

Dry Beneficiation in a Reflux Classifier

A Thesis Submitted for the Degree of

Doctor of Philosophy

By

Siubhan Ariana Macpherson

B. Eng. (Hons)

B. Math.

March 2011



This thesis contains no material which has been accepted for the award of any other degree or diploma in any university or other tertiary institution and, to the best of my knowledge and belief, contains no material previously published or written by another person, except where due reference has been made in the text. I give consent to this copy of my thesis, when deposited in the University Library, being made available for loan and photocopying subject to the provisions of the Copyright Act 1968.

I hereby certify that the work embodied in this thesis contains published papers/scholarly works of which I am a joint author. I have included as part of the thesis a written statement, endorsed by my supervisor, attesting to my contribution to the joint publication/s/scholarly work.

.....
Siubhan Ariana Macpherson

.....
Kevin P. Galvin

*Dedicated to My Family
without whom this thesis would not have been possible*

Acknowledgements

I would like to thank my supervisor, Professor Kevin Galvin for his encouragement, advice and support throughout my research project. I would also like to thank Dr Simon Iveson for his constant advice and input.

A big thank you goes to Kelly for being a sounding board for ideas and always encouraging me to continue. Further thanks to Lee, Mark, Sam, Anthony and James for their help in the lab. And thanks to Ron, Bob, Daniela, Jamie, Steve, Caitlin, Leo and Gillian for help with many little things that just kept the project moving forward.

I would also like to thank Trevor and the University's Adaptive Technology Centre for providing software, training and equipment that helped produce this thesis.

Special acknowledgement goes to Veronica for always being there throughout this project.

The financial support of the following organisations is duly acknowledged and appreciated

- The Australian Research Council
- The Australian Coal Association Research Program
- Ludowici Australia

Table of Contents

List of Figures	xix
List of Tables	xxxiii
Abstract	xxxv
Publications	xliii
Nomenclature	xliv
CHAPTER 1 INTRODUCTION	1
1.1 Aim and Objectives of Thesis	2
1.2 Background	2
1.3 Thesis Outline	6
CHAPTER 2 COAL BENEFICIATION	9
2.1 Beneficiation of Coal	10
2.2 Methods of Wet Beneficiation of Coal	11
2.2.1 Dense-Medium Cyclone	11
2.2.2 Spirals	13
2.2.3 Flotation	14
2.2.4 Reflux Classifier	14
2.2.5 Jig	15
2.3 Dry Beneficiation of Coal	16
2.3.1 Rotary Breaker	16
2.3.2 Frictional Separation	16
2.3.3 Counter-Current Fluidised Cascade	17
2.3.4 Magnetic Separation	18
2.3.5 Electrostatic Separation	18
2.3.6 FGX Separator	19
2.3.7 X-Ray Transmission	20
2.3.8 Air Dense-Medium Fluidised Bed	20
2.3.9 Vibrated Air Dense-Medium Fluidised Bed	21
2.3.10 Magnetically Stabilised Fluidised Bed	22
2.4 Summary	23
CHAPTER 3 GAS FLUIDISATION, PARTICLE TECHNOLOGY AND THE REFLUX CLASSIFIER	25
3.1 Introduction	26

3.2	Forces on a Single Particle	26
3.3	Fluidisation	29
3.4	Classes of Solid Particles	33
3.5	Elutriation	35
3.6	Dense-Medium	37
3.7	Vibration and the Vibrated Fluidised Bed	40
3.8	Inclined Fluidised Beds and Pipes	43
3.9	Dense Phase Pneumatic Conveying	45
3.10	Hindered Settling	46
3.11	Batch Vertical Sedimentation	47
3.12	Inclined Settlers	49
3.13	Reflux Classifier	51
3.14	Summary	55
	CHAPTER 4 EXPERIMENTAL METHODS	57
4.1	Introduction	58
4.2	Equipment	58
4.2.1	Reflux Classifier	58
4.2.2	Distributor Design	60
4.2.3	External Support	61
4.2.4	Feed Configuration	63
4.3	Materials	65
4.4	The Batch Experimental Apparatus	66
4.5	The Continuous Experimental Apparatus	68
4.5.1	Inclined Apparatus	68
4.5.2	Vertical Apparatus	69
4.5.3	Continuous Methodology	70
4.6	Analysis	71
4.7	Summary	73

CHAPTER 5 BEHAVIOUR OF THE SAND DENSE-MEDIUM	75
5.1 Introduction	76
5.2 Change in Sand Properties Over Time	76
5.3 Observations of the Flow Pattern	77
5.4 The Air-Sand Pseudo-Fluid	79
5.5 Proposed Segregation Mechanism	80
CHAPTER 6 BATCH TRACER PARTICLE SEPARATIONS	83
6.1 Introduction	84
6.2 Batch Elutriation Theory	86
6.3 Batch Separation Methodology	88
6.4 Tracer Particle Analysis	89
6.4.1 Equilibrium Solids Loading	89
6.4.2 Changes in Sand Properties Over Time	90
6.4.3 Movement of the Tracer Particles	92
6.4.4 Effective Partition Curves	94
6.4.5 Effect of Vibration Addition	95
6.4.6 Effect of the Time used to Calculate Effective Partition Number	96
6.4.7 Effect of Vibration Frequency and Direction	98
6.5 Two Parameter Model of Particle Velocity	101
6.5.1 Particle Species Velocity	103
6.5.2 Empirical Correlation for Slip Velocity	107
6.6 Summary	110
CHAPTER 7 CONTINUOUS TRACER PARTICLE SEPARATIONS	111
7.1 Introduction	112
7.2 Continuous Separation Methodology	112
7.3 Inclined Bed Experimental Results	114
7.3.1 Sand Flow Pattern	114
7.3.2 Partition Curve	115
7.3.3 Particle Retention	116
7.3.4 Effect of Overflow Rate	119
7.3.5 Effect of the Gas Rate	122
7.4 Vertical Bed Experimental Results	122

7.5	Modelling the Particle Velocity	126
7.6	Summary	129
	CHAPTER 8 APPLICATION TO COAL SEPARATION	131
8.1	Introduction	132
8.2	Background	132
8.3	Methodology	133
8.3.1	Batch Coal Experimental Methodology	133
8.3.2	Continuous Coal Experimental Methodology	134
8.4	Batch Coal Results	135
8.5	Continuous Coal Results	139
8.5.1	Approach to Steady State	139
8.5.2	Yield vs. Ash	142
8.6	Potential for Scale-Up	145
8.7	Summary	146
	CHAPTER 9 CONCLUSIONS AND RECOMMENDATIONS	147
9.1	Conclusions	148
9.2	Recommendations	153
	REFERENCES	155
	APPENDIX A: SAND AND VIBRATION DATA	164
	APPENDIX B: LIST OF EXPERIMENT DATES AND CONDITIONS	174
	APPENDIX C: BATCH TRACER PARTICLE DATA	178
	APPENDIX D: BATCH TRACER LEVENSPIEL RESULTS	186
	APPENDIX E: CONTINUOUS TRACER PARTICLE RAW DATA – INCLINED	188
	APPENDIX F: CONTINUOUS TRACER PARTICLE RAW DATA – VERTICAL	218
	APPENDIX G: COAL SEPARATION DATA	248

APPENDIX H: CONTINUOUS TRACER PARTICLE PARTITION CURVE DATA	252
APPENDIX I: CONTINUOUS TRACER PARTICLE ERROR BARS	257
APPENDIX J: SAMPLE CALCULATIONS	259
APPENDIX K: PHOTOS OF REFLUX CLASSIFIER	262
APPENDIX L: SPRING DESIGN	267

List of Figures

Figure 1-1: Schematic representation of the Reflux Classifier illustrating the parallel inclined plates at angle θ above the fluidised bed.	4
Figure 2-1: Schematic of a typical Australian coal preparation circuit as inferred from Sanders (2007).	12
Figure 2-2: Illustration of the circulation of particles in a spiral showing the splitter and the segregation mechanism (Kelly & Spottiswood, 1982).	14
Figure 2-3: The Beresford Plate Separator (Sanders, 2007).	17
Figure 3-1: The forces acting on a particle in a fluid.	27
Figure 3-2: Different fluidisation regimes that occur as the gas velocity increases moving from left to right (Grace, 1986).	31
Figure 3-3: The relationship between particle classification and diameter and density (Geldart, 1973).	34
Figure 3-4: The zones in the gas fluidised bed freeboard (Rhodes, 2002).	36
Figure 3-5: Mass on spring (Hoult, 2007).	41
Figure 3-6: Flow regime transition in an inclined fluidised bed (a) packed bed; (b) channel initiation; (c) channelled bed. (O'Dea et al., 1990).	44
Figure 3-7: Schematic of horizontal plug conveying (Konrad, 1986).	45
Figure 3-8: Schematic of vertical plug conveying (Konrad, 1986).	46
Figure 3-9: The regions that develop during the sedimentation of a mixture of three distinct species of particles. Region 1 contains all three species of particles, region 2 is devoid of the fastest-settling species and region 3 contains only the slowest-settling species (Davis & Acrivos, 1985).	48
Figure 3-10: Schematic of a continuous inclined settler containing four particle species, with an overflow rate such that only the two slowest-settling species reach the overflow (Davis & Gecol, 1996).	50
Figure 3-11: Schematic of the Reflux Classifier, shown here with three channels although any number is possible.	51
Figure 3-12: Two-dimensional schematic representation of the inclined channel section of the Reflux Classifier (Laskovski et al., 2006).	52

- Figure 4-1:** Schematic of the overflow arrangement showing the 20 mm wide channel opening into the overflow chamber before exiting through the 25 mm exit hole. See Appendix K for photos. **60**
- Figure 4-2:** Schematic representation of the batch Reflux Classifier apparatus showing the main vertical and inclined channel and the attached vibratory motors. For further photos of the apparatus, see Appendix K. **67**
- Figure 4-3:** Schematic of the continuous Reflux Classifier apparatus showing the main vertical and inclined channel and the attached vibratory motors and underflow pinch valves. **69**
- Figure 4-4:** Schematic of the continuous vertical fluidised bed apparatus showing the main vertical channel and the attached vibratory motors and underflow pinch valves. **70**
- Figure 4-5:** An example of a partition curve illustrating the partition number, PN, the particle density, ρ_p , and the densities, ρ_{25} , ρ_{50} and ρ_{75} . **72**
- Figure 5-1:** The change in the size distribution of the sand over time. It can be seen that the longer the sand was used, the finer the sand became. **76**
- Figure 5-2:** Sketch of the appearance of bubbles in the incline taken from video footage. The bubble extends across the entire width of the channel and there is a constant layer of downward sliding sand on the upward facing incline. **78**
- Figure 5-3:** The average measured (a) gas bubble length and (b) sand plug length in the inclined bed from video analysis of the air-sand dense-medium Reflux Classifier shown for gas rates of 10%, 15%, 20% and 25%. Each value is the average of several measurements and the error bars are the range of those values. The raw data is given in Appendix A. **79**
- Figure 5-4:** Schematic representation of the behaviour of low density (white) and high density (black) particles in the experimental apparatus illustrating (a) particles at rest at the base of a plug, (b) high density particle accelerates from rest at a greater rate than low density particle, (c) high density particle partially buried by falling sand before the low density particle arrives, and high density particle penetrates further into the fluidised upper surface of the plug beneath, (d) high density particle has travelled further down than low density particle (Macpherson et al., 2010). **81**
- Figure 6-1:** Schematic of the product fractionation pathway that was found to produce the best results (Walton et al., 2007). **85**

- Figure 6-2:** Output tracer concentration diagrams for (a) plug flow, (b) plug flow with some longitudinal mixing, (c) complete mixing, (d) dead water (Danckwerts, 1953) versus the number of flow volumes that have exited the bed. In dead water a large part of the fluid is trapped in eddies and spends a longer than average time in the pipe while the remainder travels quickly through a narrowed channel. **87**
- Figure 6-3:** The calculated mass of sand in the Reflux Classifier over the 54 minutes of each experiment. The vibration conditions are given together in the legend together with the sand feed rate in g/min. The gas rate was $3.22 \times 10^{-4} \text{ m}^3/\text{s}$ in every case. **90**
- Figure 6-4:** Plots of cumulative mass elutriated versus time showing the effect of coal on the rate of elutriation of 1600 kg/m^3 tracer particles from the Reflux Classifier under conditions of 0.005 kg/s sand feed rate, gas flowrate of $3.22 \times 10^{-4} \text{ m}^3/\text{s}$ and 595V vibration. (a) New sand containing un-ground coal, (b) and (c) show duplicate results on the same day using the same sand as in (a) after two months of constant use, and (d) shows the performance with new sand containing no coal. **91**
- Figure 6-5:** The rate of elutriation of $-6.35 +1.00 \text{ mm}$ particles from the air-sand dense-medium Reflux Classifier fitted with first order elutriation curves according to Equation (6-1) taking into account the time delay. The bed was fluidised at $3.22 \times 10^{-4} \text{ m}^3/\text{s}$ gas rate, with a sand feed rate of 0.0050 kg/s , vibrated at 595V . The 2400 kg/m^3 density experiment was one of the first conducted, before the experimental method was standardised, so less data was collected and over a shorter (40 minute) time period. **93**
- Figure 6-6:** 30 minute effective partition curve for $-6.35 +1.00 \text{ mm}$ tracer particles from the air-sand dense-medium Reflux Classifier, fluidised at $3.22 \times 10^{-4} \text{ m}^3/\text{s}$ gas rate, with a sand feed rate of 0.0050 kg/s and vibrated at 595V . **94**
- Figure 6-7:** The effect of the addition of vibration on the separation efficiency of the effective partition curve after 30 minutes for $-2.0 +1.0 \text{ mm}$ particles and $-6.35 +4.0 \text{ mm}$ tracer particles with a sand feed rate of 0.0050 kg/s and gas flowrate of $3.22 \times 10^{-4} \text{ m}^3/\text{s}$. The lines are the least square error fit of Equation (4-1) to the data. **95**
- Figure 6-8:** Effective partition curves for $-2.0 +1.0 \text{ mm}$ particles under the 595H vibration condition evaluated at different processing times. Sand feed rate of 0.0050 kg/s and gas flowrate of $3.22 \times 10^{-4} \text{ m}^3/\text{s}$. **96**
- Figure 6-9:** The effect of residence time on the (a) ρ_{50} and (b) Ep under the 595H vibration condition for the tracer particle size fractions $-6.35 +4.0 \text{ mm}$, $-4.0 +2.0 \text{ mm}$ and $-2.0 +1.0 \text{ mm}$. Sand feed rate of 0.0050 kg/s and gas flowrate of $3.22 \times 10^{-4} \text{ m}^3/\text{s}$. **97**

- Figure 6-10:** Effective batch partition curves after 30 minutes processing for -4.0 +2.0 mm tracer particles at the three vibration conditions 325H, 595V and 595H, sand feed rate of 0.0050 kg/s and gas flowrate of $3.22 \times 10^{-4} \text{ m}^3/\text{s}$. The data points show the experimental data and the curves are the best fit of Equation (4-1) to the data. **98**
- Figure 6-11:** The effect of the different vibration conditions on the (a) ρ_{50} and (b) Ep for the three size fractions studied after 30 minutes of processing. Sand feed rate of 0.0050 kg/s and gas flowrate of $3.22 \times 10^{-4} \text{ m}^3/\text{s}$. **99**
- Figure 6-12:** Two parameter fit of Equation (6-4) to experimental data for 595H vibration conditions and $1300 \text{ kg}/\text{m}^3$ density tracer particles. **103**
- Figure 6-13:** Species velocity versus particle size for 3 different tracer densities for 595V with a feed rate of 0.0050 kg/s. The trend lines are linear best fits to the species velocity data, all forced to converge at the same point at zero particle size, which is the inferred medium convective velocity. The slip velocity is the difference between the species and convective velocities. **104**
- Figure 6-14:** The species velocity versus particle size for 325 H with a feed rate of 0.0050 kg/s. The linear best fits were forced to intersect the ordinate at a single point. **104**
- Figure 6-15:** The relationship between the slip velocity and the particle size and density for three vibration conditions, particularly showing the independence from vibration frequency and direction. **108**
- Figure 7-1:** The mass of sand in the overflow and underflow in each three minute sample interval during an experiment. Lines are drawn to connect points and do not necessarily represent the actual trend. It can be seen that the underflow rate is very steady and the overflow rate varies significantly. **114**
- Figure 7-2:** An example of the partition curves obtained in one experiment. Each data point represents the experimental partition of particles of a particular size and density that had exited the bed by the end of the experiment (that is, ignoring particles still in the bed). The curves are Equation (4-1) fitted to the data with the sum of the square errors minimised. The conditions were an inclined bed fluidised with a gas rate of $4.03 \times 10^{-4} \text{ m}^3/\text{s}$, a feed rate of 560 g/min and underflow rate of 305 g/min. The horizontal dotted line represents the partition to overflow that would be expected if the separation was based solely on convection of neutrally buoyant particles. The arrows on this and subsequent figures indicate the progression from small to large particles. **115**

- Figure 7-3:** The distribution of tracer particles by (a) size fraction and (b) density in the inclined system at the end of an experiment, where Layer 1 is at the base of the bed and Layer 9 is at the top, showing the approximate positions of the feed inlet and the base of the incline based on an even distribution of sand throughout the bed. An accumulation of particles partway up the incline is observed. Lines are drawn to connect the points and do not necessarily reflect actual trends. 117
- Figure 7-4:** The determination of the experimental uncertainty associated with the calculated ρ_{50} for -4.0 +2.8 mm particles under conditions of an inclined bed fluidised with a gas rate of $4.03 \times 10^{-4} \text{ m}^3/\text{s}$, a feed rate of 560 g/min and underflow rate of 305 g/min. The triangular data points, with the vertical error bars, are the experimental partition numbers for the particles that exited the bed fitted with the smallest square error partition curve according to Equation (4-1) as in Figure 7-2. The vertical error bars represent the 90% confidence intervals of the final partition of all the particles, assuming each particle remaining in the bed has a 50% probability of exiting through the overflow. The more particles remaining in the bed at the end of the experiment, the larger the error bars. Two partition curves were fitted to these two scenarios, shown with dotted and dashed lines. So, the experimental ρ_{50} (shown with the square) could lie anywhere between these two other partition curve, giving the experimental uncertainty (shown by horizontal error bars). 119
- Figure 7-5:** Fitted (a) ρ_{50} and (b) Ep values versus the ratio of the mass flowrate of sand in the overflow to sand in the feed (i.e the variable x in Equation (7-1)). 120
- Figure 7-6:** The relationship between the ρ_{50} (ordinate) and the proportion of feed reporting to the overflow (abscissa) showing 90% confidence error bars as in Figure 7-4. The experimental data is fitted according to Equation (7-1). 121
- Figure 7-7:** How the separation (a) cut-point (ρ_{50}) and (b) efficiency (Ep) vary with changes in the gas flowrate at a fixed overflow rate. From the figure it is clear that a gas rate of 25% produced the least variation in ρ_{50} with size and the lowest Eps . 122
- Figure 7-8:** Comparing the (a) ρ_{50} in the inclined bed, (b) ρ_{50} in the vertical bed, (c) Ep in the inclined bed and (d) Ep in the vertical bed, with changes in the proportion of feed sand reporting to the overflow. The ρ_{50} data have been fitted with the minimum sum square errors equation of the form $y = Ax^n + C$. For the inclined system, $2 \leq n \leq 7$, for the vertical system $n = 6.8$. 123

- Figure 7-9:** Comparing the (a) ρ_{50} in the inclined bed, (b) ρ_{50} in the vertical bed, (c) Ep in the inclined bed and (d) Ep in the vertical bed with changes in the gas flowrate. **124**
- Figure 7-10:** The rate of elutriation of 1600 kg/m^3 density particles from an inclined fluidised bed and a vertical fluidised bed with a gas rate of 25%, feed rate of 560 g/min and an underflow rate of 185 g/min. **125**
- Figure 7-11:** The species velocity in the vertical system, with a feed rate of 560 g/min, vibration rate of 595V and gas rate of 25%, as predicted by Equation (7-2) and fitted to an Intermediate flow regime model (that is dependent on $d^{1.14}$). (a) Illustrates the overflow stream converging to a single convective velocity of 0.0023 m/s with an overflow rate of 276 g/min. (b) Illustrates the underflow stream converging to a single convective velocity of 0.0022 m/s with an overflow rate of 114 g/min. Fitted lines forced to converge to a single point. **127**
- Figure 7-12:** The species velocity in the inclined system, with a feed rate of 560 g/min, vibration rate of 595V and gas rate of 25%, as predicted by Equation (7-2) and fitted to an intermediate flow regime model (that is dependent on $d^{1.14}$) in (a) the overflow stream with an overflow rate of 297 g/min and (b) the underflow stream with an overflow rate of 176 g/min. **128**
- Figure 8-1:** Compares a single stage coal (-4.0 +1.0 mm) separation in a sand medium with vibration with the coal washability data (-4.0 +1.0 mm) and a multi-stage magnetite medium coal (-4.0 +1.0 mm) separation without vibration. **136**
- Figure 8-2:** The effect of vibration on the separation efficiency of the air-sand dense-medium Reflux Classifier on coal in the size range -4.0 +0.5 mm, comparing experimental results for No Vibration, 595V and 750M vibration conditions with the coal washability data (-4.0 +0.5 mm). **137**
- Figure 8-3:** The separation achieved using the air-sand dense-medium Reflux Classifier system with 595V vibration on -8.0 +1.0 mm coal, compared with the coal washability data (-8.0 +1.0 mm). **138**
- Figure 8-4:** The changes in the overflow and underflow composition over time for (a) sand mass and (b) coal mass. In particular showing the approach to steady state at 70 minutes, 160 minutes and 200 minutes. **140**
- Figure 8-5:** The approach to steady state of individual size fractions. (a) -5.6 +4.0 and -4.0 +2.8 mm, (b) -2.8 +2.0, -2.0 +1.4 and -1.4 +1.0 mm. **140**

- Figure 8-6:** The distribution of coal within the bed after 210 minutes of continuous coal feed at a concentration of 5.8 mass%. The approximate positions of the feed and the base of the incline are indicated. A higher concentration of coal is clearly apparent at the base of the incline. The horizontal dotted line indicates the feed concentration. **141**
- Figure 8-7:** The cumulative size distribution of (a) the combined overflow and underflow samples for 70, 80, 160, 170, 200 and 210 minutes and (b) the separate overflow and underflow compared with the feed size distribution for an overflow rate of 221 g/min (170 minutes). The different dotted lines in (a) represent the different time samples. **142**
- Figure 8-8:** The Cumulative Yield (%) vs Cumulative Ash (%) separation results achieved in the air-sand dense-medium Reflux Classifier (RC) with vibration on a continuous coal feed (-5.6 +1.0 mm), compared with the coal washability data and the separation obtained in the water-based Reflux Classifier (Callen et al., 2007b) in each appropriate size fraction: (a) -8.0 +4.0 mm, (b) -4.0 +2.0 mm, (c) -2.0 +1.0 mm (d) -8.0 +1.0 mm. **144**

List of Tables

Table 3-1: The drag coefficient and terminal velocity of spherical particles for the Stokes', Intermediate and Newton's regimes.	28
Table 3-2: Hydrodynamic features of different regimes of fluidisation which can exist between the onset of fluidisation and pneumatic transport for Geldart Group B systems (Arnaldos & Casal, 1996).	32
Table 6-1: The elutriation rate constants, K_i (min^{-1}), for the plots in Figure 6-4.	92
Table 6-2: The theoretical and inferred convective velocities for the three vibration conditions with a sand feed rate of 0.0050 kg/s. The steady state mass of sand in the bed from which the theoretical velocity is calculated is also included.	106
Table 6-3: The average bed density, the inferred separation density using the slip velocities ($\rho_{m,i}$) and the separation density (ρ_{50}) for the three different tracer sizes calculated from partition curves after 30 minutes at the three different vibration conditions.	106

Abstract

It is common practice in industry to beneficiate coal (and other minerals) to meet contractual obligations. This beneficiation increases the concentration of the valuable component in the product by removing the unwanted gangue or mineral matter in predominantly density based separations. Current beneficiation technology relies heavily on water-based separation devices that are highly efficient. However these require extensive water recovery operations and result in a wet product that has a reduced value and higher transport cost than an equivalent dry product. As water supplies in the mining areas of Australia become less reliable, there is renewed interest in beneficiation technologies that do not require water or water recovery operations and can produce a product of equivalent value to water-based beneficiation. This thesis considers dry beneficiation in a novel gas-solid fluidised bed, known as the Reflux Classifier, with the addition of a dense-medium and vibration.

Prior to this work, the application of the water-based Reflux Classifier to the separation of particles on the basis of size and/or density had been extensively studied and the use of the pneumatic Reflux Classifier as a size separation device had also been investigated. The application of the pneumatic Reflux Classifier to the density based beneficiation of particles had not been previously considered.

In the present study, the density based separation of particles in a laboratory scale pneumatic Reflux Classifier was considered. The apparatus was constructed of stainless steel and had a cross-sectional area of 20 mm × 100 mm with a plenum chamber and distributor below a 1 m vertical fluidised bed and a 2 m channel inclined at 70° to the horizontal above. A sand dense-medium was used to encourage density based separations and sand was continually fed to the bed in all experiments. The bed could be configured for batch separations with continuous overflow removal, or continuous separations with both continuous overflow and underflow removal. The whole apparatus could be vibrated to study the effect of the addition of vibration to the separations. The separations obtained in the Reflux Classifier were compared to separations in a 3 m vertical fluidised bed to determine the effect of the incline on the separation performance of the vessel.

The majority of the separation experiments were conducted on batch quantities of plastic tracer particles in the size range $-6.35 +1.0$ mm with densities of 1300, 1600, 1800, 2100 and 2400 kg/m³. In batch experiments, tracer particles of a single density were placed on the distributor and the bed filled with silica sand (density 2600 kg/m³, $-355 +90$ μ m). The gas and vibration were introduced simultaneously with a continuous feed of sand medium and the rate of elutriation of particles (both sand and tracer) from the bed was measured. The batch experiments investigated the effect of changing the vibration frequency and direction, including separations with no vibration, across the range of tracer particle densities. In continuous experiments, steady state between the feed and the continuous overflow and underflow of sand was established. The tracer particles in single density samples were fed into the bed in 10 minute intervals over a period of 40 minutes and their rate of exit through the overflow and underflow was measured. The continuous experiments investigated the effect of changing the overflow rate of particles at a constant feed rate and the effect of changing the gas rate.

The sand fluidised bed acted as a dense-medium, or pseudo-fluid, enhancing the density separation of particles. Increasing the gas rate, or decreasing the vibration frequency both acted to increase the size of bubbles in the bed, which resulted in less homogeneity in the medium and thus less effective separations. As with all dense media operations, the effectiveness of the medium increased for larger tracer particles. An almost perfect density separation of particles greater than 4 mm in diameter was observed while for particles less than 2 mm in diameter the separation was more dependent on the convective velocity of the medium than the particle size.

The rate of particle elutriation from the bed was first order dependent on particle concentration. The elutriation rate data for the batch experiments was modelled using a two-parameter model for dispersed plug flow to find the particle velocity and dispersion. The particle velocity was found to consist of a convective velocity due to the flowrate of the sand through the vessel that affected all particles equally, and a buoyant velocity dependent on particle size and density. This buoyant velocity could be predicted from an equation for particle terminal velocity in the Intermediate regime, with the density and viscosity of the medium dependent on the vibration conditions.

The density cut-point of the separations could be varied by changing the overflow rate, the vibration rate and the gas rate. Increasing the overflow rate or the gas rate led to a higher density cut-point while increasing the vibration frequency reduced the density cut-point. The separation efficiency decreased with decreasing particle size or increasing gas rate, but was largely unaffected by the overflow rate. The inclusion of the incline increased the separation efficiency by encouraging the refluxing of near density particles, as observed in the water-based Reflux Classifier. This refluxing is a unique characteristic of the inclined channel that was not observed in the vertical fluidised bed.

The separation performance of the experimental apparatus was very good for the largest particles in comparison to water-based beneficiation devices but poor for particles below 2.0 mm. For particles in the size range -6.35 +4.0 mm the separation efficiency, measured by the Ep , was 0.04 for the batch separations and 0.06 for the continuous separations. This compares well with the 0.02-0.03 Ep of water-based dense-medium cyclones on the same size coal particles. The Ep for particles in the size range -2.0 +1.0 mm was 0.16 in the batch separations and 0.35 in the continuous separations which is significantly higher than the 0.07 Ep of the water-based Reflux Classifier and the 0.14 to 0.18 Ep of water-based spirals.

From the tracer particle experiments the best conditions for a continuous coal separation were determined to be high frequency vibration, and minimal gas and overflow rates, with the Reflux Classifier performing better than a vertical fluidised bed. A separation of coal confirmed that the dense-medium pneumatic Reflux Classifier with vibration can perform good density based separations. The geometry used in this work restricted the processing capacity (tonnage) of the unit to approximately 1.5 t/m².h, with higher feed rates resulting in particles accumulating in the bed and causing blockages. A water-based Reflux Classifier has a throughput capacity as high as 47 t/m².h.

This thesis describes the first attempt to characterise the behaviour of a Reflux Classifier with sand dense-medium. The intention was to determine if such an apparatus could be used to separate particles on the basis of density and the potential for its application as an industrial process. The focus was on the changes in behaviour and the

separation cut-point and efficiency with changing conditions. From this work it was concluded that the laboratory scale Reflux Classifier can separate particles on the basis of density with similar efficiency and cut-point to current industrial standards but the processing capacity is significantly below that of similar footprint water-based technologies.

Publications

Macpherson, S., Moghtaderi, B., Walton, K., and Galvin, K.P. (2007) Dry Processing using an Air-Magnetite Dense-medium in the Reflux Classifier, *Proceedings, 37th Annual Australasian Chemical Engineering Conference, CHEMECA 2007*, Melbourne, Australia.

Macpherson, S.A. and Galvin, K.P. (2008) The Effect of Vibration on Dry Coal Beneficiation in The Reflux Classifier, *Proceedings, The 25th Annual International Pittsburgh Coal Conference 2008*, Pittsburgh, USA.

Macpherson, S.A., Callen, A.M., Walton, K.J. and Galvin, K.P. (2008) Dry Processing of Coal in an Air-Sand Dense-Medium Reflux Classifier with Vibration, *Proceedings, 12th Australian Coal Preparation Society Conference 2008*, Sydney, Australia.

Macpherson, S. A., Iveson, S. M. and Galvin, K. P. (2010) Density based separations in the Reflux Classifier with an air-sand dense-medium and vibration. *Minerals Engineering*, 23, 74-82.

Macpherson, S. A., Iveson, S. M. and Galvin, K. P. (2010) Density-based separation in a vibrated Reflux Classifier with an air-sand dense-medium: tracer studies with simultaneous underflow and overflow removal, *Manuscript submitted for publication to Minerals Engineering*.

Nomenclature

Symbol	Definition	Units
A	Area of bed	m^2
a	Amplitude	m
Ar	Archimedes Number	-
C	Concentration	-
C_D	Drag coefficient	-
D	Dispersion coefficient	m^2/s
D_v	Vessel diameter	m
d_o	Diameter of falling object	m
d_p	Diameter of particle	m
d_{SV}	Diameter of sphere having same surface area as target particle	m
Ep	Ecart probable	kg/m^3
F	Theoretical throughput advantage	-
f	Frequency	1/s
F_B	Buoyancy force	$kg.m/s^2$
F_D	Drag force	$kg.m/s^2$
F_G	Gravitational force	$kg.m/s^2$
F_w	Weight force	$kg.m/s^2$
$f(\epsilon)$	Hindered settling function	-
g	Gravitational acceleration, 9.81	m/s^2
H	Height of bed	m
k	Spring constant or restoring force	N/m
K_i	First order elutriation constant of particles of size d_{pi}	$kg/m^2.s$
L	Length	m
m	Mass	kg
\dot{m}	Tracer particle mass fraction elutriation rate	1/s
M_B	Mass of particles in bed	kg
M_{bed}	Steady state holdup of sand	kg
\dot{M}_{feed}	Rate of sand addition	kg/s

P	Pressure	Pa
PN	Partition number	-
ΔP	Pressure difference	Pa
ΔP_{mf}	Pressure difference at minimum fluidisation	Pa
Q	Volume of tracer	m^3
Re	Reynolds number	-
Re_m	Reynolds number of the medium	-
Re_{mf}	Reynolds number at minimum fluidisation	-
Re_p	Particle Reynolds number	-
R_i	Rate of elutriation	kg/s
t	Time	s
U	Velocity	m/s
U_c	Fluidisation velocity where pressure fluctuations are at a maximum	m/s
U_{cb}	Minimum channelled bed velocity	m/s
U_{conv}	Convective velocity	m/s
$U_{conv,i}$	Inferred convective velocity	m/s
$U_{conv,t}$	Theoretical convective velocity	m/s
U_f	Fluid superficial velocity	m/s
U_i	Initial fluidisation velocity in an inclined bed	m/s
U_k	Fluidisation velocity where pressure fluctuations stabilise	m/s
U_{mf}	Minimum fluidisation velocity	m/s
U_p	Particle velocity	m/s
U_r	Relative velocity between object and medium particles	m/s
U_{slip}	Particle slip velocity	m/s
U_{TFS}	Terminal Free Settling Velocity	m/s
U_{tr}	Fluidisation velocity where particle transport commences	m/s
V	Volume	m^3
V_B	Volume of the bed	m^3
X_i	Concentration of particles of size d_{pi}	-
x	Linear displacement	m
\ddot{x}	Acceleration in x-direction	m/s^2
z	Perpendicular gap	m

Greek Letters

Symbol	Definition	Units
ε	Voidage	-
ε_{mf}	Voidage at minimum fluidisation	-
ϕ	Sphericity	-
ϕ_i	Volume fraction of species i	-
η	Segregation efficiency	-
θ	Angle of inclination to the horizontal	°
μ_e	Effective viscosity	Pa s
μ_f	Fluid viscosity	Pa.s
ρ	Density	kg/m ³
ρ_f	Density of fluid	kg/m ³
ρ_g	Density of gas	kg/m ³
ρ_i	Density of species i	kg/m ³
ρ_m	Density of medium	kg/m ³
$\rho_{m,i}$	Inferred medium density	kg/m ³
ρ_p	Density of particle	kg/m ³
ρ_s	Density of solid	kg/m ³
ρ_{50}	Cut-point density	kg/m ³
ρ_{25}	Particle with 25% probability of reporting to overflow	kg/m ³
ρ_{75}	Particle with 75% probability of reporting to overflow	kg/m ³
τ	Period	s
τ_o	Yield stress of Bingham fluid	kg/m ² .s
ω	Vibration frequency	1/s
ω_n	Natural frequency	1/s

Chapter 1

Introduction

1.1 Aim and Objectives of Thesis

The Reflux Classifier consists of a vertical fluidised bed with a system of inclined channels above as shown in Figure 1-1. It is noted, however, that in this study the system was simplified to just one inclined channel above the vertical section. The focus of the study was on the potential of the system to separate particles on the basis of density under dry conditions, with specific emphasis on dry coal beneficiation. In previous studies using water as the fluidising medium, the Reflux Classifier has been shown to be effective in achieving efficient size (Doroodchi et al., 2006) and also density based separations (Galvin et al., 2005). Similarly efficient size separation has been achieved using air as the fluidising medium (Callen et al., 2007a). However the separation of particles on the basis of density has not been investigated previously using air as the fluidising medium.

The aim of this study was to establish the optimal conditions under which a pneumatic Reflux Classifier can be used to separate particles on the basis of density, and to compare the separations with those obtained using the water-based Reflux Classifier. This work incorporated the effects of both a dense-medium and vibration with air fluidisation. The significance of the inclined section on the density separation in the pneumatic device was also investigated, with reference to the separation achieved in the conventional vertical system.

1.2 Background

Beneficiation is the separation of a feed into its valuable and waste components. In the minerals industry, this separation is usually done based on the physical property of density, although other physical properties like electrical or magnetic susceptibility, or surface properties may be exploited. Density is the mass per unit volume of a substance and depends on the chemical composition.

Run-of-mine coal consists of combustible carbon-based material and non-combustible mineral matter, also known as gangue, which typically is composed of silica based material. Often, before it can be utilised to produce energy or metallurgical coke, the

coal must be beneficiated to remove much of the non-combustible material. A typical coal beneficiation process involves breaking the coal to pass a 50 mm screen before classifying into three parallel streams. The coarse stream is separated on the basis of density in dense-medium cyclones, the fines are often beneficiated in spirals and the ultrafines via flotation. All three of these processes are water-based and thus coal is traditionally mined in areas that have a good water supply. The final wet coal product must be de-watered to meet contractual moisture levels.

The efficiency of water-based processing is undeniable, with near ideal density based separations achieved. However, water processing is not without disadvantages. For example, these processes result in significant product moisture, tailings disposal problems and a need for water recovery processes such as filters, centrifuges and thickeners.

The development of dry beneficiation methods has been largely ignored in the past, due to the superior separation provided by water-based technologies. However, as the reliability of water in many mining regions decreases, interest in dry beneficiation methods for coal is increasing. This is particularly so in Australia, the fourth largest coal producer and largest exporter in the world (World Coal Institute, 2008), which also happens to be the driest inhabited continent on Earth (Commonwealth of Australia, 2009).

In addition to not needing a reliable water supply, a dry beneficiation process provides a dry coal product with higher calorific value and reduced transport cost as less water is retained in the coal. Furthermore, a dry coal processing facility does not require the large capital investment of water recovery operations and large areas for tailings ponds. Potential disadvantages of dry beneficiation include the need for a dry feed, greater need for dust control measures and the risk of explosion of fines.

The Reflux Classifier consists of parallel inclined channels located above a conventional fluidised bed as illustrated in Figure 1-1. Water-based units are being used commercially to separate coal from mineral matter (Ludowici, 2007). The inclined channels provide a larger effective segregation area due to the Boycott Effect (Boycott,

1920), thus permitting much higher operating velocities than used in conventional fluidised beds (Galvin & Nguyentranlam, 2002). A reflux action also develops as a result of particle segregation onto the upward facing inclined surfaces. The settled particles then slide down the inclined surfaces and return to the fluidised zone. The particles are subsequently re-fluidised and return to the inclined channels for further possible separation to the overflow. Particles, especially low density ones, can also experience a mechanism of re-suspension in the channels due to shear-induced lift forces (Laskovski et al., 2006).

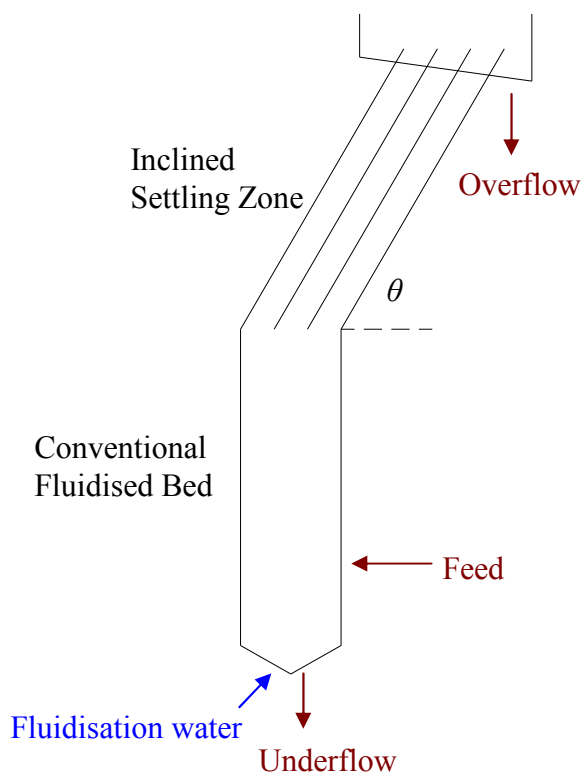


Figure 1-1: Schematic representation of the Reflux Classifier illustrating the parallel inclined plates at angle θ above the fluidised bed.

Fluidised beds are known to provide an excellent mixing environment, hence their application as a separation device requires conditions that minimise mixing especially at the exit locations of the separating particles. The separation in a fluidised bed occurs due to the difference in terminal settling velocity of the particles within the bed, with the particles having the highest settling velocity segregating to the bottom of the bed and the lowest settling velocity particles congregating at the top of the bed (Rhodes,

2002). In a high density fluid the difference in terminal settling velocity of two particles of different density is more pronounced than in a low density fluid. Thus a water fluidised bed will segregate particles on the basis of their settling velocity more easily than an air fluidised bed.

One way to potentially overcome this problem is to use an air fluidised bed of fine particles as the separating medium. This dense-medium acts as a pseudo-fluid with an effective density intermediate between the densities of the gas and constituent solid particles. To another particle significantly bigger than the medium particles, the gas-solid suspension acts as a continuum (pseudo-fluid) rather than as individual particles buoyed by a gas. The use of such a dense-medium with a much higher effective fluid density promotes better density based separation of the larger particles.

The gas fluidisation properties of the medium particles depend on their size and density. Geldart (1973) identified four different regimes of behaviour, of which the two bubbling regimes, Group A and B, are of interest. Bubbling results in large areas of inconsistent density within the bed and also causes more violent mixing, both of which are detrimental. To provide an effective gravity separation the density of the medium needs to be consistent (Jin et al., 2005).

Vibration reduces the bubble size (Jin et al., 2005) and thus provides a more consistent density throughout the bed. Furthermore, vibration decreases the minimum fluidisation velocity of the particles (Wang et al., 1997), which has the benefits in a dry system of decreasing the gas velocity required to achieve fluidisation. In the Reflux Classifier, vibration may also assist in the re-suspension of particles in the inclined settling zone.

In a review of developed dry beneficiation processes, Lockhart (1984) concluded that gas fluidisation was the most appropriate method for the gravity separation of coal particles. However, the potential of the Reflux Classifier as a dry separation device has only recently been considered. Callen et al. (2007) conducted the first study of the gas-solid fluidisation of particles in a Reflux Classifier. They considered the effect of parallel inclined channels on the elutriation of particles from the dilute phase freeboard of an air-fluidised bed, and concluded the action was very similar to the water-based

system. However, their objective was to examine the transport of particles of one density, covering a broad range of particle sizes. The inclined channels permitted higher operating velocities for the same separation size. Indeed, further work confirmed that for particles of different densities, the separation of coal particles proceeded primarily on the basis of the particle size (Walton et al., 2007). However, with the addition of magnetite as a dense-medium it was observed that the coal separation was no longer governed by the particle size, and that the separation exhibited significant density dependence (Walton et al., 2007).

The work of this thesis follows on from the work of Walton et al. (2007). The magnetite dense-medium used in that study was replaced with lower density sand at a higher concentration. The fluidised bed was also vibrated to improve the consistency of the bed. The separation performance of the system in both semi-batch and continuous configurations was investigated.

1.3 Thesis Outline

This thesis commences with a literature review in Chapters 2 and 3. This review is followed by a description of the experimental methods in Chapter 4 and observations about the fluidising behaviour of the sand medium in Chapter 5. Tracer particles of different size and density were used to probe the transport of different particle species. The results of the tracer particle experiments are reported in Chapter 6 for the batch system and Chapter 7 for the continuous system, with the coal separation experiments discussed in Chapter 8. Chapter 9 contains the concluding discussion and the recommendations arising from this work.

The background of the current state of coal beneficiation in Australia is given in Chapter 2 before discussing the existing dry coal beneficiation technologies and their effectiveness. This review provides the context for the opportunity of a new dry gravity separation device, the subject of this thesis.

Chapter 3 provides a comprehensive review of the established theory behind various aspects of the Reflux Classifier performance. The review commences with gas

fluidisation and the different Geldart particle classifications (Geldart, 1973). This is followed by discussion of the elutriation of particles from fluidised beds, the use of dense media in particle separations, and the effect that vibration has on the behaviour of a gas fluidised bed. Following consideration of the effect of hindered settling, inclined settlers and inclined fluidised beds are examined leading into a discussion of the theory that underpins the Reflux Classifier.

The development design and construction of the air-sand dense-medium Reflux Classifier with vibration is the subject of Chapter 4. The discussion covers the multiple designs, an overview of the different experimental techniques used, and assessments on the results obtained. The behaviour of the sand medium was observed in a transparent channel, and these observations are discussed in Chapter 5.

Once the system was designed and built, its performance was evaluated by performing density separations. Tracer particles were chosen for these initial separations because they provide an immediate measure of their density based on their colour. Chapters 6 and 7 discuss the density separations obtained in the batch and continuous systems respectively using tracer particles. Those chapters also contains the findings of how the system behaved under differing conditions of vibration frequency and direction, sand rate, gas rate and system geometry. Using the findings from this work, coal separations were performed and these results given in Chapter 8.

Conclusions from these results were then made and discussed in Chapter 9 together with recommendations for further work.

Chapter 2

Coal Beneficiation

2.1 Beneficiation of Coal

Beneficiation, through gravity separation, is the separation of a feed into its density components without reference to particle size or any other physical property. Coal has been beneficiated for many decades in (generally) water-based operations for several reasons: removing the non-combustible material from the coal provides a cleaner burning product with a higher calorific value; metallurgical coal quality improves; transport costs on a per tonne of combustible basis are reduced. As mining techniques have become more mechanical, beneficiation has become an expected practice as there are large amounts of gangue removed from the seam and outside of the seam. In addition, the coal currently being mined is often of lower quality than in the past, further adding to the desirability of beneficiation.

At face value, dry beneficiation is more attractive than water-based processing. The logic is inescapable: coal is removed from the ground in a water saturated state, breakage produces a significant increase in surface area, and hence the moisture content falls below the saturation level producing a dry-like state and finally, after processing a coal product of low moisture is required. However it must be acknowledged that in the past dry beneficiation technologies have generally been less efficient than water separations. Dry separations have also been more sensitive to feed composition and rate, and dust containment and spontaneous combustion associated with dry coal have also been of significant concern (Lockhart, 1984).

In his review of the dry beneficiation of coal, Lockhart (1984) asserts that the dust control operations necessary for dry beneficiation are simpler than water recovery operations and require less land area and capital investment. In addition, drying as-mined coal is simpler than de-watering coal after wet processing. Wet coal is also more likely to absorb further water than dry coal and may freeze, causing handling difficulties in cold weather.

Dry processing of coal has not been widely adopted due to the simplicity and efficiency of water-based beneficiation technology. Without a paradigm shift in mining there are only limited circumstances where dry beneficiation would be considered as the

preferred option over traditional beneficiation techniques. These include mining in areas where the water supply is limited or unreliable; if the coal contains large amounts of clay that can swell or cause the feed to become high in slimes content and hence difficult to handle; if the temperature of the site is likely to fall below 0°C; or if there is the possibility of damaging the product or contaminating the process water.

2.2 Methods of Wet Beneficiation of Coal

Before discussing the technologies available for dry beneficiation of coal, the major industrial water-based beneficiation methods used in Australia will be outlined as well as the technologies pertinent to this thesis. Figure 2-1 illustrates a typical coal beneficiation circuit. As-mined coal contains coal and mineral matter. This feed is crushed to reduce the large particles to a manageable size, typically below 50 mm, in turn liberating the coal from the mineral matter. The feed is then sieved to separate the coarse fraction which is generally beneficiated in a dense-medium cyclone (Sanders, 2007). The undersize coal from the sieve bend may be further separated into fine coal and ultrafine coal in a hydrocyclone. The fine coal is beneficiated using spiral classifiers and the ultrafine coal by flotation. Both dense-medium cyclones and spirals separate on the basis of density while flotation exploits the hydrophobicity of the coal. These unit operations are described in more detail below.

2.2.1 Dense-Medium Cyclone

The dense-medium cyclone is the most prevalent coal beneficiation device in Australia. In 2007, between 60 and 70% of the coal processed in Australia had been through a dense-medium cyclone separation (Sanders, 2007). There are two main advantages of a dense-medium cyclone. Firstly the addition of a dense-medium increases the density of the coal-water suspension which allows the separation to take place on the basis of density with very little effects of particle size. Secondly, the increased acceleration force in a cyclone, when compared to gravity alone, allows the separation to take place at a high rate.

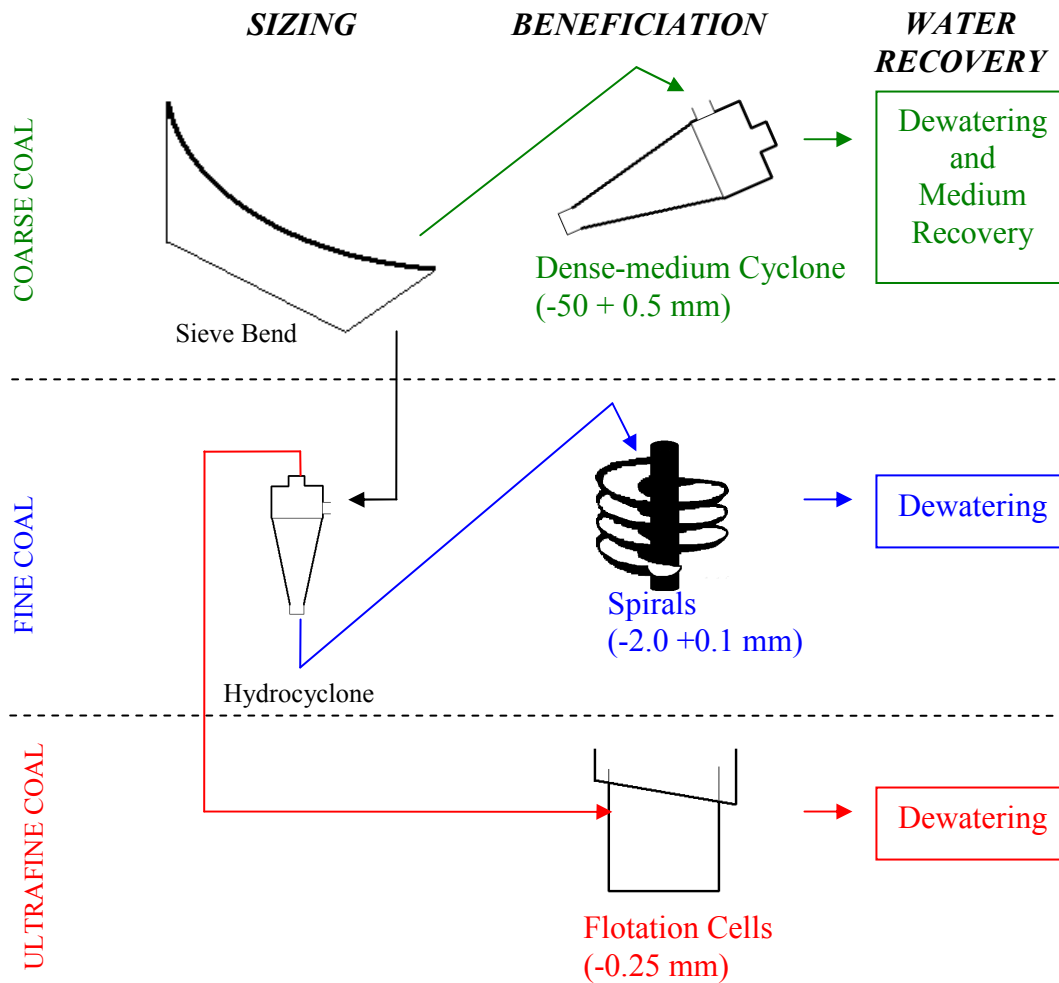


Figure 2-1: Schematic of a typical Australian coal preparation circuit as inferred from Sanders (2007).

In a dense-medium separation, particles denser than the medium suspension will sink while the lower density particles will float. In Australia, magnetite is the medium of choice with the majority of the magnetite particles being smaller than $60\ \mu\text{m}$ (Sanders, 2007). Because magnetite has a high density only a small amount is needed to provide the required medium density thus minimising any increase in the viscosity of the suspension due to added particles. In addition, magnetite is ferromagnetic which allows it to be more easily recovered from the coal product and reject using a high gradient magnetic separator.

A cyclone increases the rate of separation by increasing the acceleration force experienced by the particles. In a dense-medium cyclone the high density particles are flung to the outer walls and removed through the underflow while the low density particles migrate to the vortex in the centre of the cyclone and are recovered via the overflow. Very large particles, which already have high settling rates, may not need the additional acceleration of a cyclone and so may be processed in dense-medium baths.

Dense-medium cyclones are very effective at separating particles down to 0.5 mm in diameter with an Ep of generally 0.02 to 0.03. While they can be used for fine particles, the added complexity of the circuit has not made it a popular choice in Australian coal processing (Sanders, 2007).

2.2.2 Spirals

Spirals are the most commonly used technology for the beneficiation of fine coal, that is, coal approximately -2.0 +0.1 mm in size (Sanders, 2007). The segregation mechanism in a spiral, like a cyclone, also relies on centrifugal forces. The feed forms a thin film layer in the spiral, and centrifugal forces cause a circulation pattern in the water. The water is flung to the outside of the channel, aided by the wash water (Figure 2-2) preferentially entraining the low density (low terminal velocity) particles. These particles then begin to settle back to the centre via gravity, but are resuspended by the water flowing outwards. This arrangement provides segregation of the dense material to the centre, where it is removed via the splitters (see Figure 2-2), and the low density material to the outer walls for removal at the base of the spiral.

Because spirals operate best with a thin slurry film they are a relatively low capacity device. Thus, many spirals are used concurrently in a coal processing plant, often with three spirals nested together to reduce the floor area required. Spirals generally separate between the densities of 1600-1800 kg/m³ with Eps of 0.14 to 0.18 (Sanders, 2007) which is a fairly narrow range of operation.

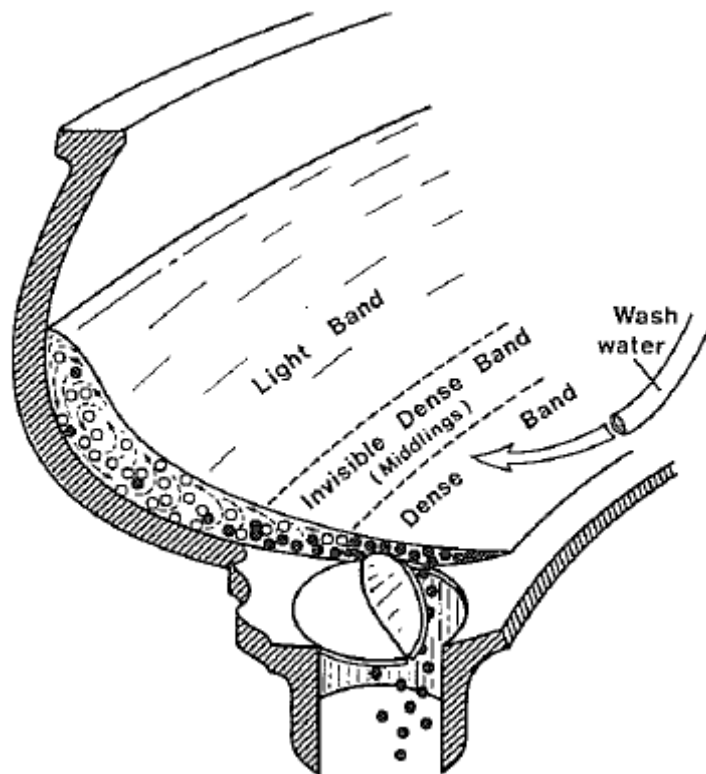


Figure 2-2: Illustration of the circulation of particles in a spiral showing the splitter and the segregation mechanism (Kelly & Spottiswood, 1982).

2.2.3 Flotation

Flotation is used to beneficiate ultrafine coal, in the size range of approximately -0.2 mm. Unlike spirals and dense-medium cyclones, flotation does not separate particles on the basis of density. Instead, flotation utilises the difference in surface hydrophobicity of coal and mineral matter. A reagent is added to the coal feed to make the coal particles more hydrophobic while leaving the mineral matter hydrophilic. In a flotation column, the feed is aerated and bubbles are formed with the aid of a surfactant. The hydrophobic particles attach to the bubbles and float to the overflow, while the hydrophilic particles settle out. Flotation works best when the coal is fully liberated.

2.2.4 Reflux Classifier

The Reflux Classifier is discussed in detail in Chapter 3. It has been investigated as a smaller footprint option to replace spirals in commercial water-based coal processing. Recent work by Galvin et al. (2009) has provided evidence that the Reflux Classifier

can be used as a density separation device to much smaller sizes and has the potential to replace spirals and other fluidised bed devices.

2.2.5 Jig

A jig operates on the principle of differential acceleration (Kelly & Spottiswood, 1982). When a particle accelerates from rest, the drag is negligible since the velocity is initially very small. Thus the buoyant weight of the particle can be equated with the mass of the particle, m , multiplied by its acceleration, a , as given by Newton's Second Law. The full derivation of the buoyant weight is given in Chapter 3. Here the mass is given by the product of the particle volume and density. Hence,

$$(\rho_p - \rho_f)g \frac{\pi}{6} d_p^3 = F_w = ma = -\rho_p \frac{\pi}{6} d_p^3 \frac{dU_{slip}}{dt} \quad (2-1)$$

where ρ_p is the density of the particle, ρ_f the density of the fluid, d_p the diameter of the particle, U_{slip} the slip velocity of the particle relative to the fluid and t time. It is noted that the so-called "added mass" effect of the water is neglected in Equation (2-1). Therefore, from Equation (2-1), the initial acceleration, dU_{slip}/dt , is,

$$\frac{dU_{slip}}{dt} = -\left(1 - \frac{\rho_f}{\rho_p}\right)g, \quad (2-2)$$

which is independent of the particle size.

A jig utilises a pulsating current of fluid to expand a bed of particles and then allow them to settle. The different accelerations of the coal and gangue cause the bed to segregate. Thus the low density coal can be skimmed from the top of the bed and the gangue removed from the bottom. By controlling the rate of pulsation of the fluid and the size range of the feed, a near perfect density separation can, in principle, be obtained from a water-based jig (Kelly & Spottiswood, 1982).

2.3 Dry Beneficiation of Coal

A brief outline and review of the technologies that have been developed for the dry beneficiation of coal is given below. The purpose of this review is to place the apparatus used in this thesis within the context of other dry beneficiation methods. It is not intended to provide a detailed understanding of the theory and operation of existing dry beneficiation technology.

2.3.1 Rotary Breaker

Rotary breakers effectively separate friable coals from mineral matter by frequently lifting and dropping the feed material. The coal is more likely to break than the gangue and thus a subsequent sizing operation will separate the coal and mineral matter. The design of the rotary breaker is important in determining the effectiveness of the separation, and they do not work well on hard coals (Dwari & Rao, 2007). This process has a low selectivity and high energy and maintenance requirement.

2.3.2 Frictional Separation

The Beresford plate separator (Sanders, 2007) exploits the difference in the frictional resistance and resilience of coal and mineral matter. Particles in a narrow size range are dropped onto a highly polished, inclined glass plate. The coal particles are more likely to bounce off the plate and gain a higher fall velocity due to the reduced contact time with the plate. As a result, the coal particles have more momentum when they fall off the edge of the plate and travel further than the mineral matter. The particles are able to be separated into different hoppers as seen in Figure 2-3. It is possible however that this method is of limited use as the glass plate is likely to need repolishing frequently due to the constant rain of particles.

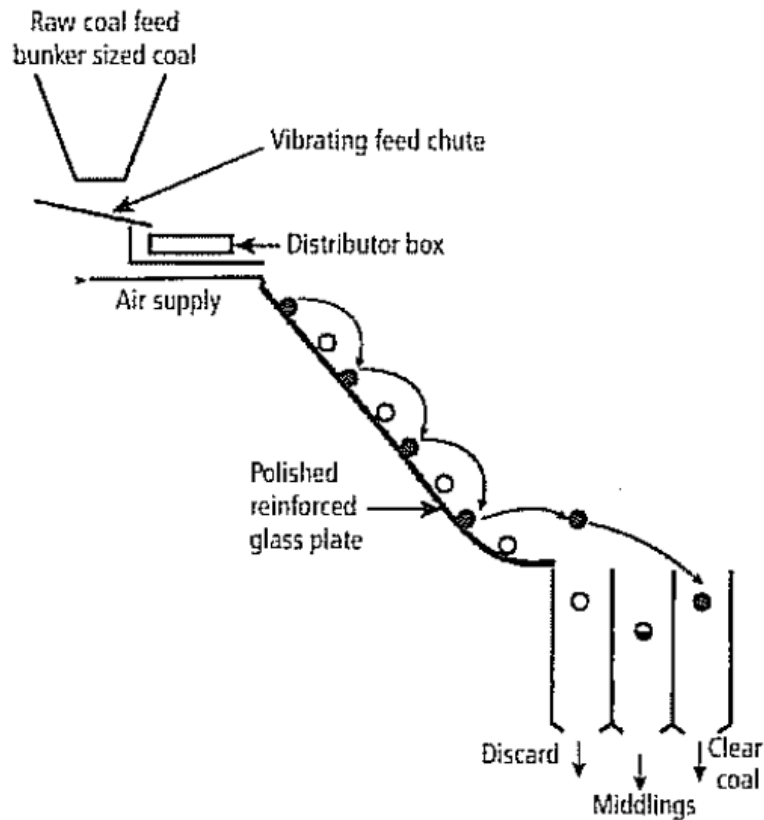


Figure 2-3: The Beresford Plate Separator (Sanders, 2007).

2.3.3 Counter-Current Fluidised Cascade

The counter-current fluidised cascade was designed in the 1970's to separate sulphurous matter from coal (Chan & Beekmans, 1982). The counter-current fluidised cascade consists of a fluidised bed on a slight slope with a chain running through the base of the bed. The reject matter sinks to the bottom of the bed and is carried by the chain up the incline to exit. The product material is skimmed from the top at the opposite end of the bed. Significant reductions in the pyrite and ash content of the product coal of a -400 μm feed sample were observed (Chan & Beekmans, 1982). There was some comminution due to the use of the chain. In order to reduce this comminution effect, Dong & Beekmans (1990) investigated the possibility of using a crossflow of air, but discovered that this resulted in the de-fluidisation of particles. The counter-current fluidised cascade is an effective density separation device but the comminution could damage the product and cause dust control problems.

2.3.4 Magnetic Separation

Magnetic separation techniques exploit the fact that inorganic mineral matter is moderately paramagnetic and coal is slightly diamagnetic (Hise, 1982). Two common methods of magnetic separation are High Gradient Magnetic Separation which separates the coal in a high intensity magnetic field over a short distance, and Open Gradient Magnetic Separation which separates over a longer distance with a lower intensity magnetic field.

Pyrite is another non-combustible material that is commonly found in coal. Pyrite is high in iron, and is weakly paramagnetic, and thus can be separated from coal in a strong magnetic field. If the pyrite is converted to the strongly paramagnetic pyrrhotite by irradiating the sample with microwaves, only a moderate magnetic field is required. However, the irradiation process may also damage or destroy the coal product. (Dwari & Rao, 2007)

Magnetic separation techniques can be effective, but they are energy intensive and may also require pre-treatment of the coal. In addition, the size range needs to be restricted to minimise the effects of the momentum of the particles. Magnetic separation could find application as an alternative to floatation for the beneficiation of coal fines.

2.3.5 Electrostatic Separation

Electrostatic separation techniques exploit the fact that coal and mineral matter have different electrical properties and will exhibit different charges when bombarded with ions. Electrostatic separation methods work best for fine coals (Dwari & Rao, 2007) due to their high surface-area-to-volume ratio. There are several different ways of electrically separating particles, but two of particular interest are the corona discharge and triboelectric separation.

A corona discharge can be applied in a batch process in a rotating drum. The coal and mineral matter are bombarded with charged particles giving them a charge of their own. The particles are flung onto the walls where the charge is conducted away. The charge

dissipates at different rates depending on whether the particle is coal or mineral matter and so one particle species is removed from the walls before the other (Lockhart, 1984).

In triboelectric separation coal and mineral matter are charged by bringing them into contact with other particles or a surface. This is frequently done in a pipe where, if the material is chosen correctly, the coal will take on a positive charge and the mineral matter a negative charge (Anderson et al., 1979). The charged particles are then passed through an electric field which deflects their path depending on their charge and so they can be separated into different vessels.

For electrostatic separation techniques to be effective the coal needs to be well ground to maximise liberation and make the particles easier to charge. This adds a significant energy requirement to an already energy intensive process. Thus, like magnetic separation, electrostatic separation can only reasonably replace the flotation circuit of a coal beneficiation process. In addition, charging fine particles increases the risk of explosion and so electrostatic separation may not be appropriate in all circumstances.

2.3.6 FGX Separator

The FGX separator passes a feed of coal over a table, blowing air from below and vibrating from the side to separate the particles on the basis of density. The lowest density particles are imparted with the most velocity and so exit the table first with the densest travelling right to the end (Caner Orhan et al., 2010).

The FGX separator was developed in China as a de-stoning operating. It generally separates coal at a density of 2000 kg/m^3 with typical Ep between 0.2 and 0.25. It is now used throughout the world, even in areas with a good fresh water supply (Caner Orhan et al., 2010). The FGX Separator is useful as a first step in dry coal beneficiation to reduce the volume of feed to the remainder of the plant.

2.3.7 X-Ray Transmission

Von Ketelhodt (2010) described the use of Dual Energy X-Ray Transmission to separate coal from mineral matter. The coal is passed by an X-Ray scanner and its composition determined. The particle is then sorted by a mechanical or air device. This technology is appropriate to coal in the size range -100 +30 mm and operates between 1400 and 1600 kg/m³. The separation efficiency varies between 0.75 and 0.2 and current industrial units have a capacity of up to 80 t/h (von Ketelhodt, 2010).

2.3.8 Air Dense-Medium Fluidised Bed

Although there are many different dry beneficiation techniques, according to Lockhart (1984) those based on an air-fluidised bed with a dense-medium are the most effective. Air dense-medium fluidised beds have been used for almost a century to beneficiate coal. One of the earliest reported coal beneficiation methods using an air dense-medium fluidised bed was the Fraser & Yancey (1926) separation that utilised a sand dense-medium.

Very coarse coal (+50 mm) was successfully separated at laboratory scale by Chen & Yang (2003) in an air dense-medium fluidised bed. They found that increasing the bed depth minimised the bubble formation to provide a more stable fluidised bed. An *Ep* of 0.02 was achieved for this separation, equivalent to the high performance values normally reported for dense-medium cyclones.

Many laboratory scale air dense-medium fluidised bed separations of coal have been on coarse coal in the size range -50 +6 mm. An excellent example is the work of Luo et al. (2002a) who achieved an *Ep* of 0.03 over the entire size range of -50 +6 mm using a magnetite medium. It was observed that larger particles exhibited higher recovery and efficiency and were easier to separate. Small particles were more prone to back mixing with the medium solids (Luo & Chen, 2001), and were also more affected by the bed viscosity. This finding is consistent with water-based dense-medium operations, which are more effective for large particles, and can only process particles down to a certain size (Kelly & Spottiswood, 1982).

Currently in China there is a 50 t/h capacity dry processing plant for -50 +6 mm coal utilising air dense-medium fluidised bed technology (Dwari & Rao, 2007). The medium used is a mixture of magnetite and coal, with the proportion of the two adjusted to set the density of the air dense-medium fluidised bed to between 1300-2200 kg/m³ as required. No comment was made about whether there was any segregation of this mixed media.

The separation of fine coal (-6 +1 mm) in a laboratory air dense medium fluidised bed was studied by Prashant et al. (2010). Using magnetite or silica sand as the dense medium, batch and continuous separations of coal were conducted. Reductions in ash content from 24% to 12% for batch and 9% for continuous separations were observed. It was necessary to have very short residence times to minimise mixing. This is an example of existing technology being adapted to a smaller size range. It will be interesting to observe whether these promising results can be replicated on a larger scale.

A clear separation of silica stone and prophyllite, which have only a 250 kg/m³ density difference, was obtained by Oshitani et al. (2003) in the size range -50 +10 mm in an air dense-medium fluidised bed. The fluidised bed medium consisted of glass beads and stainless steel shot. The minimum fluidisation velocity of the two components was chosen to be roughly the same to minimise segregation of the medium. The density of the medium was adjusted by varying the volume fractions of the two components and the fluidisation gas velocity with great success and minimal segregation of the medium. It was found that the velocity of the fluidisation affects the separation time and quality. At low fluidisation velocities the particles took considerable time to sink, and at high velocities there was sufficient momentum in the gas stream to prevent the complete sinking of the dense particles.

2.3.9 Vibrated Air Dense-Medium Fluidised Bed

Vibrating a dense-medium fluidised bed enables smaller particles to be fluidised to form the medium by overcoming cohesive forces (Luo et al., 2000; Xu & Zhu, 2006). Vibration also shears the bubbles of excess fluidisation gas (Wang et al., 1997; Jin et al.,

2005) as they form at the distributor (Luo et al., 2008), resulting in a more stable dense-medium. The height of a vibrated fluidised bed should be small to minimise the coalescence of bubbles further from the distributor. This topic is covered in detail in Chapter 3.

The separation of coal particles in a vibrated dense-medium fluidised bed was investigated by Luo et al. (2008) who achieved an Ep of 0.07 on a -6.0 +0.5 mm feed in a batch test. It was unclear whether this value is based on the entire feed or on only the coal obtained from the very top and very bottom strata of the fluidised bed at the end of the experiment.

A novel vibrated fluidised bed, called the AKAFLOW, is described by Weitkaemper et al. (2010) for the separation of coal particles smaller than 3 mm. The process combines fluidisation and vibration to form a system similar to an air jig. The material is passed along a screen that is eccentrically vibrated and fluidised from below. As it passes along the screen the heavy material is progressively removed from the below. This process has been successful in reducing the ash content by one quarter although the recovery is less than optimal. The unit is capable of processing up to 6 t/h. This technology is significantly less energy intensive than electrostatic separations and with improvement could form a standard part of a dry coal beneficiation circuit.

2.3.10 Magnetically Stabilised Fluidised Bed

When using a magnetic medium such as magnetite, a fluidised bed can be stabilised by a magnetic field, rather than vibration. The magnetically stabilised fluidised bed has much smaller bubbles than an air dense-medium fluidised bed alone and has been the subject of many investigations. Luo et al. (2002a) observed that increasing the intensity of the magnetic field did not affect the minimum fluidisation velocity but increased the gas velocity at which unstable bubbling occurred, thus ultimately increasing the range of stability of the bed. Using a stable fluidised bed (that is, before unstable bubbling occurs), Luo et al. (2002b) achieved a reasonable separation of coal from mineral matter, although the yield was poor.

Fan et al. (2001; 2002) created a magnetically stabilised fluidised bed of the required density and then poured the coal (-6 +1 mm) into the top of the bed with the dense coal sinking to the bottom and the remainder floating. This produced a separation with an Ep of 0.066 (Fan et al., 2001; 2002). According to Fan et al. (2001) the bed density can be adjusted to between 1300 and 2200 kg/m³ although it is not explained how this occurs.

2.4 Summary

As-mined coal is beneficiated before selling to the consumer to remove the non-combustible components and thus increase the calorific value of the final product. In conventional coal processing this beneficiation occurs in a variety of water-based processes including dense-medium cyclones, spirals and floatation cells.

Dry beneficiation presents a unique opportunity to separate coal from mineral matter resulting in a dry coal product that has a higher calorific value than a water processed coal having the same mineral matter content. Dry beneficiation research has been largely overlooked in the past as most processes were much less efficient than the water-based alternatives. However recent results, particularly in dense-medium fluidised beds have provided encouragement that dry beneficiation can become a viable alternative.

Chapter 3

Gas Fluidisation, Particle Technology and The Reflux Classifier

3.1 Introduction

This chapter provides the theoretical framework needed to support the work contained in this thesis. This chapter begins with a description of the forces acting on a single particle in a fluid, followed by an explanation of fluidisation. Gas fluidisation is then discussed with a particular focus on the Geldart classification scheme (Geldart, 1973). The terms elutriation and entrainment are defined. The use of a dense-medium in a gas fluidised bed to promote separations on the basis of particle density, and the benefit of vibrated fluidised beds are discussed. These topics are of particular relevance to this study. Finally the transport of particles in inclined fluidised beds and pipes, especially dense phase pneumatic conveying, are explored.

The focus then shifts to a description of particle transport in a Reflux Classifier. The discussion begins with hindered settling in vertical and inclined sedimentation vessels, followed by a brief history of the Reflux Classifier incorporating both water and gas fluidised systems.

3.2 Forces on a Single Particle

A spherical particle falling through a static fluid exhibits a weight force due to gravity, F_G , and experiences a buoyancy force due to the support of the fluid against gravity, F_B , and a drag force due to the friction of the fluid flowing past the particle surface, F_D as illustrated in Figure 3-1.

The weight force is given by the product of the particle mass and the acceleration due to gravity, g (9.81 m/s^2),

$$F_G = \frac{\pi \rho_p d_p^3 g}{6}, \quad (3-1)$$

where ρ_p is the particle density (kg/m^3) and d_p the particle diameter (m).

Similarly, the buoyancy force is the mass of fluid displaced by the particle multiplied by the gravitational acceleration,

$$F_B = \frac{\pi\rho_f d_p^3 g}{6}, \quad (3-2)$$

where ρ_f is the fluid density.

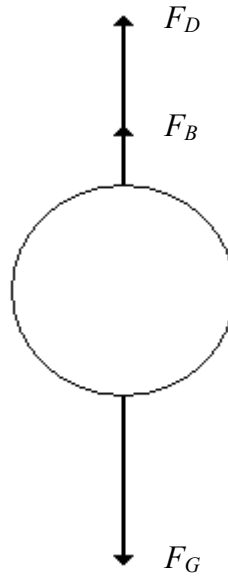


Figure 3-1: The forces acting on a particle in a fluid.

The drag force on the particle, arising from the relative motion between the particle and the fluid, is (Rhodes, 2002):

$$F_D = \frac{C_D \pi \rho_f U_{slip}^2 d_p^2}{8}, \quad (3-3)$$

where U_{slip} is the particle velocity (m/s) through the fluid and C_D a drag coefficient dependant on the particle Reynolds number. The particle Reynolds number is given by:

$$Re_p = \frac{U d_p \rho_f}{\mu_f}, \quad (3-4)$$

where μ_f is the viscosity of the fluid.

When a particle reaches its terminal velocity, U_{TFS} , the acceleration of the particle is zero. Thus, from Newton's Second Law, the sum of the three forces F_G , F_B and F_D is zero. That is:

$$\frac{\pi\rho_p d_p^3 g}{6} - \frac{\pi\rho_f d_p^3 g}{6} - \frac{C_D \pi\rho_f U_{TFS}^2 d_p^2}{8} = 0. \quad (3-5)$$

There are three settling regimes typically encountered in minerals processing; the Stokes' regime, characterised by low particle Reynolds number and laminar flow, Newton's regime, characterised by high particle Reynolds number and turbulent flow, and an Intermediate regime in between. The drag coefficients, C_D , for the three regimes and their range as defined by Rhodes (2002) are given in Table 3-1 with the corresponding terminal velocities calculated by solving Equation (3-5). The precise definitions of the regimes vary, with different texts stating different boundaries, although the same overall description is presented. There are also numerous correlations for the drag coefficient in the Intermediate regime that can be found in various texts on fluidisation.

Table 3-1: The drag coefficient and terminal velocity of spherical particles for the Stokes', Intermediate and Newton's regimes.

Regime	Reynolds Number	Drag Coefficient, C_D	Terminal velocity
Stokes'	$Re_p < 2$	$C_D = \frac{24}{Re_p} = \frac{24\mu_f}{\rho_f d_p U_{slip}}$ (Rhodes, 2002)	$U_{TFS} = \frac{d_p^2 (\rho_p - \rho_f) g}{18\mu_f}$ (3-6)
Intermediate	$2 < Re_p < 500$	$C_D = \frac{18.5}{Re_p^{0.6}}$ (Vance & Moulton, 1965)	$U_{TFS} = 0.153 \frac{d_p^{8/7} (\rho_p - \rho_f)^{5/7} g^{5/7}}{\mu_f^{3/7} \rho_f^{2/7}}$ (3-7)
Newton's	$500 < Re_p < 10^5$	$C_D = 0.44$ (Rhodes, 2002)	$U_{TFS} = \sqrt{\frac{3(\rho_p - \rho_f) g d_p}{\rho_f}}$ (3-8)

The above expressions for the terminal velocity of a particle refer to what can be termed the free settling terminal velocity or U_{TFS} . Hindered settling is the reduction of the

particle velocity due to the presence of other particles in the fluid and is discussed in Section 3.10 below.

A non-spherical particle can be modelled in the same manner as a spherical particle by taking into account its sphericity. The sphericity, ϕ , of a particle is the surface area of the particle divided by the surface area of a sphere of the same volume (Rhodes, 2002). Similarly, the diameter of the particle can be approximated by the diameter of an equivalent volume sphere (Rhodes, 2002).

3.3 Fluidisation

Consider a packed bed of particles with a fluid percolating upwards through the base of the bed. As the fluid velocity increases the bed will expand. The bed is said to be fluidised when the weight of each particle is supported by the drag of the fluid. The superficial velocity at which fluidisation first occurs is called the minimum fluidisation velocity.

The expansion in the bed is characterised by an increase in the pressure drop across the bed due to greater frictional resistance with rising fluid velocity. At minimum fluidisation the pressure drop across the bed is equal to the weight force of the particles minus the buoyancy force of the particles per unit area. Thus the pressure drop, ΔP , across a fluidised bed of particles is given by:

$$\Delta P = \frac{F_D}{A} = \frac{F_G - F_B}{A} = \frac{V_B(1 - \varepsilon)(\rho_p - \rho_f)g}{A} = \frac{M_B}{\rho_p} \frac{(\rho_p - \rho_f)g}{A}, \quad (3-9)$$

where V_B is the volume of the bed, ε the void fraction of the bed, A the cross-sectional area of the bed and M_B the mass of particles in the bed.

The minimum fluidisation velocity can be calculated by equating the pressure drop across a fluidised bed (Equation (3-9)) with the pressure drop across a packed bed, given by the Ergun (1952) equation:

$$\frac{-\Delta P}{H} = 150 \frac{(1-\varepsilon)^2 \mu_f U_f}{\varepsilon^3 d_{SV}^2} + 1.75 \frac{(1-\varepsilon) \rho_f U_f^2}{\varepsilon^3 d_{SV}} \quad (3-10)$$

where H is the height of the bed, U_f the superficial fluid velocity and d_{SV} refers to the diameter of a sphere having the same surface area to volume ratio as the particles in the bed. Thus after rearranging the following is derived:

$$Ar = 150 \frac{(1-\varepsilon_{mf})}{\varepsilon_{mf}^3} Re_{mf} + 1.75 \frac{1}{\varepsilon_{mf}^3} Re_{mf}^2, \quad (3-11)$$

where ε_{mf} is the voidage at minimum fluidisation, Re_{mf} the particle Reynolds number (Equation (3-4)) at $U = U_{mf}$, and Ar the Archimedes number (also called the Galileo number in some texts) defined by:

$$Ar = \frac{\rho_f (\rho_p - \rho_f) g d_{SV}^3}{\mu_f^2}. \quad (3-12)$$

In order to solve Equation (3-11), it is necessary to know ε_{mf} . The bed voidage at minimum fluidisation may be approximated by the packed bed voidage. Alternatively, the empirical correlation of Wen and Yu (1966) can be used to calculate Ar for spheres with $0.01 < Re_{mf} < 1000$:

$$Ar = 1060 Re_{mf} + 159 Re_{mf}^{1.687}. \quad (3-13)$$

Equation (3-13) can be solved iteratively by guessing a value of U_{mf} , or using the approximation:

$$Re_{mf} = 33.7 \left((1 + 3.59 \times 10^{-5} Ar)^{0.5} - 1 \right). \quad (3-14)$$

which assumes that the exponent of Re_{mf} in Equation (3-13) is 2, not 1.687.

In a gas fluidised system, there are six fluidisation regimes that are typically exhibited (Arnaldos & Casal, 1996) depending on the superficial gas velocity and the type of particles being fluidised (see Section 3.4 for more on particle classification). These six regimes are illustrated in Figure 3-2 and their properties outlined in Table 3-2. According to Arnaldos and Casal (1996), the transitions between the fluidisation regimes are delineated by three transition velocities U_c , U_k and U_{tr} . The fixed bed is descriptive of the bed prior to the onset of fluidisation. A bubbling or slugging bed (depending on particle properties) is apparent from minimum fluidisation for Geldart group B and D particles (see Section 3.4) until the first transition velocity U_c , the onset of the transition regime. Turbulent fluidisation occurs from U_k until U_{tr} , which marks the start of fast fluidisation.

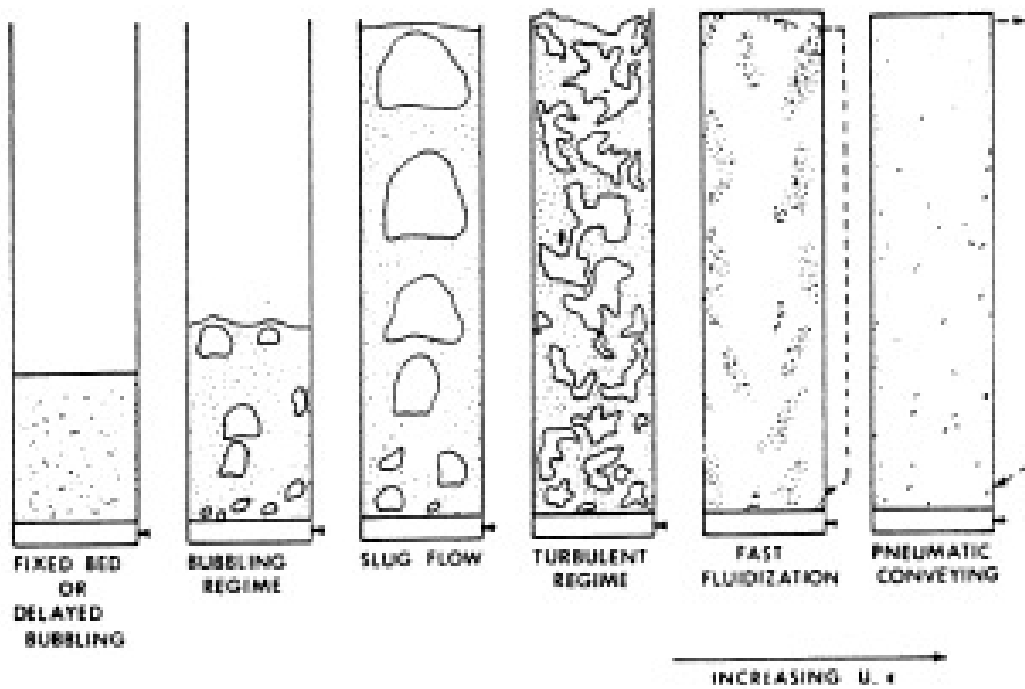
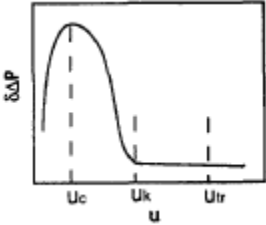


Figure 3-2: Different fluidisation regimes that occur as the gas velocity increases moving from left to right (Grace, 1986).

Figure 3-2 illustrates that there are two phases in a gas fluidised bed of particles; the emulsion phase, which consists of the particles and the fluidisation gas, and the gas phase, which contains the gas in excess of that required for fluidisation. In bubbling/slugging fluidisation the emulsion forms the continuous phase, but in fast fluidisation the gas becomes the continuous phase.

Table 3-2: Hydrodynamic features of different regimes of fluidisation which can exist between the onset of fluidisation and pneumatic transport for Geldart Group B systems (Arnaldos & Casal, 1996).

Range of velocities	Bubbling Fluidisation $U_{mf} \leq U \leq U_c$	Transition to turbulence $U_c < U \leq U_k$	Turbulent fluidisation $U_k < U < U_{tr}$	Fast Fluidisation $U \geq U_{tr}$
	<p>Two phases: emulsion and bubbles</p> <p>Bed surface relatively well defined</p> <p>Solids concentration constant with height</p>	<p>Bubbles break down</p> <p>Solid particles strongly agitated</p> <p>Bed surface poorly defined</p> <p>Solids entrainment increases with velocity</p>	<p>No bubbles</p> <p>Bed surface does not exist or is difficult to see</p> <p>Continuous decrease of solids concentration with height</p> <p>A significant solids recirculation is required to maintain solids inventory</p> <p>Bed density does not depend on solids recirculation rate</p>	<p>Clusters of solids play an important role</p> <p>Solids concentration is practically constant over most of bed height; a denser bed in the lowest zone</p> <p>A very good solids recirculation is required to maintain solids inventory</p> <p>Bed density depends on solids recirculation rate</p>
	<p>The bed can be maintained without solids recirculation</p>			

As seen in column 1 of Table 3-2, U_c is defined as the fluid velocity where the fluctuations in the pressure drop due to turbulence are at a maximum. U_k is the point where there are no further changes in the pressure drop fluctuations despite increasing fluid velocity and U_{tr} occurs when it is possible for particles to be transported out of the system. Correlations for the three transition velocities by different authors under different operating conditions are summarised in the paper of Arnaldos and Casal (1996).

Rhodes (1996) suggests that turbulent fluidisation occurs from U_c to U_k and dilute transport occurs between U_k and U_{tr} . These new definitions are contrary to the definitions previously proposed and accepted in the literature by others (Avidan & Yerushalmi, 1982; Yerushalmi et al., 1978; Yerushalmi & Cankurt, 1979; Arnaldos & Casal, 1996). However they are in agreement with the experimental observations of the many workers in the field. Rhodes (1996) adds that although these new definitions are supported by experiment, there does not exist a clear description of turbulent fluidisation. The definitions of Rhodes (1996) are supported by Smoulders and Baeyens

(2001) and have become generally accepted in the literature. This demonstrates that in the field of gas fluidisation there is still a great deal of evolution in the understanding of fluidisation. Although researchers do not always agree on definitions it is clear that ultimately the results are consistent. For the purposes of this work, and to avoid any confusion, the definitions of Arnaldos and Casal (1996) will be used throughout.

The fluidisation behaviour of a bubbling fluidised bed of sand particles, similar to that used in this thesis, was studied by Mostoufi and Chaouki (2004). The bed circulated with particles ascending in clusters through the centre of the bed and descending in larger aggregates down the annular region adjacent to the walls. It was also observed that as the superficial gas velocity increased, the volume of bubbles increased, while the concentration of the particles in the emulsion phase remained fixed.

The work described in this thesis was conducted in the bubbling or slugging regime of Group B particles, and so the vast body of literature covering the transition, turbulent and fast fluidisation regimes was considered outside the scope of this work.

3.4 Classes of Solid Particles

According to Geldart (1973), solids can be divided into four groups based on their fluidisation behaviour. The distinctions between the four groups, A, B, C, and D are illustrated in Figure 3-3.

Geldart Group C particles are very fine, generally of low density, and very difficult to fluidise. These particles primarily exhibit channelling behaviour, or the particles rise as clumps due to the dominance of cohesive forces over all other forces (Geldart, 1973).

Geldart Group A particles are typically fine or have a low particle density. At minimum fluidisation the bed expands, and gradually exhibits bubbling as the superficial gas velocity increases. The bubbles tend to rise faster than the superficial gas velocity. These beds exhibit a high degree of particle circulation and expand and contract with increasing and decreasing gas velocity respectively (Geldart, 1973).

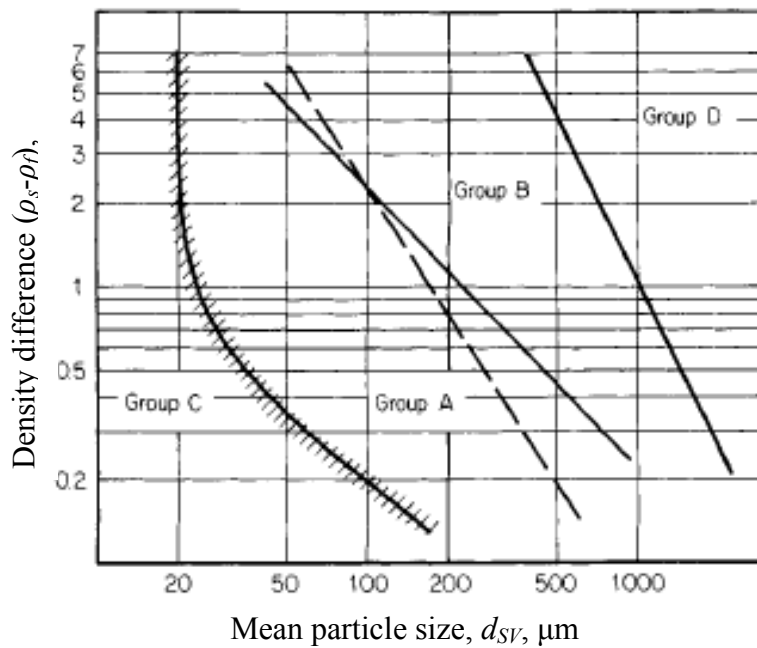


Figure 3-3: The relationship between particle classification and diameter and density (Geldart, 1973).

Group B particles are larger and denser than Group A and exhibit bubbling at minimum fluidisation conditions. A fluidised bed of Group B particles has poor circulation (Geldart, 1973).

Group D particles are very large and dense and the bubbles rise much more slowly than the superficial gas velocity, unlike Group A and B particles (Geldart, 1973).

The distinctions between the first three groups are due to inter-particle forces (Molerus, 1982). For type C particles, the cohesive forces dominate over all other forces acting on the particles. Cohesive forces are significant, though not dominant, for Group A particles, but play no role in the fluidisation behaviour of Group B particles. Molerus (1982) suggests that the distinction between groups B and D is due to the way in which the bed becomes fluidised. Group D particles tend to fluidise with a spouting bed which is characterised by a larger pressure drop across the bed at minimum fluidisation than that defined by Equation (3-9) due to the larger inertial forces involved.

3.5 Elutriation

Entrainment and elutriation are phenomena that occur in a fluidised bed. Entrainment occurs when the particles are supported and carried by the fluid upwards in the bed (Geldart, 1986). In general this occurs when the fluid velocity is greater than the terminal velocity of the particle. Entrainment can also occur for particles that settle faster than the gas velocity due to the particles being flung from the surface during bubble rupture, and via momentum transfer due to collisions with other particles. Elutriation is the process by which a particle exits a fluidised bed. As with entrainment, some particles with terminal velocity greater than the gas velocity are elutriated although in general it is particles with $U_{TFS} < U_f$ that are elutriated. Entrainment and elutriation could be confused for the same phenomenon however they are distinct. A particle may become entrained in the gas low in the bed, but as the particle rises above the bed surface the actual gas velocity decreases (with decreasing solids concentration) and the particle may be released from the gas. Elutriation requires the particle to exit the bed, and the term is often used to refer to the separation of particles on the basis of size (Geldart, 1986).

There are no theoretical models of entrainment due to the complexity of the system, resulting in a reliance on empirical correlations (Geldart, 1986). Empirical correlations are very dependant on the geometry of the system and the properties of the particles used.

There are many zones of a fluidised bed as illustrated in Figure 3-4. The splash zone is the region where particles with terminal velocity greater than the gas velocity are found in the freeboard because they have been propelled into this zone by bursting bubbles. In theory, only the particles with terminal velocity lower than the gas velocity of the remaining stream (so in effect, the superficial gas velocity) will continue into the transport disengagement zone. However, if there is sufficient concentration of fines then momentum transfer can occur between the fine particles and the coarse particles allowing the high terminal velocity particles to continue to rise and ultimately to be elutriated (Geldart et al., 1979).

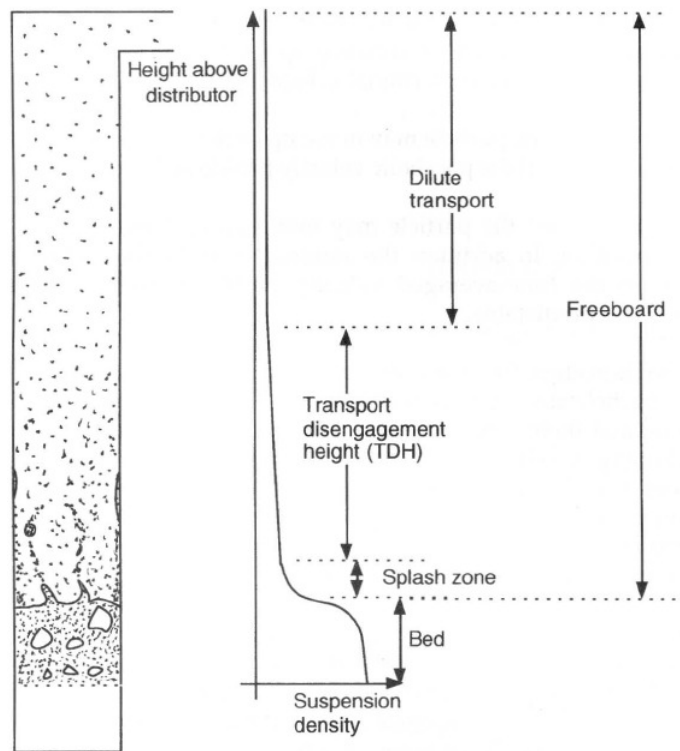


Figure 3-4: The zones in the gas fluidised bed freeboard (Rhodes, 2002).

The mechanism of how particles enter the freeboard zone was argued for some time in the literature. It was known that when bubbles burst at the surface particles were ejected into the freeboard but there was much disagreement in the literature as to whether the particles came from the surface or the wake of the bubbles. This was thoroughly examined by Pemberton and Davidson (1986a) who concluded that particles were ejected from both the surface and the wake. Pemberton and Davidson (1986b) also concluded that the disengagement of particles from the freeboard zone occurs at the walls of the vessel.

Several authors, including Leva (1951) and Tasirin and Geldart (1998), have established that the rate of elutriation, R_i , of particles from the freeboard zone of a fluidised bed is directly proportional to the concentration of particles within the bed. That is:

$$R_i = \frac{d(X_i M_B)}{dt} = K_i A X_i, \quad (3-15)$$

where X_i is the concentration of particles of size d_{pi} in the bed and K_i the first order elutriation rate constant for the size fraction d_{pi} .

There is no accepted correlation for the elutriation rate constant K_i encompassing all conditions. Many empirical correlations have been proposed over the years (Yagi & Aochi, 1955; Zenz & Weil, 1958; Wen & Hashinger, 1960; Tanaka et al., 1972; Merrick & Highley, 1974; Geldart et al., 1979; Colakyan et al., 1979; Lin et al., 1980; Colakyan et al., 1981; Kato et al., 1985; Subbarao, 1986; Sciazko et al., 1991; Baeyens et al., 1992; Nakagawa et al., 1994) but all were found to be highly dependant on the bed geometry and the particles used (Tasirin & Geldart, 1998). It is observed that K_i is less dependent on the gas velocity as the particle diameter decreases or as the gas velocity increases (Tasirin & Geldart, 1998). In the context of this work it can be concluded that K_i would best be calculated from experiment although using a correlation from a bed with similar geometry may be sufficient.

3.6 Dense-Medium

The elutriation of coarse particles from a fluidised bed is less when the bed contains only coarse particles compared to when the bed includes fine as well as coarse particles (Geldart et al., 1979; Choi et al., 2001). The complete mechanism is not understood but Geldart et al. (1979) suggest that the fines in the gas stream increase the apparent density of the fluid resulting in a reduced terminal velocity for the coarse particles and so allow their elutriation. In addition, it is believed that there is some momentum transfer between the fine particles and the coarse particles (Geldart et al., 1979; Choi et al., 2001). That is, the fine particles impart their excess momentum to coarse particles via collisions. Geldart et al. (1979) observed that this was more likely to occur in particles with a larger surface area for contact. This phenomenon is known as the dense-medium effect.

The effect of increasing the suspension density is to decrease the particle terminal velocity as given in Table 3-1. This has the double advantage of automatically forcing particles with density lower than the suspension density to the top of the bed and of allowing lower fluidisation rates. However the increase in the viscosity of the

suspension somewhat negates these advantages by lowering the rate of separation and thus a balance needs to be maintained.

The addition of fine, dense solids to a fluidised bed changes the suspension density which can result in different separation properties for the larger particles. The effect of a dense-medium on the separation performance of a water fluidised teetered bed separator was studied by Galvin et al. (1999b), who considered several solids as media including the coal as an autogenous dense-medium. The dense-medium should ideally be formed using particles denser than the target particles.

Dense media have been extensively used in air fluidised beds to aid in coal separations. Magnetite has been the preferred medium of several workers (Fan et al., 2001; Fan et al., 2006; Luo et al., 2002b; Zhenfu & Qingru, 2001; Luo et al., 2008) who exploited its ferromagnetism to stabilise the fluidised bed through use of a magnetic field. The combination of the fluidisation gas and magnetic field provided further control over the density of the medium, with the intensity of the magnetic field and the gas velocity both contributing to the final density of the bed.

A stable air dense-medium fluidised bed behaves as a dense liquid or pseudo-fluid (Choung et al., 2006), with particles denser than the bulk density of the bed sinking and lower density particles rising (Dwari & Rao, 2007). That is, the gas stream with entrained media behaves as a fluid in its own right, with a density dependent on the concentration of particles in the gas stream. The density, ρ_m , of the fluidised bed is given by Luo & Chen (2001):

$$\rho_m = (1 - \varepsilon)\rho_p + \varepsilon\rho_g \quad (3-16)$$

where ρ_p is the density of the particles, ρ_g the density of the gas and ε the voidage, or volume fraction of the bed occupied by the gas. The effective density of the medium depends on the size of the particles to be separated; the largest particles experience the densest pseudo-fluid (Choung et al., 2006). When particles are close in size to the media particles they behave as a particle in a gas stream surrounded by many other similar particles, while larger particles behave as they would in a dense liquid. Thus is it

important for the media particles to be significantly smaller than the particles to be separated (Jin et al., 2005; Choung et al., 2006).

The presence of air bubbles in the air dense-medium fluidised bed causes instability and an inconsistent medium density. The best density based separation results occur when the bed is fluidised with micro bubbles (stable bed density) and when the bed has a low viscosity and high fluidity (Dwari & Rao, 2007).

Smaller particles are more likely to be affected by the mixing of the media in the bed and the bed viscosity (Luo et al., 2008). The viscosity of a dense-medium fluidised bed can range between 0.1 Pa s and 2.5 Pa s (Rees et al., 2007) depending on the size and density of the medium particles. In addition, as the size of particles to be separated decreases the size of the media must likewise decrease. However it is more difficult to fluidise small particles with Geldart type C (Geldart, 1973) cohesive behaviour. Thus, there are some inherent difficulties when attempting to separate fine coal in a dense-medium fluidised bed.

The drag force on a particle in an air dense-medium fluidised bed was calculated by Wei and Chen (2001) (in Dwari and Rao (2007)) who measured the terminal velocity of spheres falling through a fluidised bed. It was assumed that the fluidised bed behaved as a Newtonian fluid, but the results indicated it was in fact a Bingham fluid. The drag coefficient, C_D , was empirically determined to be (Dwari & Rao, 2007):

$$C_D = \frac{24}{Re_m} (1 + 0.15 Re_m^{0.687}), \quad (3-17)$$

where Re_m is the Reynolds number of the medium given by:

$$Re_m = \frac{d_o U_r \rho_m}{\mu_e}, \quad (3-18)$$

where d_o is the diameter of the falling object, U_r the relative velocity between the falling sphere and the fluidised particles and μ_e the effective viscosity given by:

$$\mu_e = \frac{\mu + \tau_o d_o}{3U_r} \quad (3-19)$$

where τ_o is the yield stress of the Bingham fluid.

3.7 Vibration and the Vibrated Fluidised Bed

Vibration can be simply defined as the oscillation of a system about a point. The frequency of vibration, f , is the number of oscillations per unit time, while the period, τ , is the time taken for one complete oscillation (Church, 1967). The amplitude of vibration, a , is the linear distance between the centre reference point and the maximum extension of vibration (Church, 1967), hence the total oscillation distance is twice the amplitude.

If an undamped system is disturbed it will vibrate at its natural frequency, ω_n . Exciting a system at its natural frequency will result in the amplitude of vibration continuing to increase until the system fails. A system will have several natural frequencies depending on the number of coordinates required to define its position at any time (Church, 1967). A rigid bar has six natural frequencies since it requires a pair of coordinates, $[(x_1, y_1, z_1), (x_2, y_2, z_2)]$ to define its position in space.

Simple Harmonic Motion (SHM) is the most commonly occurring vibration and is governed by the equation (Church, 1967):

$$\ddot{x} = \frac{d^2 x}{dt^2} = -\omega^2 x \quad (3-20)$$

where x is the linear displacement from equilibrium, t time and ω the vibration frequency of the system. That is, the acceleration of the system is proportional to its distance from the equilibrium position. SHM is typically described by the oscillation of a mass on a spring as illustrated in Figure 3-5. When a spring is displaced, a restoring force of magnitude k (N/m) acts in the direction opposite to the original displacement. This k is known as the spring constant.

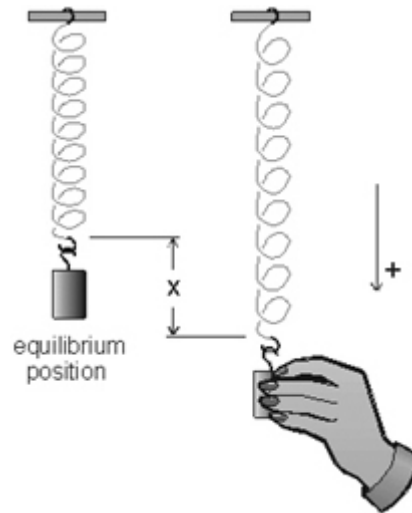


Figure 3-5: Mass on spring (Hoult, 2007).

If the mass on the end of the spring is m then the equation governing the motion of the spring is:

$$-kx = m\ddot{x} \Rightarrow \ddot{x} = -\frac{k}{m}x, \quad (3-21)$$

which has the general solution:

$$x = A \cos\left(\sqrt{\frac{k}{m}}t\right) + B \sin\left(\sqrt{\frac{k}{m}}t\right) \quad (3-22)$$

where A and B are constants.

Springs are an excellent form of passive (no external input) vibration isolator. Vibration isolators prevent damage to equipment and bases due to vibration (Rao, 1995). In general the spring constant determines the natural frequency of the system. A low system natural frequency reduces the damage to the supporting structure (Rao, 1995).

Vibrating a fluidised bed has several effects on the general characteristics. In the first place, vibration tends to decrease the minimum fluidisation velocity (Erdesz & Mujumdar, 1986; Wang et al., 1997) by decreasing the bed voidage (Marring et al., 1994) and by providing energy to the particles thus reducing the energy barrier to fluidisation. Secondly the bubbles in a vibrating fluidised bed do not coalesce as readily and are often sheared apart by the vibration (Wang et al., 1997; Jin et al., 2005) resulting in a more stable fluidised bed, particularly for Geldart group A and B particles which are more prone to bubbling behaviour. Vibration also acts to stabilise the

dispersion of particles, and in particular a dense-medium, throughout the bed (Jin et al., 2005). Thus, when attempting to separate particles in an air dense-medium fluidised bed, vibration is a useful tool in providing a more stable separation medium.

Vibration increases the region of stable fluidisation for group A particles (Marring et al., 1994) and the vibration intensity required for stable fluidisation decreases with increasing particle diameter due to the decrease in cohesive forces with increased diameter (Marring et al., 1994; Mawatari et al., 2002; 2005). Vibration greatly aids in fluidising a bed of group C powders and irregular particles as it helps overcome the interparticle forces (Xu & Zhu, 2006). According to Xu and Zhu (2006) the effect of vibration on a fluidised bed of fine particles depends on the direction of the vibration with horizontal vibration having a significantly larger effect than vertical vibration. It was further observed that increasing the vibration frequency decreased the minimum fluidisation velocity, but once a critical frequency was reached, no further reduction occurred.

Vibrated fluidised beds behave very differently to liquid fluidised beds (Fraas, 2005), exhibiting pure slug flow while liquid fluidised beds have a velocity profile (Fraas, 2005). Further, a vibrated gas fluidised bed is different from a gas fluidised bed with particle momentum and kinetic energy playing a more significant role in the vibrated case than the gas fluidised case which is dominated by hydrostatic and hydrodynamic forces (Fraas, 2005).

In researching the difference between a bed of particles fluidised by vibration or gas, Daleffe et al. (2007) found that in a vertically vibrated bed large particles tended to migrate to the top of the bed, due to the vibration forces dominating, while with gas fluidisation the small particles prevail at the top due to the dominance of particle drag forces. In a bed fluidised by both gas and vibration these forces can be balanced to provide a well mixed bed of particles and minimise segregation. This will be an advantage in designing a density separation process as it may be possible to reduce the effects of particle size on the separation in a vibrated fluidised bed.

When studying a vibrated fluidised bed of coarse particles (from 300 μm to 1.64 mm) Jin et al. (2007) made two key observations on the effects of vibration on a bed of

Geldart type B particles. Vibration tended to stabilise the bed voidage in the axial and radial directions as well as reducing the overall voidage. Vibration has a more significant impact on the voidage of a short bed than a tall bed and at lower fluidisation velocities.

When a large particle in a bed of smaller particles is vibrated vertically the large particle segregates to the top due to the “Brazil-nut” effect (Rosato et al., 1987), as also happens to a mixture of large and small particles. This phenomenon occurs regardless of the densities of the particles due to the migration of smaller particles below a larger one as it rises when shaken, making it impossible for the large particle to return to the bottom.

3.8 Inclined Fluidised Beds and Pipes

The flow behaviour of a gas fluidised bed with inclination angles of 30°, 45°, 60° and 75° to the horizontal was investigated by Chong et al. (1984). An angle of 30° exhibited channelling and poor solids movement and was not considered fluidised. Three fluidisation regimes were observed; the fixed bed, where the gas percolates through the interstices of the bed, the partially fluidised bed with bubbles of gas forming on the upper inclined plate creating a mobile upper section, leaving a fixed lower section of the bed, and the fully fluidised bed (Figure 3-6). The gas velocities distinguishing these two regimes are U_i , the initial fluidisation velocity, and U_{mf} , the minimum fluidisation velocity. The plot of U/U_{mf} vs $\Delta P/\Delta P_{mf}$ for the fixed bed regime is independent of the inclination angle. For an inclined bed, U_{mf} is much greater than for a vertical bed.

O’Dea et al. (1990), following on from Chong et al. (1984), also studied inclined fluidised beds with angles between 45° and 90° but did not observe full fluidisation. Instead the main bed was fluidised at U_{cb} and the excess fluidisation gas formed a channel at the upward incline as shown in Figure 3-6.

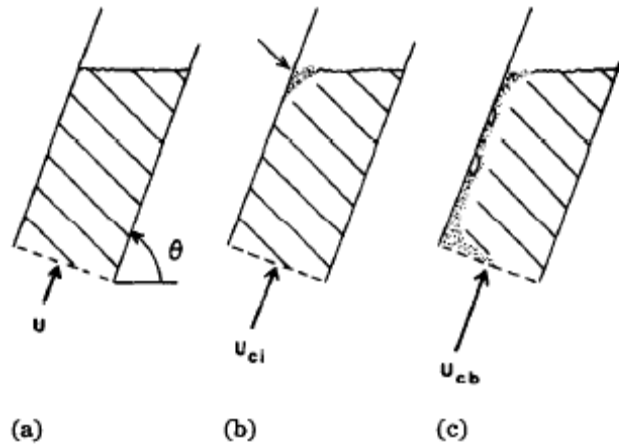


Figure 3-6: Flow regime transition in an inclined fluidised bed (a) packed bed; (b) channel initiation; (c) channelled bed. (O'Dea et al., 1990).

According to O'Dea et al. (1990), in a channelled bed the pressure drop is independent of the gas velocity, while in a fixed bed the pressure drop is proportional to the gas velocity. Hence, channelling could be considered the equivalent of minimum fluidisation for an inclined fluidised bed. This suggests that the observations of Chong et al. (1984) may not have been accurate, and that a channelled bed may have been mistaken for a fully fluidised bed. As there is no complete description of the Chong et al. (1984) apparatus it is difficult to determine how easily they could visually observe the fluidisation behaviour of the bed. Both the channelling pressure drop and gas velocity decrease as the angle of inclination decreases from 90° to 45°. O'Dea et al. (1990) found that the simplified Ergun equation is applicable to packed beds of any inclination:

$$\frac{\Delta p}{L} = 150\mu \frac{(1-\varepsilon)^2}{(\phi d_p)^2 \varepsilon^3} U \quad (3-23)$$

The transport of solids in inclined pipes has been studied by various authors. There is a critical inclination angle at which the pressure gradient in an inclined fluidised bed is at a maximum (Levy et al., 1997; Hong & Zhu, 1997, 2002). That is, as the inclination angle relative to the horizontal increases, the pressure gradient increases until the critical inclination angle and then decreases to a vertical bed. The critical angle is proportional to the ratio of superficial gas velocity to particle terminal velocity (Levy et

al., 1997). At low angles of inclination the frictional forces dominate the transport, but gravitational forces are more important in systems with a high angle of inclination (Hong & Zhu, 1997). At low gas rates and high inclination angles, coarse particles tend to settle and flow downwards (Hong & Zhu, 2002; Ginestet et al., 1993).

3.9 Dense Phase Pneumatic Conveying

Dense phase pneumatic conveying can be defined in a number of ways (Konrad, 1986) but a simple definition that covers a variety of particle properties is ‘the transport of solids where the pipe is full of solids at a cross-section’. This can also be called plug conveying, where (non-fluidised) plugs of solids are transported between air bubbles. Dense phase pneumatic conveying is characterised by low gas rates, resulting in less particle attrition than in a lean phase conveying system.

Plug conveying occurs in both horizontal and vertical pipes (Konrad, 1986) and by corollary would also occur in inclined pipes. The flow patterns are illustrated schematically in Figure 3-7 and Figure 3-8. The flow can be essentially described as a solid (non-fluidised) plug of particles that is forced through a pipe by air bubbles. The front of the plug of solids sweeps up the solids at the base of the bubble in front and deposits solids behind into the next bubble. There may be some particles suspended in the gas bubble. Vertical dense phase pneumatic conveying resembles a slugging fluidised bed (Konrad, 1986).

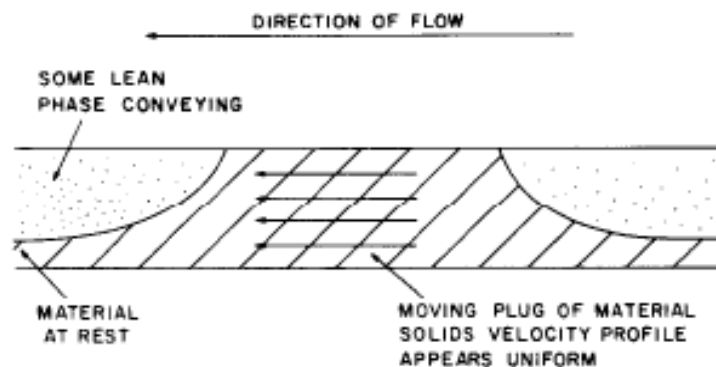


Figure 3-7: Schematic of horizontal plug conveying (Konrad, 1986).

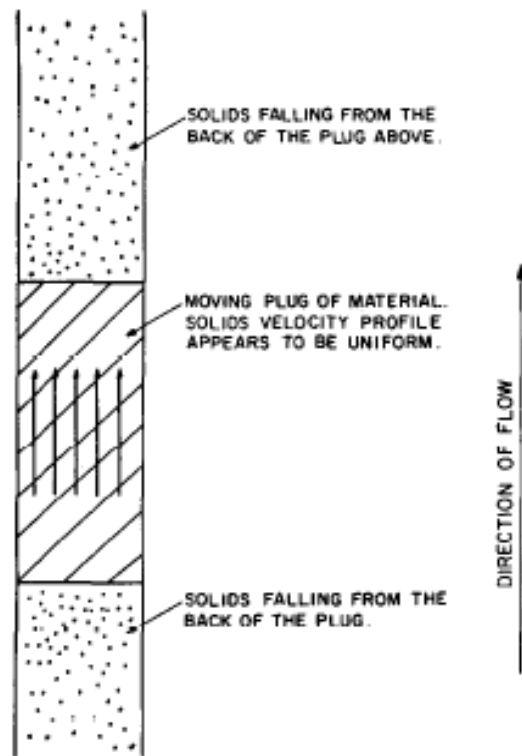


Figure 3-8: Schematic of vertical plug conveying (Konrad, 1986).

3.10 Hindered Settling

At very low solid concentrations and particle Reynolds numbers the settling velocity of a particle is given by the Stokes settling velocity, also known as the terminal free settling velocity, U_{TFS} . As a particle settles it displaces fluid causing a slight upwards fluid flow. At higher particle concentrations this flow increases, as does particle shear due to the reduced distance between individual particles. This has the effect of reducing the settling velocity, a phenomenon known as hindered settling.

Hindered settling effects in a mono-component (single size and density) system were experimentally investigated by Richardson and Zaki (1954) and their correlation is still in use today:

$$U_p = U_{TFS} f(\varepsilon) = U_{TFS} \varepsilon^n, \quad (3-24)$$

where U_p is the hindered settling velocity of the particle, ε the void fraction of the bed and n a constant dependant on the Reynolds number and the ratio of the particle size to

the vessel diameter. Richardson and Zaki (1954) provided several correlations for the coefficient, n , depending on the Reynolds number. One correlation used for determining the value of n independent of the Reynolds number is the Khan and Richardson (1989) equation:

$$\frac{4.8 - n}{n - 2.4} = 0.043 Ar^{0.57} \left[1 - 2.4 \left(\frac{d_p}{D_v} \right)^{0.27} \right], \quad (3-25)$$

where D_v is the diameter of the vessel.

Other correlations for the hindered settling function, $f(\epsilon)$, have been published in the literature but they tend to be specific to the experimental system and so in general it is best to compare the system being studied with the conditions of the published correlations and select the most appropriate (Davis & Acrivos, 1985).

3.11 Batch Vertical Sedimentation

If an initially well mixed suspension of particles ($\epsilon > 0.6$) in a vertical column is left to stand, the particles will eventually settle out into a sediment layer and clear fluid. The rate of settling is determined by the hindered settling velocity of the particles, given by Equation (3-24) above. The time for settling also depends on the area of sedimentation and the initial height and concentration of the suspension.

Figure 3-9 illustrates the zones that develop during the settling of a batch system containing three species with different U_{TFS} . The different rates of settling of the particles create three regions in the bed; the lowest region containing all three particle species in their original concentrations, region 2 devoid of the fastest settling species and region 3 containing only the slowest settling particles; the remaining particles having settled into slurry. This behaviour only occurs with solids volume fractions less than 0.4, above which the close packing results in bulk settling. This view can be extended to a polydisperse system. Although illustrated in a batch configuration, this principle equally applies in a continuous situation.

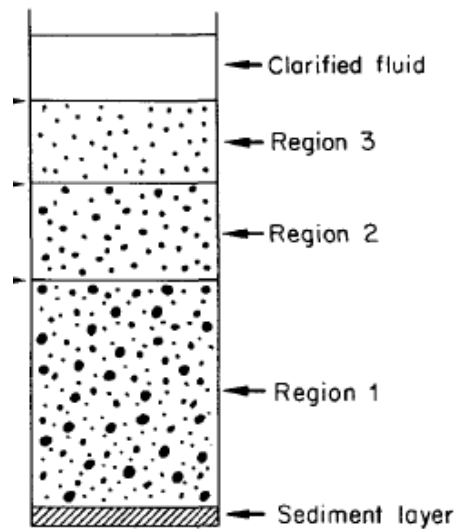


Figure 3-9: The regions that develop during the sedimentation of a mixture of three distinct species of particles. Region 1 contains all three species of particles, region 2 is devoid of the fastest-settling species and region 3 contains only the slowest-settling species (Davis & Acrivos, 1985).

The presence of more than one particle size and/or density in the system affects the hindered settling function, $f(\varepsilon)$. The voidage is calculated as the volume fraction of the fluid, rather than the volume of the bed not occupied by the species in question, since all particles will be settling and also affect the hindered settling function as particles, not fluid (di Felice, 1995). Thus,

$$\varepsilon = 1 - \sum \phi_i \tag{3-26}$$

where ϕ_i is the volume fraction of species i .

di Felice (1995) summarises the debate in the literature concerning whether the terminal free settling velocity, U_{TFS} , in Equation (3-24) should be calculated based on a modified fluid density and viscosity, taking into account the effect of the other particles suspended in the fluid. According to di Felice (1995), some consider that treating the suspension of fluid and particles as a pseudo-fluid gives a better representation of the forces acting on the system than simply ignoring the presence of the particles. In general, the density of the pseudo-fluid is the density of the suspension (di Felice,

1995). The pseudo-fluid theory is likely to be of greater effect in a system with a low fluid density and viscosity, such as gas, than for a water system.

A modified form of the Richardson-Zaki equation was proposed by Galvin et al. (1999a) for a water-based system with a dense-medium to take into account this effect of density. That is,

$$U_p = U_{TFS} \left(\frac{\rho_i - \rho_m}{\rho_i - \rho_f} \right)^{n-1}, \quad (3-27)$$

where ρ_i is the species density and ρ_m the density of the medium. Equation (3-27) shows that the advantages of a dense-medium (see Section 3.6), while beneficial to aiding a density separation are tempered by the hindered settling effect. Thus there is a limit to how high a concentration of dense-medium can be used in a gravity separation before hindered settling negates its inherent benefit.

3.12 Inclined Settlers

The main advantage of an inclined settler over a vertical settler is the significantly increased surface area for settling. This effect was first reported by Boycott (1920) who observed that blood corpuscles settled out faster in inclined test tubes than vertical ones. Much of the work on inclined settlers was completed by Robert Davis and co-workers in the 1980's and 1990's. They used a kinematic approach based on the work of Ponder (1925) and Nakamura and Kuroda (1937); the so called PNK theory. The initial theoretical framework was laid out for a polydisperse system with a finite number of fractions and then extended to a continuous dispersion (Davis et al., 1982).

Similar to a vertical system, a settler inclined from the vertical at angle θ exhibits segregation zones as illustrated for a continuous quaternary system in Figure 3-10 where species 1 has the highest terminal free settling velocity. This is very similar to Figure 3-9 although there is a larger sedimentation area due to the inclination angle. And, as in the vertical system, region 1 contains species 1, 2, 3 and 4 in their original

concentrations, except on the upward facing incline where the concentration is greater due to the settled sediment.

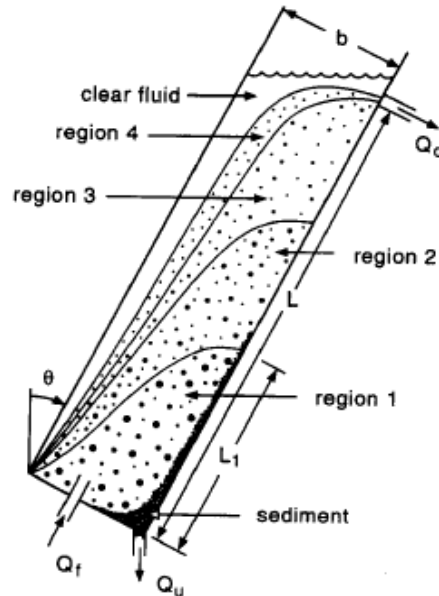


Figure 3-10: Schematic of a continuous inclined settler containing four particle species, with an overflow rate such that only the two slowest-settling species reach the overflow (Davis & Gecol, 1996).

Several works (Davis et al., 1989; Davis & Gecol, 1996; Zhang & Davis, 1990) discussed the use of an inclined settler to separate suspensions on the basis of size or density. From this work, mathematical models were developed using PNK theory and validated. Davis et al. (1989) noted that the best conditions for separation occurred with an angle of inclination to the vertical no more than 30° to prevent sediment build-up and that vibrating the settling plate also assisted in the sedimentation process.

The density separation of two species with the same terminal velocity but different density was achieved by Nelson et al. (1997) in an inclined settler. They discovered that the slurry formed an autogenous dense-medium that allowed for the density separation. They noted however that the system was very sensitive to the rate of solids in and out of the system. This suggests they were operating near the region where hindered settling negates the dense-medium effect.

The sedimentation of particles is also dependant on the particle shape with Romero et al. (1993) noting that particles of the same diameter but different shape had markedly different settling velocities due to their different settling orbits and rotations. The implication of this is that performing a size separation on a feed of particles of different shapes is not a trivial exercise.

3.13 Reflux Classifier

The Reflux Classifier consists of parallel inclined plates similar to a lamella settler above a fluidised bed (Galvin, 2004) as illustrated in Figure 3-11. The inclined plates allow for effective particle separation on the basis of size or density as noted in Section 3.12 for an inclined settler, but the multiple plates provide a greater area for segregation. With multiple channels it is important that each channel operates with a common superficial velocity, otherwise a varied separation could arise, resulting in a loss of separation efficiency. The fluidised bed below the lamella settler provides a consistent slurry feed into each of the channels (Nguyentranlam & Galvin, 2001). In the lamellae section, particles can segregate onto the inclined plates and return to the fluidised bed. This results in a refluxing or recycling of the particles in the system reducing the probability of misplaced particles.

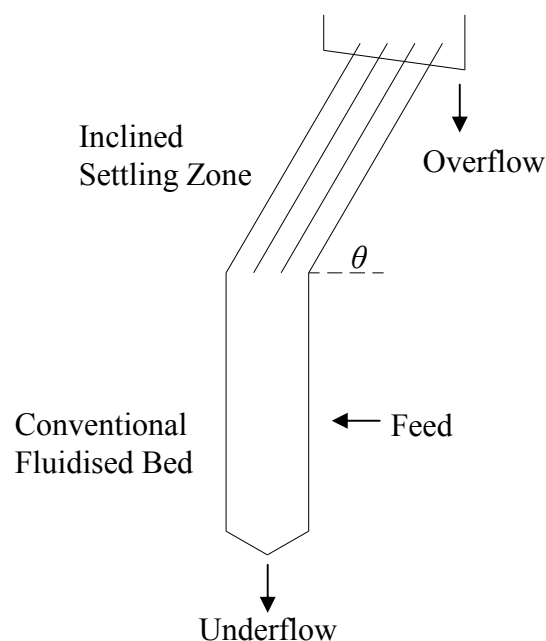


Figure 3-11: Schematic of the Reflux Classifier, shown here with three channels although any number is possible.

A major advantage of the Reflux Classifier over more conventional separation methods is that the Reflux Classifier is a high throughput system. That is, it has a higher processing capacity due to a larger effective settling area than a conventional vertical settler. The increased vessel area is determined geometrically to be (Laskovski et al., 2006):

$$F = 1 + \left(\frac{L}{z}\right) \cos \theta \sin \theta \quad (3-28)$$

where F is the theoretical throughput advantage (the area is F times larger than the cross-sectional area of the vertical section), L the length of the inclined channels, z the perpendicular gap and θ the angle of inclination with respect to the horizontal (see Figure 3-12).

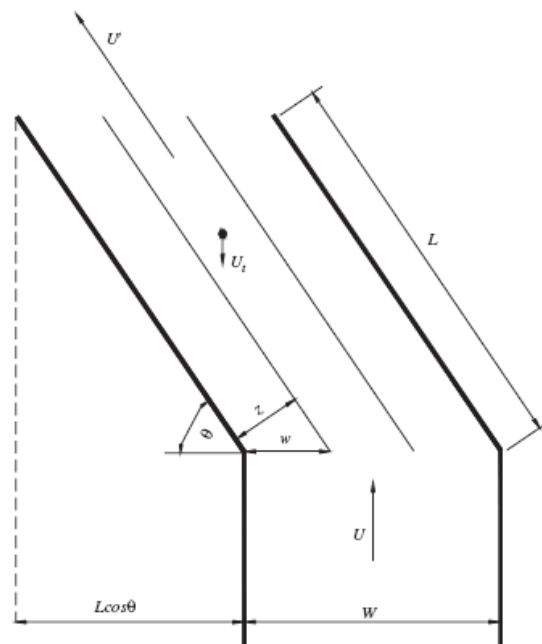


Figure 3-12: Two-dimensional schematic representation of the inclined channel section of the Reflux Classifier (Laskovski et al., 2006).

Equation (3-28) implies that the throughput advantage, F , could increase indefinitely by changing the aspect ratio, L/z . Indeed, the aspect ratio of the inclined settler has an effect on the performance of size separations in the Reflux Classifier, as observed by Zhou et al. (2006) in the size separation of mineral sands. For a fixed flow velocity,

increasing the aspect ratio by reducing z will initially reduce the separation size due to the increase in effective settling area. Further narrowing of the channels results in an increase in the separation size as particles are resuspended due to shear forces.

Laskovski et al. (2006) proved that the throughput advantage is limited by the segregation efficiency, η , as given by:

$$\eta = \frac{U/U_{TFS}}{F}. \quad (3-29)$$

The competing tendency for particles to segregate or convey is also determined from dimensional analysis by the segregation efficiency (Laskovski et al., 2006):

$$\eta = \frac{1}{1 + 0.133 \cos \theta Re_t^{1/3} (L/z)} \quad (3-30)$$

where Re_t is the particle Reynolds number at terminal velocity.

In density separations, the recycling action of the Reflux Classifier significantly reduces the effects of particle size on the separation. Additionally, in continuous operations, which have higher particle concentrations than batch operations, the dense phase forms an autogenous dense-medium, promoting the upward movement of the low density particles to the overflow.

When using very narrow channels with less than a 2 mm gap in the Reflux Classifier for density separations the effects of size on the separation can be very efficiently suppressed (Galvin, 2009). The reason for this is twofold. In the first place there are higher shear rates in the narrow channels which promote particle transport up the incline as demonstrated by Laskovski et al. (2006). In the second place, the flow in these channels is laminar, giving a parabolic flow profile, with the result that particles resting on the incline will experience different flow velocities depending on their diameter. In

this way the effect of the particle size on the terminal velocity of the particle is negated. As a result the separation takes place almost exclusively on the basis of density.

Callen et al. (2007a) conducted a gas-solid fluidisation study of the Reflux Classifier, examining the particle size classification achieved using different inclined channel lengths, L , and gaps, z . Remarkably, they reported a result very similar to that obtained by Laskovski et al. (2006), as defined by Equation (3-30). For the gas-solid system Callen et al. (2007) obtained:

$$\eta = \frac{1}{1 + 0.134 \cos \theta Re_t^{0.33} (L/z)}. \quad (3-31)$$

3.14 Summary

This chapter provided a historical and theoretical context for the work of this thesis by giving a summary of the research that forms the foundation on which this thesis is built.

The forces acting on a single particle in a fluid were used to derive equations for the terminal free settling velocity of the particle in the Stokes', Intermediate and Newton's regimes. Knowledge of these velocities is very useful when studying the behaviour of particles in a fluidised bed.

The effect that the size and density of a particle have on its fluidisation properties is determined by its Geldart (1973) classification as discussed above. In particular, there was a treatise about the best particles to be used for dense media based on their Geldart group. The theory of dense-medium fluidised beds, including a discussion of a dense-medium effect, was provided to complement the practical aspects of dense-medium operations given in Chapter 2. The gas fluidisation behaviour of these particles was compared and contrasted with the behaviour of particles in dense phase pneumatic conveying.

Simple harmonic motion and the effect of vibration on a gas fluidised bed were discussed as topics of particular interest to this thesis.

From a discussion of the theory of hindered settling and inclined lamella settlers, a fundamental understanding of the Reflux Classifier was developed. In addition, a brief discussion of the applications of the Reflux Classifier to density separations and as a pneumatic size separation device was included.

Chapter 4

Experimental Methods

4.1 Introduction

This chapter provides an outline of the design of the experimental apparatus and the experimental methods used in this thesis. Three apparatus were used; a batch Reflux Classifier, a continuous Reflux Classifier and a vertical fluidised bed.

4.2 Equipment

4.2.1 Reflux Classifier

Prior to the commencement of this work, separations of coal in a pneumatic Reflux Classifier, with and without a dense-medium, were performed at this University with satisfactory results (Walton et al., 2007). The apparatus used in those experiments had a 250 mm high vertical fluidised zone below a 2 m section inclined at 70° to the horizontal both having a 20 × 100 mm cross-section.

When designing the apparatus for the experiments in this study there were several factors in the geometry that had to be considered. These were the channel width and depth; the lengths of the vertical and inclined sections; the angle of inclination to the horizontal; the overflow arrangement; how gas entered the apparatus; and how feed entered the apparatus.

With the exception of the Reflux Classifier used by Callen et al. (2007a), all the laboratory scale apparatus used in the past, and in particular that used by Walton et al. (2007), had a channel width of 100 mm, and so this was continued in the present work. Channel depths of both 10 and 20 mm were considered by Walton et al. (2007) who concluded that the narrower channel produced better separations of -2 mm coal. To prevent blockages, the channel gap needed to be at least three times the diameter of the largest particle. In this work the plan was to separate coal up to 6 mm in size. With these considerations a channel depth of 20 mm was chosen. This dimension also allowed direct comparisons to be made with results from the work of Walton et al. (2007).

As noted in the Introduction, the Reflux Classifier usually contains multiple channels in the inclined section. For this work, however, a single inclined channel was used in order to simplify the system and subsequent analysis, and hence the depth of the inclined and vertical sections were both 20 mm.

Most of the previous work on the water-based Reflux Classifier was based on a vertical fluidised bed 1 m in length below the inclined channels. This zone was used to promote an autogenous dense-medium effect, in turn causing larger particles to segregate upwards and enter the inclined zone. The work by Callen et al. (2007a), involving a pneumatic Reflux Classifier, also used a 1 m vertical fluidised zone. Walton et al. (2007) used a 250 mm high vertical fluidised bed, with the vertical zone used to help feed the particles into the inclined section where classification occurred. In the present work, involving the separation of coal in a dense-medium, a 1 m fluidised zone was chosen to assist the action of the dense-medium, and to provide sufficient space for the feed to enter, with minimal short-circuiting. In the first instance a polycarbonate apparatus consisting of two 500 mm sections was used so that the effect of the length of the vertical section could be studied.

From the work by Laskovski et al. (2006) it was known that increasing the aspect ratio (see Section 3.13) of the inclined channels increased the degree of segregation, but with a diminishing benefit at extreme aspect ratios. An inclined channel 2 m in length, providing an aspect ratio of 2000 mm/20 mm or 100, was therefore used. The incline was originally designed in two 1 m long sections so that the effect of the length of the incline could be studied.

When choosing the angle to the horizontal of the inclined channel, past work was again considered. An angle of 70° had been established as the optimum angle for performance in the water-based system with an aspect ratio of 100 (Zhou et al., 2006). Callen et al. (2007) found that the behaviour of the pneumatic Reflux Classifier was very similar to that of the water-based system, particularly in the effect of aspect ratio. In the present work an angle of inclination of 70° to the horizontal was chosen.

The overflow design used in previous work (Walton et al., 2007) was based on an imitation of the launder overflow used for water-based systems. However the exit was too narrow and tended to block frequently. The overflow arrangement that was designed and used in this work is illustrated in Figure 4-1. The particles were able to exit the incline over the whole width of the channel, and through an inverted pyramid to a 25 mm hose that carried the particles and gas to the collection point of a cyclone. Further details of the final design, including photographs are included in Appendix K.

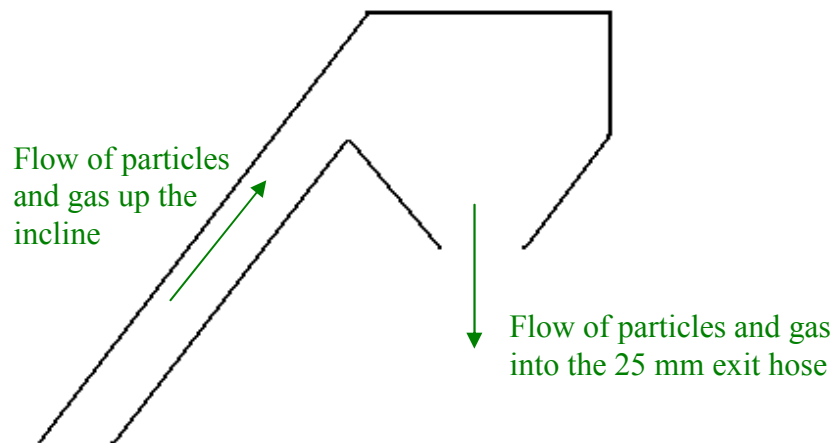


Figure 4-1: Schematic of the overflow arrangement showing the 20 mm wide channel opening into the overflow chamber before exiting through the 25 mm exit hole. See Appendix K for photos.

A range of construction materials were considered. Stainless steel was attractive because of its strength. The major disadvantage was that it was opaque, providing no capacity for visual observation of what was happening within the bed. Polycarbonate was also an attractive option, because it was transparent. Given the need to make observations of the particle transport and separation mechanism, a Polycarbonate system was constructed in the first instance, with the flanges made of polyvinyl chloride. The only metal components were the plenum chamber, distributor plate and the bolts holding the apparatus together.

4.2.2 Distributor Design

To fluidise the bed of particles, compressed air at high pressure needed to be passed through a distributor plate of small holes to ensure an even distribution of gas into the

bed. In the batch system the bed was fluidised through a distributor plate at the base of the vertical bed in the same way as the bed used by Walton et al. (2007). The gas entered the plenum chamber at the base and then passed through a distributor plate into the bed. The design of the distributor plate, 20×1 mm diameter holes in two straight lines, was maintained from the pre-existing apparatus of Walton et al. (2007).

In the continuous system the distributor design needed to be changed so that particles could be removed through the base of the bed. A new flanged channel section was constructed of stainless steel with the channel walls forming the distributor plate. The 20×1 mm diameter holes were drilled into the channel walls and surrounded by a plenum chamber. This gas feed system was bolted below the 1 m vertical bed and was found to provide the same bubbling pattern as the batch plenum chamber and distributor plate, while leaving a packed bed beneath the gas inlet holes as long as there was no path for the air to escape below. Photos of the continuous gas distributor are included in Appendix K.

4.2.3 External Support

Because the apparatus was to be vibrated it was important to separate it from its supporting structure. Springs were chosen as the cheapest and easiest passive isolator and because the behaviour of springs is easily modelled. Shock absorbers were also considered, but there was concern that because they contain a piston they might restrict the range of motion of the apparatus. By using springs the vibration could be isolated without restricting the movement of a vibrating apparatus. The springs were designed specifically for the task, taking into account the mass of the apparatus that they would be supporting and the natural frequency that would result from the spring constant. The full design of the springs is explained in the Appendix L.

The Reflux Classifier was constructed of Polycarbonate sheets that were glued together and so the channel needed to have a supporting frame that was also vibrated. The supporting frame needed to be strong but also lightweight to minimise the energy required for vibration. In addition, the frame needed to flex with the channel whilst not allowing it to bend to the point of breaking.

As noted above, the vibrating frame was mounted on four springs to isolate it from the supporting structure. Two horizontal bars were attached to a pair of springs and between these two bars were mounted both the vibration motors and the main Reflux Classifier apparatus. The supporting frames for the Reflux Classifier were constructed by welding sections of Novex Engineering N1000 (NovaStrut, 2010) into a vertical section and an inclined section at 70° to the horizontal; that is, in the same shape as the Reflux Classifier. This pair of identical inclined frames were bolted one each between the horizontal bars. This made it easy to bolt the Reflux Classifier onto the vibrating frame. In this way the Reflux Classifier was supported along its entire length whilst also being free to vibrate. This supporting frame was mounted on an existing metal structure in the laboratory. This structure supported the Reflux Classifier well above the floor, permitting movement in all directions. Photographs of this supporting frame are given in Appendix K.

The motors used to vibrate the apparatus employed an eccentric mass to produce the vibration. A pair of these motors were coupled to produce a linear vibration (Blekhman, 1988). It was noted in Section 3.7 that the system in question had six natural frequencies because it had six degrees of freedom. As the frequency of vibration increased, the direction in which the apparatus vibrated changed when passing through a multiple of the natural frequency. So, for example, if the motors were located one on top of the other, the initial vibration would be horizontal, given this direction would be perpendicular to the axis of the centres of the motors. Increasing the vibration frequency above the natural frequency would then result in the direction of vibration changing, possibly to vertical, or to some other mode of vibration.

During the commissioning of the Polycarbonate Reflux Classifier, the apparatus was tested for gas leaks and its ability to withstand the vibration. No problems were encountered with the apparatus until an experiment was performed with continuous coal and medium feed. The pressures of the gas, medium and coal in the apparatus combined with the forces of vibration caused the channel to crack, leak and become unusable. The failure was primarily caused by a build-up of coal particles close to the overflow. These particles formed a blockage that created significant back pressure resulting in the

cracking of the glued joints in the material. Since this kind of blockage was likely to re-occur, the broken apparatus was not repaired.

To replace the broken Polycarbonate Reflux Classifier, the 20 mm channel stainless steel apparatus used for previous work on dry coal beneficiation (Walton et al., 2007) in the Reflux Classifier was modified to include a 1 m vertical section. The new steel construction easily withstood the internal pressure and external vibration. The only disadvantage was that there could be no observations of what was happening during the experiments. Although the steel apparatus was heavier than the original polycarbonate channel, the total weight was still below the design limit of the springs.

4.2.4 Feed Configuration

Both the batch and continuous systems needed to be continually fed with solids during operation. This was achieved by means of a 25 mm hole set 700 mm above the gas inlet on the 1 m vertical. A flexible hose was connected at this position.

When considering how to feed the system, the two main factors considered were (i) how to regulate the feed to the system, and (ii) how to prevent loss of fluidising air from the apparatus. The first design involved a hopper with a narrow opening and sand and coal kept inside the hopper. The flow of sand and coal into the bed was controlled by a flow of gas perpendicular to the base of the hopper. It was concluded that the opening at the base of the hopper would have to be made too narrow to allow the coal to exit. Similarly, while a vibratory feeder would have provided a steady flow, for particles of all sizes, there was no way of sealing the arrangement properly from the gas in the bed.

Instead a pair of manually operated ball valves was used to feed the system. The manual operation provided adequate control for maintenance of a steady flow of solids into the apparatus. By keeping at least one of the valves closed at all times, there was minimal loss of fluidisation gas from the bed and the solids preferentially flowed into the low pressure environment of the fluidised bed.

The ball valves were functional but, over time, exhibited a number of disadvantages. Because of the constant presence of solids under some pressure, the seals became contaminated with sand and began to loosen, resulting in gas leaking from the bed. In addition, the sand made the valves harder to open and close resulting in operator fatigue. And of course there was the constant risk that sand and gas could eject from the feed tube due to the inadvertent opening of both valves. For these reasons the manual ball valves were later replaced with pneumatic pinch valves. A computer controlled system was also introduced for the continuous tracer particle work. Changing to pinch valves (*AKO Armaturen and Separations GmbH*, DN050) reduced operator error and fatigue allowing higher feed rates to be used in shorter time intervals (once every 30 s instead of once every 60 s).

In the continuous system it was necessary to remove coal and sand from the base of the Reflux Classifier in a controlled manner without loss of gas pressure in the bed. The three possibilities considered for doing this were a rotary valve, a pair of valves (either manual or pneumatic pinch) or an auger. An auger was the preferred choice because it would provide a continuous movement of underflow from the device. In the presence of coarser particles, the auger was also expected to provide better performance than a rotary valve. Thus, the speed of the motor turning the auger would determine the rate of particle removal. The only perceived disadvantage of the auger was the significant additional mass which, in turn, would modify the system vibration.

The augers were designed and constructed by *Auger Fabrications* to handle particles up to 6 mm in diameter. When tested, the solids in the auger became fluidised, probably due to the vibration, and the bed soon emptied even when the auger wasn't turning. The auger outlet was placed in a sealed vessel so that the pressure at the overflow would be less than at the underflow. This arrangement was expected to lead to the gas flowing preferentially to the overflow, preventing the fluidisation of the underflow. However despite this modification the bed continued to empty through the auger due to the vibration. In addition, the vibration caused the central axis of the auger to bend so that it could not be rotated, and large coal particles caused the rotation to jam because there was not sufficient lubrication.

With the failure of the augers, a new underflow system consisting of pneumatic pinch valves was introduced. Pinch valves (*AKO Armaturen and Separations GmbH*, DN025) were chosen over the more continuous rotary valve because there was concern that the rotary valve would experience the same jamming issues as the auger. Further, there was concern that the rotating chamber could fill with sand before the opening was sufficiently large to allow the coal particles through. The pinch valves proved to be a very robust system, providing computer control, and exhibiting no observable wear, with all particles easily transported from the device.

4.3 Materials

The bed was fluidised with compressed atmospheric air supplied by the laboratory air compressor.

In previous work (Walton et al., 2007), low concentrations of fine magnetite was used as a dense-medium to encourage density rather than size based separation of dry coal in the Reflux Classifier. This approach was used by many other workers (see Chapter 2). Because there was an observable concentration gradient in the magnetite medium across the incline, with the magnetite settling onto the incline even though the gap was only 20 mm, it was decided that a lean phase dense-medium was not sufficient and that a lower density medium at a higher concentration would be preferable. Sand, at half the density of magnetite, was the obvious choice. This medium is inexpensive, readily available and likely to be favoured by industry. Choosing the size range of the media was also very important because if it was too fine it might not fluidise, instead exhibiting cohesive Geldart type C behaviour (Geldart, 1973), and if the particles were too coarse then the medium would not be experienced as a pseudo-fluid by the coal (Choung et al., 2006). The size of the sand chosen was less than half that of the smallest coal to be separated but still large enough to be in the Geldart group B classification. When a Group A ballotini was tested as a potential medium, it was found to become very cohesive.

Coal feeds were sourced from a mine in the Bowen Basin, Queensland. The coal feed was sieved into the required size fractions and riffled to the required mass. Samples were analysed for mineral matter (ash) content. The feed sample was also analysed for

its density distribution, usually referred to as the coal washability data, using the float/sink method. The full size and ash distribution of the coal feeds used in this thesis are included in Appendix G.

Plastic tracer particles were supplied by Partition Enterprises, Indooroopilly Queensland. They were described as “Naturally Shaped” with an estimated sphericity of about 0.7. The tracer particles were in the size fraction $-6.35 +1.00$ mm and had densities of 1300, 1600, 1800, 2100 and 2400 kg/m³ which were identified by different colours. The tracer particles proved to be a very robust and provided a convenient basis for analysis.

4.4 The Batch Experimental Apparatus

The apparatus configuration used for batch experiments is illustrated in Figure 4-2. The Reflux Classifier was constructed of stainless steel and consisted of a 1000 mm vertical section with a 1925 mm inclined section at 70° to the horizontal in the standard configuration. The internal dimensions consisted of a channel perpendicular spacing of 20 mm and channel width, into the page, of 100 mm. The inclined section was constructed from two flanged sections of length 500 mm and 1250 mm, and a 175 mm long section with the overflow arrangement (Figure 4-1). Thus it was possible to assemble an incline of length 175 mm, 675 mm, 1425 mm or 1925 mm.

Compressed air was supplied at room temperature from the laboratory compressor through a gate valve and gas rotameter (1) to the plenum chamber. The gas passed through a distributor plate (2) with 20×1 mm diameter holes arranged evenly in two parallel rows. Gas and solids exited at the overflow through a 1 inch hose. The gas and solids then separated via a cyclone. The Reflux Classifier was vibrated by means of vibration exciters (4) which were controlled by a variable speed drive (5). Solids could be added during operation without loss of gas pressure through use of a two valve system (3) connected to the feed inlet located 700 mm above the distributor. 25 mm ball valves were connected via 400 mm of 25 mm hose. A further length of the same flexible hose was then extended to the feed point of the vertical zone. The hose was left with enough slack so that the Reflux Classifier could vibrate freely.

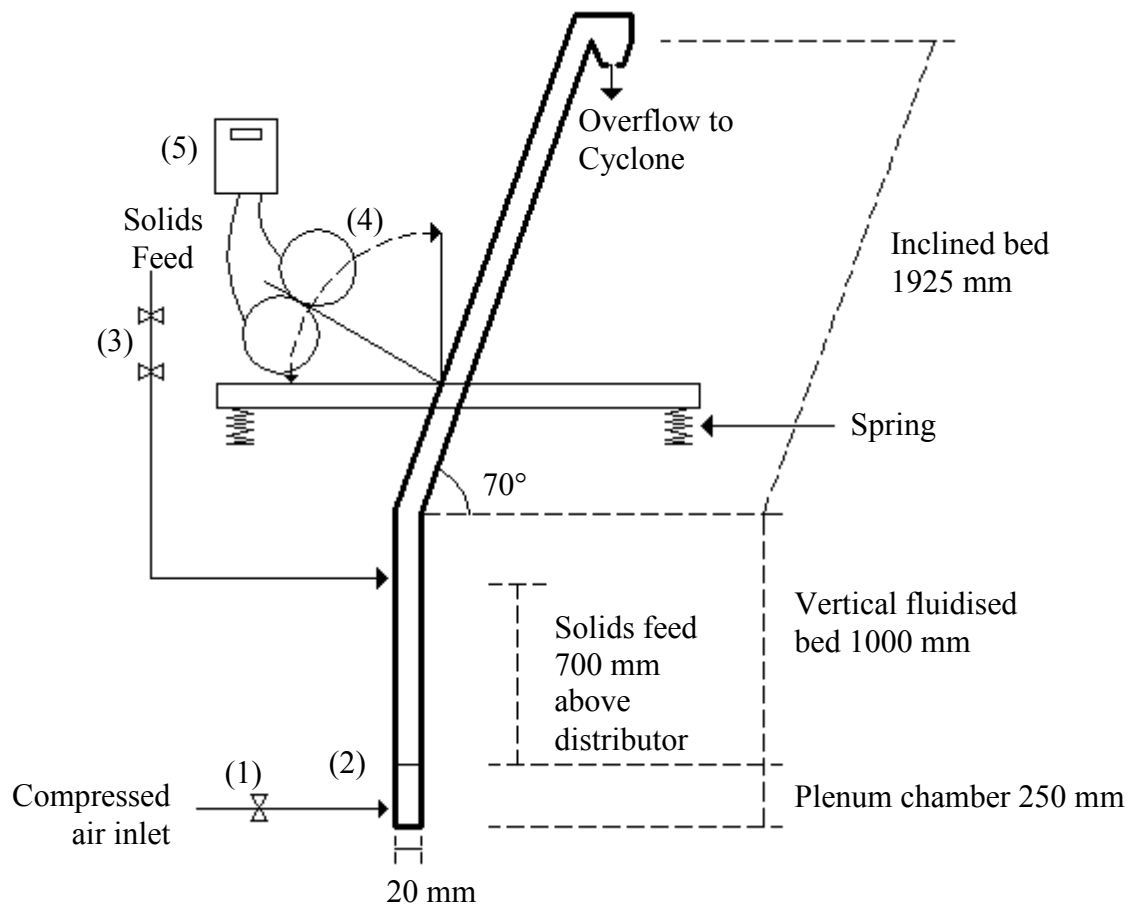


Figure 4-2: Schematic representation of the batch Reflux Classifier apparatus showing the main vertical and inclined channel and the attached vibratory motors. For further photos of the apparatus, see Appendix K.

The entire Reflux Classifier apparatus was bolted onto a steel frame which was supported on four springs for vibration isolation. The springs were provided by *Lovells Springs*, Carrington and the design specifications are given in Appendix J. This frame was vibrated by two motors that caused vibration using a rotating eccentric mass. These motors were coupled to rotate in opposite directions resulting in a linear, rather than circular, vibration. The motors were supplied by *Uras Vibrator*; model number KEE-3-4B. The angle of incidence of the vibration could be adjusted by changing the angle of the frame to which the motors were bolted. The angle could be rotated a full 90° as indicated in Figure 4-2 and shown in the Appendix K.

In a given batch experiment, 250 g of tracer particles of a single density were placed on the distributor plate. The Reflux Classifier was then filled completely with sand (approx 9 kg). The fluidising gas and vibration (if used) were switched on simultaneously. A

fixed volume of sand was fed at regular discrete intervals via the two valves on the feed hose. For example, an average feed rate of 0.0050 kg/s was obtained by feeding 300 g of sand once per minute. The overflow material was collected via the underflow stream of a cyclone. These particles were then collected via a plastic bag attached to the underflow outlet of the cyclone. The bag was changed at pre-determined intervals. These samples were analysed to determine the rates of elutriation of the sand and tracer particles.

When the experiment had been completed, the plenum chamber and distributor plate were removed and the bed emptied of sand and any remaining tracer particles.

4.5 The Continuous Experimental Apparatus

4.5.1 Inclined Apparatus

The apparatus used for the continuous separations was very similar to that used in the batch separations. The main apparatus including the inclined and vertical fluidised beds remained the same, as did the springs and motors. To allow for continuous solids removal through the bottom of the Reflux Classifier, the gas distribution system was modified as described Section 4.2.2. That is, a 160 mm length of channel was added to the base of the Reflux Classifier, still with a 20 × 100 mm cross-section and with 10 × 1 mm holes drilled in a straight line on each of the 100 mm sides. Surrounding these holes was a 38 mm pipe that served as the plenum chamber, welded on to the outside of the channel walls above and below the holes.

Below the new gas distributor the bed was constricted through a pyramid shaped hopper to a 25 mm diameter round hole where a pair of 25 mm pneumatic pinch valves was attached in series to control the underflow. The manual feed valves were also replaced by 50 mm pneumatic pinch valves to allow for automation of the feed. Each of the pinch valves was operated by a solenoid valve, and the opening and closing controlled by a LabVIEW program.

The pinch valves were provided by *AKO Armaturen and Separations GmbH*, with the catalogue numbers being DN025 and DN050 for the 25 and 50 mm valves respectively.

The vibrations were characterised by the frequency of the motors and the direction was measured using a tri-axial accelerometer as reported in Appendix A.

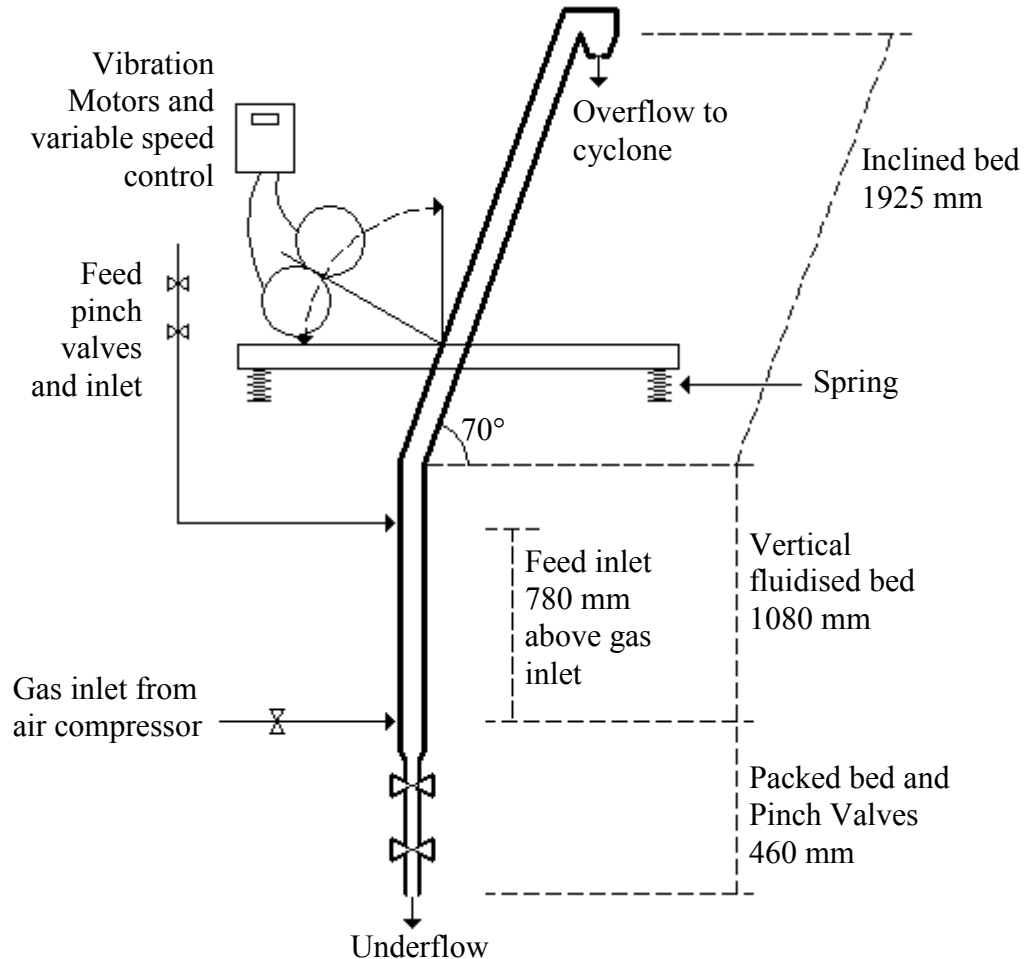


Figure 4-3: Schematic of the continuous Reflux Classifier apparatus showing the main vertical and inclined channel and the attached vibratory motors and underflow pinch valves.

4.5.2 Vertical Apparatus

The apparatus used for investigating separations using the vertical arrangement was the same as for the inclined bed described above, but the incline was replaced with a continuous vertical section. The frame was also modified to suit the changed arrangement.

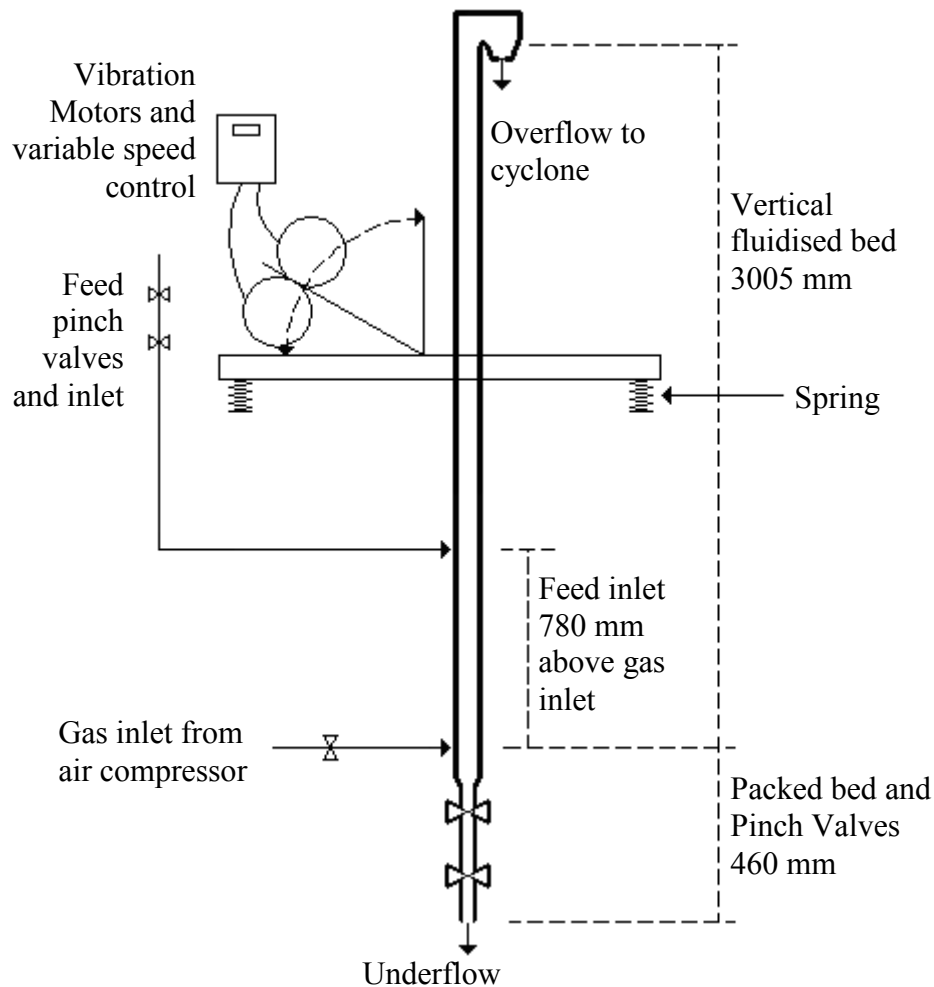


Figure 4-4: Schematic of the continuous vertical fluidised bed apparatus showing the main vertical channel and the attached vibratory motors and underflow pinch valves.

4.5.3 Continuous Methodology

For a continuous tracer particle experiment, the particles were prepared in the size fractions $-6.35 + 5.6$, $-5.6 + 4.0$, $-4.0 + 2.8$, $-2.8 + 2.0$, $-2.0 + 1.4$ and $-1.4 + 1.0$ mm in each density fraction. The number of particles of each size fraction ranged between 50 for the largest and 200 for the smallest particles in each batch. These size fractions were combined into their density fractions as one sample.

To commence an experiment, the bed was filled with sand and then the gas and vibration switched on. When any excess sand had been elutriated, feeding of sand and underflow removal commenced simultaneously. In all of the continuous experiments the sand feed rate was 560 g/min (280 g twice per minute) and the vibration rate was

595 rpm in the vertical plane. Once a steady overflow of sand had begun, the sample of one density (all size fractions) of tracer particles was fed into the bed together with the sand at a rate equivalent to the sand only feed. At this point the overflow and underflow were collected, in increments of 3 minutes. The remaining tracer particles were added at ten minute intervals, one density at a time, until all had been added. This approach made their separation and analysis much easier. Sand continued to be fed at regular intervals and the overflow and underflow collected until the vast majority of tracer particles had exited the bed, to a maximum experimental run time of two hours.

A continuous experiment with a coal feed proceeded in a similar way to the tracer particle experiment. The coal feed was sieved into the required size fraction and then riffled into small quantities of the same mass. The bed was filled with sand and a steady state flow of sand feed and overflow were established as above. Coal samples were then fed every feed interval together with sand up to the volume required. Samples of the overflow and underflow were taken at regular intervals.

4.6 Analysis

A partition curve provides the probability that a particle with a given property (in this case density) will report to a given exit stream such as the overflow (or underflow). In many cases only two parameters, the cut-point density, ρ_{50} , which is the density of a particle having a 50 % chance of reporting to a given stream, and the characteristic slope of the partition curve, are needed to adequately define a density partition curve. A separation is more efficient if the slope is steep. This is often characterised in terms of the *Ecart probable* (Ep) value, which is half the difference between the 75 % and 25 % partition densities, normalised by the density of water. Equation (4-1) is an empirical two parameter partition function used to fit the data obtained in this work:

$$PN = \frac{1}{1 + \exp\left(\frac{\ln 3(\rho_p - \rho_{50})}{Ep}\right)} \quad (4-1)$$

In Equation (4-1), ρ_p , ρ_{50} and Ep are in units of density, or g/cm^3 . A smaller value of Ep implies a more efficient separation and a steeper slope. Equation (4-1) was fitted to the

experimental data by minimising the sum of the square errors between the experimental data points and the predicted values. In Figure 4-5, the density cut-point, or ρ_{50} is 1.8 g/cm³ and the ρ_{25} and ρ_{75} are 1.6 g/cm³ and 2.0 g/cm³ respectively yielding an Ep of 0.2 g/cm³.

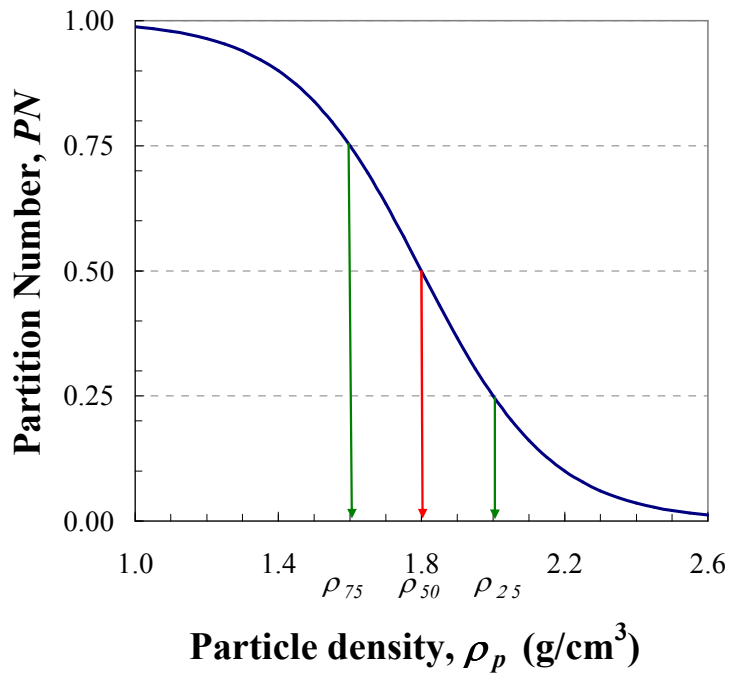


Figure 4-5: An example of a partition curve illustrating the partition number, PN, the particle density, ρ_p , and the densities, ρ_{25} , ρ_{50} and ρ_{75} .

4.7 Summary

The system described in this thesis is quite different from conventional methods of separation, combining a dense-medium and vibration with a Reflux Classifier in a way that has not been previously attempted. As a result, there were many design considerations and several failures before the final version of the apparatus was constructed and found to work.

The final vibrated Reflux Classifier consisted of a 20×100 mm cross section channel with a 1 m vertical zone and a 2 m inclined section at 70° to the horizontal located above. The channel was attached to a frame that vibrated linearly by means of a pair of motors. The Reflux Classifier arrangement was operated in semi-batch or continuous mode, with continuous feed and overflow. The materials and experimental procedures used in the experiments of this thesis were described together with the final apparatus configurations for each experiment.

Chapter 5

Behaviour of the Sand Dense-Medium

5.1 Introduction

The separations that are the subject of this thesis occur in an air-sand fluidised medium. It is important to understand and, where possible, quantify the behaviour of this sand medium in order to properly analyse the experimental separation results.

5.2 Change in Sand Properties Over Time

The sand used in this work was grade 50N, supplied by *Unimin Australia*. The true density of the sand was determined by pycnometry to be 2640 kg.m^3 .

The environment in the air fluidised, vibrated Reflux Classifier was reasonably abrasive. There was some change in the size distribution of the sand particles over time as seen in Figure 5-1. The sand became finer, although the change was gradual and minor.

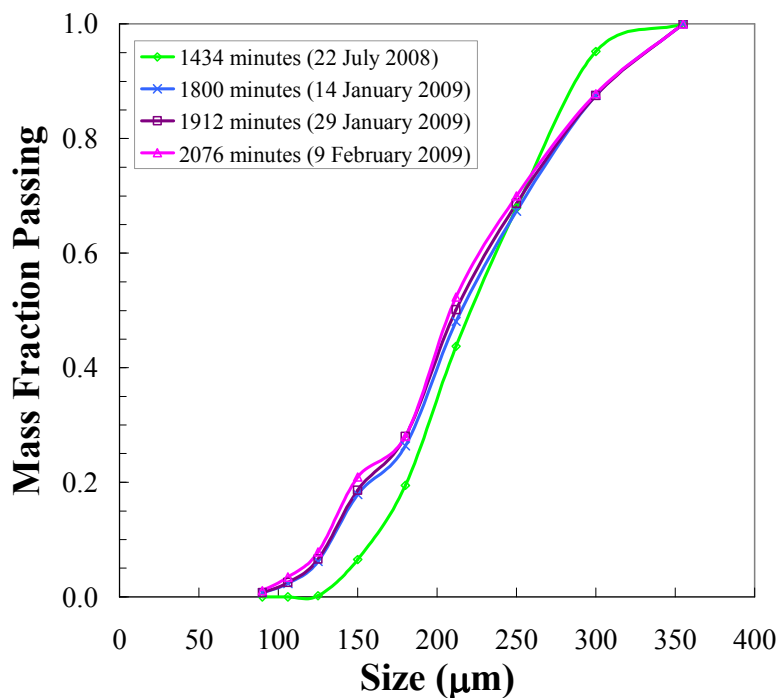


Figure 5-1: The change in the size distribution of the sand over time. It can be seen that the longer the sand was used, the finer the sand became.

When using sand as the medium to separate coal there was always a small amount of coal that would remain in the sand at the end of the experiment because it was too small to be sieved out. Over time this concentration of coal in the sand increased while the coal particles themselves reduced in size. The result of this abrasion was a darker and more cohesive medium. The cohesiveness increased to the point where the sand would no longer flow freely into the vessel and had to be replaced. This effect is typical of what would occur under plant conditions and hence was worth investigating.

Fresh sand was used for tracer particle experiments and hence the sand did not display cohesive behaviour in those experiments. It was clear that the major contribution to the stickiness of the sand was the ground coal. The impact of coal on the properties of the sand medium would be of particular importance in an industrial coal beneficiation process.

5.3 Observations of the Flow Pattern

The Polycarbonate apparatus was used to observe and film the behaviour of the batch Reflux Classifier. The vertical bed fluidisation behaviour was typical of a bubbling Geldart Group B (Geldart, 1973) fluidised bed, with the bubbles increasing in size as they rose through the vertical section. Upon entering the incline, the bubbles grew to occupy the entire column cross-section, displaying coarse slugging behaviour typical of dense phase transport (Konrad, 1986). This is illustrated in Figure 5-2. Vibrating the bed reduced the length of the slugs, with visual observations suggesting that the highest frequency vibrations resulted in the smallest bubbles.

The bed was observed to consist of discrete gas bubbles or slugs and a concentrated phase, also called the emulsion phase or sand plugs. In the incline, the concentrated phase appeared to be a packed bed with no discernible mixing of sand or tracer particles. These plugs were pushed up by the bubble/slug rising behind them. As they rose, material rained down from the base of each plug through the bubble/slug underneath and onto the upper surface of the next plug of solids. This falling material slid back along the lower surface of the channel rather than falling through the slug.

The length of the bubbles was affected by the addition of vibration, with a vibrated bed exhibiting smaller bubble slugs than the non-vibrated bed as measured from video footage (see Appendix A). This observation was consistent with previous findings (Wang et al., 1997; Jin et al., 2005). In addition, visual observations of the bed indicated that increasing the vibration rate decreased the size of the bubbles, increased the rate of bubble rise and reduced the variability in the length of the bubbles.

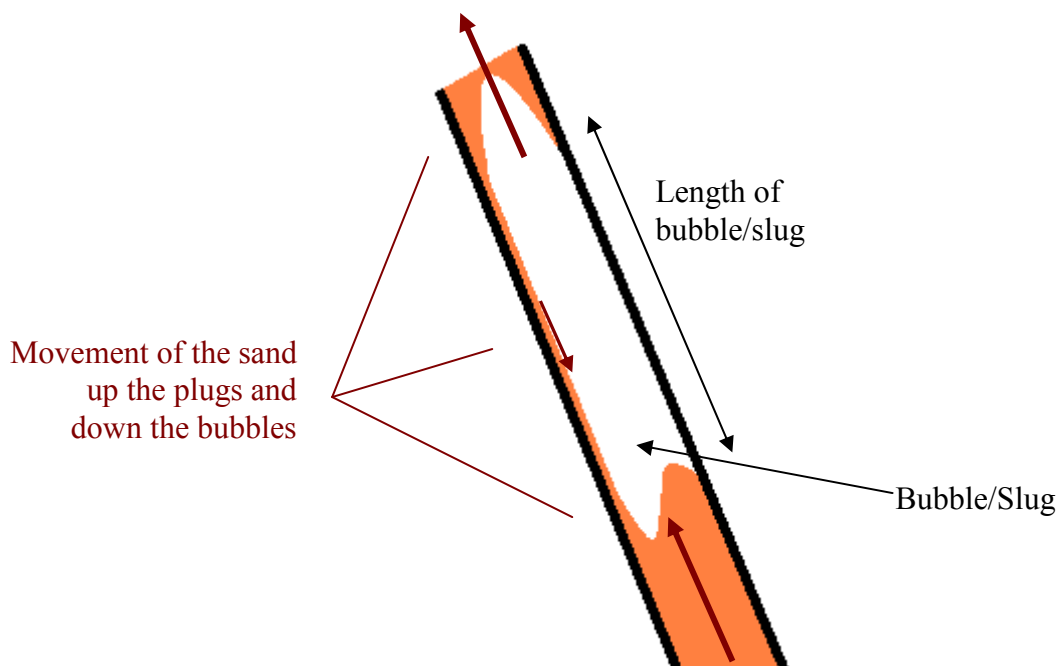


Figure 5-2: Sketch of the appearance of bubbles in the incline taken from video footage. The bubble extends across the entire width of the channel and there is a constant layer of downward sliding sand on the upward facing incline.

The gas rate had a similar effect on the length of the bubbles to the vibration rate. Increasing the gas rate caused an increase in the length of the bubbles as shown in Figure 5-3a. This increase also resulted in greater variability in the length of the bubbles, as seen in the larger error bars. The size of the sand plugs increased only moderately, (Figure 5-3b), which implies that most of the gas in excess of that required for minimum fluidisation was carried in the gas bubbles, as expected from past results (Toomey & Johnstone, 1952; O'Dea et al., 1990; Mostoufi & Chaouki, 2004). Extrapolating backwards in Figure 5-3a the minimum bubbling velocity (O'Dea et al., 1990) can be inferred to occur at a 6.5% gas rate or 0.0404 m/s.

When vibrated, the rate of rise of the bubbles was not affected by the changing gas rate, with an average rise velocity of 0.41 m/s. Without vibration, the bubbles were more infrequent, and the rate of rise increased with increasing gas rate. At 15%, the rise velocity was 0.24 m/s, at 20%, 0.29 m/s and at 25%, 0.41 m/s. This indicates that the vibration increased the fluidity of the system as expected from the literature (see Section 3.7)

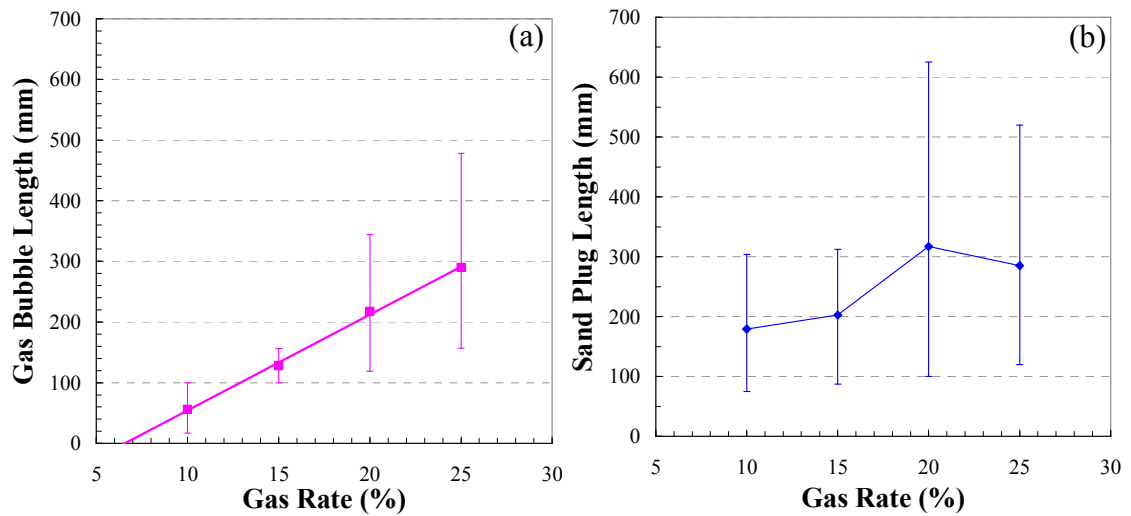


Figure 5-3: The average measured (a) gas bubble length and (b) sand plug length in the inclined bed from video analysis of the air-sand dense-medium Reflux Classifier shown for gas rates of 10%, 15%, 20% and 25%. Each value is the average of several measurements and the error bars are the range of those values. The raw data is given in Appendix A.

5.4 The Air-Sand Pseudo-Fluid

The fluidised air-sand medium forms a pseudo-fluid (see Section 3.6) in which the separation of the tracer particles occurs. It is this same pseudo-fluid that carries and separates the tracer particles. That is, the tracer particles are not fluidised by the gas, but the air-sand pseudo-fluid, and in fact the gas rates used are insufficient to fluidise the largest tracer particles. Because of the pseudo-fluid phenomenon the sand particles are no longer considered as individual particles in this analysis, but as part of the continuum of the pseudo-fluid.

A constant feed of sand is required to allow particles to exit from the bed. If there was no sand feed to the bed, the tracer particles would essentially behave as if they were in a tank of fluid with no net fluid motion. They would separate on the basis of the settling velocity only, with the low density particles floating to the top of the bed. However, without any convective flow of the air-sand pseudo-fluid through the overflow, the particles cannot escape the bed.

It is worth noting that the air-sand pseudo-fluid is a bubbling, fluidised suspension of particles, not a continuous fluid. As a result there is some inherent turbulence in the bed caused by the bubbles that will cause particles settling in the fluid to experience some dispersion and/or mixing.

5.5 Proposed Segregation Mechanism

Since there was no mixing or settling apparent in the concentrated plugs in the incline it was surmised that the majority of segregation in the inclined section of the rig must occur in the gas bubble between the plugs. Figure 5-4 provides a schematic representation of the proposed segregation mechanism.

The particles fall from rest at the base of the plug through the air bubble below and so their initial acceleration is dependant solely on the density of the particles, as described in Chapter 2. Thus, similar to jigging, the high density particles fall with greater initial velocity than the low density particles. As a result, they reach the surface of the next concentrated phase sooner and are buried in falling sand ahead of the lower density particles. In addition, the denser particles with more inertia will penetrate/punch further into the loose sand layer at the top of each plug when compared to the low-density particles. The combination of these two effects results in high density particles rising more slowly than low density particles.

Vibration caused a reduction in the bubble size, shortening the distance over which the particles accelerate as they fall through a bubble. The reduction increased with increasing vibration frequency, meaning that higher vibration frequencies led to smaller bubbles. Short falls through small bubbles should enhance the density separation effect

described above since this increases the percentage of time that particles settle in the initial acceleration phase where size is unimportant.

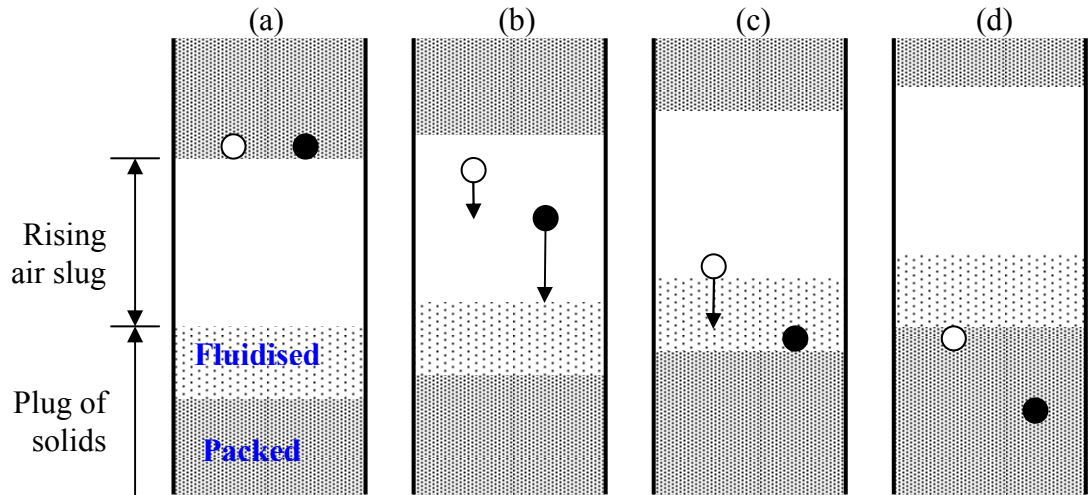


Figure 5-4: Schematic representation of the behaviour of low density (white) and high density (black) particles in the experimental apparatus illustrating (a) particles at rest at the base of a plug, (b) high density particle accelerates from rest at a greater rate than low density particle, (c) high density particle partially buried by falling sand before the low density particle arrives, and high density particle penetrates further into the fluidised upper surface of the plug beneath, (d) high density particle has travelled further down than low density particle (Macpherson et al., 2010).

Based on these observations it is clear that there are two distinct zones for possible segregation in the incline: the air bubble and the sand plug, each with very different properties for density and viscosity. The viscosity of the air bubble would be about 1×10^{-5} Pa s while the viscosity of the sand plug should be close to the viscosity measured by several workers and reported in Rees et al. (2007) of 0.6 to 1.0 Pa s. Based on the above segregation model, the viscosity of the sand plug is largely irrelevant, but its density will determine how far different particles will penetrate the upper fluidised zone.

Chapter 6

Batch

Tracer Particle

Separations

6.1 Introduction

This work is an investigation into the application of the pneumatic Reflux Classifier to coal beneficiation. Although industrial applications require continuous, steady state separations it is appropriate to first investigate the system under semi-batch conditions. Hence this chapter is concerned with the separation of particles on the basis of their density and size under batch conditions, using tracer particles to quantify the inherent particle transport. This approach then provides kinetic data fundamental to understanding a continuous system.

Coal separations in the Reflux Classifier had previously been researched at the University of Newcastle by Walton et al. (2007) using an apparatus similar to that used in this work. They found that when air alone was used as the fluidising medium, the separation took place mainly on the basis of the particle size, and that increasing the gas rate increased the separation size while decreasing the separation efficiency.

By adding a magnetite dense-medium, Walton et al. (2007) found that the separation proceeded largely on the basis of density, with some effects due to particle size evident in the smaller size fractions as is typical of dense-medium separations (Kelly & Spottiswood, 1982). Several different processing configurations, the best of which is illustrated in Figure 6-1, were considered by Walton et al. (2007). They found that when using a magnetite dense-medium in the Reflux Classifier multiple separation stages were required to produce a satisfactory coal product. A single stage separation is preferred by industry. It was clear from the work of Walton et al. (2007) that the magnetite medium alone was not capable of producing an efficient density based separation of coal in the Reflux Classifier.

It is believed that the difficulty encountered by Walton et al. (2007) in using a magnetite dense-medium was due to the small volume of medium used, resulting in an uneven concentration throughout the bed. This is discussed further in Chapter 8. By using medium particles of lower density such as sand at a higher concentration, the consistency of the medium should be improved.

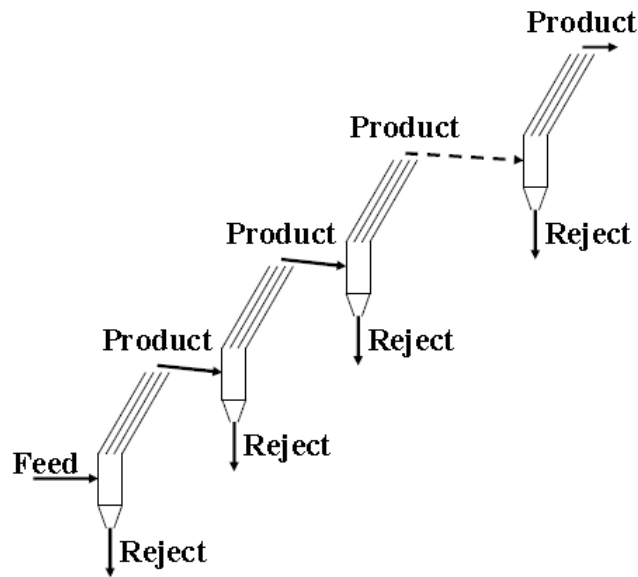


Figure 6-1: Schematic of the product fractionation pathway that was found to produce the best results (Walton et al., 2007).

In the dry beneficiation of coal using a dense-medium, bubbling that occurs when the fluidisation velocity exceeds the minimum fluidisation velocity produces an inconsistent density and encourages mixing. In previous studies (Luo et al., 2000; Luo et al., 2008; Xu & Zhu, 2005; Wang et al., 1997; Jin et al., 2005), vibration was introduced in order to reduce the size of the bubbles and thus the negative effects on the separation. In the present study the effects of introducing a medium and the benefits of introducing vibration on the separations achieved using a pneumatic Reflux Classifier are examined. This chapter examines the separations achieved under semi-batch conditions using tracer particles.

6.2 Batch Elutriation Theory

Modelling the elutriation of particles from a gas fluidised bed has been investigated by many researchers. Much of this work was summarised by Tasirin and Geldart (1998) with the conclusion that the rate of elutriation of particles from a gas fluidised bed, R_i , is given by the empirical equation:

$$R_i = \frac{d(X_i M_B)}{dt} = K_i A X_i, \quad (6-1)$$

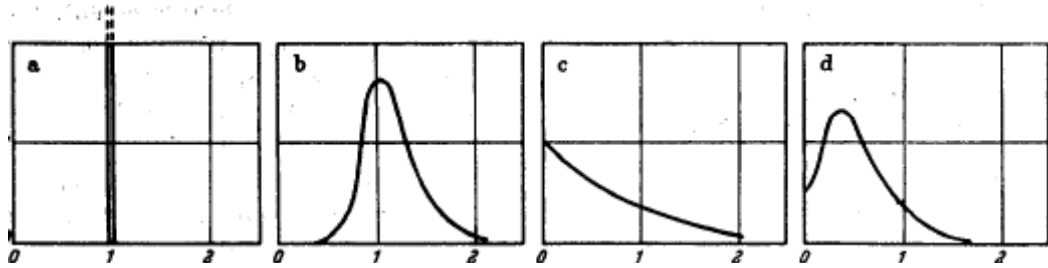
where X_i is the mass fraction of particles of size d_{pi} in the bed, M_B the total mass of solids in the bed, A the cross-sectional area of the bed and K_i the first order elutriation rate constant for the size fraction d_{pi} . The value of K_i varies greatly depending on the geometry of the system, and so there is no theoretical value for this constant. Many empirical values of K_i are reported in the literature (see Section 3.5) and one can be chosen that best suits the system being studied.

Equation (6-1) states that the rate of elutriation from a fluidised bed is first-order dependant on the concentration of particles in the bed. Callen et al. (2007a) observed that the elutriation of particles from the Reflux Classifier also obeys Equation (6-1).

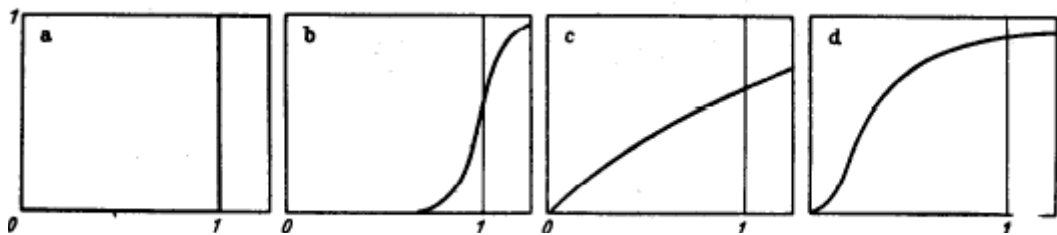
When an pulse of tracer is introduced into a flowing fluid in a vessel, the pulse will spread as it travels due to longitudinal molecular diffusion (Danckwerts, 1953; Levenspiel & Smith, 1957) with the rate of spread depending on the flow conditions in the vessel. The diffusion model had been the subject of many papers in the literature including the seminal work by Danckwerts (1953), as well as follow-up communications by Levenspiel and Smith (1957) and van der Laan (1958). This diffusion can be modelled or calculated from experimental data and is represented by the diffusion coefficient D (m^2/s). The diffusion model should also take into account back mixing that occurs along the length of the vessel.

The plot of the concentration of tracer at the sample point of a vessel and a cumulative plot of the same data for four flow conditions are given in Figure 6-2. By analysing the

output data of an experiment one can easily determine which of the four flow conditions is most like the flow condition in the system.



(i) Instantaneous tracer concentration vs dimensionless vessel flow volume



(ii) Cumulative tracer concentration vs dimensionless vessel flow volume

Figure 6-2: Output tracer concentration diagrams for (a) plug flow, (b) plug flow with some longitudinal mixing, (c) complete mixing, (d) dead water (Danckwerts, 1953) versus the number of flow volumes that have exited the bed. In dead water a large part of the fluid is trapped in eddies and spends a longer than average time in the pipe while the remainder travels quickly through a narrowed channel.

These data can be modelled in a number of ways depending on the flow and boundary conditions. For example, in the manner of Levenspiel and Smith (1957) consider a pipe of infinite length with a fluid flowing through it in plug flow. A section of this pipe of length, L , with corresponding volume, V , has an injection point at one end of the length and a sampling point at the other. If an impulse of tracer is injected and the concentration monitored at the other end, the output will resemble one of the plots in Figure 6-2. The dispersion of this tracer in the fluid is defined by (Levenspiel & Smith, 1957):

$$\frac{\partial C}{\partial t} = D \frac{\partial^2 C}{\partial x^2}, \quad (6-2)$$

where $C(x,t)$ is the concentration of tracer in the fluid (dimensionless), D the diffusion coefficient, t time (s) and x the distance (m) from the injection point. A solution to the open boundary condition problem of Equation (6-2) is (Levenspiel & Smith, 1957):

$$C = \frac{QL}{V\sqrt{4\pi Dt}} \exp\left[-\frac{(L-Ut)^2}{4Dt}\right], \quad (6-3)$$

where Q is the volume occupied by the injected tracer and U the flow velocity. Equations for systems with other boundary conditions are given by van der Laan (1958), however as they cannot be solved analytically, for simplicity they are not considered here.

The above model is for molecular diffusion in a flowing fluid. However the effects of dispersion on solid particles in a fluid can be modelled in the same way as is shown in Section 6.5.

6.3 Batch Separation Methodology

The apparatus used in these experiments is detailed in Section 4.4 and illustrated in Figure 4-2. The stainless steel Reflux Classifier apparatus had a 1000 mm vertical fluidised bed with a 1925 mm channel inclined at 70° to the horizontal above. The internal channel dimensions were 20 × 100 mm. Sand was fed into the bed by means of two ball valves. The bed was vibrated by two motors as described in Section 4.2.3. The frequency of the vibration was given by the frequency setting on the motor (595 rpm or 325 rpm), and was confirmed by strobe measurements. These frequencies were chosen in order to avoid the resonant frequencies of the vessel and the supporting frame. For convenience the direction of the vibration was defined as either horizontal (H) or vertical (V) throughout this thesis as determined by visual observations of the predominant direction of vibration of the Reflux Classifier. The more thorough description of the vibration conditions is given in Appendix A.

The tracer and sand particles described in Chapters 4 and 5 respectively were used in these experiments. In a given experiment tracer particles of a single density were placed

on the distributor plate. The Reflux Classifier was then filled completely with sand (approximately 9 kg). The fluidising gas and vibration (if used) were switched on simultaneously. 300 g of sand was fed at one minute intervals via the two valves on the feed hose yielding an average feed rate of 0.0050 kg/s. The overflow material was collected via a plastic bag attached to the underflow outlet of the cyclone on the exit line. The bag was changed at pre-determined intervals. These samples were analysed to determine the rates of elutriation of the sand and tracer particles.

When each experiment had been completed, the plenum chamber and distributor plate were removed and the bed emptied of sand and any remaining tracer particles.

6.4 Tracer Particle Analysis

A series of experiments was carried out at a single gas flowrate of 3.22×10^{-4} m³/s, equivalent to a superficial velocity of 0.16 m/s, with vibration applied to the system. The three modes of vibration studied were 595V, 595H and 325H, where the number refers to the vibration frequency in rpm and the letter denotes the predominant direction of vibration, either vertical (V) or horizontal (H). The vibration is completely defined in Appendix A. While other gas rates were considered, particles tended to remain in the bed at low gas flowrates, giving minimal useful information. Separations of coal using higher gas flowrate produced an unacceptably high density product. The chosen rate was found to be highly effective in comparison. From this work the effect of the vibration frequency and direction on the separation performance was determined.

6.4.1 Equilibrium Solids Loading

At the commencement of an experiment the bed was full of sand. When fluidised, the bed expanded and some sand exited until the bed reached its equilibrium loading of sand. The mass of sand in the bed at any time could be back-calculated from a knowledge of the final mass in the bed at the end of the experiment, the sand feed rate and the rate at which sand had exited in the overflow.

The addition of vibration affected the equilibrium solids loading of the bed as illustrated in Figure 6-3. Vibrating the bed at 325 rpm did not make a significant difference to the equilibrium mass of sand in the vessel when compared to the non vibrated bed, with the bed in both cases containing about 6 kg of sand. However, increasing the vibration frequency further to 595 rpm caused the equilibrium mass of sand in the bed to increase to between 7 and 8 kg of sand. The vertical vibration mode appeared to give slightly higher bed masses than the horizontal mode. The sand feed rate did not appear to have a significant effect. The number and size of the slugs/bubbles was not measured, so it is not known how the density of the concentrated emulsion phase between the bubbles was varying.

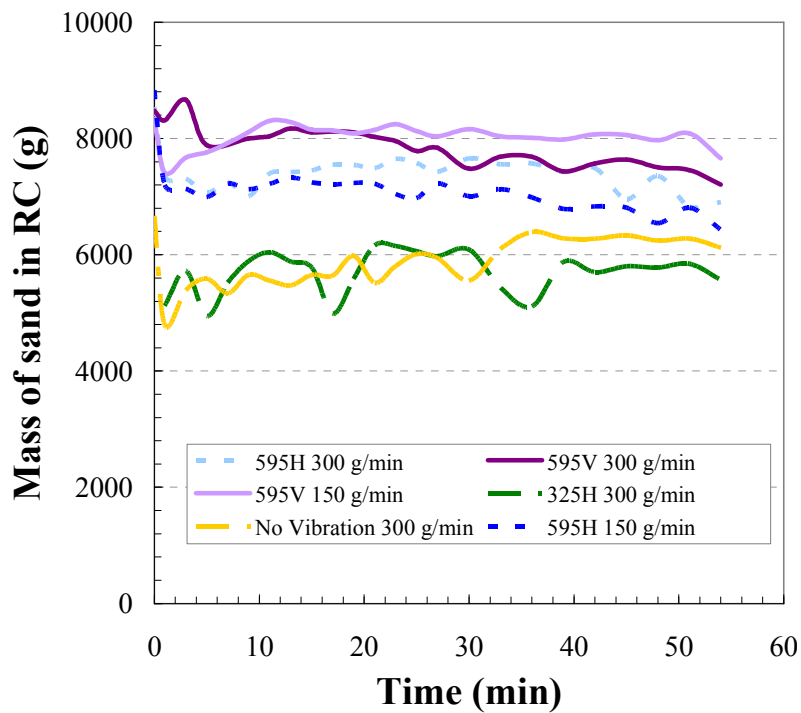


Figure 6-3: The calculated mass of sand in the Reflux Classifier over the 54 minutes of each experiment. The vibration conditions are given together in the legend together with the sand feed rate in g/min. The gas rate was $3.22 \times 10^{-4} \text{ m}^3/\text{s}$ in every case.

6.4.2 Changes in Sand Properties Over Time

The sand which was used in these tracer particle experiments had previously been used for coal experiments. As a result, there were traces of coal left in the sand that were too small to be sieved out. Over time the abrasive environment in the Reflux Classifier ground down these coal particles and caused the sand to become observably more

sticky/cohesive. In the following discussion, the term clean medium refers to sand that is relatively clean, containing either no coal particles or unground coal particles. The term contaminated medium refers to sand with a significant concentration of fine coal.

Experimental results clearly indicate that the elutriation of tracer particles is significantly inhibited by the use of contaminated medium as shown in Figure 6-4. The elutriation constants for Figure 6-4 are included in Table 6-1. Cases (a) and (d) correspond to elutriation experiments using clean medium and cases (b) and (c) were experiments with contaminated medium.

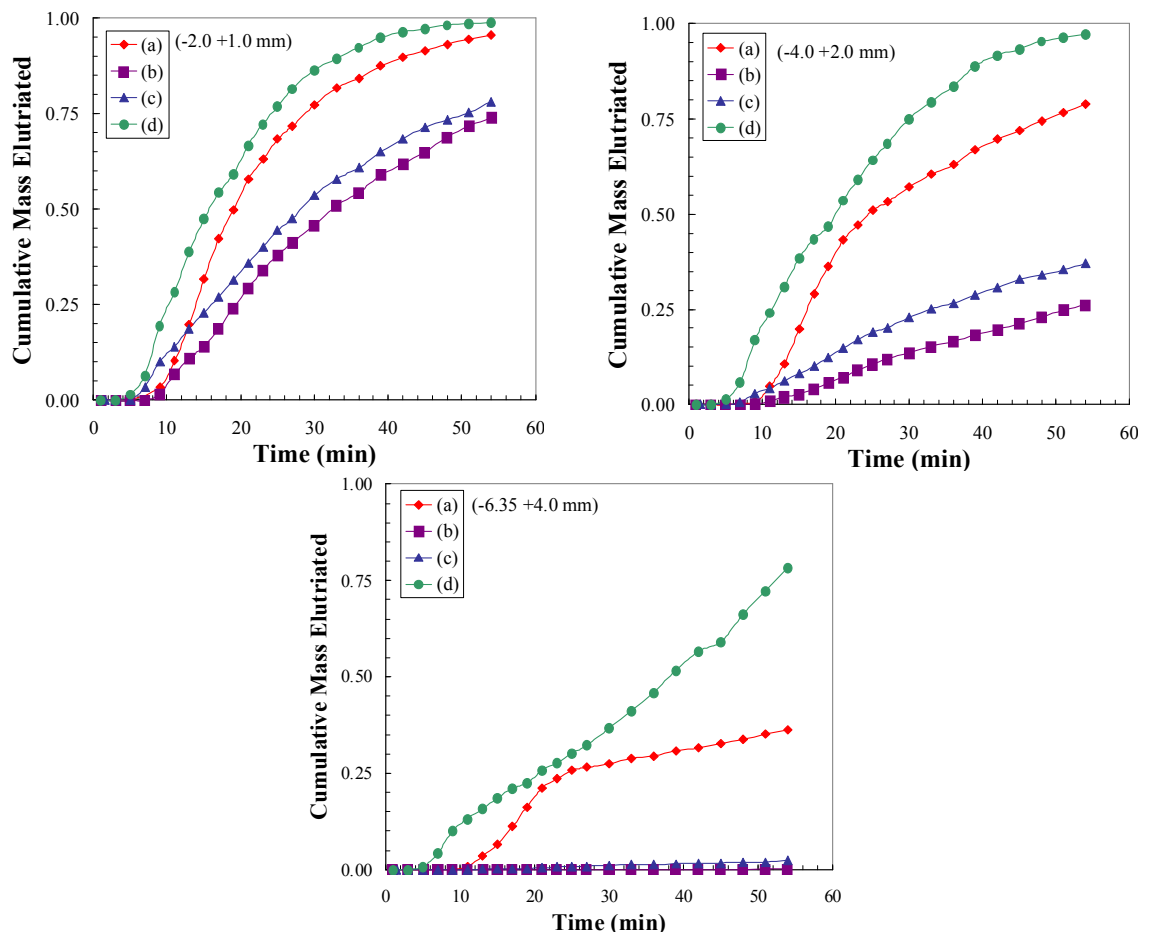


Figure 6-4: Plots of cumulative mass elutriated versus time showing the effect of coal on the rate of elutriation of 1600 kg/m^3 tracer particles from the Reflux Classifier under conditions of 0.005 kg/s sand feed rate, gas flowrate of $3.22 \times 10^{-4} \text{ m}^3/\text{s}$ and 595 V vibration. (a) New sand containing un-ground coal, (b) and (c) show duplicate results on the same day using the same sand as in (a) after two months of constant use, and (d) shows the performance with new sand containing no coal.

The elutriation constants for the clean medium experiments (a) and (d) are clearly very similar with a slight difference in the intermediate size range. Similarly, the elutriation constants for the contaminated medium experiments (b) and (c) are closely related, with minor differences at intermediate size. Clearly in general the elutriation constants are significantly higher for the clean medium than for the contaminated medium indicating that the contaminated medium inhibited particle elutriation.

Table 6-1: The elutriation rate constants, K_i (min^{-1}), for the plots in Figure 6-4.

	Elutriation Rate constant (K_i , min^{-1})		
	-2.0 +1.0 mm	-4.0 +2.0 mm	-6.35 +4.0 mm
(a)	0.075	0.0375	0.02
(b)	0.03	0.007	0
(c)	0.033	0.011	0.0004
(d)	0.075	0.06	0.02

It is also observed in Figure 6-4 that there was no elutriation of the -6.35 +4.0 mm particles from the contaminated medium. This particle retention is indicative of the refluxing phenomenon present in the incline that is discussed in detail later in the thesis (see Section 7.3.3 Particle Retention).

The experiments at each vibration condition were completed consecutively so the effects of the sand deterioration within a vibration condition would be minimal. However comparisons between different vibration conditions are more problematic because of the potential confounding effect of sand ageing. A full list of the experiments conducted and the dates that they were conducted on is included in Appendix B.

6.4.3 Movement of the Tracer Particles

Figure 6-5 shows the total mass percent of different density tracer particles of size -6.35 +1.00 mm that had elutriated from the bed as a function of time for the 595V case with a sand feed rate of 0.0050 kg/s.

There was an initial delay period during which no tracer particles exited the bed. This represents the time taken for the first set of particles to be lifted the three metre distance from their initial position at the base of the bed. The low density tracer particles rose

much more quickly than the high density particles, with nearly all of the 1300 kg/m³ tracer particles having exited the system after 30 minutes, while over 90% of the 2400 kg/m³ tracers were still within the bed. At the end of the experiment when the bed was emptied, it was noted that most of the tracer particles that failed to leave the system were located at the base, immediately above the gas distributor plate. This suggests that they would have exited through the underflow stream, had there been one.

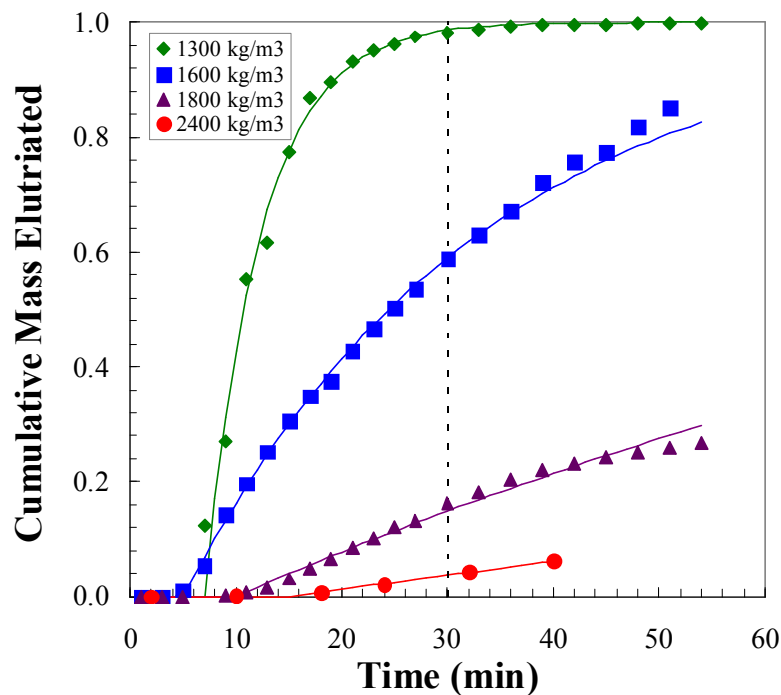


Figure 6-5: The rate of elutriation of $-6.35 +1.00$ mm particles from the air-sand dense-medium Reflux Classifier fitted with first order elutriation curves according to Equation (6-1) taking into account the time delay. The bed was fluidised at 3.22×10^{-4} m³/s gas rate, with a sand feed rate of 0.0050 kg/s, vibrated at 595V. The 2400 kg/m³ density experiment was one of the first conducted, before the experimental method was standardised, so less data was collected and over a shorter (40 minute) time period.

What Figure 6-5 illustrates in particular is that the rate of elutriation is defined by a first order exponential decay as given in Equation (6-1). This is in keeping with literature results on the concentration dependence of particle elutriation. Particle elutriation from a gas fluidised bed occurs because particles enter the freeboard through the bursting of bubbles at the bed surface. The mechanism for particle elutriation in this system is more likely to be due to particles being carried over with the dense-medium as it exits the bed. However, this appears to display a similar concentration dependence.

6.4.4 Effective Partition Curves

From the semi-batch elutriation experiments, it was possible to construct what have been termed “effective” partition curves. Normally, a partition curve describes the probability of a particle reporting to the overflow of a process, with the balance of the particles reporting to the underflow. In the present case, however, there was no underflow stream, and hence there was no steady state partition between two streams. Instead the mass percentages of the initial charge of tracer particles in each size fraction that had elutriated at a given time (as seen in Figure 6-5) were used as the partition numbers and curves were fitted through these data points according to Equation (4-1). That is, the particles that had elutriated in the chosen time were considered the overflow stream and those remaining in the bed were considered the underflow. An example of a partition curve formed from the data in Figure 6-5 at a time of 30 minutes is given in Figure 6-6 with a partition curve fitted through the data according to Equation (4-1) by minimising the sum of the errors squared.

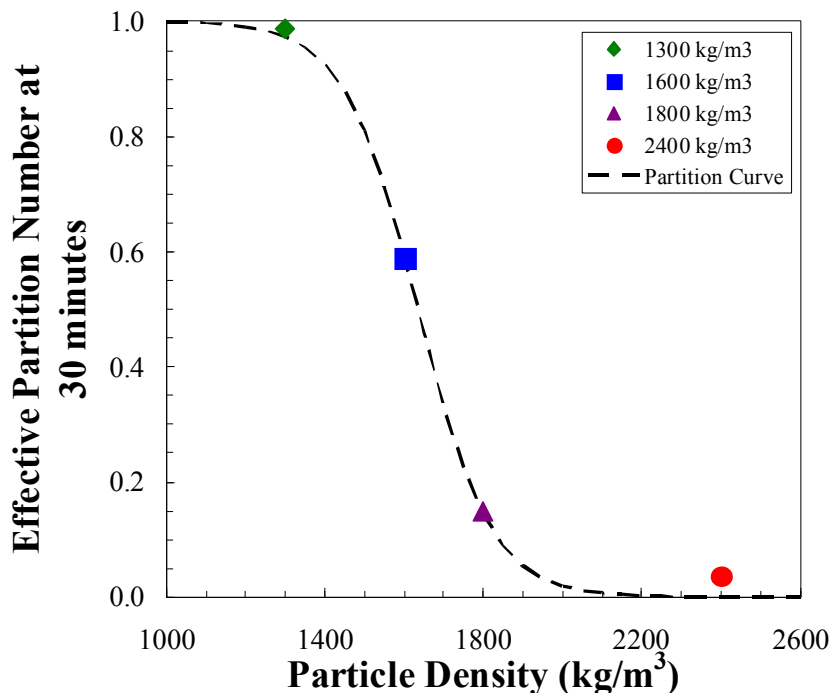


Figure 6-6: 30 minute effective partition curve for $-6.35 +1.00$ mm tracer particles from the air-sand dense-medium Reflux Classifier, fluidised at 3.22×10^{-4} m³/s gas rate, with a sand feed rate of 0.0050 kg/s and vibrated at 595V.

6.4.5 Effect of Vibration Addition

When comparing the separation obtained in a vibrated fluidised bed with a non-vibrated bed in Figure 6-7, vibration clearly improves the sharpness of separation for the larger -6.35 +4.0 mm particles. There was also a slight sharpening in the partition curve for the -4.0 +2.0 mm particles with vibration (not shown for simplicity). However, there was no significant change for the -2.0 +1.0 mm particles.

Because of the clear positive benefits to be gained from vibrating the Reflux Classifier apparatus, it was decided not to complete further non-vibrated experiments in a batch system. The experiments in Figure 6-7 were both conducted using the “new sand” consecutively and so the deterioration of the sand mentioned in Section 6.4.2 was unlikely to have any effect on the result. The benefits of the addition of vibration were also confirmed in the batch separations of coal (see Chapter 8).

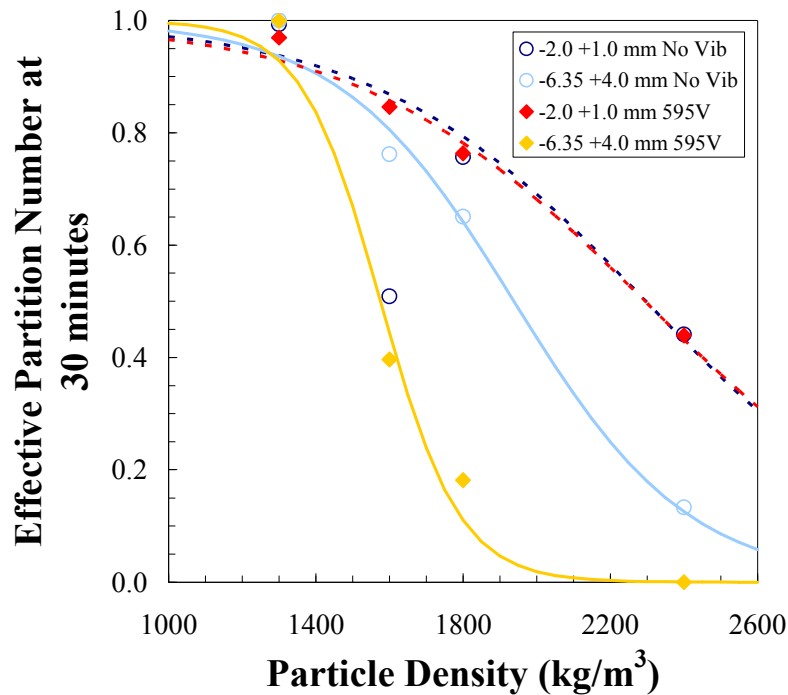


Figure 6-7: The effect of the addition of vibration on the separation efficiency of the effective partition curve after 30 minutes for -2.0 +1.0 mm particles and -6.35 +4.0 mm tracer particles with a sand feed rate of 0.0050 kg/s and gas flowrate of $3.22 \times 10^{-4} \text{ m}^3/\text{s}$. The lines are the least square error fit of Equation (4-1) to the data.

6.4.6 Effect of the Time used to Calculate Effective Partition Number

The variation in the effective partition curves with the choice of time is illustrated in Figure 6-8 for the -2.0 +1.0 mm particles and Figure 6-9 for three different size fractions. It can be seen that after about 30 minutes the efficiency (E_p), of the separation remains approximately constant. The cut-point density increases with longer processing time. This shift in the cut-point is to be expected since the percentage of particles in the overflow tends to increase as time passes (Figure 6-5). The change in the cut-point density is most pronounced for the smallest size fraction. The effect of particle size on the separation is discussed in Section 6.5.1.

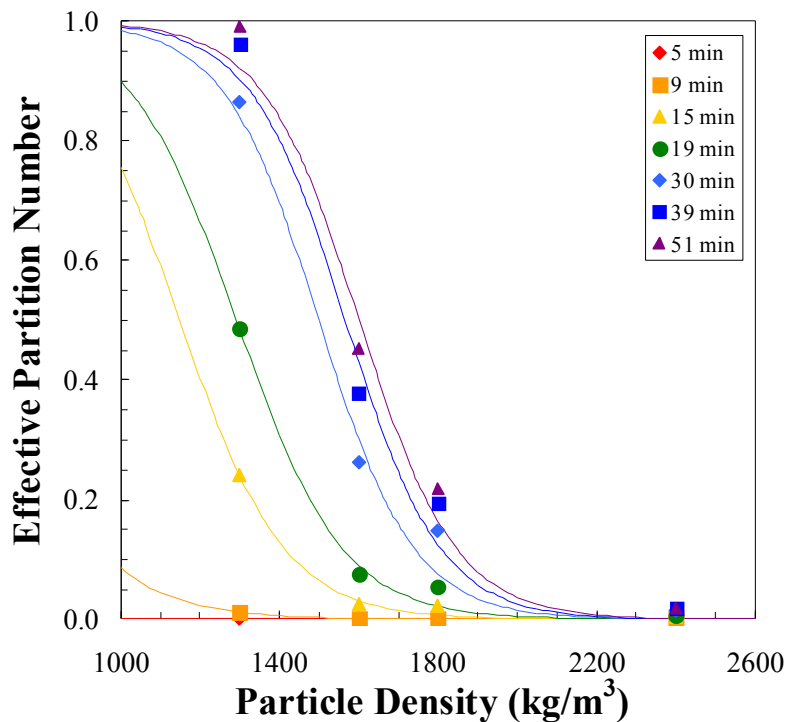


Figure 6-8: Effective partition curves for -2.0 +1.0 mm particles under the 595H vibration condition evaluated at different processing times. Sand feed rate of 0.0050 kg/s and gas flowrate of $3.22 \times 10^{-4} \text{ m}^3/\text{s}$.

It can be seen in Figure 6-9 that for the 595H case the ρ_{50} does not change significantly with particle size, but that the E_p is significantly decreased as the particle size increases. These trends are also observed in the 595V and 325H vibration conditions suggesting that the effects of size on the ρ_{50} are effectively suppressed by the air-sand dense-medium Reflux Classifier with vibration but that the E_p is still very much size dependent. This strongly suggests that the separation mechanism is a dense-medium

separation, where the density cut-point is independent of particle size, but the relatively low settling rates of small particles makes them harder to separate.

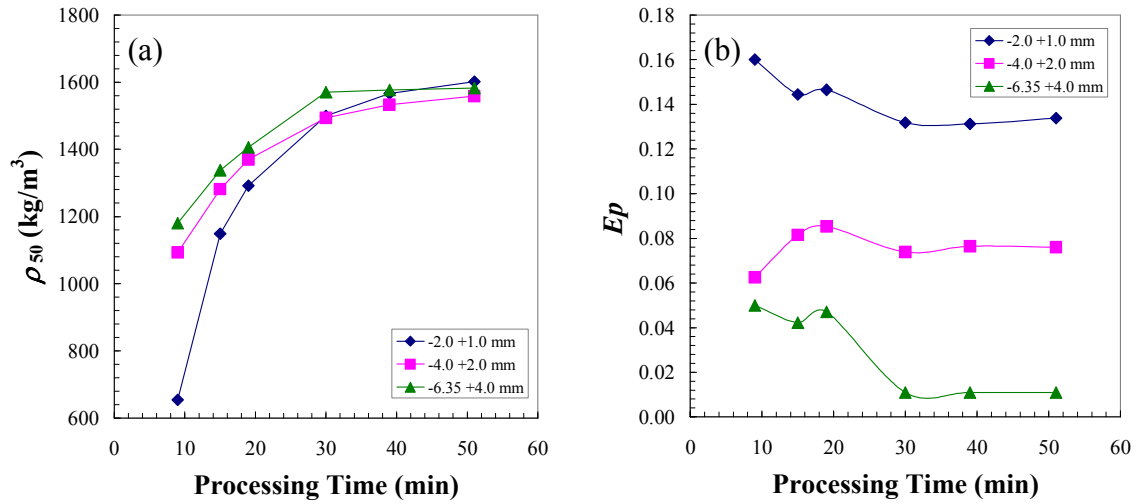


Figure 6-9: The effect of residence time on the (a) ρ_{50} and (b) Ep under the 595H vibration condition for the tracer particle size fractions -6.35 +4.0 mm, -4.0 +2.0 mm and -2.0 +1.0 mm. Sand feed rate of 0.0050 kg/s and gas flowrate of 3.22×10^{-4} m³/s.

6.4.7 Effect of Vibration Frequency and Direction

Since it was clear from Figures 6-8 and 6-9 that the separation efficiency does not change significantly after 30 minutes of processing, a separation time of 30 minutes was chosen to compare the effects of different vibration modes on the separation efficiency and cut-point. Figure 6-10 compares the separations obtained for the three vibration conditions used, for tracers in the size range -4.0 +2.0 mm, and Figure 6-11 compares the ρ_{50} and E_p for the three vibration conditions for all three size fractions of tracer particles.

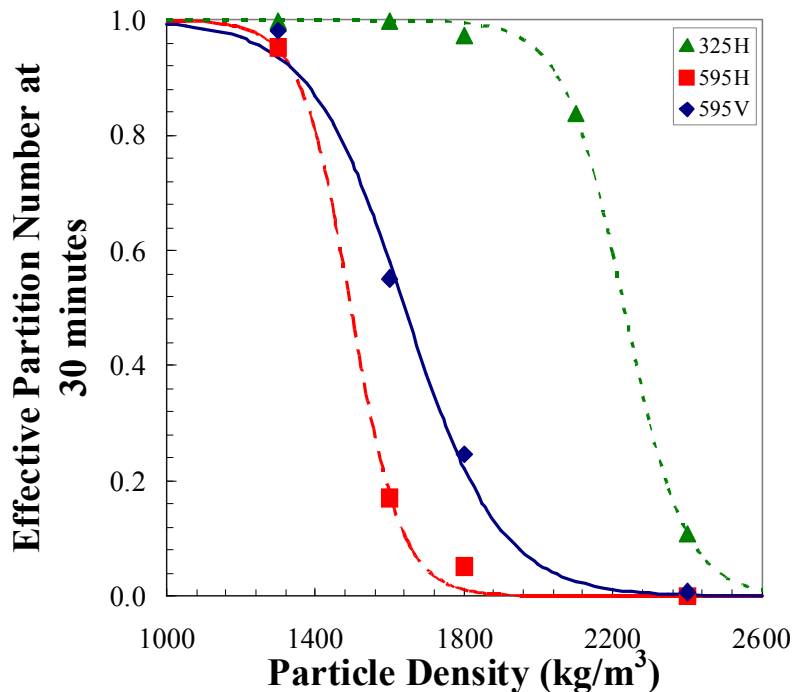


Figure 6-10: Effective batch partition curves after 30 minutes processing for -4.0 +2.0 mm tracer particles at the three vibration conditions 325H, 595V and 595H, sand feed rate of 0.0050 kg/s and gas flowrate of $3.22 \times 10^{-4} \text{ m}^3/\text{s}$. The data points show the experimental data and the curves are the best fit of Equation (4-1) to the data.

The direction and frequency of the vibration have an impact on the separation density but for the size range -4.0 +2.0 mm there is very little effect on the separation efficiency evident in Figure 6-10. The fit of Equation (4-1) to the experimental data is generally very good. Note that each batch experiment only studied a single tracer density and vibration mode, so the results in Figure 6-10 are compiled from 13 experiments. The

self-consistency of the data further demonstrates how reproducible the experiments were (see Figure 6-4).

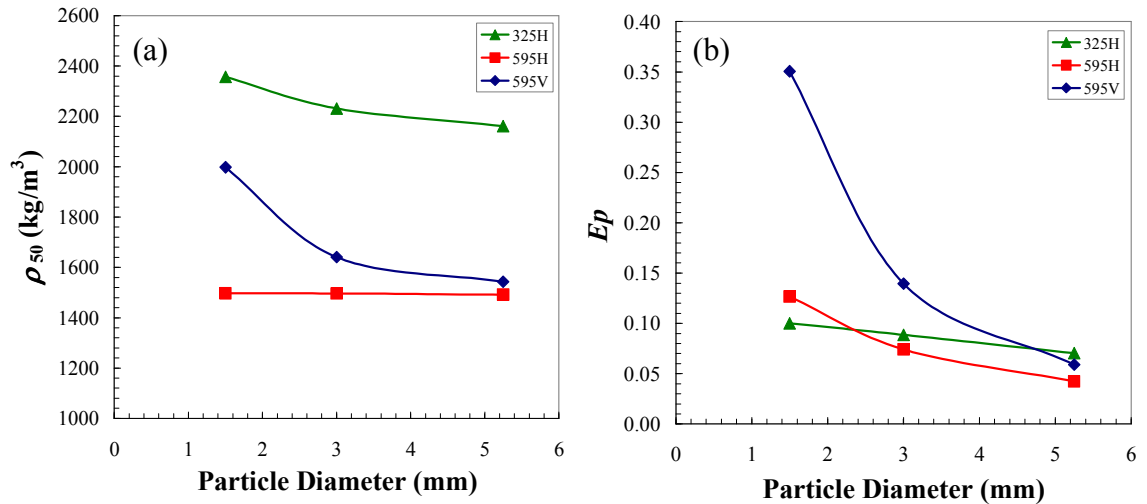


Figure 6-11: The effect of the different vibration conditions on the (a) ρ_{50} and (b) E_p for the three size fractions studied after 30 minutes of processing. Sand feed rate of 0.0050 kg/s and gas flowrate of $3.22 \times 10^{-4} \text{ m}^3/\text{s}$.

The density cut-point, or ρ_{50} , remained largely unchanged with particle size (Figure 6-11a). However, the E_p decreased significantly as the particle size increased (Figures 6-9b, 6-11b). This is consistent with the observation made in other dense-medium operations that the dense-medium effect is more pronounced for particles significantly larger than the dense-medium particles (Kelly & Spottiswood, 1982).

There are at least two theories of how fine particles in suspension can act as a dense-medium. Fine particles increase the effective density of the suspension experienced by coarser particles. That is, the fine particle suspension acts as a pseudo-fluid (Choung et al., 2006) on the larger particles, enhancing a density separation. Alternatively, fine particles can transfer some of their momentum to larger particles thus providing an upwards force on particles that would not exit the bed under the flow of the fluidising gas alone (Geldart, 1973; Choi et al., 2001).

Although the dense-medium effect partially accounts for the lower E_p s of the largest particles another factor that cannot be ignored is the two velocities that act on the particles; the medium convective velocity and the particle buoyant velocity. Particles of

all sizes and densities experience the same medium convective velocity, however the buoyant velocity depends on both the particle size and density relative to the medium. Because the larger particles have a larger buoyant velocity than the small particles, the effect of the medium convective velocity is dampened resulting in a more efficient separation. This is further discussed in Section 6.5.1.

The frequency and, to a lesser extent, the direction of the vibration clearly affect the cut-point density of the separation. The low frequency 325H vibration has a much higher cut-point than the 595V and 595H vibration cases. If the separation were due only to a dense-medium effect then that would imply that the 325H case had a higher medium density than the 595V case.

The mass of sand contained in the Reflux Classifier was higher for the 595V and 595H vibration cases than for the 325H case (Figure 6-3 and Table 6-2). Superficially, this suggests that the bed density was lower for 325H than 595V, opposite to the above inference based on the separation density. However, the density of the emulsion phase is what is significant to the separation, and this density is determined by the volume of gas present to fluidise the medium. Both the gas flowrate and vibration affect the emulsion phase density.

Vibration acts to fluidise the bed (Wang et al., 1997; Marring et al., 1994) as well as break up the bubbles. So it is likely that the increased frequency caused the emulsion density at minimum fluidisation to be lowered. Thus, it is expected that as the vibration frequency increases, the emulsion phase density decreases resulting in the observed lower cut point.

The cut-point density, as shown in Figures 6-10 and 6-11, is not a true measure of the separation performance of the air-sand dense-medium Reflux Classifier with vibration. The ρ_{50s} are based on data for effective partition curves from batch experiments, not true partition curves from continuous experiments, and hence are dependent on the processing time as discussed in Section 6.4.6 above.

What can be concluded from the batch partition curves is the ease with which particles of a particular size and density are transported through the bed. A high cut-point in the batch partition curve indicates that particles are more easily transported to the overflow of the bed than in a separation with a lower cut-point. The high ρ_{50} values for the 325H case demonstrate that particles of density as high as 2100 kg/m^3 will tend to elutriate while at a higher vibration frequency of 595V with a cut-point of about 1600 kg/m^3 , they will remain in the bed. That is, increasing the vibration frequency tends to suppress the transport of particles to the overflow.

An examination of the batch separation performance provides some insight into the behaviour of particles in the air-sand dense-medium Reflux Classifier with vibration. However, further work in a continuous system is required before conclusions can be drawn about the mechanism of the separation.

6.5 Two Parameter Model of Particle Velocity

The particle elutriation data were fitted to a two-parameter model for dispersed plug flow with open boundary conditions at each end (Levenspiel, 1972):

$$\dot{m} = \frac{U}{\sqrt{4\pi Dt}} \exp\left[-\frac{(L-Ut)^2}{4Dt}\right], \quad (6-4)$$

where \dot{m} is the tracer mass fraction elutriation rate (1/s), U the species velocity (m/s), D the dispersion coefficient (m^2/s), t the time (s) and L the length (m) of the Reflux Classifier, assumed to be the length of the vertical and inclined sections added together. The mass fraction elutriation rate is defined as the mass of particles elutriated in a time interval divided by the product of the time interval and the total mass of particles of that size fraction in the initial tracer charge. Equation (6-4) is a modified form of Equation (6-3) which is valid for open boundary conditions provided $D/UL < 0.01$, but it is also approximately valid for closed boundary conditions (Levenspiel, 1999).

The species velocity, U , is the velocity of a particle relative to the vessel and consists of two components; a convective velocity, U_{conv} , due to the movement of the medium and a slip velocity, U_{slip} , of the particle relative to the medium. This can be expressed as:

$$U = U_{conv} + U_{slip} \quad (6-5)$$

where a positive slip velocity implies that the particle rises faster than the medium and a negative slip velocity implies the particle sinks relative to the medium.

The Reflux Classifier apparatus used in these experiments has closed, not open, boundary conditions. The particles are unable to return to the bed if they exit at the overflow nor can they exit beneath the distributor plate. However, the experimental value of D/UL was always less than 0.01, which was within the limits of applicability of the model. Because the dispersion was low the differences between the open and closed systems would have been minimal. And so, because there is no analytical solution to the closed boundary condition case, this model was used despite its shortcomings.

Equation (6-4) assumes that all particles are free to leave the apparatus and that eventually all of them will if given sufficient time. In reality this is not the case as within the given experiment time of 54 minutes, 100% of the particles rarely exited the bed. In particular, for high density particles, the probability of particles exiting the bed is very low as they tend to migrate to the underflow which in the batch system does not exist, so they ended up accumulating/remaining on the distributor plate. Because of this, Equation (6-4) was not applied to experimental results where less than 50% of the particles had been elutriated.

Equation (6-4) applies to a uniform plug flow situation. However, the convective velocity in the apparatus was not constant. Below the feed point there was effectively no convective velocity of sand. Also one might expect that behaviour within the inclined channel will be different to that in the vertical channel. However, as the dispersion rates were not measured in each section, these could not be separately modelled. Hence, in order to simplify the analysis, the apparatus was effectively treated as a 3 m long black-box, ignoring the varied convective velocities and any effects of the incline. So this

analysis was only intended to provide a very general understanding of the bulk transport of particles through the system.

A typical model fit to the experimental data is shown in Figure 6-12 for the 1300 kg/m^3 particles with 595H vibration and 0.0050 kg/s sand feed rate. In spite of the questionable validity of some of the assumptions behind it, the model can be made to give a very good fit to the data. In each case there are two fitted parameters, the dispersion coefficient D and the species velocity U .

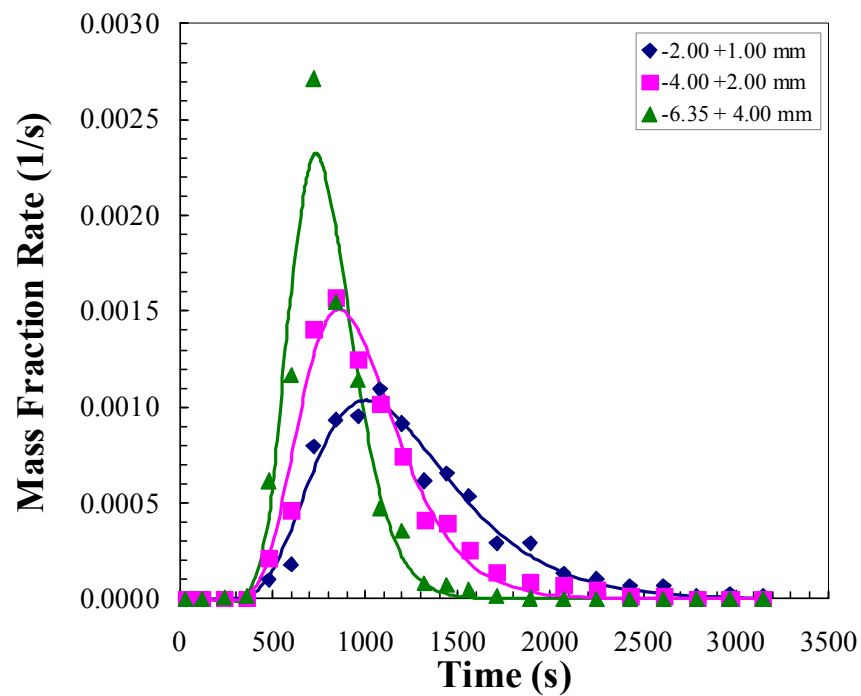


Figure 6-12: Two parameter fit of Equation (6-4) to experimental data for 595H vibration conditions and 1300 kg/m^3 density tracer particles.

6.5.1 Particle Species Velocity

By plotting the species velocity, U , for each size fraction, density and vibration condition, and extrapolating the data to zero particle size it was possible to infer the apparent convective velocity U_{conv} due to the movement of the medium through the system. Then, as shown in Equation (6-5), the slip velocity, U_{slip} , is the difference between the actual particle velocity relative to the vessel and the convective velocity relative to the vessel. This is illustrated in Figures 6-13 and 6-14.

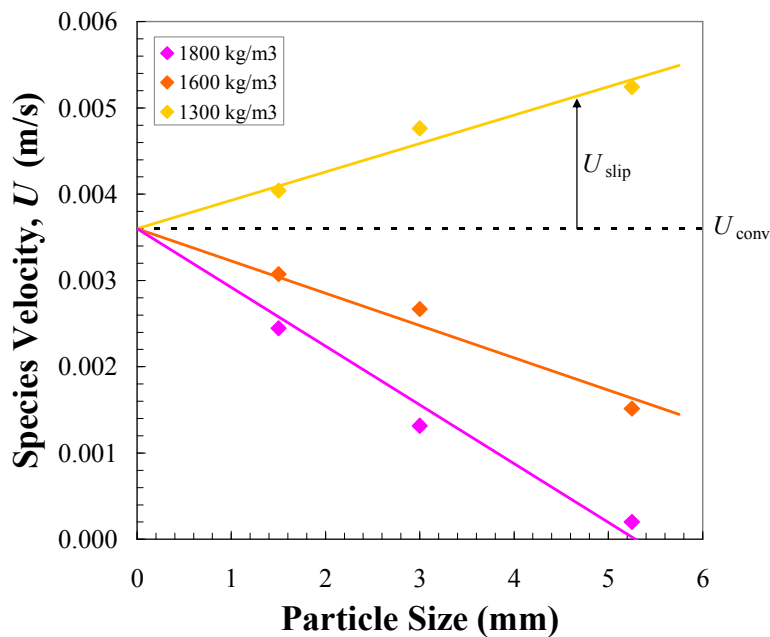


Figure 6-13: Species velocity versus particle size for 3 different tracer densities for 595V with a feed rate of 0.0050 kg/s. The trend lines are linear best fits to the species velocity data, all forced to converge at the same point at zero particle size, which is the inferred medium convective velocity. The slip velocity is the difference between the species and convective velocities.

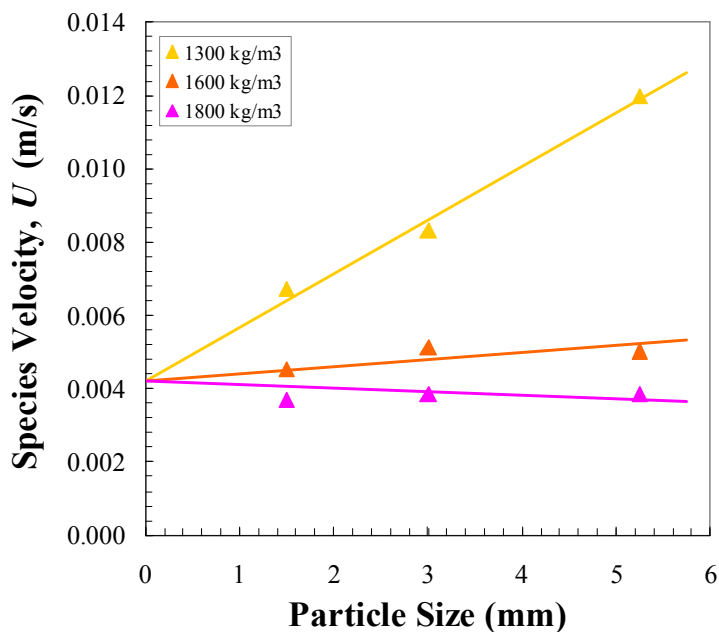


Figure 6-14: The species velocity versus particle size for 325 H with a feed rate of 0.0050 kg/s. The linear best fits were forced to intersect the ordinate at a single point.

Figure 6-13 illustrates the species velocity calculated by Equation (6-4), plotted versus particle size for the 595V vibration condition and Figure 6-14 gives the 325H case. In the 595H case Equation (6-4) was not applied because less than 10% of the particles had elutriated for all densities except the 1300 kg/m³ and so no results are reported. In Figure 6-13 and 6-14 the species velocities have been linearly extrapolated to the same point for all three particle densities. In both vibration cases, which had the same sand feed rate, the inferred convective velocity, $U_{conv,i}$, is approximately 0.004 m/s.

The theoretical sand convective velocity $U_{conv,t}$, is given by,

$$U_{conv,t} = \frac{\dot{M}_{feed} L}{M_{bed}} \quad (6-6)$$

where \dot{M}_{feed} is the rate of sand addition (kg/s), M_{bed} is the steady state hold-up (kg) of sand as given in Figure 6-3 and L is the total length of the apparatus (m). Equation (6-6) assumes that the entire mass of sand in the bed is involved, whereas in reality sand below the feed point is in a dead zone with zero convective velocity. This was neglected since the model assumes uniform conditions throughout the column. Adding sand at a rate of 0.0050 kg/s to a 3 m long column containing between 5.7 and 8 kg of sand corresponds to a convective velocity in the range 0.0026 to 0.0019 m/s. Although this is lower than the inferred value of 0.004 m/s, it is encouragingly of the same order of magnitude as the apparent value. And when the effect of the volume of sand below the feed point that does not contribute to the convective velocity is considered, the difference between the theoretical and inferred values will reduce. The inferred and theoretical convective velocities are given in Table 6-2.

In Figure 6-13, the slip velocity was positive and increased with increasing diameter for 1300 kg/m³ density particles but was negative and decreased for 1600 and 1800 kg/m³ density particles. These results suggest a dense-medium separation occurred with the medium density somewhere between 1300 and 1600 kg/m³. The inferred medium density, $\rho_{m,i}$ was determined using linear interpolation of the slope of the best-fit U line versus tracer density to estimate the density at which the slope was zero. For the 595V case, $\rho_{m,i} = 1440$ kg/m³ and for the 325H case $\rho_{m,i} = 1730$ kg/m³. These inferred medium

densities are given in Table 6-3 with the densities calculated from the partition curves and from the mass of sand in the bed.

Table 6-2: The theoretical and inferred convective velocities for the three vibration conditions with a sand feed rate of 0.0050 kg/s. The steady state mass of sand in the bed from which the theoretical velocity is calculated is also included.

Fluidisation State	Steady State Mass (kg)	Average Bed Voidage	Theoretical Convective Velocity, $U_{conv,t}$ (m/s)	Inferred Convective Velocity, $U_{conv,i}$ (m/s)
Not fluidised; no vibration	9.3	0.404		
Fluidised; no vibration.	6.3	0.618		
325H	5.7	0.638	0.0026	0.0041
595V	8.0	0.505	0.0019	0.0036
595H	7.5	0.528	0.0020	

Table 6-3: The average bed density, the inferred separation density using the slip velocities ($\rho_{m,i}$) and the separation density (ρ_{50}) for the three different tracer sizes calculated from partition curves after 30 minutes at the three different vibration conditions.

Fluidisation State	Average Bed Density ($\times 10^{-3}$ kg/m ³)	Inferred Separation Density, $\rho_{m,i}$ ($\times 10^{-3}$ kg/m ³)	ρ_{50} ($\times 10^{-3}$ kg/m ³) -2.0 +1.0 mm	ρ_{50} ($\times 10^{-3}$ kg/m ³) -4.0 +2.0 mm	ρ_{50} ($\times 10^{-3}$ kg/m ³) -6.35 +4.0 mm
325H	0.94	1.73	2.28	2.20	2.06
595V	1.29	1.44	1.87	1.65	1.55
595H	1.23	1.54	1.50	1.49	1.57

The average bed density, calculated from the mass of sand in the bed, has no relationship to the observed density of the system from the slip velocities, or the partition data. This, as discussed above, is because the average bed density does not take into account the distribution of the gas in the bubbles and emulsion. The inferred separation density from the slip velocities and the ρ_{50} s from the partition curves have good agreement, particularly in the high frequency vibration cases. This implies that the

determination of the partition curves and species velocities, while relying on assumptions, are both valid methods for analysing the batch elutriation data.

6.5.2 Empirical Correlation for Slip Velocity

The slip velocity calculated from the difference between the particle species velocity and the inferred convective velocity, as per Equation (6-6), was fitted to the following empirical equation by minimizing the square error,

$$U_{slip} = k(\rho_p - \rho_{m,i})^x d_p^y \quad (6-7)$$

where k , x and y are constants and $\rho_{m,i}$ is the inferred medium density as in Table 6-3. Equation (6-7) is of the same form as the equations for the calculation of the terminal velocity of a particle given in Table 3-1. Different values of x and y , corresponding to the Stokes', Intermediate and Newton's regimes were substituted into Equation (6-7) which was then fitted to the experimental data. For all three vibration conditions, the Intermediate regime provided the best fit to the data. This is unsurprising since the relationship between the diameter and slip velocity as seen in Figure 6-13 and 6-14 is approximately linear. The fit of Equation (6-7) in the Intermediate regime is illustrated in Figure 6-15, with k equal to 0.0254 with SI units, when $x = 5/7$ and $y = 8/7$, giving a correlation coefficient of 0.82.

What is most important to observe is that the relationship between the slip velocity and the particle diameter and density in Figure 6-15 is for data from all three vibration conditions. Thus the slip velocity is independent of the vibration direction or frequency, and depends only on the effective density of the medium and the particle diameter. That is, while the vibration affects the separation by determining the density of the medium, it does not appear to affect the movement of the particles relative to the medium.

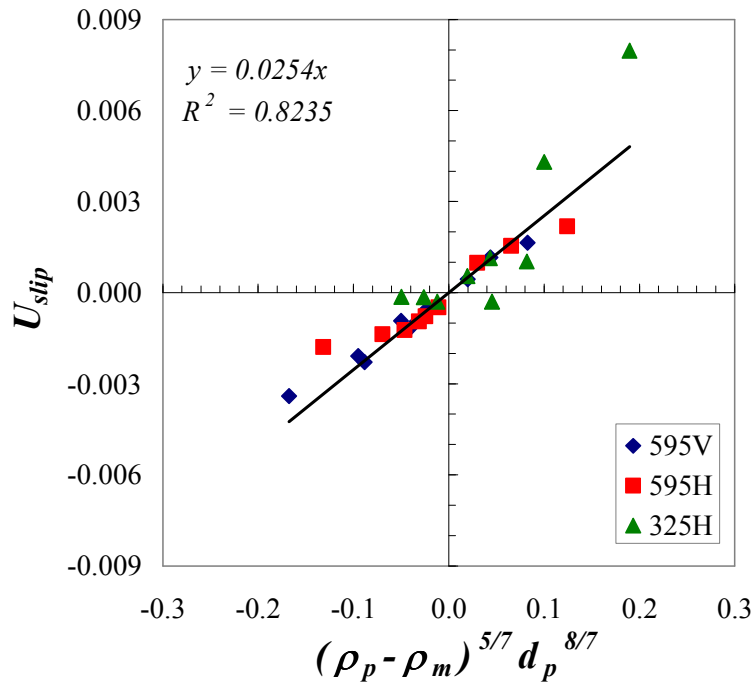


Figure 6-15: The relationship between the slip velocity and the particle size and density for three vibration conditions, particularly showing the independence from vibration frequency and direction.

The terminal free settling velocity of a particle in the Intermediate regime with diameter d_p and density ρ_p in a fluid of density ρ_f and viscosity μ_f was given in Chapter 3 as (Vance & Moulton, 1965):

$$U_{TFS} = 0.153 \frac{d_p^{8/7} (\rho_p - \rho_f)^{5/7} g^{5/7}}{\mu_f^{3/7} \rho_f^{2/7}} \quad (3-7)$$

From the relationship between $(\rho_p - \rho_f)^{5/7} d_p^{8/7}$ and the experimental slip velocity in Figure 6-15 it is possible to calculate the viscosity of the pseudo-fluid medium since

$$0.153 \frac{g^{5/7}}{\mu_f^{3/7} \rho_f^{2/7}} = 0.0256 \quad (6-8)$$

Thus the viscosity of the medium is calculated to be approximately 22 Pa s for all three vibration conditions. This is significantly larger than the viscosity of an air-sand

fluidised bed, indicated by Rees et al. (2007) to be approximately 1.0 Pa s for the sand used in this work. If a viscosity of 1.0 Pa s is substituted into Equation (3-7), the experimental slip velocity is 3.75 times smaller than the theoretical value. However, the calculation above does not take into account the significant effects of the narrow channel walls on the apparent viscosity and assumes that the particles are experiencing a true pseudo-fluid and reach their terminal velocity. It is also worth noting that the presence of de-fluidised sand particles in the emulsion phase would also affect the rise velocity of the particles.

Further work in a continuous system will need to be done to be definitive about the exact functional dependency of U_{slip} on particle density and size since the current data set does not show enough sensitivity to these two values. Further investigation may also provide confirmation of whether the particles reach their terminal velocity in the bed, which was assumed above. It may also provide insight into whether the overall behaviour of the particles is a combination of flow in two different regimes, one in the gas slugs and another in the upper region of the solid plugs as suggested in Chapter 5.

6.6 Summary

The separation performance of the batch air-sand dense-medium Reflux Classifier was assessed through a series of tracer particle experiments. The separations of the tracer particles proceeded largely on the basis of density, with some size effects. It was found that by vibrating the bed the error in the separation, Ep , was significantly reduced for the largest particles sizes although no improvement was observed smallest particles. The Eps for the vibrated system of between 0.04 and 0.16 are of the same order of magnitude as those accepted by industry for coal density separations.

The rate of particles exiting the bed was first-order dependent on their concentration, with a time delay due to the need for particles to migrate from the base of the bed to the overflow. Although this relationship is consistent with observations of the rate of elutriation of particles from a fluidised bed, further work needs to be done to better understand the mechanism that causes the particles to exit the overflow.

Effective partition curves were constructed from the elutriation data based on a fixed residence time. It was observed that a lower vibration frequency encourages denser particles to elutriate when compared to a higher vibration frequency. From these partition curves it was concluded that the batch air-sand dense-medium Reflux Classifier with vibration is capable of separating particles on the basis of density with high efficiency at the cut-point and Ep required for coal separations.

An empirical relationship between the particle slip velocity and the particle diameter and density was found to be of the same form as equations in the literature for the terminal velocity of a particle in the Intermediate regime. This allowed the calculation of the apparent viscosity of the medium pseudo-fluid. Further work needs to be done to confirm the relationship.

Further work needs to be done to characterise the effects of changing the gas rate, and determining what benefit, if any, the inclined channel above the fluidised bed provides. It is also important to investigate if the system can be used continuously, as this is necessary for it to be of any use industrially. That is the subject of the next chapter.

Chapter 7

Continuous Tracer Particle Separations

7.1 Introduction

It is clear from Chapter 6 that it is possible to obtain a good density separation in a vibrated Reflux Classifier when using a sand dense-medium in a batch operation. However, if the process is to be of any use in an industrial context, good separation performance also needs to be achieved in a continuous system. This chapter discusses the application of the pneumatic Reflux Classifier with a sand dense-medium described in Chapter 4 to a continuous steady state separation.

From the batch experiments conducted in Chapter 6 it was found that the density separations obtained in the air-sand dense-medium Reflux Classifier depended on the vibration rate. Without vibration the separation efficiency significantly decreased as particle size increased. It was also possible to calculate the particle slip velocities.

This chapter extends the work of the previous chapter into a system with continuous overflow and underflow removal, although still with a batch quantity of tracer particles. The aim is to determine whether and how underflow removal affects density separation performance. The effect of changing the gas rate is also investigated. Finally, the performance of the Reflux Classifier is compared with that of a vertical section of the same total length, in order to establish whether the incline plays a significant role in determining the separation performance.

From these experiments, a very clear picture is obtained of the main factors affecting the density separation, including: vibration rate and direction; underflow rate; gas rate; and system geometry. Hence, the best conditions for a continuous steady state separation of a coal feed are established.

7.2 Continuous Separation Methodology

The apparatus used in these experiments is described in detail in Chapter 4 and illustrated in Figure 4-3 and Figure 4-4. As in the batch experiments, the continuous Reflux Classifier had a 1080 mm vertical fluidised bed with a 1925 mm long inclined channel above. Below the fluidised bed the continuous gas distributor and pinch valves

were attached. The channel internal dimensions were 20×100 mm and sand and tracer particles were fed into the bed through a hose sealed by a pair of pinch valves. The bed was vibrated by two motors as described in Section 4.2.3.

The experiments undertaken in the Reflux Classifier were repeated in a vibrated vertical fluidised bed of length 3005 mm with the same underflow apparatus as the inclined bed. The work involving a vertical system provided a basis for assessing the benefits of the inclined section. The supporting frame was also modified to suit the changed arrangement. This allowed the effect of the incline on the separations to be studied (see Section 4.5.2).

Samples of plastic tracer particles were prepared into their density size fractions, as detailed in Section 4.3. To commence an experiment, the bed was filled with sand and then the gas and vibration were switched on simultaneously. When any excess sand had been elutriated, the feeding of the sand and the underflow removal were commenced. In all of the experiments the sand feed rate of 560 g/min was achieved by feeding 280 g twice per minute, with the vibration set at 595 rpm in the vertical plane. Once a steady overflow of sand was established, the sample of one density (all size fractions) of tracers was fed into the bed together with sand to make up the same volume as a normal 30 s feed increment. At this point samples of the overflow and underflow were taken at three minute intervals. The remaining samples of tracer particles were added at ten minute intervals, one density at a time, until all had been added. Sand continued to be fed at 30 s intervals and the overflow and underflow taken every three minutes until the vast majority of tracer particles had exited the bed, to a maximum experimental run time of two hours.

The air rate was varied between 4.03 and 5.64×10^{-4} m³/s and the underflow rate between 260 and 460 g/min. The air rate was measured using a gas rotameter in % of maximum flow. A flow rate of 4.03×10^{-4} m³/s corresponded to 25% of maximum flow. Experimental results are reported in terms of the rotameter % reading for simplicity.

Each overflow and underflow sample was screened at 710 μ m to remove the sand, which was then weighed. Any tracer particles in the stream were then sieved into their

size fractions, sorted and counted to determine the number of each size and density of tracer particles that were in that sample. This work provided information on the elutriation rates of particles, and therefore the slip velocities, as well as the overall partition curve for the experiment.

7.3 Inclined Bed Experimental Results

7.3.1 Sand Flow Pattern

Figure 7-1 illustrates the mass of sand exiting the bed through the overflow and the underflow in each three minute interval of an experiment. The underflow rate was constant because a fixed volume of material was removed in each time interval. The variability of the overflow reflects the slugging fluidisation in the incline. The upper surface of the bed in the incline was significantly below the overflow, with the slugs of gas causing it to rise and fall as they pushed up and broke through. Over time, the volume of sand in the bed increased until a bubble slug forced a large volume of sand into the overflow at once.

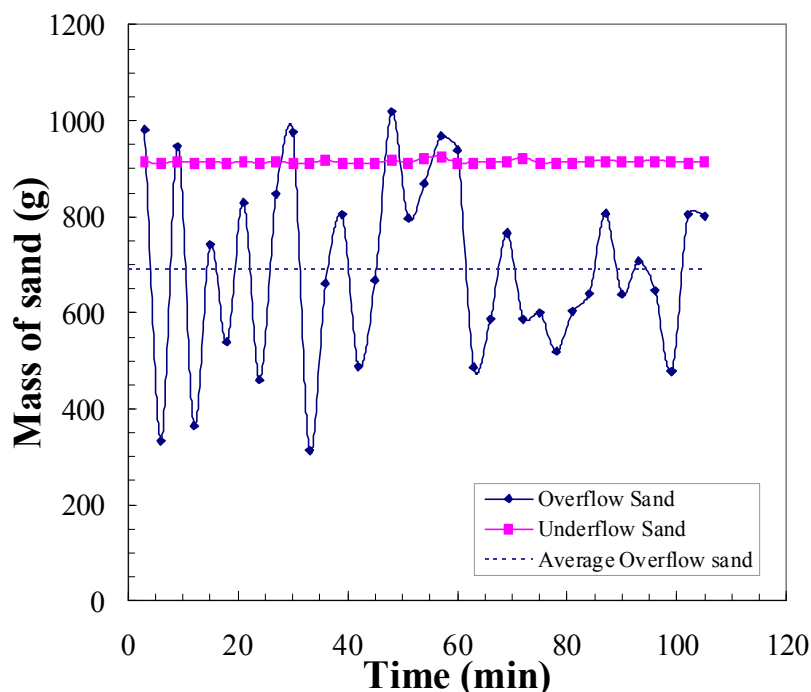


Figure 7-1: The mass of sand in the overflow and underflow in each three minute sample interval during an experiment. Lines are drawn to connect points and do not necessarily represent the actual trend. It can be seen that the underflow rate is very steady and the overflow rate varies significantly.

7.3.2 Partition Curve

Figure 7-2 shows a typical set of partition data for different size ranges of tracer particles in the inclined bed with a sand feed rate of 560 g/min (280 g per 30 s) and an underflow rate of 305 g/min (92 g per 18 s). These curves show the least square error fit of Equation (4-1) which was used to obtain the ρ_{50} and Ep values. The particle separation efficiency clearly increases with increasing particle size, consistent with observations made in Chapter 6. The separation cut-point, ρ_{50} , changes with tracer particle size. The ρ_{50} of the smallest particles is 1860 kg/m³ and of the largest particles, 1600 kg/m³. The trend of ρ_{50} changing with particle size is also consistent with the observations made in Chapter 6 and with density separations in the water-based Reflux Classifier (Galvin et al., 2002).

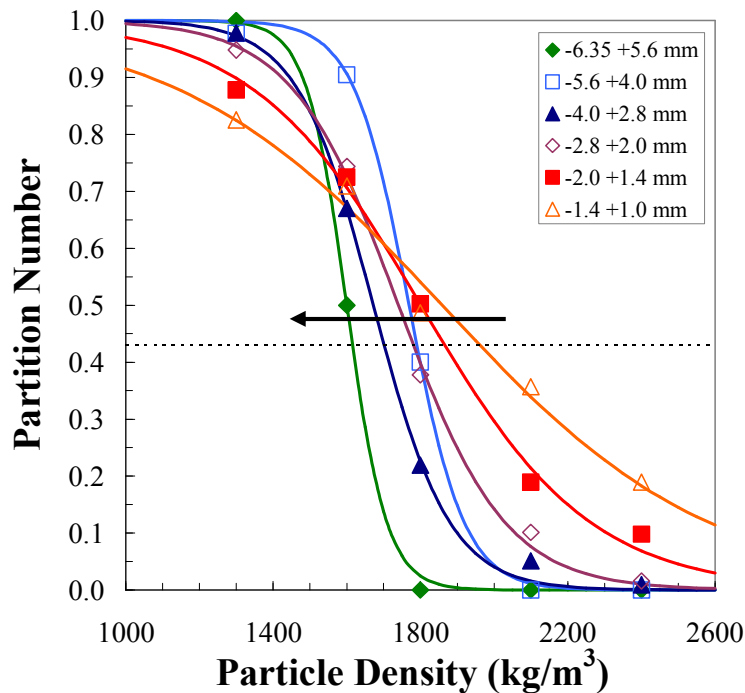


Figure 7-2: An example of the partition curves obtained in one experiment. Each data point represents the experimental partition of particles of a particular size and density that had exited the bed by the end of the experiment (that is, ignoring particles still in the bed). The curves are Equation (4-1) fitted to the data with the sum of the square errors minimised. The conditions were an inclined bed fluidised with a gas rate of $4.03 \times 10^{-4} \text{ m}^3/\text{s}$, a feed rate of 560 g/min and underflow rate of 305 g/min. The horizontal dotted line represents the partition to overflow that would be expected if the separation was based solely on convection of neutrally buoyant particles. The arrows on this and subsequent figures indicate the progression from small to large particles.

The change in the ρ_{50} and E_p with particle size is due to the effects of the density driven particle-buoyant velocity and the medium-convective velocity acting on the particles in the bed.

The buoyant velocity will more greatly affect larger particles than small ones. This is due in part to the dense-medium effect, where particles “see” the air-sand emulsion as a continuum rather than as discrete sand particles suspended in air, which is more effective on larger particles. Additionally, the buoyant force increases with particle size more rapidly than particle drag since it depends on volume, not surface area. As a result, the terminal rise/settling velocity of particles is greater for large particles than small particles and so large particles are more likely to overcome local turbulence than small particles, resulting in lower E_p s.

The medium-convective velocity is the same for all particles, as observed in Chapter 6. However, because the buoyant velocity of small particles is so low compared to large particles, the effect of the medium convective velocity is greater for smaller particles. That is, small particles are more likely to follow the flow of the medium than be separated according to their density, resulting in higher E_p s. In the extreme case, very small particles will experience no density based separation but will split in the same ratio as the sand medium.

The combination of the effects of the two velocities results in lower E_p s and less variability in the ρ_{50} with overflow rate for large particles than for small particles as.

7.3.3 Particle Retention

In some experiments, significant numbers of tracer particles were retained within the inclined bed. A sample distribution of particles remaining in the bed at the end of an experiment is given in Figure 7-3. This data was obtained by emptying the bed in small increments called ‘layers’ through the valves at the base and then analysing each layer for sand and tracer particle content. It is clear that the particles that were retained in the bed were concentrated towards the base of the incline and that it was mostly the largest particles that were retained. Furthermore, there was a high concentration of 2100 kg/m^3

density particles close to the base of the incline, a high concentration of 2400 kg/m^3 particles in the vertical bed and a high concentration of 1800 kg/m^3 particles half way up the incline. This suggests that there is also some density classification of the retained particles with the lower density particles residing higher in the bed. The higher concentration of 2100 kg/m^3 particles compared to 1800 kg/m^3 particles may be due to their 20 minutes shorter residence time in the bed.

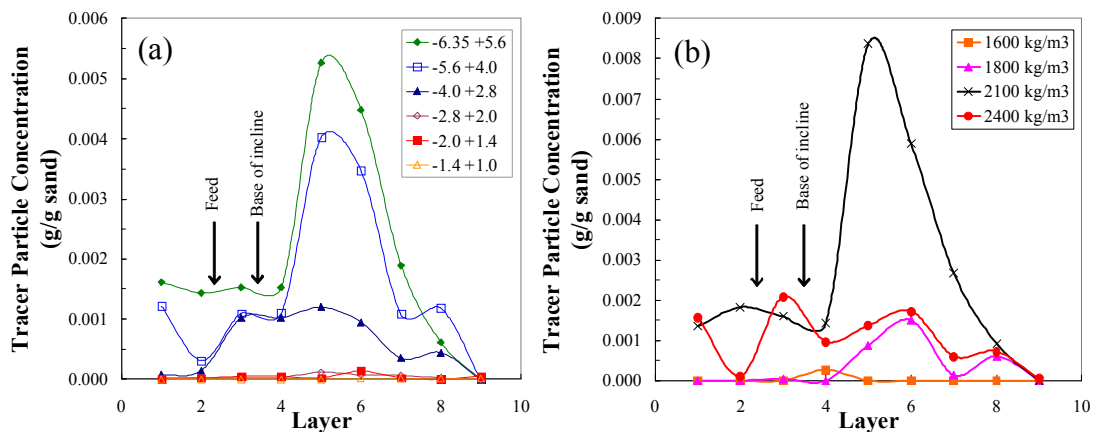


Figure 7-3: The distribution of tracer particles by (a) size fraction and (b) density in the inclined system at the end of an experiment, where Layer 1 is at the base of the bed and Layer 9 is at the top, showing the approximate positions of the feed inlet and the base of the incline based on an even distribution of sand throughout the bed. An accumulation of particles partway up the incline is observed. Lines are drawn to connect the points and do not necessarily reflect actual trends.

In the water-based Reflux Classifier with a batch feed, particles also can become trapped in the inclined section of the bed. This is because the convective velocity of the water in the vertical direction is lower in the inclined bed than in the vertical bed, as can be seen from the geometry. So particles with terminal settling velocity between these two velocities will flow into the incline but then settle out and return to the vertical bed, thus becoming trapped in the system. The similar retention of particles in the apparatus used in this thesis could be due to the same refluxing mechanism.

The retention in the water-based Reflux Classifier tends to be for small, high density particles and large, low density particles, while in the pneumatic Reflux Classifier it was the large, moderate density particles and middle sized high density particles that were retained. This is likely due to the higher density of the dense-medium in the pneumatic

Reflux Classifier causing a shift in the size and density of the particles retained. The 1300 kg/m^3 particles were not retained in the system because they had a lower density than the medium and were not prone to refluxing.

Retention of particles was observed in experiments with a very low overflow rate. The particles retained were mostly the larger 1600 , 1800 and 2100 kg/m^3 density particles. Hence particles may be retained in the bed due to there being insufficient sand to transport them through the overflow or they may be trapped within the incline due to an equilibrium between their convective and buoyant velocities. If there was insufficient sand for transport the particles would congregate at the top of the bed, otherwise the particles would be spread throughout the incline as they were refluxed, with a concentration towards the base. Figure 7-3 suggests that it is a refluxing action, and not a lack of sand convective velocity that caused the retention of particles.

In the vertical system, where the same feed and underflow rates were used, a similar retention of particles was not observed, with very few tracer particles remaining in the bed at the end of the experiment. This further supports the theory that particles reflux in the incline. The refluxing of the coarse particles suggests that in a continuous steady state system there would be an initial accumulation of particles in the incline before a steady state concentration is reached.

In Figure 7-2 the data points were based only on the particles that had exited the bed at the end of an experiment. Because of the retention of particles there was a certain amount of experimental uncertainty associated with each data point. To quantify this uncertainty it was assumed that the particles remaining in the bed had an equal chance of reporting to the overflow or the underflow. Thus the probable distribution of retained particles at the end of an experiment was Gaussian. From a normal distribution, the 90% confidence range of the separation of the particles remaining in the bed was determined. This is illustrated in Figure 7-4 where the two dashed lines show the boundaries of the 90% confidence intervals (shown by the vertical error bars) fitted to Equation (4-1). Thus, the experimental error associated with the ρ_{50} can be determined as illustrated by the horizontal line at $PN = 0.5$.

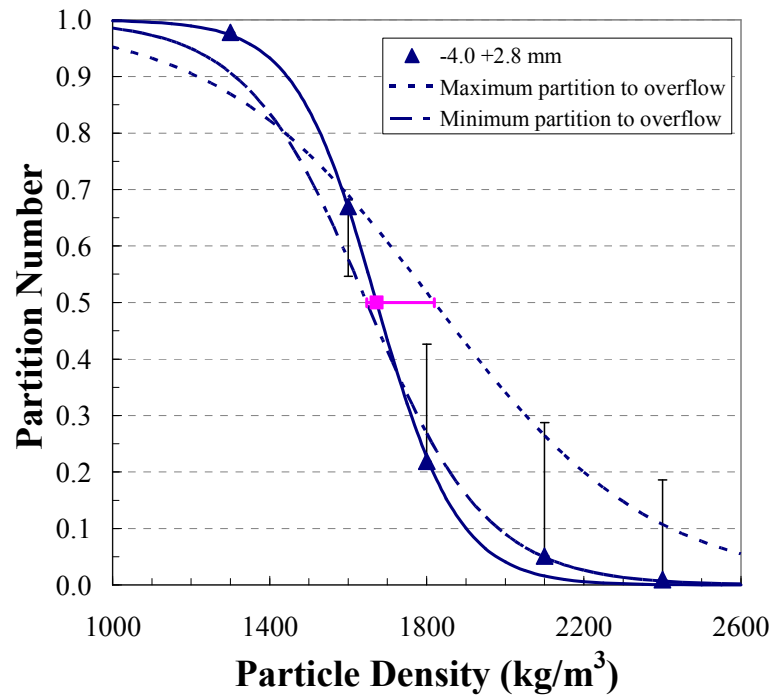


Figure 7-4: The determination of the experimental uncertainty associated with the calculated ρ_{50} for $-4.0 +2.8$ mm particles under conditions of an inclined bed fluidised with a gas rate of $4.03 \times 10^{-4} \text{ m}^3/\text{s}$, a feed rate of 560 g/min and underflow rate of 305 g/min. The triangular data points, with the vertical error bars, are the experimental partition numbers for the particles that exited the bed fitted with the smallest square error partition curve according to Equation (4-1) as in Figure 7-2. The vertical error bars represent the 90% confidence intervals of the final partition of all the particles, assuming each particle remaining in the bed has a 50% probability of exiting through the overflow. The more particles remaining in the bed at the end of the experiment, the larger the error bars. Two partition curves were fitted to these two scenarios, shown with dotted and dashed lines. So, the experimental ρ_{50} (shown with the square) could lie anywhere between these two other partition curve, giving the experimental uncertainty (shown by horizontal error bars).

7.3.4 Effect of Overflow Rate

The experimental values of the ρ_{50} , calculated using Equation (4-1) as seen in Figure 7-2, are shown in Figure 7-5 for the full range of overflow conditions. This is repeated in detail in Figure 7-6 for each size fraction individually to show the error bars. The data points in Figures 7-5 and 7-6 were fitted to a monotonically increasing empirical equation of the form:

$$\rho_{50} = Ax^n + C \quad (7-1)$$

where x is the dimensionless ratio of the mass of sand in the overflow to mass of sand in the feed and n , A and C are fitted constants (kg/m^3). This relationship was chosen since the ρ_{50} increases as the overflow rate increases. It is noted that the value of n increases with increasing particle size, reflecting the change from a convective velocity driven separation for small tracer particles, when $n \approx 2$, to a buoyancy driven separation for the larger particles when $n \approx 7$. The values of A , C and n are given in Appendix H.

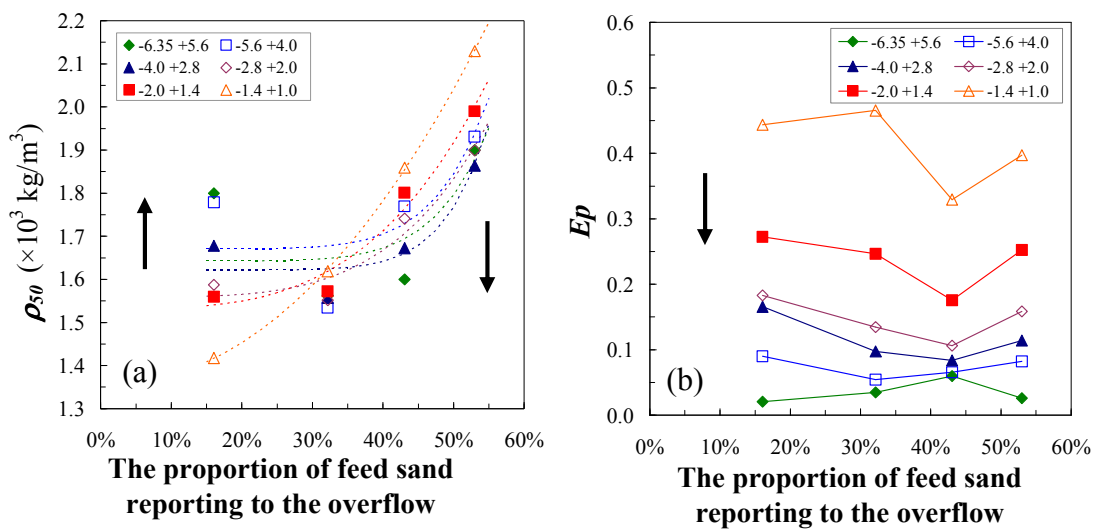


Figure 7-5: Fitted (a) ρ_{50} and (b) Ep values versus the ratio of the mass flowrate of sand in the overflow to sand in the feed (i.e. the variable x in Equation (7-1)).

Figure 7-5a clearly shows that the ρ_{50} varies less as the particle size increases, showing the decreased dependence on the convective velocity as the buoyant velocity dominates. This is also reflected in the reduction of the Ep values (Figure 7-5b) with increasing particle size.

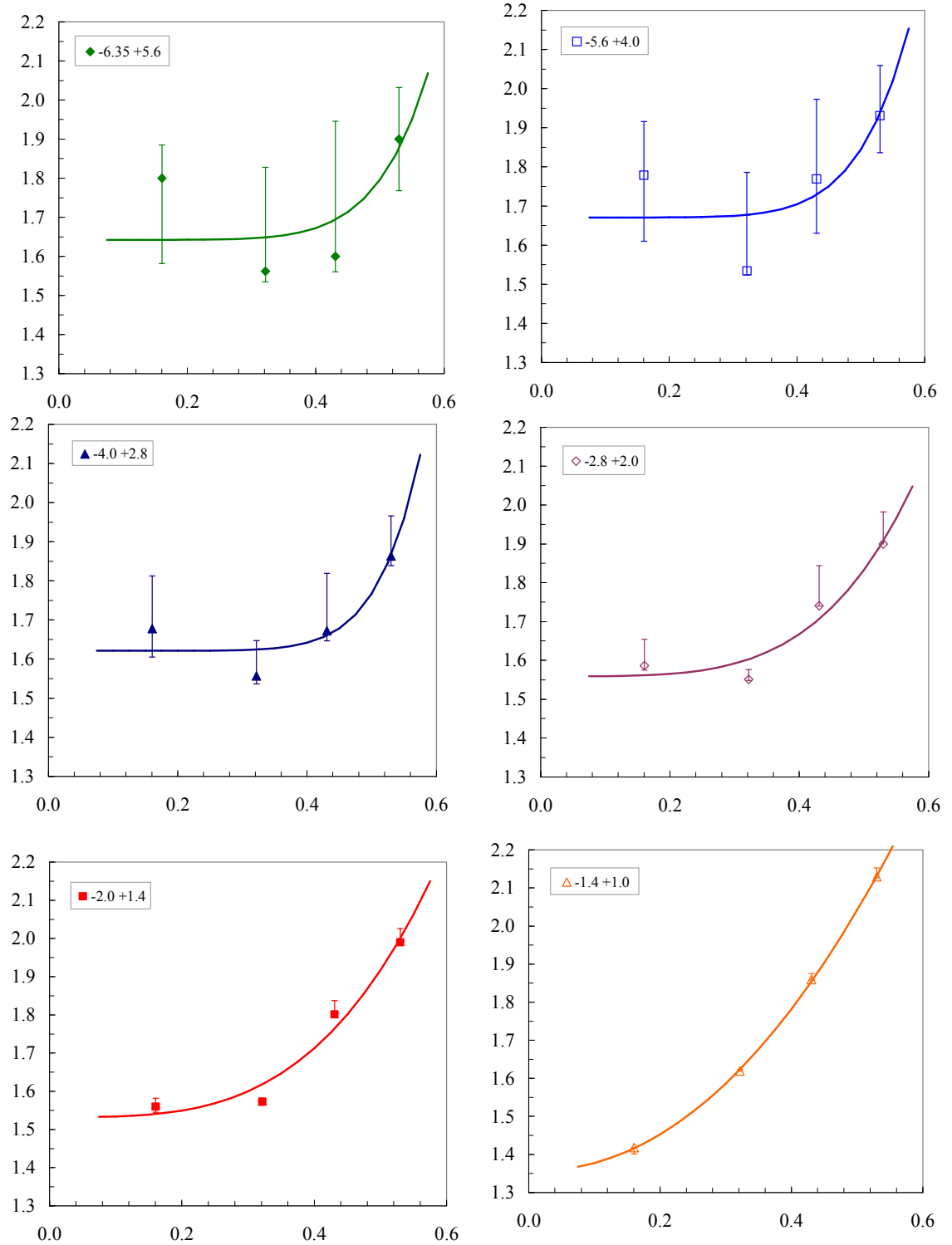


Figure 7-6: The relationship between the p_{50} (ordinate) and the proportion of feed reporting to the overflow (abscissa) showing 90% confidence error bars as in Figure 7-4. The experimental data is fitted according to Equation (7-1).

7.3.5 Effect of the Gas Rate

It was noted in Chapter 5 that increasing the gas flowrate caused the size of the bubbles in the bed to increase with a corresponding increase in the variability of the medium. Decreasing the rate of vibration also increases the size of the bubbles and the variability of the system, as observed in Chapter 6. This had the effect of increasing the density cut-point of the separation. In the same way, increasing the gas rate also increases the ρ_{50} , as seen in Figure 7-7.

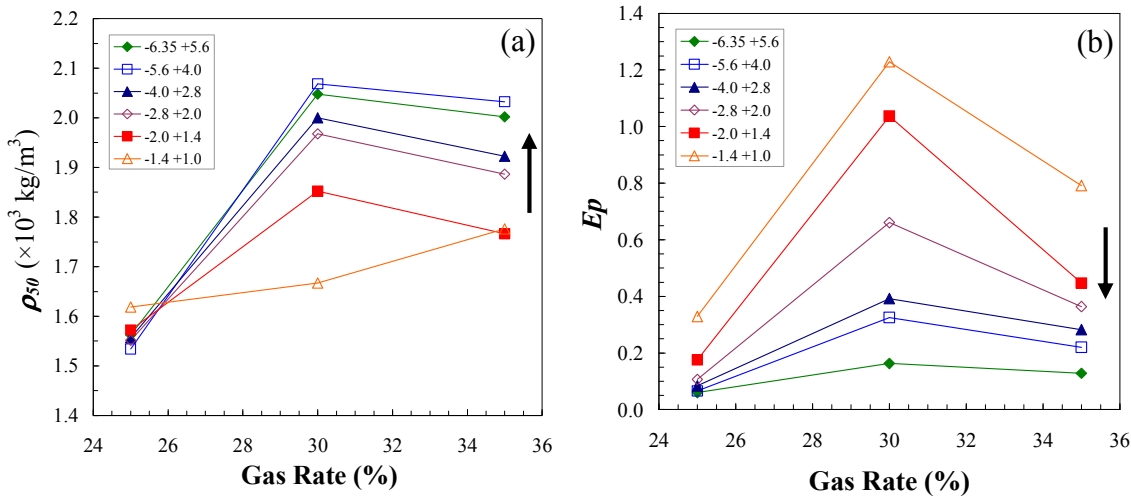


Figure 7-7: How the separation (a) cut-point (ρ_{50}) and (b) efficiency (Ep) vary with changes in the gas flowrate at a fixed overflow rate. From the figure it is clear that a gas rate of 25% produced the least variation in ρ_{50} with size and the lowest Eps .

Figure 7-7b shows an increase in the Ep with increasing gas rate, but then a reduction as the gas rate is further increased. The increase in the variability of the system, due to larger bubbles that have more inconsistency in their size, is expected to increase the Ep . It is not clear why the Ep peaks at a gas rate of 30%. However, it is clear that a low gas rate produces a better separation efficiency, and that the separation is less size dependent at a lower gas rate.

7.4 Vertical Bed Experimental Results

The effect of the presence of the incline on the separation was investigated by repeating the experiments described above in a vertical fluidised bed of the same length. The effect of the proportion of sand in the feed reporting to the overflow is illustrated in Figure 7-8, and the effect of gas flowrate in Figure 7-9.

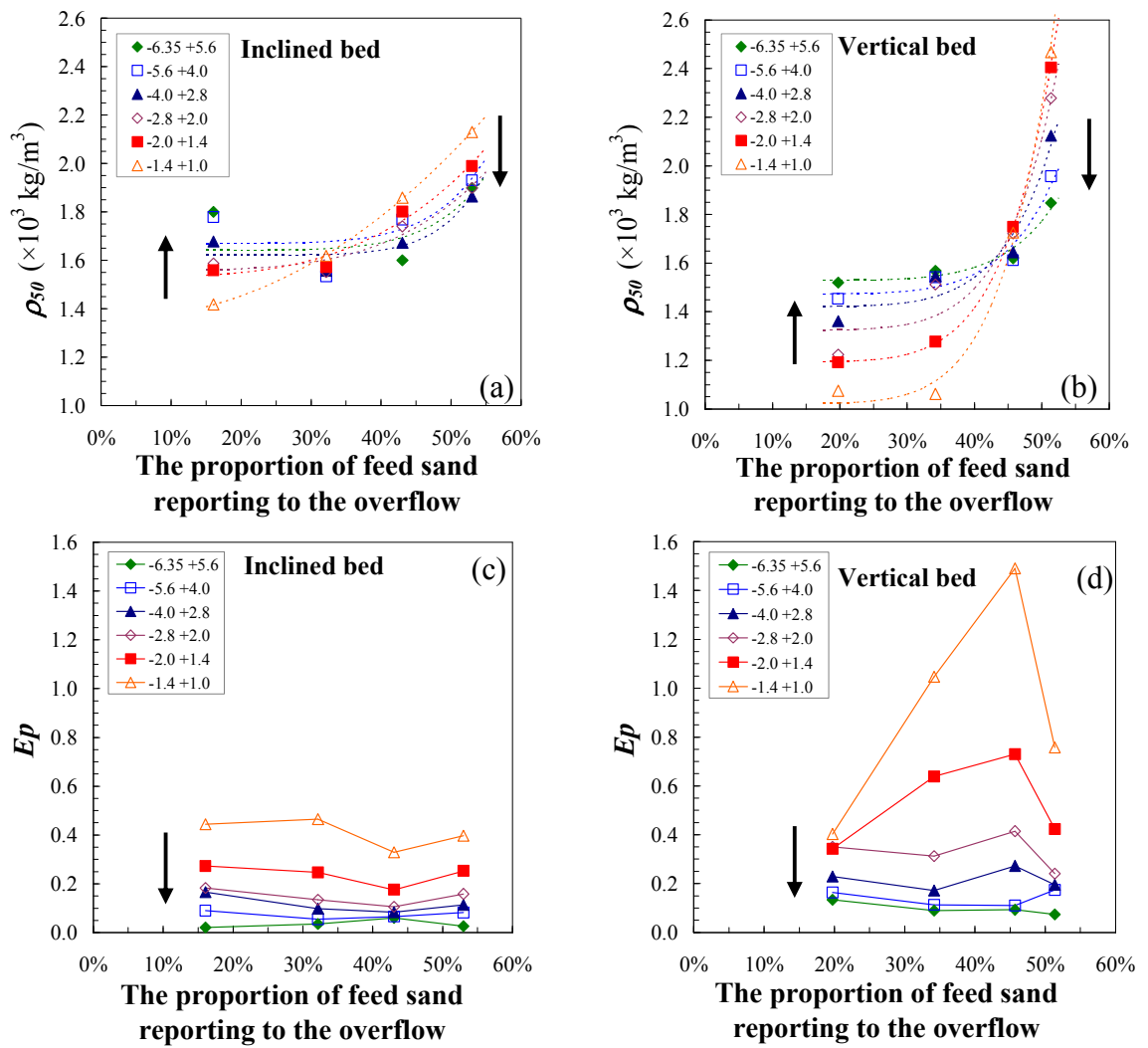


Figure 7-8: Comparing the (a) ρ_{50} in the inclined bed, (b) ρ_{50} in the vertical bed, (c) Ep in the inclined bed and (d) Ep in the vertical bed, with changes in the proportion of feed sand reporting to the overflow. The ρ_{50} data have been fitted with the minimum sum square errors equation of the form $y = Ax^n + C$. For the inclined system, $2 \leq n \leq 7$, for the vertical system $n = 6.8$.

Figure 7-8 and 7-9 show that the presence of the incline acts to stabilise the separation. This is clear from the increased variation in the ρ_{50} over the same range of overflow and gas rate conditions in the vertical system (Figure 7-8b and Figure 7-9b) when compared to the inclined system (Figure 7-8a and Figure 7-9a). In addition, the inclined system consistently has a lower Ep , and thus higher separation efficiency, than the vertical system. This leads to the conclusion that the inclined system provides a more stable and efficient arrangement for separating particles on the basis of density.

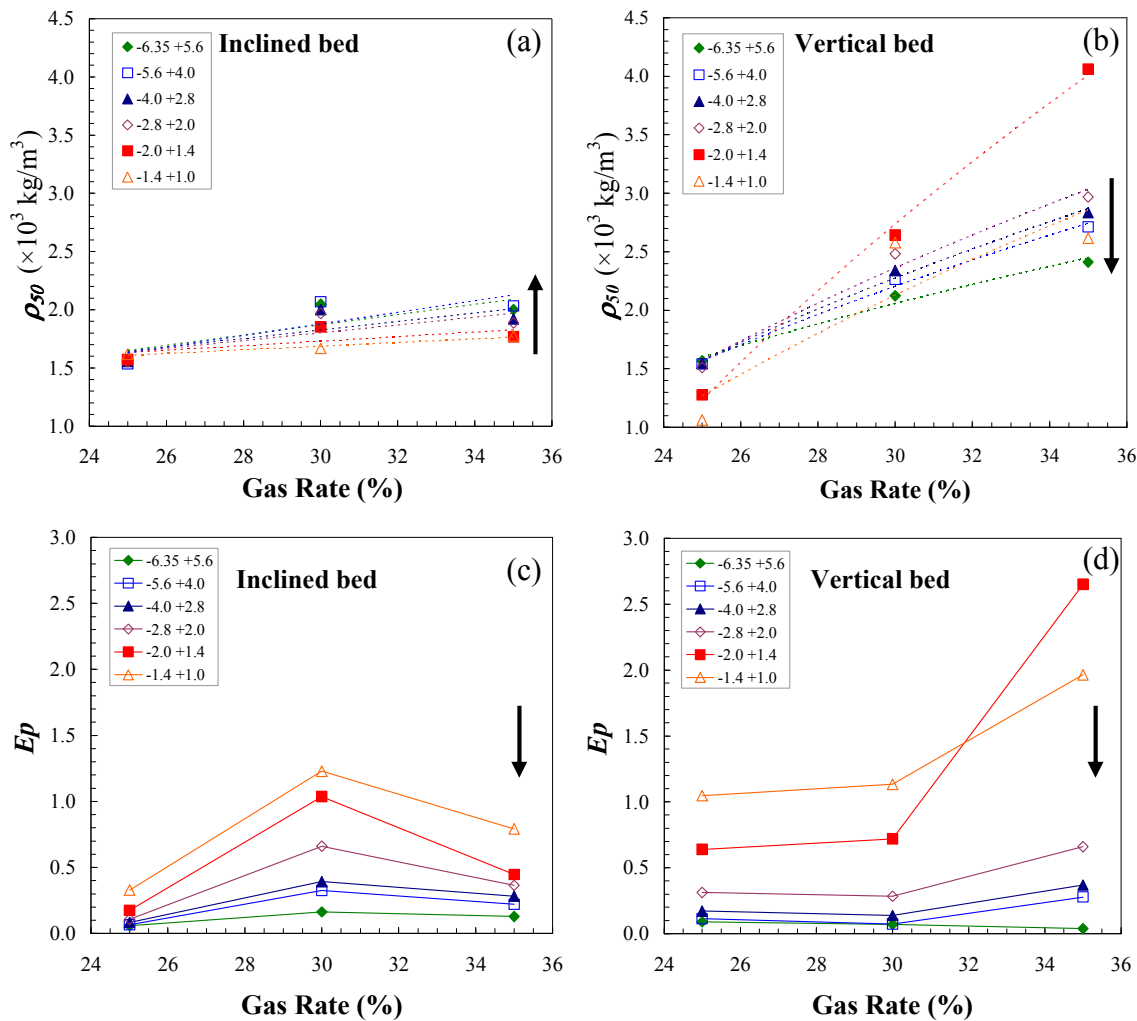


Figure 7-9: Comparing the (a) ρ_{50} in the inclined bed, (b) ρ_{50} in the vertical bed, (c) Ep in the inclined bed and (d) Ep in the vertical bed with changes in the gas flowrate.

The incline causes a refluxing of particles, as noted in Section 7.3.3, particularly of the largest particles. This refluxing is not observed in the vertical system, as seen in Figure 7-10 which illustrates the rate of elutriation of particles of density 1600 kg/m³ from the

vertical and inclined beds. In the inclined bed, the largest particles are mostly retained in the bed, while the smallest particles are elutriated within an hour. By comparison, the size of the particles in the vertical bed makes almost no difference to the elutriation kinetics, with particles of all sizes being elutriated at the same rate.

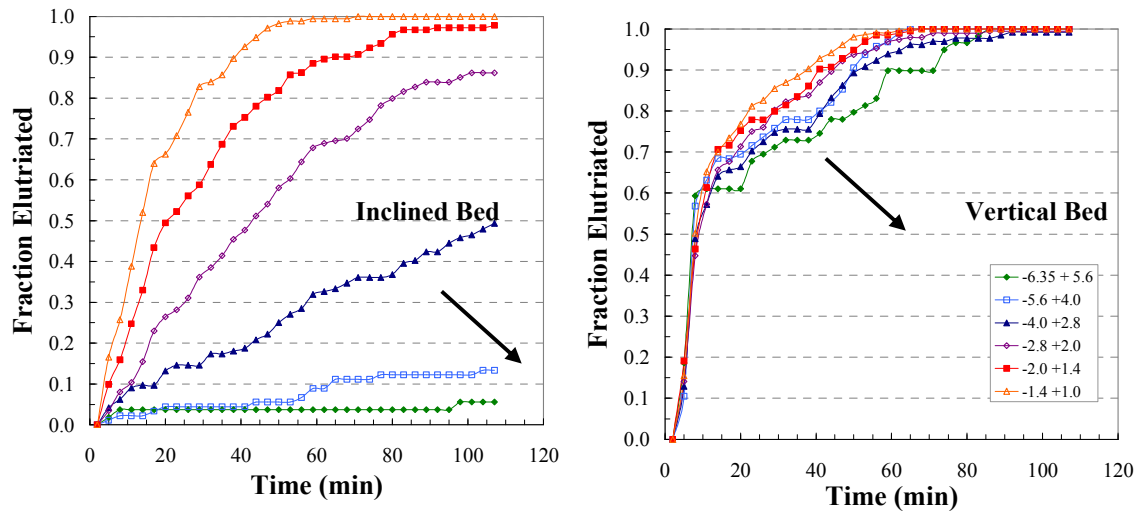


Figure 7-10: The rate of elutriation of 1600 kg/m^3 density particles from an inclined fluidised bed and a vertical fluidised bed with a gas rate of 25%, feed rate of 560 g/min and an underflow rate of 185 g/min.

The increased separation efficiency of the inclined bed, as observed in Figure 7-8 and 7-9 is due, at least in part, to this refluxing of particles that allows for a greater opportunity for misplaced particles to be reprocessed. In the vertical system particles that reach the top of the fluidised bed are most likely transported through the overflow, regardless of their density, without any opportunity for reprocessing. Thus, the addition of the incline provides an additional classification zone which results in an improved separation efficiency.

It was proposed in Chapter 5 that the separation of particles on the basis of density in the air-sand dense-medium Reflux Classifier is due to a jiggling action. A jiggling separation mechanism would certainly benefit from longer processing times and so the observed difference in separation efficiency between the inclined and vertical systems would support this theory. However, if the separation mechanism was similar to jiggling, the particles would be most likely to congregate at the top of the bed and not show the obvious signs of recirculation that are seen in the Reflux Classifier (Figure 7-3). In addition, the greatest change in separation efficiency between the vertical and inclined

beds occurs in the smallest particles which have the same residence times in both systems.

From the results of these continuous experiments, a new, two-stage separation mechanism is proposed. The particles initially enter a bubbling fluidised bed where a preliminary density separation occurs due to the dense-medium effect. This separation is most effective on the largest particles. The particles that proceed above the feed point are then further classified in the slugging zone while those that proceed below are transported out through the underflow. The advantage of the presence of the incline in the secondary classification is that the particles have a longer residence period and a greater potential to re-enter the vertical fluidised bed for further classification before being transported out by the convective velocity of the medium as well as buoyancy effects.

7.5 Modelling the Particle Velocity

From the previous work in a batch system, (see Chapter 6) the velocity of the particles in the system could be modelled by an equation for dispersed plug flow from Levenspiel (1999):

$$\dot{m} = \frac{U}{\sqrt{4\pi Dt}} \exp\left[\frac{-(L - Ut)^2}{4Dt}\right]. \quad (7-2)$$

This method of analysis was again used in the continuous system to calculate the velocity of particles in both the overflow and the underflow streams. It was assumed that the length of the underflow stream was the distance between the feed point and the first underflow valve (860 mm) and the length, L , of the overflow stream was thus 2300 mm. It was also assumed that once particles entered one stream they did not reflux back through the stream or into the other path. Typical examples of the results obtained are shown in the following figures. The equation was only applied to streams where more than 25% of the feed reported to that stream.

As is clearly illustrated in Figure 7-11, the velocities of the particles in the vertical system as predicted by Equation (7-2) can be forced to converge to a single convective velocity within a reasonable margin of error. Considering the variability inherent in the vibrated, slugging fluidised bed the correlation of the results is very good. These results suggest that the particles are in the Intermediate flow regime which is consistent with the observation made in Chapter 6.

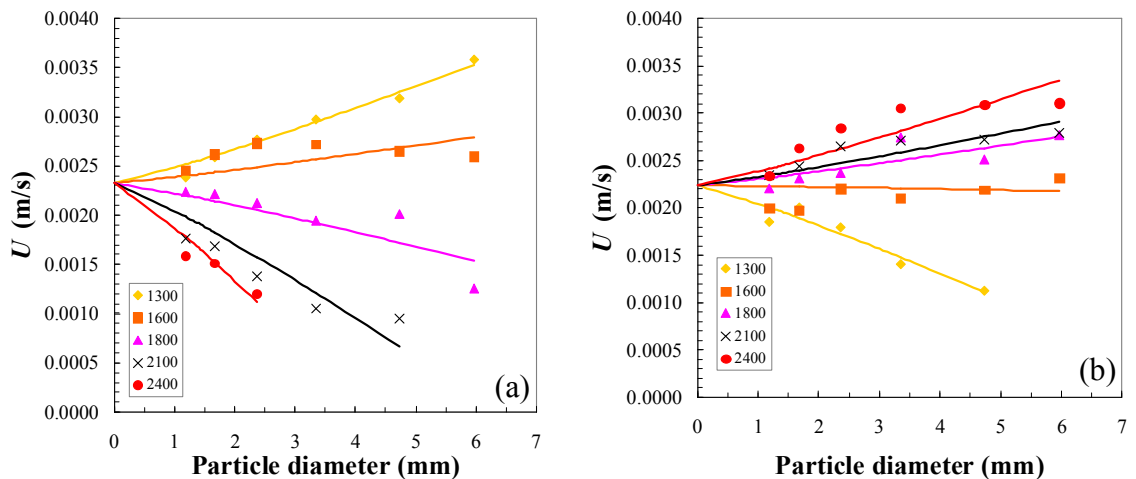


Figure 7-11: The species velocity in the vertical system, with a feed rate of 560 g/min, vibration rate of 595V and gas rate of 25%, as predicted by Equation (7-2) and fitted to an Intermediate flow regime model (that is dependent on $d^{1.14}$). (a) Illustrates the overflow stream converging to a single convective velocity of 0.0023 m/s with an overflow rate of 276 g/min. (b) Illustrates the underflow stream converging to a single convective velocity of 0.0022 m/s with an overflow rate of 114 g/min. Fitted lines forced to converge to a single point.

However, the good correlations seen in the vertical system are not observed in the inclined system. As can be seen in Figure 7-12, not only do the velocities not converge to a single convective velocity but they do not even fit the Intermediate regime model. This is due to the refluxing of particles that occurs in the inclined system. Why this refluxing did not seem to affect results in the batch experimental work is possibly due to the lack of an underflow that thus provided particles with only one option of travel, which was to the overflow.

It is clear, that the treatment of the system as a “black box”, while appropriate for the batch work and the continuous vertical system, is quite inappropriate for modelling the

continuous Reflux Classifier. While it is interesting to observe the lack of correlation between the batch and the continuous systems with regard to Equation (7-2) the most probable explanation is that the equation was designed for a system that did not experience any refluxing of particles (other than by dispersion) and had a convective flow of fluid in only one direction. The assumptions that were made when applying Equation (7-2) to the continuous system were too great for it to remain valid.

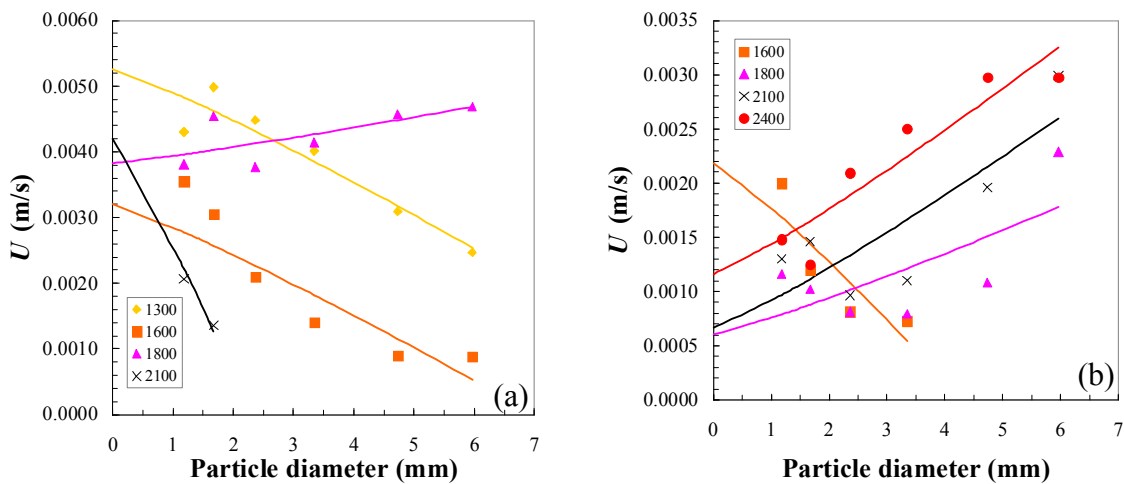


Figure 7-12: The species velocity in the inclined system, with a feed rate of 560 g/min, vibration rate of 595V and gas rate of 25%, as predicted by Equation (7-2) and fitted to an intermediate flow regime model (that is dependent on $d^{1.14}$) in (a) the overflow stream with an overflow rate of 297 g/min and (b) the underflow stream with an overflow rate of 176 g/min.

7.6 Summary

Density based separations of batch quantities of tracer particles were carried out in the air-sand dense-medium Reflux Classifier with vibration and continuous overflow and underflow removal. The effects of changing the overflow rate and the gas rate at a fixed rate of feed were determined. These results were compared with separations carried out in a vertical fluidised bed.

It was observed that increasing the overflow rate or the gas rate increased the density cut-point. The variation in the ρ_{50} was greatest in the smallest particles. The separation efficiency, measured with the Ep , increased with increasing particle size, consistent with observations made in Chapter 6. This is a clear indication of the dense-medium effect.

The vertical fluidised bed did not separate particles on the basis of density as effectively as the Reflux Classifier, although the observed trends with changing the overflow rate or gas rate were the same. The variation in the ρ_{50} was also greater for the vertical system than the inclined system.

The determination of the velocity of the particles in the bed, using the dispersed plug flow equation of Levenspiel (1999) as in Chapter 6, is valid for the vertical fluidised bed, showing the separation is in the Intermediate regime. However, the assumptions needed to apply the equation are not valid in an inclined system that experiences significant refluxing.

It is possible to effectively separate particles on the basis of density, with minimal size effects, in the air-sand dense-medium Reflux Classifier with vibration. The Reflux Classifier performs favourably when compared with a vertical fluidised bed under the same conditions and there is clear evidence that the refluxing action observed in the water-based Reflux Classifier (Nguyentranlam & Galvin, 2001) also occurs in the air-sand dense-medium system.

Chapter 8

Application to Coal Separation

8.1 Introduction

In the previous two chapters it was shown that the air-sand dense-medium Reflux Classifier with vibration can be used to separate tracer particles on the basis of density in both batch and continuous configurations. The density cut-points and Ep values of these separations were in the range that would be appropriate for coal beneficiation.

This chapter is focussed on the separations achieved using a coal feed, with a continuous distribution of particle size and density. Batch coal separations were used to examine separation performance as a function of particle size and vibration. The expectation was that the system should perform according to the batch tracer particle experiments. The batch separations were also compared with the separations performed by Walton et al. (2007) using a magnetite dense-medium. The second part of this chapter is concerned with separations of coal under continuous conditions. The gas rate, vibration frequency and feed and overflow rates were chosen from the continuous tracer particle work as those producing optimal density based separation conditions for coal.

8.2 Background

Prior to the density based separations of tracer particles that were the subject of the preceding two chapters, Walton et al. (2007) performed density based separations using a magnetite medium in a Reflux Classifier with a similar geometry to the one used in this thesis. Magnetite was a natural choice as it is the preferred dense-medium in the coal industry for water-based density separation. One of its advantages was that it is ferromagnetic and thus easy to recover from the coal product and gangue using a magnetic separator. Magnetite had also been the chosen medium in most of the previous studies on density separations of coal in air fluidised beds including by Luo et al. (2001; 2002a; 2003) and Fan et al. (2001).

Walton et al. (2007) used the magnetite dense-medium (-212 +150 μm) at a very low concentration of about 6.5 volume percent of the vessel. This, when combined with the experimental gas rates, provided the correct medium density for coal separation. At higher magnetite concentrations, Walton et al. (2007) found that the high density

mineral matter particles were transported to the overflow with the low density coal product. However, because such a small volume of medium was required, a concentration gradient of dense-medium in the inclined channels was observed, with the medium concentrating on the lower face of the channels and only the fluidisation gas present at the upper face.

To fluidise the magnetite medium in the incline, high gas rates were needed, which in turn emptied the bed of the medium within minutes of processing. As a result, Walton et al. (2007) found that several processing steps were required to achieve a good separation. The best approach involved reprocessing the product multiple times with the same inventory of magnetite but at progressively lower gas rates, resulting in gradual removal of the highest density material (see Figure 6-1).

It was thought that the effects of the inconsistent density of the medium, due to its low concentration, could be reduced by using a lower absolute density medium at a higher concentration resulting in the same overall medium density. As a result, in this thesis the magnetite medium was replaced with a sand dense-medium as discussed previously in Chapter 6. Sand is readily available and has a true density about half that of magnetite. The batch coal separation results obtained using the new sand medium reported below are compared with the best separations obtained by Walton et al. (2007) to determine if the new medium provided any benefit.

8.3 Methodology

The apparatus and materials used for the coal experiments are described in Chapter 4 and the experimental methods are given below.

8.3.1 Batch Coal Experimental Methodology

A riffled 300 g coal sample was mixed with an equal mass of sand. The Reflux Classifier was filled with about 6 kg of sand and the gas and vibration (if used) were commenced simultaneously. Sand was fed through the feed valves and hose in 200 mL amounts (~300 g) until a steady overflow was produced, that is, until the bed had

reached equilibrium capacity. The coal-sand mixture was then added in 200 mL amounts every 60 seconds until all had been added. After this, sand continued to be added at the same rate until the completion of the experiment. The overflow sand and coal were collected periodically throughout the experiment. When the experiment had been completed, the plenum chamber and distributor plate were removed and the bed emptied of sand and any remaining coal.

The overflow samples and the bed material were screened at 1.0 mm to remove the sand and the coal samples were sieved into their size fractions and analysed for mineral matter content.

8.3.2 Continuous Coal Experimental Methodology

Before commencing the experiment the coal was divided into ~18 g samples using a rotary sample divider. The Reflux Classifier was then filled with sand and the gas turned on to $4.03 \times 10^{-4} \text{ m}^3/\text{s}$ (25% of maximum flow). When the bed became fluidised, indicated by sand exiting the overflow, the vibration was introduced at 595 rpm, with the motors in vertical alignment as in the tracer particle experiments. The computer program controlling the feed and underflow valves was commenced, with the underflow valves opening initially every 12 s and the feed valves every 30 s. 290 g of sand was fed every 30 s until present in the overflow. At this point an 18 g coal sample was then mixed with 290 g of sand and this mixture fed every 30 seconds (a total feed of 36 g coal and 580 g sand per minute) until the completion of the experiment.

The overflow and underflow were collected every ten minutes. The sand was then removed through a 710 μm screen and the retained coal sample further separated into different size fractions. The masses of both the coal and sand samples were recorded.

The initial underflow valve opening rate of once per 12 s led to an overflow rate of 129 g/min, or an overflow to feed solids ratio of 0.223. After steady state had been reached at 80 minutes, the underflow removal rate was reduced to one opening every 15 s yielding an overflow rate of 221 g/min, and overflow to feed solids ratio of 0.381. At

170 minutes the underflow valve rate was again reduced to once every 18 s for an overflow rate of 279 g/min and overflow to feed solids ratio of 0.481.

At the end of the experiment, when the gas and vibration had ceased, the bed was removed gradually through the underflow valves to obtain a picture of the distribution of material in the bed at steady state.

8.4 Batch Coal Results

The sand medium behaved quite differently to the magnetite medium. It was present at a high concentration, or dense phase, and so in the sand plugs there was no concentration gradient in the direction perpendicular to the inclined channel. As discussed in Chapter 5, there was a concentration gradient in the gas slugs. The fluidisation gas rates required when using the sand medium were 7 to 15 times lower than those used for the magnetite medium. In addition, the bed exhibited slugging fluidised behaviour with large, apparently packed plugs of sand medium separated by large gas slugs that filled the entire cross-section of the apparatus (see Section 5.3).

The separation of coal in the vibrated, pneumatic Reflux Classifier with a sand dense-medium is illustrated in Figure 8-1. This separation is compared with the best of the multiple stage coal separations using a magnetite medium from Walton et al. (2007), who used the same coal feed, and the coal washability data which represents the best possible separation that can be obtained on that coal sample.

The data for the separations in the Reflux Classifier with magnetite medium were obtained by analysing each of the six successive separation steps in two size fractions for ash content and then sorting by ash content and calculating the cumulative yield versus ash. For the sand medium separations, the data were obtained by taking the overflow at five different times throughout the batch run and, after separating into two size fractions, analysing for ash content. In both cases they were organised by ash content before calculating the cumulative ash percentage.

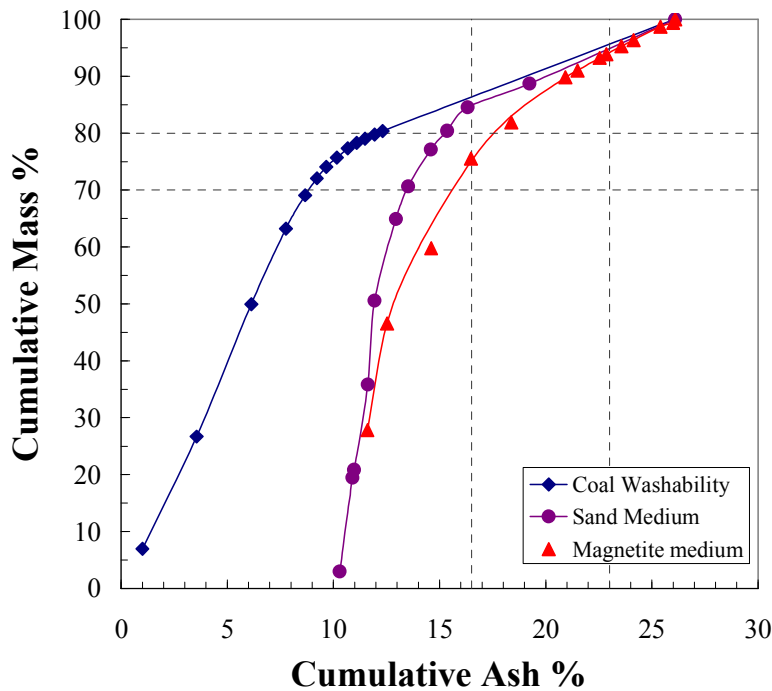


Figure 8-1: Compares a single stage coal (-4.0 +1.0 mm) separation in a sand medium with vibration with the coal washability data (-4.0 +1.0 mm) and a multi-stage magnetite medium coal (-4.0 +1.0 mm) separation without vibration.

It is clear from Figure 8-1 that changing the medium from magnetite to sand significantly improved the separation performance. The single stage coal separation with a sand medium and vibration is near ideal, closely following the coal washability separation, down to a yield of 85% (or cumulative ash of 16.5%) after which the separation efficiency rapidly decreases. However, the almost vertical nature of the separation curve at an ash of 11% between yields of 0 and 70% strongly indicates a dense-medium separation, as expected from the tracer particle experiments. In comparison, the multiple-stage magnetite medium separation deviated from the ideal separation below ash of 23%. Furthermore, in the yield range of 70 to 80%, the magnetite medium produced a coal product with a 3% higher absolute ash content than the sand medium. Thus it is clear that the sand medium with vibration provides significant benefits for coal separation when compared with a magnetite medium in the same apparatus.

Figure 8-1 shows that changing the medium from magnetite to sand and adding vibration allowed the separation design to be changed from a complex multistage

operation to a single stage split with an increase in separation efficiency. This is of particular advantage when considering industrial applications where a simple process is always preferred.

Once it was established that a sand medium performed much better than the original magnetite medium used by Walton et al. (2007), a range of experiments were undertaken to find the most favourable gas and vibration rates. A gas rate of $3.22 \times 10^{-4} \text{ m}^3/\text{s}$ was found to produce the best separation efficiency and it was clear that the addition of vibration improved the separation as seen in Figure 8-2 below. Two modes of vibration were used; 595V, as previously defined in Chapter 4, and 750M, which was vibrated at 750 rpm and the direction of the vibration alternated between predominantly vertical and predominantly horizontal. In both the 595V and 750M cases the axis of the centres of the motors was at 70° to the horizontal, that is parallel to the incline.

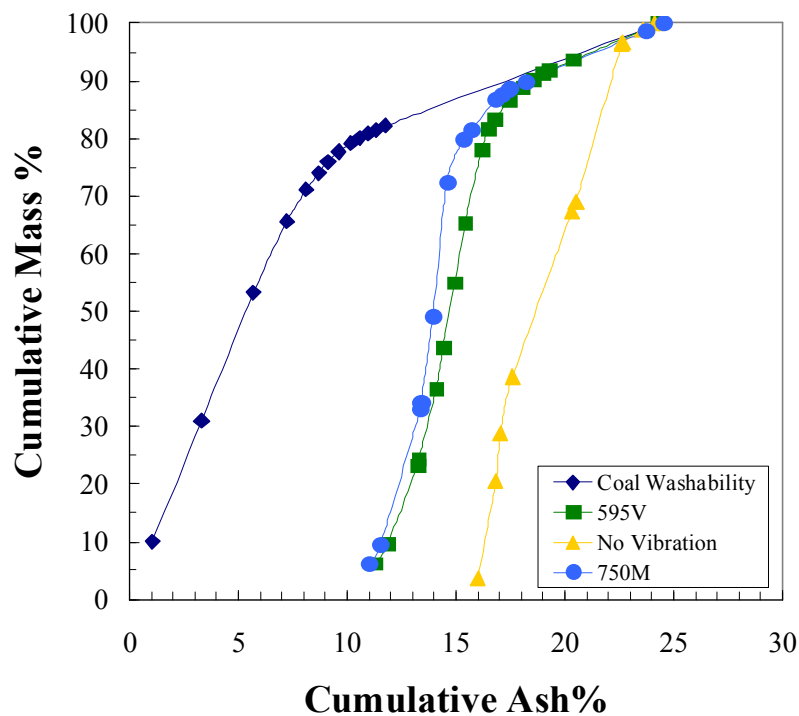


Figure 8-2: The effect of vibration on the separation efficiency of the air-sand dense-medium Reflux Classifier on coal in the size range $-4.0 +0.5 \text{ mm}$, comparing experimental results for No Vibration, 595V and 750M vibration conditions with the coal washability data ($-4.0 +0.5 \text{ mm}$).

The No Vibration case deviated almost immediately from the coal washability data while the two vibrated cases were near ideal until a yield of 90% and product ash of

about 17%. As in the batch tracer particle separations, the frequency and direction of vibration made a small difference to the separation performance with the 595V case performing slightly better than the 750M case. This however may be due to natural variation in the experimental results. Adding vibration reduced the actual ash content in the coal product by about 5%, which is a significant improvement in ash removal for the same yield.

Figure 8-3 shows the separation of the same coal as in Figures 8-1 and 8-2 over the size range of -8 +1 mm under vibration conditions of 595V. Up to a 78% yield, the separation performance provides an accurate match of the washability data, reducing the feed ash content from almost 30% to a final product of 15%. This excellent separation was achieved because, as was observed in Chapters 6 and 7, the separation of the largest particles is the more effective, typical of dense medium separations.

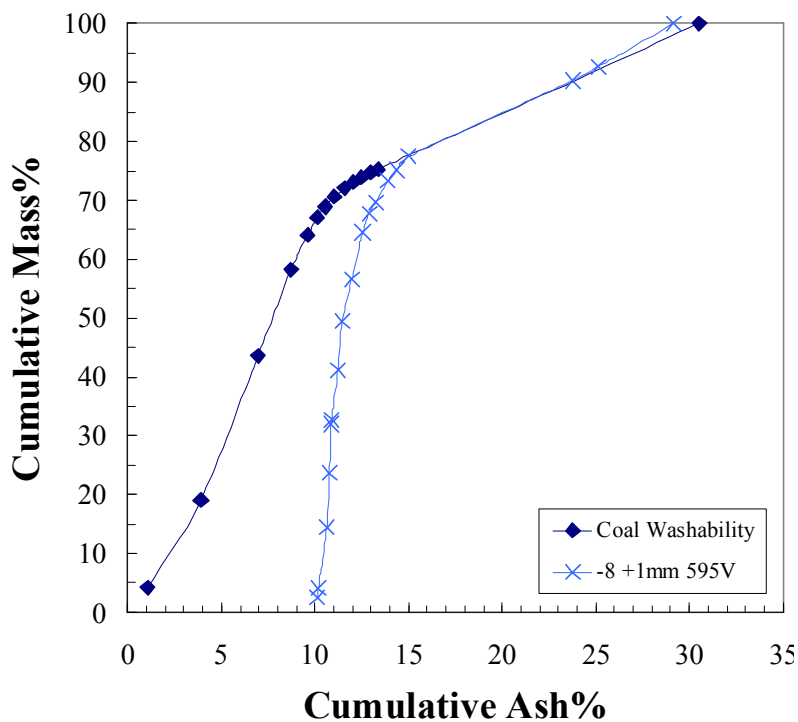


Figure 8-3: The separation achieved using the air-sand dense-medium Reflux Classifier system with 595V vibration on -8.0 +1.0 mm coal, compared with the coal washability data (-8.0 +1.0 mm).

8.5 Continuous Coal Results

The final aspect of the investigation into the behaviour of this unit was to determine if the performance observed in the tracer particle experiments of Chapters 6 and 7 was the same for a continuous coal feed.

It had been observed from the batch tracer particle work that vibration plays a key role in improving the separation efficiency of large particles and that the transport of particles to the overflow was suppressed at higher vibration frequencies. The continuous tracer particle separations showed that minimising the gas rate improved the separation efficiency and that the ρ_{50} could be controlled by the underflow rate. From all this knowledge the conditions for a continuous separation of coal in the air-sand dense-medium Reflux Classifier with vibration were chosen.

8.5.1 Approach to Steady State

From the work with the continuous system in Chapter 7 it was known that the rate of particle escape to the overflow was sporadic and therefore could not be used to determine when steady state flow had been reached. The steady underflow was monitored throughout the experiment and when the mass of coal in the underflow was consistent within 10% the system was assumed to be at steady state. The mass of coal and sand particles in the overflow and underflow streams is given in Figure 8-4. It can be particularly observed that after 70 minutes the mass of coal in the underflow only changed when the mass of sand in the underflow changed, indicating that the system quickly adjusted to new steady state conditions when the underflow rate was changed.

Figure 8-4 shows that steady state is never reached in the overflow, as expected. The underflow data indicate that the system was probably not at steady state at 70 and 80 minutes since there was a sudden drop in the mass of coal reporting to the underflow.

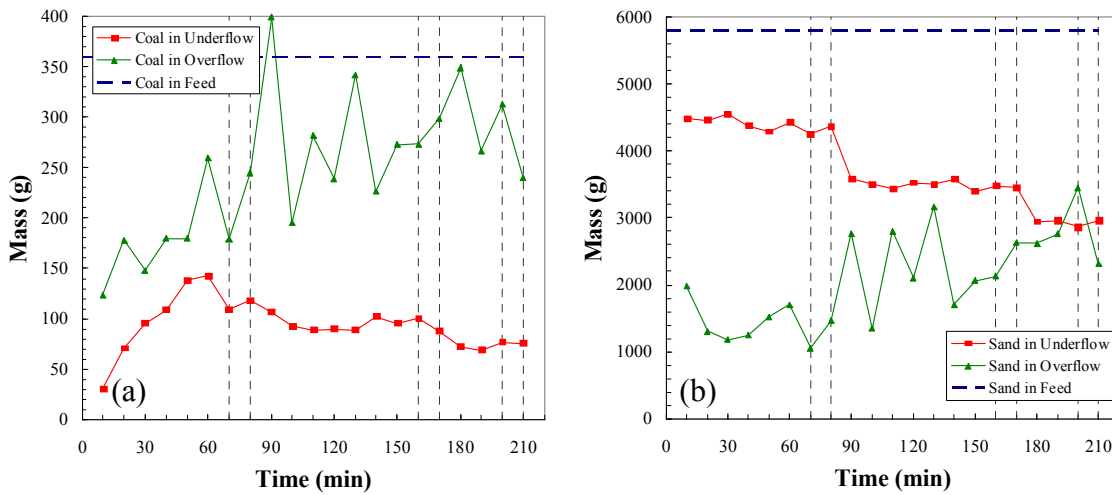


Figure 8-4: The changes in the overflow and underflow composition over time for (a) sand mass and (b) coal mass. In particular showing the approach to steady state at 70 minutes, 160 minutes and 200 minutes.

An alternative steady state condition is that the mass of particles of each size fraction in the feed is the same as the mass of particles in that size fraction exiting the bed. The rate of exit of particles on a mass basis from the bed for each size fraction is illustrated in Figure 8-5.

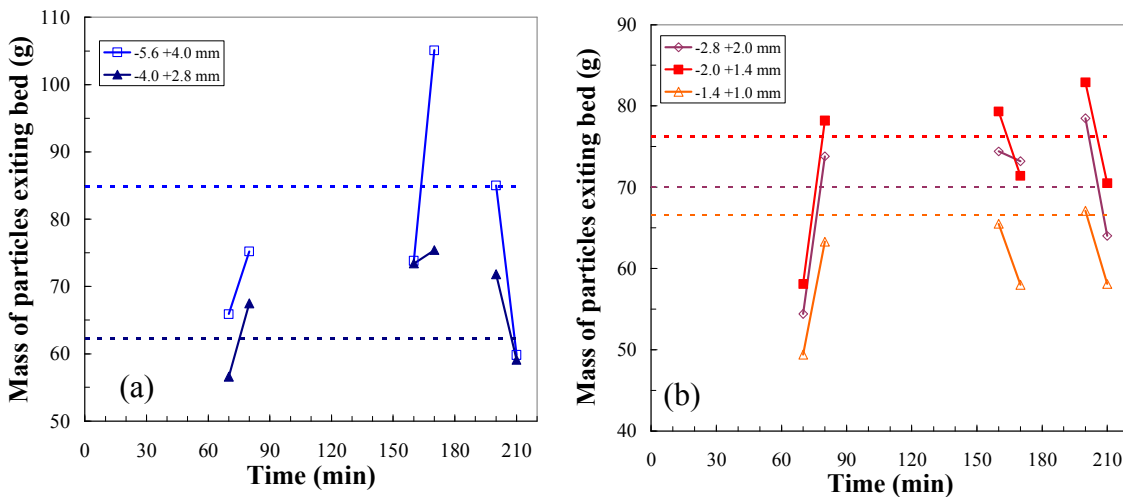


Figure 8-5: The approach to steady state of individual size fractions. (a) $-5.6 + 4.0$ and $-4.0 + 2.8$ mm, (b) $-2.8 + 2.0$, $-2.0 + 1.4$ and $-1.4 + 1.0$ mm.

Figure 8-5b shows that by 160 minutes of processing the mass of particles in the size fractions $-2.8 + 2.0$, $-2.0 + 1.4$ and $-1.4 + 1.0$ mm exiting the bed is the same as in the

feed, indicating that these particles are at steady state. This is not observed for the larger particle sizes in Figure 8-5a, possibly due to retention of these particles in the incline as observed in Chapter 7.

The presence of the incline in the tracer particle experiments caused some particles of intermediate density to be retained in the bed rather than exiting through the overflow or underflow. In a bed with a continuous feed of particles this could cause the concentration of coal within the bed to increase to the extent that the bed blocked.

With a sand to coal ratio of 17:1 (5.8 % mass) the concentration near the base of the incline increased to 14 % mass after 210 minutes, as seen in Figure 8-6. However, the bed did not block and so a significant data set was obtained. In particular it can be noted that the concentration is greatest close to the base of the incline and then drops away towards the overflow and underflow. The shape of this curve is very similar to that of the tracer particles, given in Figure 7-3.

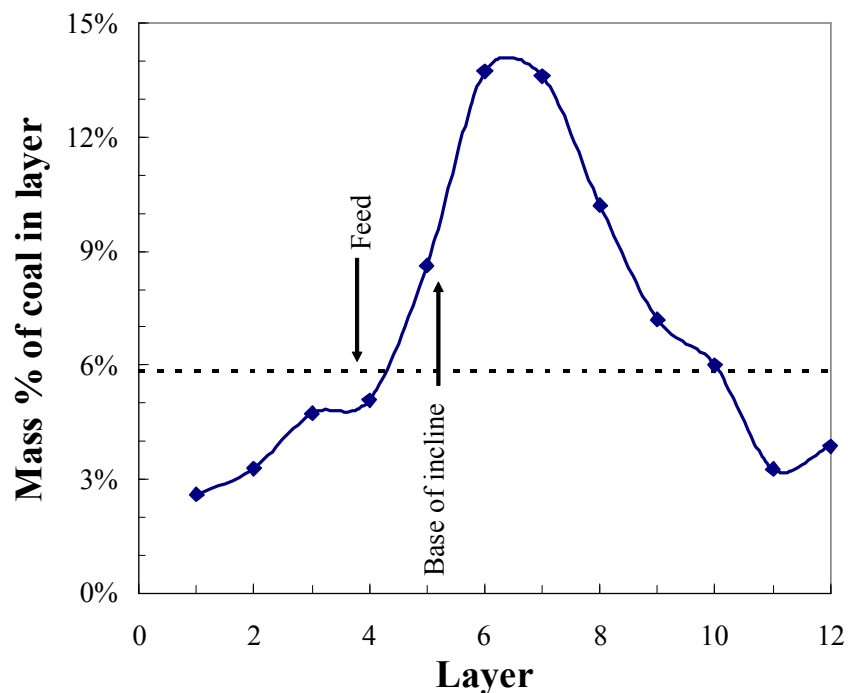


Figure 8-6: The distribution of coal within the bed after 210 minutes of continuous coal feed at a concentration of 5.8 mass%. The approximate positions of the feed and the base of the incline are indicated. A higher concentration of coal is clearly apparent at the base of the incline. The horizontal dotted line indicates the feed concentration.

The size distribution of the overflow and underflow samples at times of 70, 80, 160, 170, 200 and 210 minutes was measured to determine if particles of a particular size were more prone to retention in the bed. Figure 8-7a demonstrates that the size distribution of the combined outputs was roughly equivalent to the feed, indicating that the system was at steady state. Additionally, the size distribution of the particles in the overflow and underflow was largely equivalent to that of the feed as illustrated in Figure 8-7b.

It was also observed that the mass of particles in the size range $-5.6 +4.0$ mm reporting to the underflow in each 10 minute sample was almost the same, regardless of the underflow rate. This again is consistent with the observation in Chapter 7 that the density cut-point of particles greater than 4.0 mm is largely independent of the underflow rate.

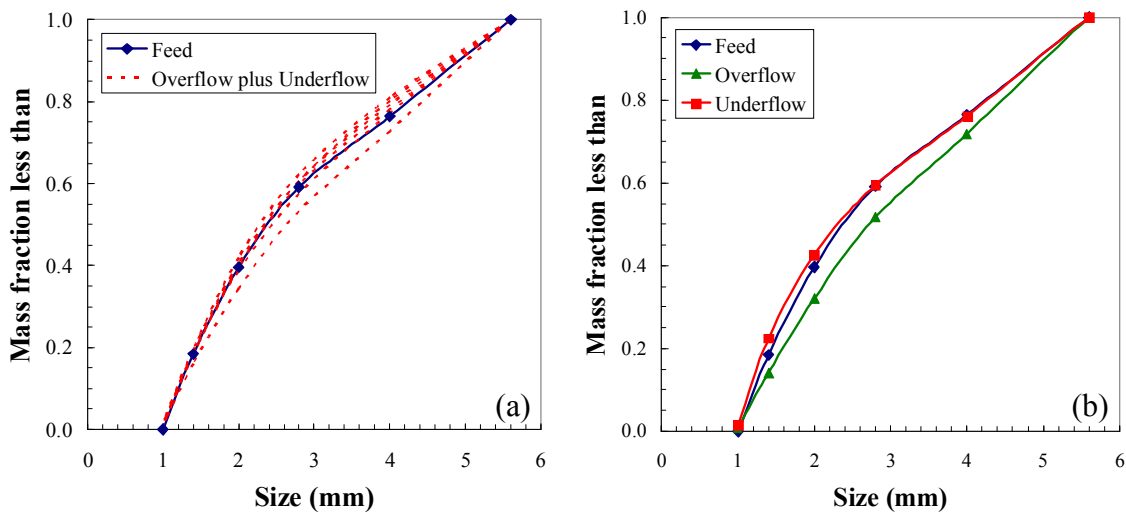


Figure 8-7: The cumulative size distribution of (a) the combined overflow and underflow samples for 70, 80, 160, 170, 200 and 210 minutes and (b) the separate overflow and underflow compared with the feed size distribution for an overflow rate of 221 g/min (170 minutes). The different dotted lines in (a) represent the different time samples.

8.5.2 Yield vs. Ash

The steady-state overflow and underflow samples from times of 70, 80, 160, 170 and 210 minutes were sieved into their size fractions and analysed for their ash content.

From this, the performance of the pneumatic Reflux Classifier with vibration and sand dense-medium could be compared with the coal washability data (as in Figures 8-1 to 8-3) and with the performance of the water-based Reflux Classifier on a batch sample of coal. This is illustrated in Figure 8-8 for four different size fractions ((a) -8.0 +4.0 mm, (b) -4.0 +2.0 mm, (c) -2.0 +1.0 mm and (d) -8.0 +1.0 mm). It should be noted that while the coal washability data and water Reflux Classifier results are for coal in the size range -8.0 +1.0 mm, the pneumatic Reflux Classifier results were for -5.6 +1.0 mm coal. It was assumed that the ash content of coal in the size range -8.0 +4.0 mm is very similar to coal in the size range -5.6 +4.0 mm. In reality, the ash content of the -8.0 +4.0 mm fraction of the coal would probably be greater than the -5.6 +4.0 mm fraction, however the advantage this gives to the pneumatic Reflux Classifier in comparison is offset by the superior performance of the unit on larger particle sizes.

The data points in Figure 8-8 are based on the underflow and feed ash results, rather than the underflow and overflow ash results. As has been mentioned previously, the rate of feed and underflow to the system are very steady, since they are controlled by valves. The overflow rate is not controllable and was observed to vary significantly (Figure 8-4). As a result, the typical method of analysing yield ash data where the overflow and underflow are mass and ash balanced with the feed was not valid here (see Figure 8-4). In some time intervals, the total mass out was much greater than the mass in, and in others, vice versa. This meant that in some cases the ash content of the reconstituted feed was significantly above or below the known feed ash. To counter this variability, the underflow and feed were used as the reference points, and the overflow mass and ash content inferred from these two values. This tended to reduce the scatter in the experimental results caused by the sporadic overflow.

The separation efficiency decreased as the particle size increased, just as expected from the tracer particle experiments. It is of particular interest to note that over the entire size range of -8.0 +1.0 mm, at a yield of 75%, the performance of the pneumatic Reflux Classifier is equivalent to the water-based Reflux Classifier. It is also very interesting to observe that the separations obtained for an overflow to feed ratio of 0.381 were almost exactly the same for the -8.0 +4.0 and -4.0 +2.0 mm size fractions. This is in complete agreement with the observations made in Chapter 7 that the effects of particle size on

the separation are suppressed at these flow conditions, validating the tracer particle experiments.

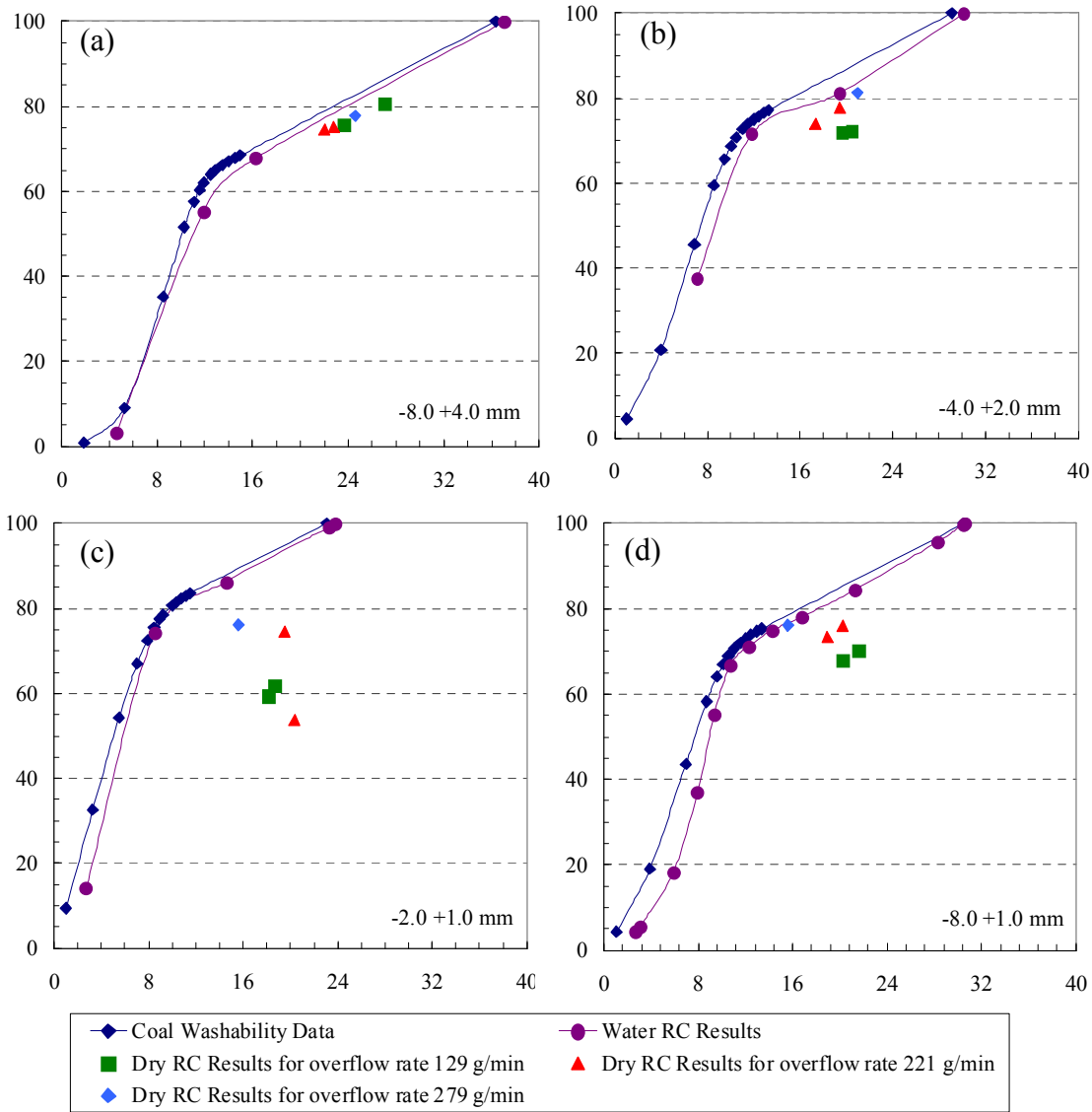


Figure 8-8: The Cumulative Yield (%) vs Cumulative Ash (%) separation results achieved in the air-sand dense-medium Reflux Classifier (RC) with vibration on a continuous coal feed (-5.6 +1.0 mm), compared with the coal washability data and the separation obtained in the water-based Reflux Classifier (Callen et al., 2007b) in each appropriate size fraction: (a) -8.0 +4.0 mm, (b) -4.0 +2.0 mm, (c) -2.0 +1.0 mm (d) -8.0 +1.0 mm.

Figure 8-8 suggests that as the length of the experiment increased so did the separation efficiency, with the separation points approaching the coal washability data. This supports the observation in Figure 8-4 that the system was not at steady state for the early samples. It also is apparent that the amount of scatter increases as the particle size

decreases, suggesting that the large particles reach their steady state density partition to the underflow much faster than the smaller particles. It is natural to observe that smaller particles, with lower buoyant velocities, take longer to reach steady state density partition, even though it was observed in Figure 8-5 that they reach steady state in the system faster than the large particles.

8.6 Potential for Scale-Up

From experiments with different ratios of sand to coal in the feed it was found that the bed was very sensitive to the amount of coal in the feed. If the amount was too great the observed increase in particle concentration at the base of the incline would increase to such an extent that the bed would block. A sand to coal ratio of 10:1 on a mass basis was sufficient to prevent blocking of the bed during an experiment of at least 4 hours duration. At a ratio of 5:1, the concentration of coal particles near the feed increased to almost 50% mass (or 66% volume) within 100 minutes and caused the apparatus to block.

At the sand feed rates used in these experiments, which were the maximum for the vibration and gas flow conditions, the maximum coal feed rate would be 50 g per minute. This corresponds to a throughput of 1.5 tonnes per m² per hour. The water-based Reflux Classifier can handle a throughput of about 47 t/m².h (Galvin et al., 2002). The blocking of the pneumatic Reflux Classifier could be due to the narrow geometry of the unit used in this work, and a larger apparatus may be able to handle a significantly higher throughput.

8.7 Summary

Separations of a coal feed were conducted in both the batch and continuous air-sand dense-medium Reflux Classifier with vibration. A significant reduction in the product ash content was observed for both the batch and continuous separations and the separation was particularly effective at removing the largest and densest fraction of the feed. There is potential for this process to be used as a “de-stoning” operation to remove the densest components of the feed before the product is further beneficiated in other processes. Any potential uses would have to take into account the limited throughput capacity of the apparatus.

The results of the coal separations performed in this Chapter confirm that the observations of the system made using tracer particles in Chapters 6 and 7 are also valid for a real feed.

Chapter 9

Conclusions and Recommendations

9.1 Conclusions

This study was concerned with the investigation of a modified fluidised bed, known as the Reflux Classifier, and its potential application to dry coal beneficiation. The apparatus, which consisted of a 1 m vertical fluidised zone below a 2 m inclined channel at 70° to the horizontal, was subjected to vibration. The particles fed to the device were separated using an air-sand dense-medium. The effects of vibration frequency, vibration direction, overflow rate and gas rate on the separation performance were studied. The findings were then compared with those for a non-vibrated Reflux Classifier and a purely vertical fluidised bed.

Particles of sand were fed to the device in order to develop a dense-medium and, in turn, promote a density based separation. The dense-medium effect occurs in fluidised suspensions of particles, resulting in a pseudo-fluid with a density between that of the fluidising gas and the solids. The dense-medium effect is greatest for particles that are significantly larger than the particles forming the media.

A series of experiments on batch quantities of tracer particles was conducted at a single gas rate and sand feed rate with vibration set at 0 rpm, 325 rpm or 595 rpm in either the vertical or horizontal direction. Fluidising gas was fed through a distributor plate at the base of the bed, sand was continually fed through a hose 700 mm above the base, and sand and tracer particles were removed through the overflow at the top.

The apparatus used in the batch experiments was modified so that underflow could be continuously removed from the base of the bed. A series of experiments on batch quantities of tracer particles was carried out with continuous overflow and underflow removal to determine the effects of changing the overflow rate or the gas rate. A second modification - changing the 2 m incline to a 2 m vertical channel was also made in order to assess the effect of the incline on the separation performance. The experiments carried out using the continuous system, with an inclined channel, were repeated using the vertical channel.

The rate of elutriation of particles from the Reflux Classifier was first order dependent on their concentration in the unit, which is the same as from conventional fluidised beds. The elutriation data obtained from the batch Reflux Classifier experiments were fitted to a two parameter model for dispersed plug flow (Equation (5-4)). The modelling of the velocity of the particles using Equation (5-4) could not reliably be applied to the continuous system.

The separation of particles in the air-sand dense-medium Reflux Classifier with vibration is driven by both the dense-medium effect and the convective velocity of the medium. The dense-medium effect resulted in an apparent buoyant, or slip velocity, either up or down depending on whether particle density was less than or greater than the medium density. For particles of a specific density, this buoyant velocity is greatest for the larger particles (see Equation (3-2)). The convective velocity affects all particles equally, but has a greater proportional impact on the smallest particles due to their small buoyant velocity.

Separations in the air-sand dense-medium Reflux Classifier are driven largely by the dense-medium effect. This is made clear by the particle separation efficiency increasing with increasing particle diameter and by the effects of particle size on the density cut-point being effectively suppressed at certain flow conditions in the continuous system. However, the convective velocity of the medium is also a significant driver of the separations, particularly in the smallest size fractions where the dense-medium effect is less. As particle size decreased the partition curve values approached the steady state partition of the sand medium to the overflow.

The relationship between the slip velocity and the particle size and density was found to be the same as for the terminal free settling velocity of particles in the Intermediate regime, that is (Vance & Moulton, 1965):

$$U_{slip} = 0.153 \frac{d_p^{8/7} (\rho_p - \rho_m)^{5/7} g^{5/7}}{\rho_m^{2/7} \mu_m^{3/7}} \quad (3-7)$$

From the experimental data the viscosity of the medium was determined to be approximately 22 Pa.s. This viscosity is significantly higher than the effective viscosities of sand fluidised beds measured by Rees et al. (2007). The large value of the apparent viscosity was attributed to the narrow channel, and the associated wall effects, and to the de-fluidisation of the sand medium in the inclined channel.

Vibration of any frequency or direction significantly improved the density based separation efficiency of the largest particles but had no impact on the smallest particles, *ca* 1.0 to 2.0 mm. The results demonstrated that the vibration affected the action of the dense-medium. The effect of vibration on the sand medium was to reduce the size of the bubbles resulting in a more homogeneous separation environment.

The vibration frequency had an effect on the density separation cut-point (ρ_{50}). Increasing the vibration frequency led to a lower density cut-point in the batch system. That is, a higher vibration frequency led to greater particle retention in the Reflux Classifier. The increased homogeneity of the medium due to smaller bubbles in the vibrated bed decreased the misplacement of particles to the overflow and hence led to a reduction in the density cut-point.

The density cut-point in both the inclined and the vertical systems, can be increased by increasing either the overflow rate or the gas flow rate. The ρ_{50} increased with the overflow rate because of the higher convective velocity driving particles to the overflow. Increasing the gas rate caused greater inconsistency in the size of the bubbles in the device, the same effect as decreasing the vibration rate, and in the same way led to an increase in the ρ_{50} .

The separation efficiency decreased slightly with an increase in the gas rate for both the inclined and the vertical systems. This decrease occurred because increasing the gas rate increased the inconsistency in the size of the bubbles in the bed, leading to higher rates of misplaced particles and so a reduced separation efficiency. Changing the overflow rate had no major effect on the separation efficiency.

The separation efficiency of the experimental apparatus was very good for the largest particles in comparison to water-based beneficiation devices but poor for particles below 2.0 mm. For particles in the size range -6.35 +4.0 mm the separation efficiency, measured by the Ep , was 0.04 for the batch separations and 0.06 for the continuous separations. This compares well with the 0.02-0.03 Ep of water-based dense-medium cyclones on the same size coal particles. The Ep for particles in the size range -2.0 +1.0 mm was 0.16 in the batch separations and 0.35 in the continuous separations which is significantly higher than the 0.07 Ep of the water-based Reflux Classifier and the 0.14 to 0.18 Ep of water-based spirals.

The Reflux Classifier consistently produced lower separation efficiencies than the vertical fluidised bed at the same gas and sand flowrate conditions. There was also less change in the density cut-point observed in the Reflux Classifier over the same range of conditions. That is, the Reflux Classifier provided a more stable and consistent separation environment than a vertical fluidised bed alone.

It was also observed that the incline promoted a refluxing of particles of density close to the density separation cut-point. This refluxing, similar to that observed in the water-based Reflux Classifier, increased the residence time of these particles and so allowed for misplaced particles to have a greater chance of exiting in the correct stream. This reflux action led to an increase in the separation efficiency.

Separations of batch and continuous coal feeds were also completed in the apparatus. The results of these separations confirmed that the observations made using tracer particles also apply for a real continuous feed.

From the results of these experiments it was evident that the pneumatic Reflux Classifier with a sand dense-medium and vibration could separate particles on the basis of density. At certain conditions, the effects of particle size on the separation were suppressed. The ideal conditions for a density based separation include vibration at a high frequency, as low a gas rate as possible, an overflow rate just sufficient to transport the low density particles, and a high medium to coal ratio. Because of the necessity for a high medium to coal ratio, this system has a limited throughput of 1.5 t/m².h which is

well below the water based Reflux Classifier throughput of 47 t/m².h. This system will find greatest application in the removal of the highest density components from a coal feed; that is as a de-stoning operation.

9.2 Recommendations

The results of this work are encouraging and suggest that the Reflux Classifier can be successfully used as a dry beneficiation device for coal at very low coal concentrations. This promise leads to openings for future research work.

1. A new apparatus could be made using a combination of stainless steel and polycarbonate. The stainless steel would provide extra strength while the polycarbonate will allow for observations to still be made during the course of an experiment. Stainless steel would form the backbone of the apparatus, being used for the flanges, plenum chamber, distributor plate and the 20 mm channel walls. The 20 mm channel walls would be made of U-shaped stainless steel so that polycarbonate sheets can be glued and bolted on to the front and back to form the 100 mm channel walls.
2. The separation of particles in a larger apparatus with multiple channels should be investigated to determine scale-up potential. In this larger apparatus, it should be observed if the slugging flow behaviour continues, or if it was a function of the narrow geometry. If it is not present, then the effects of this on the separation quality should be determined.
3. In a larger unit, the maximum throughput per unit area may be greater than in the present study, since the wall effects observed in the narrow channels of this study greatly exacerbated the blocking tendency as coarse particles accumulate. The capacity of the unit as a function of geometry is of interest in scale-up considerations.
4. Larger particles, up to 50 mm, could be studied in a larger single channel apparatus since it was clear that the separation was most efficient for the largest particles.

References

- Anderson, J. M., Parobek, L., Bergougnou, M. A. & Inculet, I. I. (1979) Electrostatic separation of coal macerals [power plant fuel]. *IEEE Transactions on Industry Applications*, IA-15, 291-3.
- Arnaldos, J. & Casal, J. (1996) Prediction of transition velocities and hydrodynamical regimes in fluidized beds. *Powder Technology*, 86, 285-298.
- Avidan, A. A. & Yerushalmi, J. (1982) Bed Expansion in High Velocity Fluidization. *Powder Technology*, 32, 223-232.
- Baeyens, J., Geldart, D. & Wu, S. Y. (1992) Elutriation of fines from gas fluidized beds of Geldart A-type powders - effect of adding superfines. *Powder Technology*, 71, 71-80.
- Blekhman, I. I. (1988) *Synchronization in Science and Technology*, New York, ASME Press.
- Boycott, A. E. (1920) Sedimentation of blood corpuscles. *Nature*, 104, 152.
- Callen, A., Moghtaderi, B. & Galvin, K. P. (2007a) Use of parallel inclined plates to control elutriation from a gas fluidized bed. *Chemical Engineering Science*, 62, 356-370.
- Callen, A. M., Patel, B., Zhou, J. & Galvin, K. P. (2007b) Washability analysis by water fluidisation and jigging. *ACARP End of grant report, Project C14066*.
- Caner Orhan, E., Ergun, L. & Altiparmak, B. (2010) Application of the FGX Separator in the enrichment of Catalagzi coal: a Simulation Study. IN Honaker, R. Q. (Ed.) *International Coal Preparation Congress*. Society for Mining, Metallurgy and Exploration.
- Chan, E. W. & Beeckmans, J. M. (1982) Pneumatic Beneficiation of Coal Fines Using the Counter-Current Fluidized Cascade. *International Journal of Mineral Processing*, 9, 157-165.
- Chen, Q. & Yang, Y. (2003) Development of dry beneficiation of coal in China. *Coal Preparation: A Multinational Journal*, 23, 3-12.
- Choi, J.-H., Suh, J.-M., Chang, I.-Y., Shun, D.-W., Yi, C.-K., Son, J.-E. & Kim, S.-D. (2001) The effect of fine particles on elutriation of coarse particles in a gas fluidized bed. *Powder Technology*, 121, 190-194.
- Chong, Y. O., Nguyen, T.-H., Leung, L. S. & Teo, C. S. (1984) Inclined Fluidised Bed. *Fluidization and Fluid Particle Systems: Recent Advances. Selected papers presented at the 76th Annual Meeting of the American Institute of Chemical Engineers*. San Francisco, CA, USA, AIChE, New York, NY, USA.

- Choung, J., Mak, C. & Xu, Z. (2006) Fine coal beneficiation using an air dense medium fluidized bed. *Coal Preparation*, 26, 1-15.
- Church, A. H. (1967) *Mechanical Vibration*, New York, John Wiley and Sons Inc.
- Colakyan, M., Catipovic, N., Jovanovic, G. & Fitzgerald, F. (1979) *72nd Annual Meeting AIChE*. San Francisco, CA, USA.
- Colakyan, M., Catipovic, N., Jovanovic, G. & Fitzgerald, T. (1981) Elutriation from a Large Particle Fluidized Bed With and Without Immersed Heat Transfer Tubes. *Recent Adv in Fluid and Fluid-Part Syst, Pap Presented at 72nd Annu Meet of AIChE, Dec 1979 AIChE Symposium Series*, 66-75.
- Daleffe, R. V., Ferreira, M. C. & Freire, J. T. (2007) Analysis of the effect of particle size distributions on the fluid dynamic behavior and segregation patterns of fluidized, vibrated and vibrofluidized beds. *Asia-Pacific Journal of Chemical Engineering*, 2, 3-11.
- Danckwerts, P. V. (1953) Continuous flow systems : Distribution of residence times. *Chemical Engineering Science*, 2, 1-13.
- Davis, R. H. & Acrivos, A. (1985) Sedimentation of Noncolloidal Particles at Low Reynolds Numbers. 17 ed., Annual Reviews Inc, Palo Alto, CA, USA.
- Davis, R. H. & Gecol, H. (1996) Classification of concentrated suspensions using inclined settlers. *International Journal of Multiphase Flow*, 22, 563-574.
- Davis, R. H., Herbolzhiemer, E. & Acrivos, A. (1982) Sedimentation of Polydisperse Suspensions in Vessels Having Inclined Walls. *International Journal of Multiphase Flow*, 8, 571-585.
- Davis, R. H., Zhang, X. & Agarwala, J. P. (1989) Particle classification for dilute suspensions using an inclined settler. *Industrial & Engineering Chemistry Research*, 28, 785-793.
- Di Felice, R. (1995) Hydrodynamics of Liquid Fluidisation. *Chemical Engineering Science*, 50, 1213-1245.
- Dong, X. & Beeckmans, J. M. (1990) Separation of particulate solids in a pneumatically driven counter-current fluidized cascade. *Powder Technology*, 62, 261-267.
- Doroodchi, E., Zhou, J., Fletcher, D. F. & Galvin, K. P. (2006) Particle size classification in a fluidized bed containing parallel inclined plates. *Minerals Engineering*, 19, 162-171.
- Dwari, R. K. & Rao, K. H. (2007) Dry beneficiation of coal - A review. *Mineral Processing and Extractive Metallurgy Review*, 28, 177-234.

- Erdesz, K. & Mujumdar, A. S. (1986) Hydrodynamic Aspects of Conventional and Vibrofluidized Beds - A Comparative Evaluation. *Powder Technology*, 46, 167-172.
- Ergun, S. (1952) Mass-transfer rate in packed columns -- Its analogy to pressure loss. *Chemical Engineering Progress*, 48, 227-236.
- Fan, M., Chen, Q., Zhao, Y. & Luo, Z. (2001) Fine coal (6-1 mm) separation in magnetically stabilized fluidized beds. *International Journal of Mineral Processing*, 63, 225-232.
- Fan, M., Chen, Q., Zhao, Y., Tao, D., Luo, Z., Zhang, X., Tao, X. & Yang, G. (2006) Fine coal dry classification and separation. *Minerals and Metallurgical Processing*, 23, 17-21.
- Fan, M., Chen, Q., Zhao, Y., Yuping Guan, Z. L. & Li, B. (2002) Magnetically stabilized fluidized beds for fine coal separation. *Powder Technology*, 123, 208-211.
- Fraas, A. P. (2005) Application of complex-mode vibration-fluidized beds to the separation of granular materials of different density. US.
- Fraser, T. & Yancey, H. F. (1926) The air-sand process of cleaning coal. *American Institute of Mining and Metallurgical Engineers -- Transactions*, 6.
- Galvin, K. P. (2004) Reflux classifier. US, The University of Newcastle Research Associates Limited.
- Galvin, K. P. (2009) Water based fractionation of particles. *Chemical Engineering Research and Design*, 87, 1085-1099.
- Galvin, K. P., Callen, A., Zhou, J. & Doroodchi, E. (2005) Performance of the Reflux Classifier for gravity separation at full scale. *Minerals Engineering*, 18, 19-24.
- Galvin, K. P., Doroodchi, E., Callen, A. M., Lambert, N. & Pratten, S. J. (2002) Pilot plant trial of the reflux classifier. *Minerals Engineering*, 15, 19-25.
- Galvin, K. P. & Nguyentranlam, G. (2002) Influence of parallel inclined plates in a liquid fluidized bed system. *Chemical Engineering Science*, 57, 1231-1234.
- Galvin, K. P., Pratten, S. & Nguyen Tran Lam, G. (1999a) A generalized empirical description for particle slip velocities in liquid fluidized beds. *Chemical Engineering Science*, 54, 1045-1052.
- Galvin, K. P., Pratten, S. J. & Nicol, S. K. (1999b) Dense medium separation using a Teetered Bed Separator. *Minerals Engineering*, 12, 1059-1081.
- Geldart, D. (1973) Types of Gas Fluidization. *Powder Technology*, 7, 285-292.

- Geldart, D. (1986) *Gas Fluidisation Technology*, Chichester, Wiley Interscience.
- Geldart, D., Cullinan, J., Georghiades, S., Gilvray, D. & Pope, D. J. (1979) Effect of Fines on Entrainment from Gas Fluidised Beds. *Transactions of the Institution of Chemical Engineers*, 57, 269-275.
- Ginestet, A., Guigon, P., Large, J. F., Gupta, S. S. & Beeckmans, J. M. (1993) Hydrodynamics of a flowing gas-solids suspension in a tube at high angles of inclination. *Canadian Journal of Chemical Engineering*, 71, 177-182.
- Grace, J. R. (1986) CONTACTING MODES AND BEHAVIOUR CLASSIFICATION OF GAS - SOLID AND OTHER TWO-PHASE SUSPENSIONS. *Canadian Journal of Chemical Engineering*, 64, 353-363.
- Hise, E. C. (1982) DEVELOPMENT OF HIGH-GRADIENT AND OPEN GRADIENT MAGNETIC SEPARATION. *Ieee Transactions on Magnetics*, 18, 847-857.
- Hong, J. & Zhu, J.-X. (1997) Effect of pipe orientation on dense-phase transport. I. Critical angle in inclined upflow. *Powder Technology*, 91, 115-122.
- Hong, J. & Zhu, J.-X. (2002) Effect of pipe orientation on dense-phase transport in inclined upward and downward flows. *Chemical Engineering Communications*, 189, 489-509.
- Hoult, D. (2007) Mass/Spring Oscillator. *The open book website*.
- Jin, H., Tong, Z., Schlaberg, H. I. & Zhang, J. (2005) Separation of fine binary mixtures under vibration in a gas-solid fluidized bed with dense medium. *Waste Management and Research*, 23, 534-540.
- Jin, H., Zhang, J. & Zhang, B. (2007) The effect of vibration on bed voidage behaviors in fluidized beds with large particles. *Brazilian Journal of Chemical Engineering*, 24, 389-397.
- Kato, K., Tajima, T., Mao, M. & Iwamoto, H. (1985) IN Kwauk, M., Kunii, D., Zheng, J. & Hasatani, M. (Eds.) *Science and Technology*. Amsterdam, Elsevier.
- Kelly, E. J. & Spottiswood, D. J. (1982) *Introduction to Mineral Processing*, New York, John Wiley & Sons.
- Khan, A. R., Richardson, J.F. (1989) Fluid-particle interactions and flow characteristics of fluidised beds and settling suspensions of spherical particles. *Chemical Engineering Communications*, 78, 111.
- Konrad, K. (1986) Dense-phase pneumatic conveying: A review. *Powder Technology*, 49, 1-35.

- Laskovski, D., Duncan, P., Stevenson, P., Zhou, J. & Galvin, K. P. (2006) Segregation of hydraulically suspended particles in inclined channels. *Chemical Engineering Science*, 61, 7269-7278.
- Leva, M. (1951) Elutriation of fines from fluidized systems. *Chemical Engineering Progress*, 47, 39-45.
- Levenspiel, O. (1999) *Chemical Reaction Engineering*, New York, John Wiley and Sons.
- Levenspiel, O. & Smith, W. K. (1957) Notes on the diffusion-type model for the longitudinal mixing of fluids in flow. *Chemical Engineering Science*, 6, 227-235.
- Levy, A., Mooney, T., Marjanovic, P. & Mason, D. J. (1997) Comparison of analytical and numerical models with experimental data for gas-solid flow through a straight pipe at different inclinations. *Powder Technology*, 93, 253-260.
- Lin, L., Sears, J. T. & Wen, C. Y. (1980) Elutriation and attrition of char from a large fluidized bed. *Powder Technology*, 27, 105-115.
- Lockhart, N. C. (1984) Dry Beneficiation of Coal. *Powder Technology*, 40, 17-42.
- Ludowici (2007) <http://www.ludowici.com.au/web/news.html?newsId=323>.
- Luo, Z. & Chen, Q. (2001) Dry beneficiation technology of coal with an air dense-medium fluidized bed. *International Journal of Mineral Processing*, 63, 167-175.
- Luo, Z., Chen, Q. & Tao, X. (2000) Formation mechanism of vibration fluidized bed (VFB). *Journal of China University of Mining Technology*, 29, 230-234.
- Luo, Z., Chen, Q. & Yaomin, Z. (2002a) Dry Beneficiation of coarse coal using air dense medium fluidized bed (ADMFB). *Coal Preparation: A Multinational Journal*, 22, 57-64.
- Luo, Z., Fan, M., Zhao, Y., Tao, X., Chen, Q. & Chen, Z. (2008) Density-dependent separation of dry fine coal in a vibrated fluidized bed. *Powder Technology*, 187, 119-123.
- Luo, Z., Zhao, Y., Chen, Q., Fan, M. & Tao, X. (2002b) Separation characteristics for fine coal of the magnetically fluidized bed. *Fuel Processing Technology*, 79, 63-69.
- Luo, Z., Zhao, Y., Tao, X., Fan, M., Chen, Q. & Wei, L. (2003) Progress in dry coal cleaning using air-dense medium fluidized beds. *Coal Preparation: A Multinational Journal*, 23, 13-20.

- Macpherson, S. A., Iveson, S. M. & Galvin, K. P. (2010) Density based separations in the Reflux Classifier with an air-sand dense-medium and vibration. *Minerals Engineering*, 23, 74-82.
- Marring, E., Hoffmann, A. C. & Janssen, L., P,B,M (1994) The effect of vibration on the fluidisation behaviour of some cohesive powders. *Powder Technology*, 79, 1-10.
- Mawatari, Y., Akune, T., Tatemoto, Y. & Noda, K. (2002) Bubbling and bed expansion behaviour under vibration in a gas- solid fluidized bed. *Chemical Engineering and Technology*, 25, 1095-1100.
- Mawatari, Y., Tsunekawa, M., Tatemoto, Y. & Noda, K. (2005) Favorable vibrated fluidization conditions for cohesive fine particles. *Powder Technology*, 154, 54-60.
- Merrick, D. & Highley, J. (1974) *AIChE Symposium Series*, 70, 366-378.
- Molerus, O. (1982) Interpretation Of Geldart's Type A, B, C And D Powders By Taking Into Account Interparticle Cohesion Forces. *Powder Technology*, 33, 81-87.
- Mostoufi, N. & Chaouki, J. (2004) Flow structure of the solids in gas-solid fluidized beds. *Chemical Engineering Science*, 59, 4217-4227.
- Nakagawa, N., Arita, S., Uchida, S., Takamura, H., Takarada, T. & Kato, K. (1994) *J. Chem. Eng. Jpn.*, 27, 79.
- Nakamura, H. & Kuroda, K. (1937) La cause de l'acceleration de la vitesse de sedimentation des suspensions dans les recipients inclines. *Keizyo Journal of medicine*, 8, 256-296.
- Nelson, D., Liu, J. & Galvin, K. P. (1997) Autogenous dense medium separation using an inclined counterflow settler. *Minerals Engineering*, 10, 871-881.
- Nguyentranlam, G. & Galvin, K. P. (2001) Particle classification in The Reflux Classifier. *Minerals Engineering*, 14, 1081-1091.
- Novastrut (2010) <http://www.novastrut.com.au/catalogue.pdf>. Mortdale, Novex Engineering.
- O'dea, D. P., Rudolph, V., Chong, Y. O. & Leung, L. S. (1990) Effect of inclination on fluidized beds. *Powder Technology*, 63, 169-178.
- Oshitani, J., Kondo, M., Nishi, H. & Tanaka, Z. (2003) Separation of silicestone and pyrophyllite by a gas-solid fluidized bed utilising slight difference in density. *Advanced Powder Technology*, 14, 247-258.

- Pemberton, S. T. & Davidson, J. F. (1986a) Elutriation from Fluidized Beds - I. Particle Ejection from the Dense Phase into the Freeboard. *Chemical Engineering Science*, 41, 243-251.
- Pemberton, S. T. & Davidson, J. F. (1986b) Elutriation from Fluidized Beds - II. Disengagement of Particles from Gas in the Freeboard. *Chemical Engineering Science*, 41, 253-262.
- Ponder, P. (1925) On sedimentation and rouleaux formation. *Quarterly Journal of Experimental Physiology*, 15, 235-252.
- Prashant, D., Xu, Z., Szymanski, J., Gupta, R. & Boddez, J. (2010) Dry Cleaning of Coal by a Laboratory Continuous Air Dense Medium Fluidized Bed Separator. IN Honaker, R. Q. (Ed.) *International Coal Preparation Congress*. Society for Mining, Metallurgy and Exploration.
- Rao, S. S. (1995) *Mechanical Vibrations*, Reading, Massachusetts, Addison-Wesley Publishing Company.
- Rees, A. C., Davidson, J. F., Dennis, J. S. & Hayhurst, A. N. (2007) The Apparent Viscosity of the Particulate Phase of Bubbling Gas-Fluidized Beds: A Comparison of the Falling or Rising Sphere Technique with Other Methods. *Chemical Engineering Research and Design*, 85, 1341-1347.
- Rhodes, M. (1996) What is turbulent fluidization? *Powder Technology*, 88, 3-14.
- Rhodes, M. (2002) *Introduction to Particle Technology*, Chichester, John Wiley and Sons Ltd.
- Richardson, J. F. & Zaki, W. N. (1954) Sedimentation and fluidization: Part I. *Transactions of the Institution of Chemical Engineers*, 32, 35-53.
- Romero, C., Agarwala, J. P. & Davis, R. H. (1993) Separation and classification of axisymmetric particles in an inclined settler. *International Journal of Multiphase Flow*, 19, 803-816.
- Rosato, A., Strandburg, K. J., Prinz, F. & Swendsen, R. H. (1987) Why the Brazil nuts are on top: size segregation of particulate matter by shaking. *Physical Review Letters*, 58, 1038-40.
- Sanders, G. J. (2007) *The Principles of Coal Preparation*, Newcastle, Australian Coal Preparation Society.
- Sciazko, M., Bandrowski, J. & Raczek, J. (1991) On the entrainment of solid particles from a fluidized bed. *Powder Technology*, 66, 33-39.
- Smolders, K. & Baeyens, J. (2001) Gas fluidized beds operating at high velocities: A critical review of occurring regimes. *Powder Technology*, 119, 269-291.

- Subbarao, D. (1986) Clusters and Lean-Phase Behaviour. *Powder Technology*, 46, 101-107.
- Tanaka, I., Shinohara, H., Hirose & Tanaka, Y. (1972) *J. Chem. Eng. Jpn.*, 5, 57-62.
- Tasirin, S. M. & Geldart, D. (1998) Entrainment of FCC from fluidized beds - a new correlation for the elutriation rate constants K^*_{∞} . *Powder Technology*, 95, 240-247.
- Toomey, R. D. & Johnstone, H. F. (1952) Gaseous fluidization of solid particles. *Chemical Engineering Progress*, 48, 220-226.
- Van Der Laan, E. (1958) Letters to the editors. *Chemical Engineering Science*, 7, 187-191.
- Vance, W. H. & Moulton, R. W. (1965) A study of slip ratios for the flow of steam-water mixtures at high void fractions. *A.I.Ch.E. Journal*, 11, 1114-1124.
- Von Ketelhodt, L. (2010) Deshaling of Coal by Dual Energy X-Ray Transmission Sorting. IN Honaker, R. Q. (Ed.) *International Coal Preparation Congress*. Society for Mining, Metallurgy and Exploration.
- Walton, K. J., Galvin, K. P. & Callen, A. M. (2007) Dry Classification of Fine Coal. *ACARP End of grant report, Project C15055*.
- Wang, T., Jin, Y., Wang, Z. & Yu, Z. (1997) Characteristics of wave propagation in a vibrating fluidized bed. *Chemical Engineering & Technology*, 20, 606-611.
- Wei, L. & Chen, Q. (2001) Calculation of drag force on an object settling in gas-solid fluidized beds. *Particulate Science Technology*, 19, 229-238.
- Weitkaemper, L., Wotruba, H. & Hoffman Sampaio, C. (2010) Effective Dry Density Beneficiation of Fine Coal Using a New Developed Fluidized Bed Separator. IN Honaker, R. Q. (Ed.) *International Coal Preparation Congress*. Society for Mining, Metallurgy and Exploration.
- Wen, C. Y. & Hashinger, R. F. (1960) Elutriation of solid particles from dense-phase fluidized bed. *A.I.Ch.E. Journal*, 6, 220-226.
- Wen, C. Y. & Yu, Y. H. (1966) Mechanics of fluidization. *Chemical Engineering Progress Symposium*, 1966.
- Xu, C. & Zhu, J. (2005) Experimental and theoretical study on the agglomeration arising from fluidization of cohesive particles - Effects of mechanical vibration. *Chemical Engineering Science*, 60, 6529-6541.
- Xu, C. & Zhu, J. (2006) Parametric study of fine particle fluidization under mechanical vibration. *Powder Technology*, 161, 135-144.

- Yagi, S. & Aochi, T. (1955) *Spring Meet. Soc Chem. Eng Jpn.*
- Yerushalmi, J. & Cankurt, N. T. (1979) *Powder Technology*, 24, 187.
- Yerushalmi, J., Cankurt, N. T., Geldart, D. & Liss, B. (1978) *AIChE Symposium Series*, 74, 176.
- Zenz, P. A. & Weil, N. A. (1958) A Theoretical-Empirical Approach to the Mechanism of Particle Entrainment from Fluidized beds. *AIChE Journal*, 4, 472-479.
- Zhang, X. & Davis, R. H. (1990) Particle classification using inclined settlers in series and with underflow recycle. *Industrial & Engineering Chemistry Research*, 29, 1894-1900.
- Zhenfu, L. & Qingru, C. (2001) Effect of fine coal accumulation on dense phase fluidized bed performance. *International Journal of Mineral Processing*, 63, 217-224.
- Zhou, J., Walton, K., Laskovski, D., Duncan, P. & Galvin, K. P. (2006) Enhanced separation of mineral sands using the Reflux Classifier. *Minerals Engineering*, 19, 1573-1579.

Appendix A: Sand and Vibration data

Raw Gas Bubble Data

The data in the following tables was taken from analysis of video footage of the sand fluidised in the Polycarbonate Apparatus without vibrations (Table A-1) and with 595V vibration (Table A-2)

Table A-1: Raw data from video observation of the bubbles in the incline of the polycarbonate apparatus without vibration and fluidised at gas rates of 15%, 20% and 25% of maximum flow.

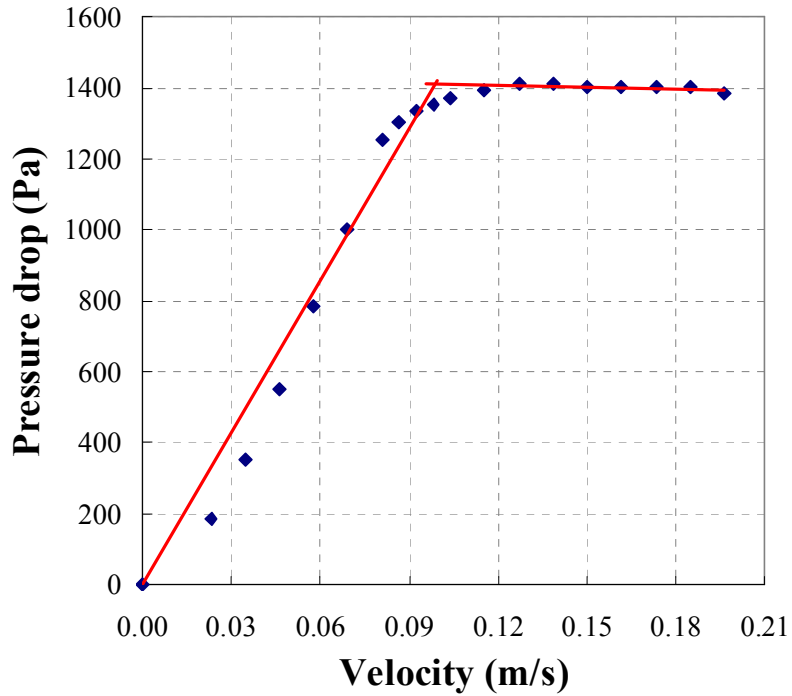
Sample Number	15%		20%			25%
	Bubble Length (mm)	Bubble Rise Velocity (m/s)	Bubble Length (mm)	Plug Length (mm)	Bubble Rise Velocity (m/s)	Bubble Rise Velocity (m/s)
1	205.1	0.259	251.6	612.9	0.288	0.441
2	102.6	0.221	212.9	367.7	0.375	0.417
3	159.0	0.259	451.6	658.1	0.183	0.357
4	210.3	0.259	322.6	522.6	0.313	
5	82.1	0.259	271.0		0.313	
6		0.192	580.6			
Average	151.8	0.241	348.4	540.3	0.294	0.405

Table A-2: Raw data from video observation of the bubbles in the incline of the polycarbonate apparatus vibrated at 595V and fluidised at gas rates of 10%, 15%, 20% and 25% of maximum flow.

Sample Number	10%			15%			20%			25%		
	Bubble Length (mm)	Plug Length (mm)	Bubble Rise Velocity (m/s)	Bubble Length (mm)	Plug Length (mm)	Bubble Rise Velocity (m/s)	Bubble Length (mm)	Plug Length (mm)	Bubble Rise Velocity (m/s)	Bubble Length (mm)	Plug Length (mm)	Bubble Rise Velocity (m/s)
1	66.7	160.7	0.375	106.3	87.5	0.417	268.8	187.5	0.441	195.7	500.0	0.500
2	16.7	125.0	0.441	156.3	275.0	0.441	137.5	187.5	0.441	195.7	160.0	0.417
3	66.7	135.7	0.375	100.0	300.0	0.341	137.5	100.0	0.375	278.3	132.0	0.375
4	100.0	303.6	0.357	112.5	187.5	0.441	175.0	187.5	0.395	234.8	240.0	0.341
5	33.3	203.6	0.417	156.3	218.8	0.417	312.5	406.3	0.395	478.3	160.0	0.300
6	23.3	139.3	0.375	143.8	206.3	0.417	343.8	625.0	0.441	478.3	340.0	0.441
7	76.7	232.1	0.417	125.0	250.0	0.441	118.8	437.5	0.469	156.5	240.0	0.536
8	66.7	125.0	0.395	125.0	112.5		150.0	487.5	0.375	391.3	440.0	0.441
9		278.6			93.8		312.5	187.5	0.357	217.4	232.0	0.536
10		228.6			281.3			187.5		169.6	120.0	0.357
11		75.0			106.3			487.5		391.3	520.0	0.469
12		142.9			312.5			500.0			340.0	
13								137.5				
Average	56.3	179.2	0.394	128.1	202.6	0.416	217.4	316.8	0.410	289.7	285.3	0.428

Minimum fluidisation velocity

The minimum fluidisation velocity of the sand was 0.1 m/s.



This velocity increased to 0.11 m/s for sand that contained the coal indicating that the sand did indeed become more cohesive with the addition of the sand.

Vibration Analysis

Measuring the vibration

To measure the vibration, a triaxial accelerometer was used. The accelerometer was provided by Crossbow Technology Inc. with product number CXL04LP3. The accelerometer measured the acceleration of the apparatus in three directions as shown in Figure A-1. The acceleration was measured at four points in the rig as illustrated in Figure A-1. Point 1 is at the overflow, point 2 is at the level of the horizontal support, point 3 at the base of the incline and point 4 at the gas inlet.

Fourier Series

The data taken from the accelerometer was converted into a Fourier Series of the form:

$$f(t) = \frac{a_0}{2} + \sum_{n=1}^5 a_n \cos\left(\frac{n\pi}{L}t\right) + \sum_{n=1}^5 b_n \sin\left(\frac{n\pi}{L}t\right)$$

where t is the time in seconds, and L is the length of half a cycle (s). $f(x)$ is the acceleration due to the vibration of the motors only. The effects of gravity have already been taken into consideration. $f(t)$ produces a result in volts, where 0.5 V corresponds to an acceleration of 1 g, or 9.81 m/s². That is, if $f(t) = 1$, the acceleration at that point in that direction is 19.62 m/s². The values of each of the constants for each of the positions are included in the following tables.

Batch Vibrations

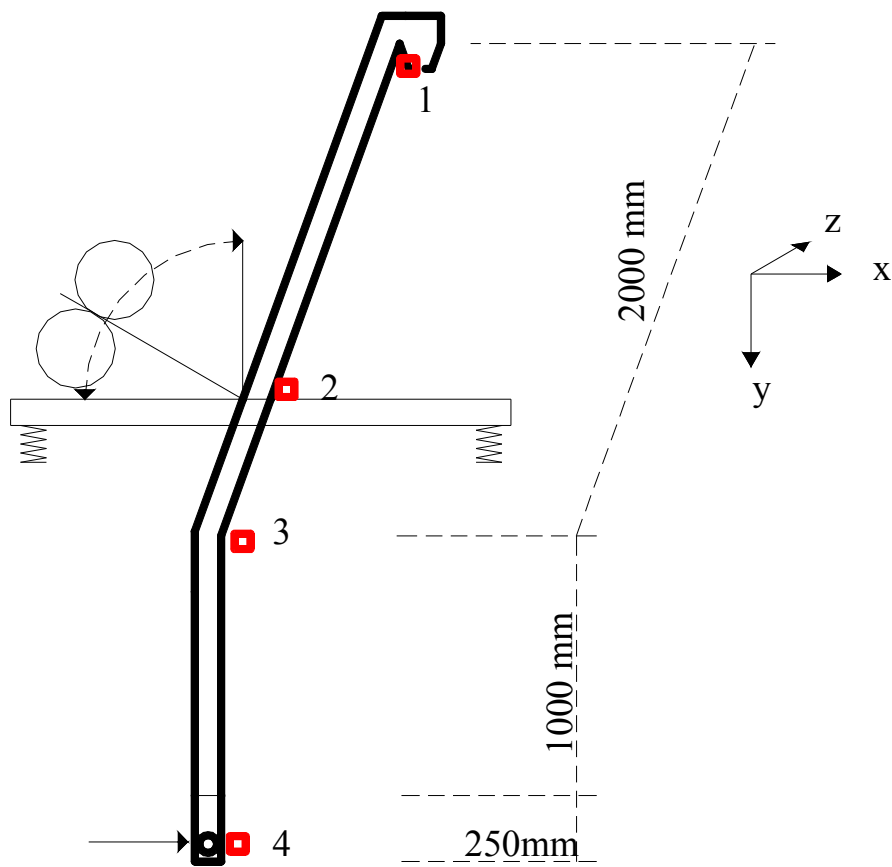


Figure A-1: Schematic of apparatus illustrating the dimensions and positioning of the accelerometer.

Table A-3: Fourier constants for 325H vibration case in the Reflux Classifier. These values give the acceleration in the x, y and z directions as shown in Figure A-1.

Accelerometer Position	Vibration direction (x, y, z)	L	a ₀	a ₁	b ₁	a ₂	b ₂	a ₃	b ₃	a ₄	b ₄	a ₅	b ₅
4	x	0.0926	-0.1133	-0.1088	-0.0572	-0.0151	0.0127	-0.0165	0.0083	-0.0009	-0.0006	-0.0011	0.0000
4	y	0.0926	-0.0490	-0.0409	-0.0076	0.0308	0.0174	0.0035	0.0044	0.0014	-0.0014	-0.0028	-0.0008
4	z	0.0926	-0.1167	-0.0090	-0.0016	0.0001	-0.0031	-0.0016	-0.0007	0.0011	-0.0032	0.0004	-0.0001
3	x	0.0926	-0.0666	0.1496	-0.0104	-0.0041	-0.0058	0.0021	0.0002	0.0012	-0.0020	-0.0006	-0.0001
3	y	0.0926	-0.0448	0.0283	-0.0138	0.0256	-0.0261	-0.0029	0.0009	0.0011	-0.0012	-0.0011	0.0007
3	z	0.0926	-0.0206	0.0104	-0.0075	-0.0002	-0.0019	0.0006	-0.0015	0.0011	-0.0024	0.0002	-0.0001
2	x	0.0926	-0.0461	0.1684	0.0206	-0.0069	-0.0135	0.0007	0.0031	0.0005	-0.0013	-0.0008	-0.0005
2	y	0.0926	-0.0422	0.0332	-0.0066	0.0291	-0.0154	-0.0037	-0.0011	0.0011	-0.0016	0.0005	0.0001
2	z	0.0926	0.0229	-0.0020	-0.0075	0.0034	0.0005	-0.0009	-0.0010	0.0007	-0.0018	0.0003	0.0000
1	x	0.0926	-0.1728	0.1940	0.1540	0.0192	-0.0415	0.0192	-0.0094	0.0009	-0.0008	-0.0006	0.0000
1	y	0.0926	-0.0391	0.0902	0.0289	0.0198	0.0105	-0.0154	-0.0317	-0.0010	-0.0027	-0.0003	-0.0018
1	z	0.0926	0.0004	-0.0108	-0.0170	-0.0021	0.0037	-0.0008	-0.0004	0.0008	-0.0032	0.0002	-0.0002

Table A-4: Fourier constants for 595H vibration case in the Reflux Classifier. These values give the acceleration in the x, y and z directions as shown in Figure A-1

Accelerometer Position	Vibration direction (x, y, z)	L	a ₀	a ₁	b ₁	a ₂	b ₂	a ₃	b ₃	a ₄	b ₄	a ₅	b ₅
4	x	0.0504	-0.1238	0.4738	-0.1763	0.0069	-0.0153	-0.0003	-0.0010	0.0009	-0.0018	-0.0001	-0.0002
4	y	0.0504	-0.0220	0.0453	-0.1919	-0.0257	-0.0330	0.0052	0.0063	0.0003	-0.0013	-0.0010	-0.0010
4	z	0.0504	-0.1208	-0.0035	-0.0118	-0.0013	-0.0051	-0.0012	-0.0017	0.0009	-0.0017	0.0001	-0.0007
3	x	0.0504	-0.1017	0.3279	-0.1320	-0.0030	0.0105	0.0005	-0.0025	0.0005	-0.0041	0.0000	0.0006
3	y	0.0504	-0.0195	-0.0130	-0.1845	-0.0354	-0.0102	0.0086	-0.0022	0.0002	-0.0014	-0.0014	-0.0008
3	z	0.0504	-0.0214	0.0149	-0.0184	0.0033	-0.0020	-0.0007	-0.0025	0.0008	-0.0023	0.0006	-0.0012
2	x	0.0504	-0.0313	0.4025	0.0243	-0.0100	0.0078	0.0005	0.0000	0.0018	-0.0007	-0.0015	-0.0002
2	y	0.0504	-0.0330	0.0541	-0.1574	-0.0200	-0.0322	0.0075	0.0063	0.0005	-0.0014	-0.0007	-0.0007
2	z	0.0504	0.0017	-0.0225	-0.0075	0.0027	-0.0028	-0.0007	-0.0015	0.0001	-0.0022	0.0018	-0.0003
1	x	0.0504	-0.0056	1.0812	-0.1970	-0.0090	0.0089	-0.0012	-0.0035	0.0018	-0.0004	0.0013	-0.0008
1	y	0.0504	-0.0361	0.0404	-0.3166	-0.0363	-0.0091	0.0041	-0.0005	0.0010	-0.0001	-0.0020	-0.0015
1	z	0.0504	0.0012	0.0100	-0.0147	0.0009	-0.0040	-0.0004	-0.0029	0.0013	-0.0025	0.0009	-0.0002

Table A-5: Fourier constants for 595H vibration case in the Reflux Classifier. These values give the acceleration in the x, y and z directions as shown in Figure A-1

Accelerometer Position	Vibration direction (x, y, z)	L	a ₀	a ₁	b ₁	a ₂	b ₂	a ₃	b ₃	a ₄	b ₄	a ₅	b ₅
4	x	0.0504	-0.1255	0.6904	-0.0142	0.0096	-0.0295	0.0003	-0.0016	0.0009	-0.0009	0.0005	0.0003
4	y	0.0504	-0.0540	0.1036	-0.3874	-0.0181	-0.0143	-0.0009	-0.0105	0.0008	-0.0020	-0.0027	-0.0012
4	z	0.0504	-0.1163	0.0089	-0.0068	0.0023	-0.0063	0.0027	-0.0027	-0.0003	-0.0026	0.0008	-0.0006
3	x	0.0504	-0.0657	0.2834	-0.1100	0.0004	0.0184	0.0058	-0.0003	0.0013	-0.0015	-0.0006	0.0004
3	y	0.0504	-0.0428	0.0131	-0.3745	-0.0153	-0.0069	-0.0026	-0.0067	0.0014	-0.0021	-0.0022	-0.0007
3	z	0.0504	-0.0212	0.0297	-0.0249	0.0008	-0.0007	-0.0004	-0.0025	0.0005	-0.0024	0.0008	-0.0003
2	x	0.0504	-0.0474	0.2788	-0.0536	-0.0070	0.0164	0.0020	-0.0012	0.0014	-0.0007	0.0000	0.0005
2	y	0.0504	-0.0468	0.0882	-0.3467	-0.0119	-0.0116	-0.0038	-0.0064	0.0002	-0.0031	-0.0020	-0.0007
2	z	0.0504	0.0262	0.0171	-0.0120	0.0016	-0.0042	-0.0021	-0.0012	0.0005	-0.0024	0.0010	-0.0014
1	x	0.0504	-0.1714	0.6211	-0.0484	0.0076	-0.0216	-0.0012	0.0011	0.0012	-0.0003	0.0020	0.0004
1	y	0.0504	-0.0484	0.1893	-0.5329	-0.0643	-0.0437	-0.0010	-0.0037	0.0004	-0.0018	0.0020	-0.0036
1	z	0.0504	-0.0047	-0.0134	-0.0039	0.0005	-0.0028	-0.0003	-0.0015	0.0000	-0.0019	0.0007	-0.0008

Table A-6: Fourier constants for 595V vibration case in the Reflux Classifier. These values give the acceleration in the x, y and z directions as shown in Figure A-1

Accelerometer Position	Vibration direction (x, y, z)	L	a ₀	a ₁	b ₁	a ₂	b ₂	a ₃	b ₃	a ₄	b ₄	a ₅	b ₅
4	x	0.0504	-0.0084	0.7862	0.1751	0.0211	-0.0002	-0.0018	0.0027	0.0002	0.0015	0.0005	0.0000
4	y	0.0504	0.0038	0.3611	-0.4914	-0.0060	-0.0433	0.0020	-0.0029	-0.0025	-0.0009	0.0017	-0.0037
4	z	0.0504	0.0001	0.0435	0.0000	0.0008	-0.0009	0.0014	0.0006	0.0015	-0.0001	-0.0005	0.0002
3	x	0.0504	-0.0490	0.1199	0.0814	-0.0076	-0.0119	0.0005	0.0019	0.0003	-0.0002	0.0003	0.0000
3	y	0.0504	-0.0059	0.3966	-0.1229	-0.0060	-0.0014	0.0094	0.0015	0.0002	-0.0029	-0.0002	0.0013
3	z	0.0504	0.0009	0.0088	0.0060	0.0004	-0.0016	-0.0001	0.0007	0.0006	-0.0008	-0.0008	0.0007
2	x	0.0504	-0.0719	0.0707	-0.0109	-0.0175	0.0024	-0.0001	0.0004	0.0004	0.0005	-0.0002	0.0001
2	y	0.0504	-0.0059	0.2684	-0.2988	-0.0006	0.0089	0.0009	-0.0055	-0.0019	-0.0009	0.0015	-0.0030
2	z	0.0504	0.0221	0.0227	0.0039	0.0007	-0.0018	0.0013	0.0005	-0.0002	-0.0012	0.0000	-0.0004
1	x	0.0504	-0.0249	0.5024	0.1169	0.0081	-0.0047	-0.0009	0.0009	0.0004	0.0012	0.0010	0.0013
1	y	0.0504	-0.0012	0.1659	-0.3699	0.0032	0.0083	-0.0040	-0.0041	-0.0005	0.0011	-0.0009	-0.0016
1	z	0.0504	0.0255	0.0272	-0.0050	0.0017	0.0000	0.0009	-0.0002	0.0008	-0.0006	-0.0002	0.0005

Table A-6: Fourier constants for 595V vibration case in the vertical fluidised bed. These values give the acceleration in the x, y and z directions as shown in Figure A-1

Position	Accelerometer direction (x, y, z)	L	a ₀	a ₁	b ₁	a ₂	b ₂	a ₃	b ₃	a ₄	b ₄	a ₅	b ₅
4	x	0.0504	-0.0020	3.5449	1.2101	-0.0172	0.0571	0.0071	0.0076	0.0002	-0.0161	-0.0013	-0.0149
4	y	0.0504	0.0730	-1.8703	3.7599	-0.0162	0.1121	0.0445	0.0522	-0.0093	0.0134	0.0064	0.0177
4	z	0.0504	-0.0109	-0.2365	-0.0159	-0.0109	0.0008	0.0133	-0.0054	0.0035	0.0121	-0.0032	0.0032
3	x	0.0504	-0.2262	1.0928	-0.4458	0.0777	-0.1579	0.0243	-0.0029	0.0010	-0.0104	-0.0065	0.0000
3	y	0.0504	-0.0018	-0.9418	4.1085	0.0211	0.1145	0.0498	0.0086	-0.0037	0.0108	0.0005	0.0017
3	z	0.0504	-0.1040	-0.1574	0.0198	0.0022	0.0033	-0.0006	-0.0067	-0.0004	0.0102	-0.0005	-0.0046
2	x	0.0504	-0.8313	2.0557	-0.1366	0.1273	-0.0798	0.0300	-0.0096	0.0160	-0.0086	-0.0107	0.0008
2	y	0.0504	-0.0335	-1.8741	3.6368	-0.0421	0.0653	0.0280	0.0445	-0.0118	0.0156	0.0105	0.0124
2	z	0.0504	-0.0732	-0.0996	-0.0289	0.0185	0.0014	-0.0050	0.0034	-0.0024	0.0012	0.0054	0.0048
1	x	0.0504	-0.1076	6.6380	-1.8416	-0.1151	0.2161	0.0132	-0.0039	0.0099	0.0007	0.0018	-0.0145
1	y	0.0504	0.0204	-0.5327	4.3310	0.0104	0.0840	0.0477	0.0046	-0.0038	0.0125	0.0137	0.0080
1	z	0.0504	-0.1545	-0.3036	0.1655	0.0023	0.0053	0.0112	-0.0307	-0.0101	0.0025	-0.0067	0.0002

Appendix B: List of Experiment Dates and Conditions

Experiment ID	Date	Apparatus configuration	Dense medium	Approximate runtime (minutes)	Cumulative age of sand (minutes)	Particles to be separated	Vibration	Gas rate	Sand feed rate (g/min)
Experiment 56	14.2.07	Batch, 1 m vertical, 2 m incline	Magnetite (2 kg)	1		Tracer particles			
Experiment 57	14.2.07	Batch, 1 m vertical, 2 m incline	Magnetite (2 kg)	6		coal A 1014			
Experiment CS7	3.8.07	Batch, 1 m vertical, 2 m incline	Sand	15		coal	325H		
Experiment CS8	6.8.07	Batch, 1 m vertical, 2 m incline	Sand	1		Coal	325H		
Experiment CS9	6.8.07	Batch, 1 m vertical, 2 m incline	Sand	12		Coal	325H		
Experiment CS10	6.8.07	Batch, 1 m vertical, 2 m incline	Sand	32		Coal	325H		
Experiment CS11	7.8.07	Batch, 1 m vertical, 2 m incline	Sand	43		Coal	595V		
Experiment CS12	9.8.07	Batch, 1 m vertical, 2 m incline	Sand	42		Coal	595V		
Experiment CS13	8.8.07	Batch, 1 m vertical, 2 m incline	Sand	30		Coal	-		
Experiment CS14	8.8.07	Batch, 1 m vertical, 2 m incline	Sand	50		Coal	595V		
Experiment CS15	10.8.07	Batch, 1 m vertical, 2 m incline	Sand	15		Coal	595V		
Experiment CS16	13.8.07	Batch, 1 m vertical, 2 m incline	Sand	18.5		Coal	595V		
Experiment CS17	13.8.07	Batch, 1 m vertical, 2 m incline	Sand	40		Coal	595V		
Experiment CS18	13.8.07	Batch, 1 m vertical, 2 m incline	Sand	16		Coal	595V		
Experiment CS19	14.8.07	Batch, 1 m vertical, 2 m incline	Sand	25		Coal	-		
Experiment CS20	15.8.09	Batch, 1 m vertical, 2 m incline	Sand	22		Coal	750M		
Experiment CBI	16.8.07	Batch, 1 m vertical, 2 m incline	Ballotini			Coal	595V		
Batch tracers 1	5.9.07	Batch, 1 m vertical, 2 m incline	Sand	40		1.3	595V	20%	300
Batch tracers 2	6.9.07	Batch, 1 m vertical, 2 m incline	Sand	40		2.4	595V	20%	300
Batch tracers 3	10.9.07	Batch, 1 m vertical, 2 m incline	Sand	54		2.4	595V	20%	150
Batch tracers 4	10.9.07	Batch, 1 m vertical, 2 m incline	Sand	54		1.8	595V	20%	300
Batch tracers 5	11.9.07	Batch, 1 m vertical, 2 m incline	Sand	54		1.3	595V	20%	300
Batch tracers 6	11.9.07	Batch, 1 m vertical, 2 m incline	Sand	54		1.6	595V	20%	300
Batch tracers 7	12.9.07	Batch, 1 m vertical, 2 m incline	Sand	30		1.3	325H	20%	300
Batch tracers 8	12.9.07	Batch, 1 m vertical, 2 m incline	Sand	54		2.4	325H	20%	300
Batch tracers 9	13.9.07	Batch, 1 m vertical, 2 m incline	Sand	54		1.3	595H	20%	300
Batch tracers 10	13.9.07	Batch, 1 m vertical, 2 m incline	Sand	54		1.8	595H	20%	300
Batch tracers 11	14.9.07	Batch, 1 m vertical, 2 m incline	Sand	54		1.6	595H	20%	300
Batch tracers 12	14.9.07	Batch, 1 m vertical, 2 m incline	Sand	54		2.4	595H	20%	300
Batch tracers 13	14.9.07	Batch, 1 m vertical, 2 m incline	Sand	54		1.6	325H	20%	300

Experiment ID	Date	Apparatus configuration	Dense medium	Approximate runtime (minutes)	Cumulative age of sand	Particles to be separated	Vibration	Gas rate	Sand feed rate (g/min)
Batch tracers 16	10.10.07	Batch, 1 m vertical, 2 m incline	Sand	54	2.1	None	None	20%	300
Batch tracers 17	16.10.07	Batch, 1 m vertical, 2 m incline	Sand	54	1.6	595V	595V	10%	300
Batch tracers 18	12.11.07	Batch, 1 m vertical, 2 m incline	Sand	54	1.6	595V	595V	20%	300
Batch tracers 19	12.11.07	Batch, 1 m vertical, 2 m incline	Sand	54	1.6	595V	595V	20%	300
Batch tracers 20	12.11.07	Batch, 1 m vertical, 2 m incline	Sand	54	1.6	595V	595V	20%	300
New sand medium introduced on November 14, 2007. Old sand no longer used but kept for reference.									
Batch tracers 21	14.11.07	Batch, 1 m vertical, 2 m incline	Sand	54	1.6	595V	595V	20%	300
Batch tracers 22	16.11.07	Batch, 1 m vertical, 2 m incline	Sand	36	90	595V	595V	20%	300
Batch tracers 23	20.11.07	Batch, 1 m vertical, 2 m incline	Sand	54	144	595V	595V	20%	300
Batch tracers 24	20.11.07	Batch, 1 m vertical, 2 m incline	Sand	54	198	595V	595V	20%	300
Batch tracers 25	20.11.07	Batch, 1 m vertical, 2 m incline	Sand	48	246	None	None	20%	300
Batch tracers 26	21.11.07	Batch, 1 m vertical, 2 m incline	Sand	54	300	595V	595V	20%	300
Batch tracers 27	22.11.07	Batch, 1 m vertical, 2 m incline	Sand	54	354	595V	595V	20%	150
Batch tracers 28	22.11.07	Batch, 1 m vertical, 2 m incline	Sand	54	408	595V	595V	20%	150
Batch tracers 29	22.11.07	Batch, 1 m vertical, 2 m incline	Sand	54	462	595V	595V	20%	150
Batch tracers 30	28.11.07	Batch, 1 m vertical, 2 m incline	Sand	36	498	595V	595V	20%	300
Batch tracers 31	28.11.07	Batch, 1 m vertical, 2 m incline	Sand	36	534	595V	595V	20%	300
Batch tracers 32	28.11.07	Batch, 1 m vertical, 2 m incline	Sand	36	570	595V	595V	20%	300
Batch tracers 33	29.11.07	Batch, 1 m vertical, 2 m incline	Sand	54	624	595V	595V	20%	300
Batch tracers 34	29.11.07	Batch, 1 m vertical, 2 m incline	Sand	54	678	595V	595V	20%	300
Batch tracers 35	29.11.07	Batch, 1 m vertical, 2 m incline	Sand	54	732	595V	595V	20%	300
Batch tracers 36	3.12.07	Batch, 1 m vertical, 2 m incline	Sand	54	786	1.8	595V	20%	300
Batch tracers 37	3.12.07	Batch, 1 m vertical, 2 m incline	Sand	54	840	1.8	595V	20%	300
Batch tracers 38	3.12.07	Batch, 1 m vertical, 2 m incline	Sand	54	894	1.8	595V	20%	300
Batch tracers 39	4.12.07	Batch, 1 m vertical, 2 m incline	Sand	54	948	1.8	595V	20%	300
Batch tracers 40	5.12.07	Batch, 1 m vertical, 2 m incline	Sand	54	1002	1.6	None	20%	300
Batch tracers 41	6.12.07	Batch, 1 m vertical, 2 m incline	Sand	54	1056	1.8	None	20%	300
Batch tracers 42	6.12.07	Batch, 1 m vertical, 2 m incline	Sand	54	1110	1.8	None	20%	300
Batch tracers 43	10.12.07	Batch, 1 m vertical, 2 m incline	Sand	54	1164	1.6	None	20%	300
Batch tracers 44	10.12.07	Batch, 1 m vertical, 2 m incline	Sand	54	1218	2.4	None	20%	300
Batch tracers 45	10.12.07	Batch, 1 m vertical, 2 m incline	Sand	54	1272	1.6	None	20%	300
Springs were replaced on 11 December 2007									
Batch tracers 46	14.12.07	Batch, 1 m vertical, 2 m incline	Sand	54	1326	1.3	595H	20%	150
Batch tracers 47	14.12.07	Batch, 1 m vertical, 2 m incline	Sand	54	1380	1.6	595H	20%	150
Batch tracers 48	14.12.07	Batch, 1 m vertical, 2 m incline	Sand	54	1434	1.8	595H	20%	150

Experiment ID	Date	Apparatus configuration	Underflow valves	Underflow rate	Dense medium	Approximate runtime (minutes)	Cumulative age of sand	Tracer particles to be separated	Particle size range	Vibration	Gas rate
WS1	7.11.08	Continuous, 1 m vertical, 2 m incline	2 inch pinch valves	One per 10 minutes	Sand	30	1464		-4+2 mm	595V	20%
WS2	24.11.08	Continuous, 1 m vertical, 2 m incline	2 inch pinch valves		Sand	40	1504	all densities	all sizes	595V	20%
WS3	26.11.08	Continuous, 1 m vertical, 2 m incline	2 inch pinch valves	one per 90 sec	Sand	30	1534	all densities	all sizes	595V	30%
WS4	8.12.08	Continuous, 1 m vertical, 2 m incline	2 inch pinch valves	1 per 90 sec	Sand	27	1561	all densities	all sizes	465 (Motors horizontal)	20%
WS5	18.12.08	Continuous, 1 m vertical, 2 m incline	2 inch pinch valves	1 per 120 sec	Sand	20	1581	all densities	-6.35 + 2 mm	595 (motors horizontal)	20%
WS6	7.1.09	Continuous, 1 m vertical, 2 m incline	2 inch pinch valves	1 per 180 sec	Sand	20	1601	all densities	-6.35 + 2 mm	595 (motors horizontal)	20%
WS7	7.1.09	Continuous, 1 m vertical, 2 m incline	2 inch pinch valves	none	Sand	20	1621	all densities	-6.35 + 2 mm	595 (motors horizontal)	20%
WS8	8.1.09	Continuous, 1 m vertical, 2 m incline	2 inch pinch valves	none	Sand	19	1640	all densities	-6.35 + 2 mm	none	20%
WS9	8.1.09	Continuous, 1 m vertical, 2 m incline	2 inch pinch valves	none	Sand	20	1660	all densities	-6.35 + 2 mm	360 (motors horizontal)	20%
WS10	9.1.09	Continuous, 1 m vertical, 2 m incline	2 inch pinch valves	1 per 240 sec	Sand	20	1680	all densities	-6.35 + 2 mm	595 (motors horizontal)	20%
WS11	12.1.09	Continuous, 1 m vertical, 2 m incline	2 inch pinch valves	1 per 120 sec	Sand	20	1700	all densities	-6.35 + 2 mm	360 (motors horizontal)	20%
WS12	12.1.09	Continuous, 1 m vertical, 2 m incline	2 inch pinch valves	1 per 120 sec	Sand	20	1720	all densities	-6.35 + 2 mm	360 (motors horizontal)	20%
WS13	13.1.09	Continuous, 1 m vertical, 2 m incline	2 inch pinch valves	1 per 240 sec	Sand	20	1740	all densities	-6.35 + 2 mm	none	20%
WS14	13.1.09	Continuous, 1 m vertical, 2 m incline	2 inch pinch valves	none	Sand	20	1760	all densities	-6.35 + 2 mm	none	20%
WS15	13.1.09	Continuous, 1 m vertical, 2 m incline	2 inch pinch valves	1 per 120 sec	Sand	20	1780	all densities	-6.35 + 2 mm	595 (motors vertical)	20%
WS16	15.1.09	Continuous, 1 m vertical, 2 m incline	2 inch pinch valves	1 per 240 sec	Sand	20	1800	all densities	-6.35 + 2 mm	595 (motors vertical)	20%
CST1	16.1.09	Continuous, 1 m vertical, 2 m incline	2 inch pinch valves	1 per 120 sec	Sand	20	1820	all densities	-6.35 + 2 mm	595 (motors vertical)	20%
CST2	16.1.09	Continuous, 1 m vertical, 2 m incline	2 inch pinch valves	1 per 240 sec	Sand	20	1840	all densities	-6.35 + 2 mm	360 (motors vertical)	20%
CST3	16.1.09	Continuous, 1 m vertical, 2 m incline	2 inch pinch valves	1 per 240 sec	Sand	20	1860	all densities	-6.35 + 2 mm	360 (motors vertical)	20%
CST4	16.1.09	Continuous, 1 m vertical, 2 m incline	2 inch pinch valves	1 per 240 sec	Sand	20	1880	all densities	-6.35 + 2 mm	360 (motors vertical)	20%
CST5	27.1.09	Continuous, 1 m vertical, 2 m incline	1 inch pinch valves	1 per 30 sec	Coal Sand	32	1912	all densities	-6.35 + 1 mm	360 (motors vertical)	20%
CST6	30.1.09	Continuous, 1 m vertical, 2 m incline	1 inch pinch valves	1 per 20 sec	Coal Sand	100	2012	all densities	-6.35 + 1 mm	360 (motors vertical)	20%
CST7	6.2.09	Continuous, 1 m vertical, 2 m incline	1 inch pinch valves	1 per 20 sec	Coal Sand	64	2076	all densities	-6.35 + 1 mm	360 (motors vertical)	20%
CST8	10.2.09	Continuous, 1 m vertical, 2 m incline	1 inch pinch valves	1 per 20 sec	Coal Sand	76	2152	all densities	-6.35 + 1 mm	360 (motors vertical)	20%
CST9	21.4.09	Continuous, 1 m vertical, 2 m incline	1 inch pinch valves	1 per 30 sec	Coal Sand	130	2382	Coal, 50g/min	-5.6 + 1 mm	550 (motors vertical)	20%
CST10	27.4.09	Continuous, 1 m vertical, 2 m incline	1 inch pinch valves	1 per 60 sec	Coal Sand	90	2472	Coal, 50g/min	-5.6 + 1 mm	550 (motors vertical)	20%
CST11	29.4.09	Continuous, 1 m vertical, 2 m incline	1 inch pinch valves	1 per 60 sec	Coal Sand	160	2632	Coal, 50g/min	-5.6 + 1 mm	550 (motors vertical)	20%
CST12	8.5.09	Continuous, 1 m vertical, 2 m incline	1 inch pinch valves	1 per 90 sec	Coal Sand	117	2749	Coal, 50g/min	-5.6 + 1 mm	550 (motors vertical)	20%
CST13	13.5.09	Continuous, 1 m vertical, 2 m incline	1 inch pinch valves	Variable	Coal Sand	81	2938	Coal, 50g/min	-5.6 + 1 mm	550 (motors vertical)	20%
CST14	19.5.09	Continuous, 1 m vertical, 2 m incline	1 inch pinch valves	Variable	Coal Sand	180	3118	Coal, 12g/min	-5.6 + 1 mm	550 (motors vertical)	20%
CST15	22.5.09	Continuous, 1 m vertical, 2 m incline	1 inch pinch valves	variable	Coal Sand	100	3218	Coal, 25g/min	-5.6 + 1 mm	300 (motors vertical)	20%
CST16	4.6.09	Continuous, 1 m vertical, 2 m incline	1 inch pinch valves	variable	Coal Sand	100	3218	Coal, 25g/min	-5.6 + 1 mm	300 (motors vertical)	20%
CST17	14.7.09	Continuous, 1 m vertical, 2 m incline	1 inch pinch valves	1 per 10 sec	Coal Sand	100	3318	Coal, 25g/min	-5.6 + 1 mm	550 (motors vertical)	20%
CST18	31.8.09	Continuous, 1 m vertical, 2 m incline	1 inch pinch valves	1 per 20 sec	Coal Sand	50	3368	Coal, 25g/min coal and tracers	-5.6 + 1 mm	326 (motors vertical)	12%
CST19	2.9.09	Continuous, 1 m vertical, 2 m incline	1 inch pinch valves	1 per 20 sec	Coal Sand	80	3448	Coal, 12g/min	-5.6 + 1 mm	326 (motors vertical)	13%
CST20	4.9.09	Continuous, 1 m vertical, 2 m incline	1 inch pinch valves	1 per 20 sec	Coal Sand	50	3498	Coal, 12g/min	-5.6 + 1 mm	326 (motors vertical)	15%
CST21	2.10.09	Continuous, 3 m vertical	1 inch pinch valves	1 per 40 sec	Coal Sand	90	3588	Coal, 25g/min	-5.6 + 1 mm	595 (motors vertical)	25%
CST22	7.10.09	Continuous, 3 m vertical	1 inch pinch valves	1 per 40 sec	Coal Sand	140	3728	Coal, 25g/min	-5.6 + 1 mm	326 (motors vertical)	25%

A new bag of 50N sand was added to the current sand. This is now known as "Coal sand"

Springs were replaced before 14 July 2009

Experiment ID	Date	Apparatus configuration	Underflow valves	Underflow rate	Dense medium	Approximate runtime (minutes)	Cumulative age of sand	Tracer particles to be separated	Particle size range	Vibration	Gas rate
WS17	22.7.09	Continuous, 1 m vertical, 0.675 m incline	1 inch pinch valves	1 per 40 sec	Tracer Sand	20	20	all densities	-6.35 + 2 mm	326 (motors vertical)	20%
WS18	22.7.09	Continuous, 1 m vertical, 0.675 m incline	1 inch pinch valves	1 per 20 sec	Tracer Sand	20	40	all densities	-6.35 + 2 mm	326 (motors vertical)	20%
WS19	22.7.09	Continuous, 1 m vertical, 0.675 m incline	1 inch pinch valves	1 per 20 sec	Tracer Sand	20	60	all densities	-6.35 + 2 mm	326 (motors vertical)	10%
WS20	22.7.09	Continuous, 1 m vertical, 0.675 m incline	1 inch pinch valves	1 per 30 sec	Tracer Sand	20	80	all densities	-6.35 + 2 mm	326 (motors vertical)	10%
WS21	29.7.09	Continuous, 1 m vertical, 0.675 m incline	1 inch pinch valves	1 per 20 sec	Tracer Sand	30	110	all densities	-6.35 + 2 mm	none	10%
WS22	29.7.09	Continuous, 1 m vertical, 0.675 m incline	1 inch pinch valves	1 per 30 sec	Tracer Sand	20	130	all densities	-6.35 + 2 mm	none	10%
WS23	29.7.09	Continuous, 1 m vertical, 0.675 m incline	1 inch pinch valves	1 per 60 sec	Tracer Sand	40	170	all densities	-6.35 + 2 mm	326 (motors vertical)	10%
WS24	30.7.09	Continuous, 1 m vertical, 0.675 m incline	1 inch pinch valves	1 per 20 sec	Tracer Sand	20	190	all densities	-6.35 + 2 mm	595 (motors vertical)	10%
WS25	30.7.09	Continuous, 1 m vertical, 0.675 m incline	1 inch pinch valves	1 per 30 sec	Tracer Sand	20	210	all densities	-6.35 + 2 mm	595 (motors vertical)	10%
WS26	30.7.09	Continuous, 1 m vertical, 0.675 m incline	1 inch pinch valves	1 per 60 sec	Tracer Sand	20	230	all densities	-6.35 + 2 mm	595 (motors vertical)	10%
WS27	10.8.09	Continuous, 1 m vertical, 0.675 m incline	1 inch pinch valves	1 per 40 sec	Tracer Sand	60	290	all densities	-6.35 + 2 mm	595 (motors horizontal)	10%
WS28	10.8.09	Continuous, 1 m vertical, 0.675 m incline	1 inch pinch valves	1 per 5 min	Tracer Sand	60	350	all densities	-6.35 + 2 mm	595 (motors horizontal)	10%
WS29	11.8.09	Continuous, 1 m vertical, 0.675 m incline	1 inch pinch valves	1 per 5 min	Tracer Sand	60	410	all densities	-6.35 + 2 mm	595 (motors horizontal)	20%
WS30	11.8.09	Continuous, 1 m vertical, 0.675 m incline	1 inch pinch valves	1 per 40 sec	Tracer Sand	60	470	all densities	-6.35 + 2 mm	595 (motors horizontal)	20%
WS31	13.8.09	Continuous, 1 m vertical, 0.675 m incline	1 inch pinch valves	1 per 40 sec	Tracer Sand	60	530	all densities	-6.35 + 2 mm	595 (motors horizontal)	15%
WS32	13.8.09	Continuous, 1 m vertical, 0.675 m incline	1 inch pinch valves	1 per 20 sec	Tracer Sand	60	590	all densities	-6.35 + 2 mm	595 (motors horizontal)	15%
WS33	17.8.09	Continuous, 1 m vertical, 0.675 m incline	1 inch pinch valves	1 per 20 sec	Tracer Sand	60	650	all densities	-6.35 + 2 mm	326 (motors vertical)	20%
WS34	17.8.09	Continuous, 1 m vertical, 0.675 m incline	1 inch pinch valves	1 per 20 sec	Tracer Sand	60	710	all densities	-6.35 + 2 mm	326 (motors vertical)	10%
WS35	18.8.09	Continuous, 1 m vertical, 0.675 m incline	1 inch pinch valves	1 per 20 sec	Tracer Sand	60	770	all densities	-6.35 + 2 mm	595 (motors vertical)	10%
WS36	19.8.09	Continuous, 1 m vertical, 0.675 m incline	1 inch pinch valves	1 per 20 sec	Tracer Sand	60	830	all densities	-6.35 + 2 mm	595 (motors vertical)	20%
WS37	25.8.09	Continuous, 1 m vertical, 2 m incline	1 inch pinch valves	1 per 20 sec	Tracer Sand	60	890	all densities	-6.35 + 2 mm	595 (motors vertical)	20%
WS38	27.8.09	Continuous, 1 m vertical, 2 m incline	1 inch pinch valves	1 per 30 sec	Tracer Sand	60	950	all densities	-6.35 + 2 mm	326 (motors vertical)	12%
WS39	27.8.09	Continuous, 1 m vertical, 2 m incline	1 inch pinch valves	1 per 20 sec	Tracer Sand	60	1010	all densities	-6.35 + 2 mm	326 (motors vertical)	12%
WS40	27.8.09	Continuous, 1 m vertical, 2 m incline	1 inch pinch valves	1 per 30 sec	Tracer Sand	60	1070	all densities	-6.35 + 2 mm	595 (motors vertical)	13%
WS41	30.9.09	continuous 3 m vertical	1 inch pinch valves	1 per 30 sec	Tracer Sand	60	1130	all densities	-6.35 + 2 mm	595 (motors vertical)	25%
WS42	1.10.09	continuous 3 m vertical	1 inch pinch valves	1 per 40 sec	Tracer Sand	60	1190	all densities	-6.35 + 2 mm	595 (motors vertical)	25%
WS43	1.10.09	continuous 3 m vertical	1 inch pinch valves	1 per 40 sec	Tracer Sand	60	1250	all densities	-6.35 + 2 mm	595 (motors vertical)	25%
CT1	14.10.09	continuous 3 m vertical	1 inch pinch valves	1 per 30 sec	Tracer Sand	117	1367	all densities	-6.35 + 1 mm	325 (motors vertical)	25%
CT2	21.10.09	continuous 3 m vertical	1 inch pinch valves	1 per 30 sec	Tracer Sand	117	1484	all densities	-6.35 + 1 mm	595 (motors vertical)	25%
CT3	26.10.09	continuous 3 m vertical	1 inch pinch valves	1 per 30 sec	Tracer Sand	117	1601	all densities	-6.35 + 1 mm	595 (motors vertical)	25%
CT4	28.10.09	continuous 3 m vertical	1 inch pinch valves	1 per 18 sec	Tracer Sand	99	1700	all densities	-6.35 + 1 mm	595 (motors vertical)	25%
CT5	4.11.09	continuous 3 m vertical	1 inch pinch valves	1 per 12 sec	Tracer Sand	105	1805	all densities	-6.35 + 1 mm	595 (motors vertical)	25%
CT6	6.11.09	continuous 3 m vertical	1 inch pinch valves	1 per 15 sec	Tracer Sand	114	1919	all densities	-6.35 + 1 mm	595 (motors vertical)	25%
CT7	11.11.09	continuous 3 m vertical	1 inch pinch valves	1 per 21 sec	Tracer Sand	90	2009	all densities	-6.35 + 1 mm	595 (motors vertical)	25%
CT8	13.11.09	continuous 3 m vertical	1 inch pinch valves	1 per 15 sec	Tracer Sand	90	2099	all densities	-6.35 + 1 mm	595 (motors vertical)	35%
CT9	18.11.09	continuous 3 m vertical	1 inch pinch valves	1 per 15 sec	Tracer Sand	117	2216	all densities	-6.35 + 1 mm	595 (motors vertical)	30%
CT10	4.12.09	Continuous, 1 m vertical, 2 m incline	1 inch pinch valves	1 per 15 sec	Tracer Sand	93	2309	all densities	-6.35 + 1 mm	595 (motors vertical)	25%
CT11	6.1.10	Continuous, 1 m vertical, 2 m incline	1 inch pinch valves	1 per 18 sec	Tracer Sand	57	2366	all densities	-6.35 + 1 mm	595 (motors vertical)	20%
CT12	9.1.10	Continuous, 1 m vertical, 2 m incline	1 inch pinch valves	1 per 12 sec	Tracer Sand	90	2456	all densities	-6.35 + 1 mm	595 (motors vertical)	25%
CT13	13.1.10	Continuous, 1 m vertical, 2 m incline	1 inch pinch valves	1 per 12 sec	Tracer Sand	30	2486	all densities	-6.35 + 1 mm	595 (motors vertical)	25%
CT14	15.1.10	Continuous, 1 m vertical, 2 m incline	1 inch pinch valves	1 per 18 sec	Tracer Sand	105	2591	all densities	-6.35 + 1 mm	595 (motors vertical)	25%
CT15	18.1.10	Continuous, 1 m vertical, 2 m incline	1 inch pinch valves	1 per 21 sec	Tracer Sand	114	2705	all densities	-6.35 + 1 mm	595 (motors vertical)	25%
CT16	20.1.10	Continuous, 1 m vertical, 2 m incline	1 inch pinch valves	1 per 15 sec	Tracer Sand	117	2822	all densities	-6.35 + 1 mm	595 (motors vertical)	25%
CT17	22.1.10	Continuous, 1 m vertical, 2 m incline	1 inch pinch valves	1 per 15 sec	Tracer Sand	114	2936	all densities	-6.35 + 1 mm	595 (motors vertical)	30%
CT18	25.1.10	Continuous, 1 m vertical, 2 m incline	1 inch pinch valves	1 per 15 sec	Tracer Sand	114	3050	all densities	-6.35 + 1 mm	595 (motors vertical)	35%

Appendix C: Batch tracer particle data

Vibration	Gas Rate (%)	Feed Rate (g/min)	Date	Tracer Density (kg/m ³)
595V	20	300	11.9.07	1600

Sample Time (min)	Mass of Tracer Particles			
	-2.0 +1.0 mm	-4.0 +2.0 mm	-6.35 +4.0 mm	
1	1523.9	0.0	0.0	
3	138.1	0.0	0.0	
5	634.5	0.0	0.0	
9	1165	2.5	0.0	
11	471.9	4.8	1.5	
13	471.1	6.9	4.6	
15	671.6	8.4	5.5	
17	552.8	7.6	7.8	
19	575.7	5.4	8.8	
21	589.1	5.7	8.5	
23	517.5	3.7	4.2	
25	722.1	3.8	3.7	
27	469.8	2.5	1.4	
30	977.8	3.9	1.8	
33	1069.1	3.2	2.2	
36	780.3	1.8	1.1	
39	1041	2.3	2.3	
42	888.1	1.7	1.4	
45	955.6	1.2	2.0	
48	897.8	1.2	1.8	
51	757.2	0.9	2.2	
54	1279.3	0.8	2.4	
Bed Remains	7167.2	3.1	22.9	110.4

Vibration	Gas Rate (%)	Feed Rate (g/min)	Date	Tracer Density (kg/m ³)
595V	20	300	11.9.07	1300

Sample Time (min)	Mass of Tracer Particles		
	-2.0 +1.0 mm	-4.0 +2.0 mm	-6.35 +4.0 mm
1	1537.6	0.0	0.0
3	231	0.0	0.0
5	577	0.1	0.0
7	477.4	2.8	19.0
9	274.3	3.8	25.3
11	966.2	8.9	44.4
13	83.4	1.5	10.4
15	383	7.1	20.3
17	774.2	6.1	9.0
19	455.3	2.2	2.1
21	973.7	3.5	2.3
23	673.8	1.7	1.4
25	465.5	0.9	0.5
27	791.8	1.3	0.8
30	739.3	0.8	0.3
33	1006.8	0.8	0.1
36	1145	0.5	0.2
39	833.2	0.3	0.1
42	1022.6	0.3	0.0
45	865	0.1	0.0
48	1054.3	0.1	0.0
51	895.2	0.1	0.0
54	1285.4	0.1	0.0
Bed Remains	7346.4	0.3	0.1

Vibration	Gas Rate (%)	Feed Rate (g/min)	Date	Tracer Density (kg/m ³)
595V	20	300	10.9.07	1800

Sample Time (min)	Mass of Tracer Particles		
	-2.0 +1.0 mm	-4.0 +2.0 mm	-6.35 +4.0 mm
1	470.3	0.0	0.0
3	244.7	0.0	0.0
5	1380.9	0.0	0.0
9	1084.7	0.1	0.0
11	561.4	1.8	0.0
13	465.5	2.0	0.0
15	666.5	3.1	0.1
17	586.1	3.1	0.1
19	613.3	3.1	0.1
21	679.8	2.9	0.0
23	669.1	2.8	0.3
25	775.1	2.4	0.5
27	545.4	2.0	0.1
30	1256.7	3.2	0.8
33	696.5	1.8	1.3
36	899.6	1.7	1.7
39	1152.1	1.5	1.5
42	764.6	1.0	1.1
45	829	0.9	0.5
48	1036.3	0.9	0.4
51	946.3	0.9	0.7
54	1148.2	0.6	0.4
Bed Remains	7208.6	6.3	176.4

Vibration	Gas Rate (%)	Feed Rate (g/min)	Date	Tracer Density (kg/m ³)
595V	20	300	6.9.07	2400

Sample Time (min)	Mass of Tracer Particles		
	-2.0 +1.0 mm	-4.0 +2.0 mm	-6.35 +4.0 mm
2	1881.2	0.0	0.0
10	1736.6	0.1	0.0
18	2305.0	2.1	0.0
24	1894.4	3.9	0.0
32	2441.8	6.1	0.0
40	2648.3	5.0	0.0
Bed Remains	7352.0	27.4	161.1

Vibration	Gas Rate (%)	Feed Rate (g/min)	Date	Tracer Density (kg/m ³)
595H	20	300	13.9.07	1300
Mass of Tracer Particles				
Sample Time (min)	Mass of Sand (g)	-2.0 +1.0 mm	-4.0 +2.0 mm	-6.35 +4.0 mm
1	1493.5	0.0	0.0	0.0
3	636.1	0.0	0.0	0.0
5	847.5	0.0	0.0	0.1
7	416.6	0.0	0.0	0.3
9	840.2	0.5	2.4	10.3
11	206.2	0.9	5.2	19.5
13	578.8	4.0	15.9	45.3
15	571.1	4.7	17.8	25.9
17	501.1	4.8	14.1	19.1
19	603.3	5.5	11.5	7.9
21	654.4	4.6	8.4	5.9
23	440.2	3.1	4.7	1.4
25	674.7	3.3	4.5	1.2
27	749.9	2.7	2.9	0.8
30	666.9	2.2	2.3	0.4
33	1003.6	2.2	1.6	0.1
36	883.1	1.0	1.2	0.0
39	1048.9	0.8	0.8	0.0
42	829.7	0.5	0.3	0.0
45	1435.6	0.5	0.3	0.0
48	503.7	0.1	0.0	0.0
51	1425.3	0.2	0.0	0.0
54	822.7	0.1	0.0	0.0
Bed Remians	6906.1	0.2	0.2	0.9

Vibration	Gas Rate (%)	Feed Rate (g/min)	Date	Tracer Density (kg/m ³)
595H	20	300	14.9.07	1600
Mass of Tracer Particles				
Sample Time (min)	Mass of Sand (g)	-2.0 +1.0 mm	-4.0 +2.0 mm	-6.35 +4.0 mm
1	1003.2	0.0	0.0	0.0
3	377.1	0.0	0.0	0.0
5	470	0.0	0.0	0.0
7	814.2	0.0	0.0	0.0
9	562.8	0.0	0.0	0.0
11	584.4	0.4	0.0	0.0
13	362.6	0.2	0.2	0.0
15	685	1.2	1.2	0.2
17	667.7	1.6	1.7	0.3
19	628.4	1.9	2.0	1.4
21	656.9	2.2	2.2	0.8
23	534.1	2.1	1.8	1.0
25	675.1	2.4	1.9	0.9
27	693.1	2.6	2.7	1.2
30	812.5	3.7	4.2	2.7
33	1095.1	3.3	4.2	2.8
36	864.1	2.4	3.4	2.2
39	1077.7	2.5	3.0	2.6
42	1040.2	1.8	3.0	2.8
45	682.8	1.1	1.7	1.4
48	1057.2	1.1	1.7	2.7
51	1003.4	1.2	2.2	3.6
54	1131.7	1.3	1.8	2.4
Bed Remians	6869.1	36.9	69.0	146.9

Vibration	Gas Rate (%)	Feed Rate (g/min)	Date	Tracer Density (kg/m ³)
595H	20	300	13.9.07	2400

Sample Time (min)	Mass of Tracer Particles		
	Mass of Sand (g)	-2.0 +1.0 mm	-4.0 +2.0 mm
1	1197.9	0.0	0.0
3	749.5	0.0	0.0
5	343.6	0.0	0.0
7	734.5	0.0	0.0
9	442.8	0.0	0.0
11	616.9	0.1	0.0
13	713.4	0.0	0.0
15	469.3	0.1	0.0
17	747.3	0.0	0.0
19	584.7	0.1	0.0
21	595.9	0.1	0.0
23	685.5	0.0	0.0
25	544.3	0.1	0.0
27	638.8	0.0	0.0
30	840.2	0.1	0.0
33	982.8	0.1	0.0
36	920.8	0.0	0.0
39	1024.7	0.1	0.0
42	986.2	0.0	0.0
45	725.6	0.0	0.0
48	1089.3	0.0	0.0
51	835.5	0.0	0.0
54	1165.7	0.2	0.0
Bed Remains	6543.9	42.0	88.0
			166.6

Vibration	Gas Rate (%)	Feed Rate (g/min)	Date	Tracer Density (kg/m ³)
595H	20	300	13.9.07	1800

Sample Time (min)	Mass of Tracer Particles		
	Mass of Sand (g)	-2.0 +1.0 mm	-4.0 +2.0 mm
1	931.4	0.0	0.0
3	378.7	0.0	0.0
5	998.1	0.0	0.0
7	419.9	0.0	0.0
9	584.9	0.0	0.0
11	519.3	0.1	0.0
13	556.2	0.3	0.1
15	674	0.5	0.4
17	645.1	0.7	0.5
19	646.2	0.7	0.5
21	618.8	0.7	0.5
23	592.3	0.8	0.7
25	623.7	0.7	0.7
27	674.1	0.7	0.6
30	1036.1	1.0	0.7
33	894.3	0.8	1.1
36	1001.9	0.5	0.8
39	886.9	0.6	0.5
42	812.9	0.3	0.5
45	999.1	0.3	0.6
48	958.7	0.2	0.5
51	917.1	0.2	0.4
54	1193.6	0.2	0.3
Bed Remains	6978.3	32.4	76.1
			184.1

Vibration	Gas Rate (%)	Feed Rate (g/min)	Date	Tracer Density (kg/m ³)
325H	20	300	12.9.07	1300
Mass of Tracer Particles				
Sample Time (min)	Mass of Sand (g)	-2.0 +1.0 mm	-4.0 +2.0 mm	-6.35 +4.0 mm
1	3513.5	0.0	0.0	0.0
3	3.4	0.0	0.0	0.0
5	921.0	11.3	34.4	62.9
7	291.3	4.6	13.7	18.2
9	17.6	0.3	0.9	4.8
11	0.0	0.0	0.0	0.0
13	381.0	8.7	22.9	31.5
15	1064.5	13.0	22.0	17.2
17	428.8	1.5	1.9	0.8
19	0.0	1.8	1.4	0.3
21	147.7	0.1	0.1	0.1
23	774.9	0.4	0.3	0.1
25	688.3	0.2	0.1	0.0
27	721.0	0.1	0.0	0.0
30	910.0	0.1	0.1	0.0
Bed Remians	5750.7	0.2	0.5	0.1

Vibration	Gas Rate (%)	Feed Rate (g/min)	Date	Tracer Density (kg/m ³)
325H	20	300	14.9.07	1600
Mass of Tracer Particles				
Sample Time (min)	Mass of Sand (g)	-2.0 +1.0 mm	-4.0 +2.0 mm	-6.35 +4.0 mm
1	3494.9	0.0	0.0	0.0
3	0.0	0.0	0.0	0.0
5	0.0	0.0	0.0	0.0
7	554.1	8.8	20.8	32.5
9	288.8	6.2	12.3	20.7
11	663.6	15.4	27.5	37.4
13	595.0	17.5	26.0	50.2
14.8	372.9	7.1	7.7	15.4
17	444.6	4.9	6.0	7.0
19	740.6	5.6	4.9	6.8
21	543.4	1.9	1.4	1.2
23	903.0	1.5	1.1	1.4
25	345.3	0.5	0.3	0.5
27	1021.3	0.6	0.4	0.1
30	611.2	0.2	0.2	0.0
33	1761.5	0.1	0.1	0.0
36	243.3	0.0	0.0	0.2
39	1735.7	0.1	0.0	0.2
42	73.5	0.0	0.0	0.0
45	1019.8	0.0	0.0	0.5
48	1319.1	0.0	0.0	0.0
51	389.6	0.0	0.0	0.0
54	1163.1	0.0	0.0	0.3
Bed Remians	5864.7	0.1	0.0	1.5

Vibration	Gas Rate (%)	Feed Rate (g/min)	Date	Tracer Density (kg/m ³)
325H	20	300	2.10.07	2100

Sample Time (min)	Mass of Tracer Particles		
	-2.0 +1.0 mm	-4.0 +2.0 mm	-6.35 +4.0 mm
1	6181.1	0.0	0.0
3	0.0	0.0	0.0
5	0.0	0.0	0.0
7	0.0	0.0	0.0
9	456.1	12.1	36.6
11	595.6	6.7	20.5
13	567.5	4.2	14.7
15	683.7	3.8	12.2
17	634.8	2.3	9.9
19	642.0	1.8	11.2
21	980.8	2.1	20.4
23	293.6	0.6	5.2
25	616.1	1.2	7.0
27	1029.0	1.2	14.5
30	414.7	0.4	5.8
33	743.9	0.7	4.3
36	1170.4	0.5	5.8
39	1323.8	0.4	5.3
42	196.5	0.2	0.7
45	1162.7	0.1	2.8
48	844.2	0.1	2.2
51	1585.3	0.1	2.9
54	770.8	0.1	0.4
Bed Remains	4985.5	0.4	20.2

Vibration	Gas Rate (%)	Feed Rate (g/min)	Date	Tracer Density (kg/m ³)
325H	20	300	18.9.07	1800

Sample Time (min)	Mass of Tracer Particles		
	-2.0 +1.0 mm	-4.0 +2.0 mm	-6.35 +4.0 mm
1	3460.4	0.0	0.0
3	0.0	0.0	0.0
5	1377.5	2.3	16.1
7	23.7	0.1	0.0
9	228.8	1.7	12.3
11	447.3	4.0	17.5
13	765.0	9.1	48.4
15	701.3	6.4	28.1
17	1393.6	9.5	35.8
19	1.8	0.0	0.0
21	20.0	0.5	1.2
23	613.9	3.4	9.6
25	689.8	1.5	3.8
27	683.0	1.0	2.1
30	787.3	0.5	1.4
33	1556.3	0.4	1.0
36	1222.8	0.1	1.5
39	133.3	0.0	0.8
42	1078.8	0.1	1.2
45	797.6	0.0	0.5
48	922.9	0.0	0.3
51	833.1	0.0	0.0
54	1179.5	0.0	0.0
Bed Remains	5564.6	0.2	4.1

Vibration	Gas Rate (%)	Feed Rate (g/min)	Date	Tracer Density (kg/m ³)
No Vibration	20	300	20.11.07	1300
Mass of Tracer Particles				
Sample Time (min)	Mass of Sand (g)	-2.0 +1.0 mm	-4.0 +2.0 mm	-6.35 +4.0 mm
1	2925.0	0.0	0.0	0.0
3	0.0	0.0	0.0	0.0
5	0.0	0.0	0.0	0.0
7	1528.5	15.2	40.9	83.6
9	0.9	0.1	0.0	0.0
11	57.4	1.0	3.5	4.1
13	1264.9	18.6	44.1	46.5
15	1.5	0.0	0.0	0.0
17	174.2	1.2	3.5	1.5
19	615.6	2.4	2.2	0.0
21	412.4	1.7	1.2	0.0
23	930.8	1.4	0.5	0.0
25	427.0	0.2	0.1	0.0
27	783.1	0.4	0.1	0.0
30	519.0	0.2	0.0	0.0
33	935.4	0.1	0.0	0.0
36	1272.1	0.0	0.0	0.0
39	673.7	0.1	0.0	0.0
42	831.6	0.0	0.0	0.0
45	945.6	0.0	0.0	0.0
48	1203.1	0.1	0.0	0.0
Bed Remians	6352.0	0.1	0.6	0.7

Vibration	Gas Rate (%)	Feed Rate (g/min)	Date	Tracer Density (kg/m ³)
No Vibration	20	300	10.12.07	1600
Mass of Tracer Particles				
Sample Time (min)	Mass of Sand (g)	-2.0 +1.0 mm	-4.0 +2.0 mm	-6.35 +4.0 mm
1	2452.8	0.0	0.0	0.0
3	0.3	0.0	0.0	0.0
5	1095.3	4.5	13.6	18.9
7	420.2	2.8	6.1	7.7
9	591.1	4.0	7.7	9.2
11	522.0	4.0	6.9	1.4
13	665.0	2.7	6.0	3.4
14.8	808.0	2.5	3.3	0.5
17	243.7	0.6	1.6	0.6
19	818.3	1.9	3.2	0.9
21	597.0	1.0	0.7	0.0
23	280.7	0.4	0.5	0.2
25	619.2	0.6	0.5	0.1
27	806.8	0.6	0.3	0.0
30	597.9	0.5	0.2	0.0
33	698.5	0.2	0.2	0.0
36	885.0	0.2	0.1	0.0
39	753.3	0.2	0.3	0.3
42	754.3	0.3	0.4	0.5
45	865.8	0.1	0.3	0.2
48	1014.7	0.2	0.4	0.1
51	754.6	0.1	0.1	0.6
54	1163.4	0.1	0.2	0.6
Bed Remians	5779.9	49.2	66.9	58.8

Vibration	Gas Rate (%)	Feed Rate (g/min)	Date	Tracer Density (kg/m ³)
No Vibration	20	300	6.12.07	1800
Mass of Tracer Particles				
Sample Time (min)	Mass of Sand (g)	-2.0 +1.0 mm	-4.0 +2.0 mm	-6.35 +4.0 mm
1	2180.1	0.0	0.0	0.0
3	0.3	0.0	0.0	0.0
5	400.6	0.2	0.2	0.1
7	853.7	0.6	0.7	4.1
9	278.9	0.2	0.3	0.7
11	700.9	0.6	0.5	0.7
13	680.9	1.0	1.5	5.9
15	421.4	1.4	1.9	5.7
17	611.5	4.1	8.6	15.0
19	260.4	1.6	3.8	11.5
21	1060.9	5.6	12.7	25.3
23	313.1	1.9	5.3	11.9
25	396.2	1.8	4.2	10.3
27	666.6	2.6	5.2	8.1
30	1288.7	4.6	14.6	24.3
33	357.4	1.1	3.1	7.8
36	604.7	1.3	2.6	6.9
39	1010.8	1.6	6.3	7.5
42	904.6	0.9	3.1	1.6
45	841.7	0.5	1.5	1.2
48	993.4	0.4	2.2	2.0
51	862.0	0.4	0.4	0.3
54	1060.6	0.2	0.2	0.1
Bed Remains	6118.1	0.2	2.2	16.8

Vibration	Gas Rate (%)	Feed Rate (g/min)	Date	Tracer Density (kg/m ³)
No Vibration	20	300	10.12.07	2400
Mass of Tracer Particles				
Sample Time (min)	Mass of Sand (g)	-2.0 +1.0 mm	-4.0 +2.0 mm	-6.35 +4.0 mm
1	1139.4	0.0	0.0	0.0
3	345.5	0.0	0.0	0.0
5	1078.7	0.0	0.1	0.1
7	607.5	0.3	1.5	1.0
9	440.6	0.7	1.8	2.3
11	751.9	2.3	3.4	2.3
13	713.7	2.6	3.6	2.1
15	481.1	2.0	2.3	1.1
17	422.1	1.4	2.1	2.2
19	806.9	2.3	3.5	3.5
21	578.0	1.3	1.5	1.1
23	534.7	1.2	3.0	3.2
25	360.7	0.6	1.2	1.5
27	669.0	0.8	1.7	1.6
30	687.6	0.7	1.5	1.7
33	1252.3	0.5	2.5	7.2
36	828.8	0.2	0.5	2.1
39	904.1	0.2	0.5	2.6
42	909.5	0.0	0.2	1.6
45	844.8	0.1	0.2	1.3
48	1049.2	0.1	0.1	2.0
51	1102.8	0.0	0.0	1.5
54	846.3	0.1	0.0	0.8
Bed Remains	6706.0	24.2	57.6	133.5

Appendix D: Batch Tracer Levenspiel results

DATE	Gas Rate	Sand Feed	Vibration	Tracer	Size	D	U (m/s)	Fraction Out
		Rate		Density	mm	m ² /s	m/s	
		g/min						
5-Sep-07	20%	300	595V	1300	-2.0+1.0	0.0007	0.0038	99.3%
5-Sep-07	20%	300	595V	1300	-4.0+2.0	0.0006	0.0038	99.7%
5-Sep-07	20%	300	595V	1300	-6.35+4.0	0.0005	0.0038	100.0%
6-Sep-07	20%	300	595V	2400	-2.0+1.0	48.9749	-53687091	38.6%
6-Sep-07	20%	300	595V	2400	-4.0+2.0	28.5884	-43218863	1.3%
6-Sep-07	20%	300	595V	2400	-6.35+4.0	1.9064	-17906437	0.0%
10-Sep-07	20%	300	595V	1800	-2.0+1.0	0.0011	0.0024	93.3%
10-Sep-07	20%	300	595V	1800	-4.0+2.0	0.0016	0.0013	92.7%
10-Sep-07	20%	300	595V	1800	-6.35+4.0	0.0035	0.0002	94.8%
10-Sep-07	20%	150	595V	2400	-2.0+1.0	0.0030	0.0005	14.2%
10-Sep-07	20%	150	595V	2400	-4.0+2.0	0.0030	0.0000	0.0%
10-Sep-07	20%	150	595V	2400	-6.35+4.0	0.0030	0.0000	0.0%
11-Sep-07	20%	300	595V	1300	-2.0+1.0	0.0014	0.0040	99.3%
11-Sep-07	20%	300	595V	1300	-4.0+2.0	0.0014	0.0048	99.8%
11-Sep-07	20%	300	595V	1300	-6.35+4.0	0.0009	0.0052	99.9%
11-Sep-07	20%	300	595V	1600	-2.0+1.0	0.0011	0.0031	94.4%
11-Sep-07	20%	300	595V	1600	-4.0+2.0	0.0015	0.0027	95.2%
11-Sep-07	20%	300	595V	1600	-6.35+4.0	0.0035	0.0015	94.1%
12-Sep-07	20%	300	325H	1300	-2.0+1.0	0.0067	0.0067	99.5%
12-Sep-07	20%	300	325H	1300	-4.0+2.0	0.0064	0.0083	99.5%
12-Sep-07	20%	300	325H	1300	-6.35+4.0	0.0025	0.0120	99.9%
12-Sep-07	20%	300	325H	2400	-2.0+1.0	0.0087	0.0018	31.6%
12-Sep-07	20%	300	325H	2400	-4.0+2.0	0.0045	0.0006	13.4%
12-Sep-07	20%	300	325H	2400	-6.35+4.0	0.0040	0.0002	4.0%
13-Sep-07	20%	300	595H	1300	-2.0+1.0	0.0006	0.0028	99.5%
13-Sep-07	20%	300	595H	1300	-4.0+2.0	0.0004	0.0033	99.8%
13-Sep-07	20%	300	595H	1300	-6.35+4.0	0.0003	0.0040	99.4%
13-Sep-07	20%	300	595H	1800	-2.0+1.0	0.0030	0.0008	22.3%
13-Sep-07	20%	300	595H	1800	-4.0+2.0	0.0020	0.0004	11.0%
13-Sep-07	20%	300	595H	1800	-6.35+4.0	0.0008	0.0000	0.2%
13-Sep-07	20%	300	595H	2400	-2.0+1.0	0.0030	0.0001	2.3%
13-Sep-07	20%	300	595H	2400	-4.0+2.0	0.0200	0.0000	0.0%
13-Sep-07	20%	300	595H	2400	-6.35+4.0	0.1000	0.0000	0.0%
14-Sep-07	20%	300	595H	1600	-2.0+1.0	0.0013	0.0013	47.2%
14-Sep-07	20%	300	595H	1600	-4.0+2.0	0.0013	0.0010	36.1%
14-Sep-07	20%	300	595H	1600	-6.35+4.0	0.0008	0.0006	16.5%
14-Sep-07	20%	300	325H	1600	-2.0+1.0	0.0009	0.0045	99.9%
14-Sep-07	20%	300	325H	1600	-4.0+2.0	0.0011	0.0051	100.0%
14-Sep-07	20%	300	325H	1600	-6.35+4.0	0.0010	0.0050	99.1%
18-Sep-07	20%	300	325H	1800	-2.0+1.0	0.0004	0.0037	99.5%
18-Sep-07	20%	300	325H	1800	-4.0+2.0	0.0005	0.0038	99.5%
18-Sep-07	20%	300	325H	1800	-6.35+4.0	0.0004	0.0039	97.8%
2-Oct-07	20%	300	325H	2100	-2.0+1.0	0.0009	0.0051	99.0%
2-Oct-07	20%	300	325H	2100	-4.0+2.0	0.0018	0.0043	96.5%
2-Oct-07	20%	300	325H	2100	-6.35+4.0	0.0023	0.0037	90.0%
10-Oct-07	20%	300	NONE	2100	-2.0+1.0	0.0070	0.0031	92.0%
10-Oct-07	20%	300	NONE	2100	-4.0+2.0	0.0058	0.0027	89.2%
10-Oct-07	20%	300	NONE	2100	-6.35+4.0	0.0042	0.0029	88.0%

DATE	Gas Rate	Sand Feed Rate	Vibration	Tracer Density	Size	D	U (m/s)	Fraction Out
		g/min		kg/m ³	mm	m ² /s	m/s	
12-Nov-07	20%	300	595V	1600	-2.0+1.0	0.0019	0.0021	74.0%
12-Nov-07	20%	300	595V	1600	-4.0+2.0	0.0022	0.0009	26.2%
12-Nov-07	20%	300	595V	1600	-6.35+4.0	0.0000	0.0015	0.2%
12-Nov-07	20%	300	595V	1600	-2.0+1.0	0.0033	0.0026	78.3%
12-Nov-07	20%	300	595V	1600	-4.0+2.0	0.0037	0.0013	37.1%
12-Nov-07	20%	300	595V	1600	-6.35+4.0	0.0010	-0.0485	2.5%
20-Nov-07	20%	300	595V	1600	-2.0+1.0	0.0024	0.0039	99.0%
20-Nov-07	20%	300	595V	1600	-4.0+2.0	0.0031	0.0034	97.3%
20-Nov-07	20%	300	595V	1600	-6.35+4.0	0.0042	0.0021	78.3%
20-Nov-07	20%	300	NONE	1300	-2.0+1.0	0.0025	0.0057	99.8%
20-Nov-07	20%	300	NONE	1300	-4.0+2.0	0.0022	0.0062	99.4%
20-Nov-07	20%	300	NONE	1300	-6.35+4.0	0.0004	0.0089	99.5%
22-Nov-07	20%	150	595V	1300	-2.0+1.0	0.0004	0.0027	99.3%
22-Nov-07	20%	150	595V	1300	-4.0+2.0	0.0005	0.0030	99.7%
22-Nov-07	20%	150	595V	1300	-6.35+4.0	0.0005	0.0036	100.0%
22-Nov-07	20%	150	595V	1600	-2.0+1.0	0.0011	0.0022	90.4%
22-Nov-07	20%	150	595V	1600	-4.0+2.0	0.0016	0.0016	62.3%
22-Nov-07	20%	150	595V	1600	-6.35+4.0	0.0020	0.0006	17.5%
22-Nov-07	20%	150	595V	1800	-2.0+1.0	0.0009	0.0022	89.6%
22-Nov-07	20%	150	595V	1800	-4.0+2.0	0.0011	0.0017	69.6%
22-Nov-07	20%	150	595V	1800	-6.35+4.0	0.0010	0.0007	21.5%
5-Dec-07	20%	300	NONE	1600	-2.0+1.0	0.0027	0.0005	11.7%
5-Dec-07	20%	300	NONE	1600	-4.0+2.0	0.0031	0.0006	16.2%
5-Dec-07	20%	300	NONE	1600	-6.35+4.0	0.0080	0.0012	24.1%
6-Dec-07	20%	300	NONE	1800	-2.0+1.0	0.0087	0.0012	19.9%
6-Dec-07	20%	300	NONE	1800	-4.0+2.0	0.0098	0.0011	17.8%
6-Dec-07	20%	300	NONE	1800	-6.35+4.0	0.0073	0.0020	35.9%
6-Dec-07	20%	300	NONE	1800	-2.0+1.0	0.0005	0.0023	99.4%
6-Dec-07	20%	300	NONE	1800	-4.0+2.0	0.0005	0.0022	97.3%
6-Dec-07	20%	300	NONE	1800	-6.35+4.0	0.0005	0.0023	90.0%
10-Dec-07	20%	300	NONE	1600	-2.0+1.0	0.0059	0.0009	22.2%
10-Dec-07	20%	300	NONE	1600	-4.0+2.0	0.0012	0.0005	17.3%
10-Dec-07	20%	300	NONE	1600	-6.35+4.0	0.0000	0.0004	10.8%
10-Dec-07	20%	300	NONE	1600	-2.0+1.0	0.0162	0.0028	35.9%
10-Dec-07	20%	300	NONE	1600	-4.0+2.0	0.0158	0.0041	44.0%
10-Dec-07	20%	300	NONE	1600	-6.35+4.0	0.0199	0.0053	43.5%
10-Dec-07	20%	300	NONE	2400	-2.0+1.0	0.0046	0.0021	41.8%
10-Dec-07	20%	300	NONE	2400	-4.0+2.0	0.0063	0.0017	35.1%
10-Dec-07	20%	300	NONE	2400	-6.35+4.0	0.0032	0.0009	24.3%
14-Dec-07	20%	150	595H	1300	-2.0+1.0	0.0005	0.0036	99.2%
14-Dec-07	20%	150	595H	1300	-4.0+2.0	0.0003	0.0039	99.8%
14-Dec-07	20%	150	595H	1300	-6.35+4.0	0.0003	0.0045	99.9%
14-Dec-07	20%	150	595H	1600	-2.0+1.0	0.0010	0.0031	98.8%
14-Dec-07	20%	150	595H	1600	-4.0+2.0	0.0011	0.0033	99.1%
14-Dec-07	20%	150	595H	1600	-6.35+4.0	0.0014	0.0036	99.9%
14-Dec-07	20%	150	595H	1800	-2.0+1.0	0.0016	0.0029	94.6%
14-Dec-07	20%	150	595H	1800	-4.0+2.0	0.0020	0.0029	76.6%
14-Dec-07	20%	150	595H	1800	-6.35+4.0	0.0055	0.0012	25.3%

Appendix E: Continuous Tracer Particle Raw Data – Inclined

Experiment Date	9/01/2010
Feed Rate (g/min sand)	546
Underflow rate (g/min sand)	459
Vibration Rate	595V
Gas rate (%)	25
Experiment run time (min)	90

1800 kg/m ³ density particles														
Time (min)	Mass of Sand to Overflow (g)	Mass of Sand to Underflow (g)	Number of particles to Overflow						Number of Particles to Underflow					
			-6.35 +5.6 mm	-5.6 mm	+4.0 mm	-4.0 mm	+2.8 mm	-2.8 mm	+2.0 mm	-2.0 mm	+1.4 mm	-1.4 mm	+1.0 mm	
3	85.1	1377.1	0	1	0	2	0	0	0	3	3	10	11	13
6	357.4	1378.8	0	3	4	9	14	9	1	0	3	10	15	12
9	402.3	1378.9	0	3	6	13	10	13	0	0	0	5	20	11
12	224.5	1378.4	0	0	0	3	3	1	0	1	1	10	19	8
15	199.9	1379.0	2	1	3	2	3	5	0	0	2	5	11	8
18	198.9	1380.1	1	1	2	5	5	3	0	1	2	8	10	13
21	85.7	1387.9	0	0	2	1	0	2	0	1	0	8	11	10
24	177.8	1376.8	0	0	0	2	3	3	0	1	4	14	10	10
27	44.6	1381.8	0	0	0	0	0	0	0	1	1	8	8	6
30	403.2	1385.5	0	0	0	0	4	5	2	2	5	16	13	9
33	456.7	1378.4	0	0	0	2	5	5	0	0	3	5	4	1
36	188.0	1380.6	0	0	0	0	1	3	0	0	0	3	4	4
39	306.8	1375.7	0	0	0	1	1	0	0	0	1	1	4	1
42	350.0	1375.4	0	1	4	3	3	1	0	0	0	4	2	1
45	298.6	1388.0	0	0	1	1	2	1	0	0	0	3	2	5
48	157.1	1374.8	0	0	0	4	0	0	0	0	1	2	0	3
51	196.7	1375.1	0	0	0	0	0	1	0	0	3	3	1	1
54	239.6	1376.1	0	0	1	0	2	3	0	1	0	0	1	0
57	123.7	1374.8	0	0	0	1	1	0	0	0	2	1	1	1
60	295.2	1374.1	0	0	0	0	0	1	0	1	0	1	0	0
63	375.5	1377.8	0	0	0	0	0	0	0	0	2	3	1	1
66	164.7	1378.5	0	0	0	0	2	0	0	0	1	4	1	0
69	290.7	1380.2	0	0	0	0	0	0	0	0	2	4	2	1
72	380.3	1379.7	0	0	0	1	1	0	0	0	1	5	1	3
75	337.4	1380.8	0	0	0	0	2	0	0	0	0	4	0	1
78	406.8	1379.4	0	0	0	1	0	0	0	0	1	0	1	2
81	251.8	1379.3	0	0	0	0	0	0	0	0	0	3	2	1
84	457.0	1312.0	0	0	0	0	0	0	0	1	2	2	1	1
87	278.4	1444.2	0	0	0	0	0	0	0	0	3	2	0	1
90	156.6	1289.3	0	0	0	0	0	0	0	0	1	2	1	1
Total	263.0	1376.0	3	10	23	51	62	56	3	13	44	146	157	129

	-6.35 +5.6 mm	-5.6 mm	+4.0 mm	-4.0 mm	+2.8 mm	-2.8 mm	+2.0 mm	-2.0 mm	+1.4 mm	-1.4 mm	+1.0 mm
Total Particles to Overflow	3	10	23	51	62	56					
Total Particles to Underflow	3	13	44	146	157	129					
Total Particles Remaining in Bed	46	75	60	41	5	2					
Total Feed	52	98	127	238	224	187					

Experiment Date	9/01/2010
Feed Rate (g/min sand)	546
Underflow rate (g/min sand)	459
Vibration Rate	595V
Gas rate (%)	25
Experiment run time (min)	90

		1600 kg/m ³ density particles																														
Time (min)	Adjusted Time (min)	Number of particles to Overflow						Number of Particles to Underflow																								
		-6.35 +5.6 mm	-5.6 mm	+4.0 mm	-4.0 mm	+2.8 mm	-2.8 mm	+2.0 mm	-2.0 mm	+1.4 mm	-1.4 mm	+1.0 mm	-6.35 +5.6 mm	-5.6 mm	+4.0 mm	-4.0 mm	+2.8 mm	-2.8 mm	+2.0 mm	-2.0 mm	+1.4 mm	-1.4 mm	+1.0 mm									
3		-	-	-	-	-	-	-	-	-	-	-	-	-	-	-	-	-	-	-	-	-	-	-								
6		-	-	-	-	-	-	-	-	-	-	-	-	-	-	-	-	-	-	-	-	-	-	-								
9		-	-	-	-	-	-	-	-	-	-	-	-	-	-	-	-	-	-	-	-	-	-	-								
12	2	0	0	0	2	0	1	0	1	0	3	2	5	0	1	0	3	2	6	9	16	30	0	0	5	9	16	30				
15	5	1	1	5	7	9	8	0	0	5	9	16	30	0	0	5	9	16	30	0	0	5	9	16	30	0	0	5	9	16	30	
18	8	1	2	7	7	6	13	0	0	0	6	9	15	0	0	0	6	9	15	0	0	0	6	9	15	0	0	0	6	9	15	
21	11	0	2	4	2	5	3	0	1	3	2	6	13	0	1	3	2	6	13	0	1	3	2	6	13	0	1	3	2	6	13	
24	14	0	2	0	0	5	7	0	0	1	6	7	7	0	0	1	6	7	7	0	0	1	6	7	7	0	0	1	6	7	7	
27	17	1	0	0	1	0	1	0	0	0	1	5	8	0	0	0	1	5	8	0	0	0	1	5	8	0	0	0	1	5	8	
30	20	0	0	1	5	5	1	0	0	2	4	5	4	0	0	2	4	5	4	0	0	2	4	5	4	0	0	2	4	5	4	
33	23	0	1	3	6	6	6	0	0	1	8	6	6	0	0	1	8	6	6	0	0	1	8	6	6	0	0	1	8	6	6	
36	26	0	0	1	1	1	0	0	0	1	3	4	3	0	0	1	3	4	3	0	0	1	3	4	3	0	0	1	3	4	3	
39	29	0	0	3	0	3	2	0	0	1	1	2	2	0	0	1	1	2	2	0	0	1	1	2	2	0	0	1	1	2	2	
42	32	6	5	6	7	10	4	0	0	0	3	3	2	0	0	0	3	3	2	0	0	0	3	3	2	0	0	0	3	3	2	
45	35	0	2	0	3	4	4	0	0	0	2	4	0	0	0	2	4	0	0	0	0	2	4	0	0	0	0	2	4	0	0	
48	38	0	0	0	0	1	0	0	0	2	2	0	0	0	0	2	2	0	0	0	0	2	2	0	0	0	0	2	2	0	0	
51	41	0	0	3	3	1	1	0	0	0	1	1	2	0	0	0	1	1	2	0	0	0	1	1	2	0	0	0	1	1	2	
54	44	0	0	1	1	1	2	0	0	1	6	1	1	0	0	1	6	1	1	0	0	1	6	1	1	0	0	1	6	1	1	
57	47	0	1	0	0	0	0	0	0	1	3	2	0	0	0	1	3	2	0	0	1	3	2	0	0	0	0	1	3	2	0	
60	50	0	0	1	2	2	1	0	0	0	1	0	0	0	0	0	1	0	0	0	0	1	0	0	0	0	0	0	1	0	0	
63	53	0	0	0	2	1	5	0	0	1	1	0	0	0	0	1	1	0	0	0	0	1	0	0	0	0	0	0	1	0	0	
66	56	0	0	2	0	2	1	0	0	0	4	1	0	0	0	0	4	1	0	0	0	0	4	1	0	0	0	0	4	1	0	
69	59	0	0	0	1	1	1	0	0	1	0	0	1	0	0	1	0	0	1	0	0	1	0	0	1	0	0	0	1	0	0	
72	62	0	1	2	3	2	0	0	0	0	0	1	0	0	0	0	0	1	0	0	0	0	1	0	0	0	0	0	1	0	0	
75	65	0	0	1	2	2	1	0	0	1	2	1	1	0	0	1	2	1	1	0	0	1	2	1	1	0	0	1	2	1	1	
78	68	0	0	1	1	1	2	0	0	2	0	0	1	0	0	2	0	0	1	0	0	2	0	0	1	0	0	2	0	0	1	
81	71	0	0	0	0	1	1	0	0	1	0	3	0	0	0	1	0	3	0	0	0	1	0	3	0	0	0	0	1	0	3	0
84	74	0	0	1	1	0	2	0	0	2	2	1	1	0	0	2	2	1	1	0	0	2	2	1	1	0	0	2	2	1	1	
87	77	0	1	0	0	0	0	0	0	0	1	1	0	0	0	0	1	1	0	0	0	1	1	0	0	0	0	0	1	1	0	
90	80	0	0	0	0	0	0	0	0	1	2	0	0	0	0	1	2	0	0	0	0	1	2	0	0	0	0	0	1	2	0	0
Total		9	18	42	57	69	67	0	2	27	73	81	102																			

	-6.35 +5.6 mm	-5.6 mm	+4.0 mm	-4.0 mm	+2.8 mm	-2.8 mm	+2.0 mm	-2.0 mm	+1.4 mm	-1.4 mm	+1.0 mm
Total Particles to Overflow	9	18	42	57	69	67					
Total Particles to Underflow	0	2	27	73	81	102					
Total Particles Remaining in Bed	44	74	71	28	16	4					
Total Feed	53	94	140	158	166	173					

Experiment Date	9/01/2010
Feed Rate (g/min sand)	546
Underflow rate (g/min sand)	459
Vibration Rate	595V
Gas rate (%)	25
Experiment run time (min)	90

2100 kg/m³ density particles

Time (min)	Adjusted Time (min)	Number of particles to Overflow						Number of Particles to Underflow					
		-6.35 +5.6 mm	-5.6 +4.0 mm	-4.0 +2.8 mm	-2.8 +2.0 mm	-2.0 +1.4 mm	-1.4 +1.0 mm	-6.35 +5.6 mm	-5.6 +4.0 mm	-4.0 +2.8 mm	-2.8 +2.0 mm	-2.0 +1.4 mm	-1.4 +1.0 mm
3		-	-	-	-	-	-	-	-	-	-	-	-
6		-	-	-	-	-	-	-	-	-	-	-	-
9		-	-	-	-	-	-	-	-	-	-	-	-
12		-	-	-	-	-	-	-	-	-	-	-	-
15		-	-	-	-	-	-	-	-	-	-	-	-
18		-	-	-	-	-	-	-	-	-	-	-	-
21	1	0	0	0	0	0	0	0	0	0	0	0	0
24	4	0	0	0	0	0	0	18	13	22	20	25	22
27	7	0	0	0	0	0	0	13	16	12	20	10	20
30	10	0	0	0	0	0	0	0	0	0	0	0	0
33	13	0	0	0	0	2	6	1	0	2	10	8	9
36	16	0	0	0	1	0	2	0	2	1	5	8	11
39	19	0	0	0	0	3	2	0	1	2	4	2	9
42	22	0	1	0	3	2	3	0	0	2	4	5	4
45	25	0	0	0	0	0	2	0	3	1	4	5	1
48	28	0	0	0	0	0	0	0	0	1	4	7	2
51	31	0	0	0	0	2	1	0	0	1	0	3	5
54	34	0	0	0	0	0	3	0	0	1	1	3	6
57	37	0	0	0	0	1	0	0	3	4	0	2	6
60	40	0	0	0	0	0	1	0	0	2	5	0	3
63	43	0	0	0	0	1	2	0	2	4	9	0	0
66	46	0	0	0	0	0	0	0	3	2	6	0	2
69	49	0	0	0	0	0	1	0	1	3	2	5	3
72	52	0	0	0	0	0	0	0	2	3	6	1	8
75	55	0	0	0	0	0	0	0	2	6	1	3	3
78	58	0	0	0	0	0	0	0	0	0	0	5	3
81	61	0	0	0	0	0	0	0	0	0	4	1	3
84	64	0	0	0	0	0	0	0	0	3	2	1	1
87	67	0	0	0	0	0	0	0	0	0	4	1	0
90	70	0	0	0	0	0	0	0	0	1	2	1	1
Total		0	1	0	4	11	23	32	48	73	113	96	122

	-6.35 +5.6 mm	-5.6 +4.0 mm	-4.0 +2.8 mm	-2.8 +2.0 mm	-2.0 +1.4 mm	-1.4 +1.0 mm
Total Particles to Overflow	0	1	0	4	11	23
Total Particles to Underflow	32	48	73	113	96	122
Total Particles Remaining in Bed	15	45	41	43	17	10
Total Feed	47	94	114	160	124	155

Experiment Date	9/01/2010
Feed Rate (g/min sand)	546
Underflow rate (g/min sand)	459
Vibration Rate	595V
Gas rate (%)	25
Experiment run time (min)	90

		1300 kg/m ³ density particles													
Time (min)	Adjusted Time (min)	Number of particles to Overflow						Number of Particles to Underflow							
		-6.35 +5.6 mm	-5.6 mm	+4.0 -4.0 +2.8 mm	-2.8 +2.0 mm	-2.0 +1.4 mm	-1.4 +1.0 mm	-6.35 +5.6 mm	-5.6 mm	+4.0 -4.0 +2.8 mm	-2.8 +2.0 mm	-2.0 +1.4 mm	-1.4 +1.0 mm		
3		-	-	-	-	-	-	-	-	-	-	-	-	-	-
6		-	-	-	-	-	-	-	-	-	-	-	-	-	-
9		-	-	-	-	-	-	-	-	-	-	-	-	-	-
12		-	-	-	-	-	-	-	-	-	-	-	-	-	-
15		-	-	-	-	-	-	-	-	-	-	-	-	-	-
18		-	-	-	-	-	-	-	-	-	-	-	-	-	-
21		-	-	-	-	-	-	-	-	-	-	-	-	-	-
24		-	-	-	-	-	-	-	-	-	-	-	-	-	-
27		-	-	-	-	-	-	-	-	-	-	-	-	-	-
30		-	-	-	-	-	-	-	-	-	-	-	-	-	-
33	3	0	0	0	0	0	0	0	0	0	0	3	9	6	
36	6	1	3	4	10	5	4	0	1	1	7	10	21		
39	9	2	7	10	22	18	14	0	0	2	1	8	13		
42	12	13	18	21	20	19	19	0	0	1	3	6	11		
45	15	4	8	8	14	14	7	0	0	0	1	1	5		
48	18	7	4	5	8	8	5	0	0	0	0	2	2		
51	21	4	2	2	7	7	8	0	0	1	2	4	1		
54	24	3	3	5	13	7	3	0	0	0	0	0	5		
57	27	3	2	6	6	8	5	0	0	2	1	1	2		
60	30	2	6	12	15	5	2	0	0	0	0	0	1		
63	33	4	3	6	9	6	6	0	0	0	0	0	0		
66	36	1	2	2	1	4	0	0	0	1	1	1	0		
69	39	3	2	3	7	2	6	0	0	1	0	1	0		
72	42	4	3	11	4	6	2	0	0	0	0	0	1		
75	45	2	2	3	3	3	3	0	0	0	1	0	2		
78	48	1	4	1	3	1	2	0	0	0	0	0	1		
81	51	0	0	0	2	3	2	0	0	0	0	1	0		
84	54	0	2	4	5	5	1	0	0	0	0	0	0		
87	57	0	0	1	3	1	0	0	0	0	1	0	0		
90	60	0	0	0	0	0	0	0	0	0	0	0	0		
Total		54	71	104	152	122	89	0	1	9	21	44	71		

	-6.35 +5.6 mm	-5.6 mm	+4.0 -4.0 +2.8 mm	-2.8 +2.0 mm	-2.0 +1.4 mm	-1.4 +1.0 mm
Total Particles to Overflow	54	71	104	152	122	89
Total Particles to Underflow	0	1	9	21	44	71
Total Particles Remaining in Bed	18	14	16	11	9	7
Total Feed	72	86	129	184	175	167

Experiment Date	9/01/2010
Feed Rate (g/min sand)	546
Underflow rate (g/min sand)	459
Vibration Rate	595V
Gas rate (%)	25
Experiment run time (min)	90

		2400 kg/m ³ density particles												
Time (min)	Adjusted Time (min)	Number of particles to Overflow						Number of Particles to Underflow						
		-6.35 +5.6 mm	-5.6 +4.0 mm	-4.0 +2.8 mm	-2.8 +2.0 mm	-2.0 +1.4 mm	-1.4 +1.0 mm	-6.35 +5.6 mm	-5.6 +4.0 mm	-4.0 +2.8 mm	-2.8 +2.0 mm	-2.0 +1.4 mm	-1.4 +1.0 mm	
3		-	-	-	-	-	-	-	-	-	-	-	-	
6		-	-	-	-	-	-	-	-	-	-	-	-	
9		-	-	-	-	-	-	-	-	-	-	-	-	
12		-	-	-	-	-	-	-	-	-	-	-	-	
15		-	-	-	-	-	-	-	-	-	-	-	-	
18		-	-	-	-	-	-	-	-	-	-	-	-	
21		-	-	-	-	-	-	-	-	-	-	-	-	
24		-	-	-	-	-	-	-	-	-	-	-	-	
27		-	-	-	-	-	-	-	-	-	-	-	-	
30		-	-	-	-	-	-	-	-	-	-	-	-	
33		-	-	-	-	-	-	-	-	-	-	-	-	
36		-	-	-	-	-	-	-	-	-	-	-	-	
39		-	-	-	-	-	-	-	-	-	-	-	-	
42	2	0	0	0	0	0	0	0	0	0	1	0	0	
45	5	0	0	0	0	0	0	0	49	64	65	53	72	49
48	8	0	0	0	0	0	0	0	4	12	19	32	22	42
51	11	0	0	0	0	0	0	2	0	2	8	13	14	17
54	14	0	0	0	0	0	0	1	0	0	5	4	4	5
57	17	0	0	0	0	0	0	0	0	0	5	3	5	5
60	20	0	0	0	0	0	0	1	0	0	1	6	6	7
63	23	0	0	0	0	0	0	1	0	2	2	5	3	8
66	26	0	0	0	0	0	0	1	0	1	0	6	1	5
69	29	0	0	0	0	0	0	0	0	0	0	5	4	4
72	32	0	0	0	0	1	1	0	0	0	0	3	3	2
75	35	0	0	0	0	0	0	0	0	0	3	4	4	5
78	38	0	0	0	0	0	0	0	0	0	0	1	2	1
81	41	0	0	0	0	0	0	0	0	0	0	2	6	3
84	44	0	0	0	0	0	0	0	0	0	0	2	3	1
87	47	0	0	0	0	0	0	0	0	0	1	3	1	3
90	50	0	0	0	0	0	0	0	0	0	2	2	0	3
Total		0	0	0	0	1	7		53	81	111	145	150	160

	-6.35 +5.6 mm	-5.6 +4.0 mm	-4.0 +2.8 mm	-2.8 +2.0 mm	-2.0 +1.4 mm	-1.4 +1.0 mm
Total Particles to Overflow	0	0	0	0	1	7
Total Particles to Underflow	53	81	111	145	150	160
Total Particles Remaining in Bed	0	7	26	26	16	17
Total Feed	53	88	137	171	167	184

Experiment Date	15/01/2010
Feed Rate (g/min sand)	536
Underflow rate (g/min sand)	305
Vibration Rate	595V
Gas rate (%)	25
Experiment run time (min)	105

1800 kg/m ³ density particles														
Time (min)	Mass of Sand to Overflow (g)	Mass of Sand to Underflow (g)	Number of particles to Overflow						Number of Particles to Underflow					
			-6.35	-5.6 +4.0	-4.0 +2.8	-2.8 +2.0	-2.0 +1.4	-1.4 +1.0	-6.35	-5.6 +4.0	-4.0 +2.8	-2.8 +2.0	-2.0 +1.4	-1.4 +1.0
			+5.6 mm	mm	mm	mm	mm	mm	+5.6 mm	mm	mm	mm	mm	mm
3	980.9	914.5	0	1	4	2	10	9	0	0	0	4	4	4
6	333.5	911.3	0	1	0	7	1	13	1	1	5	12	18	25
9	946.8	914.7	0	0	3	10	21	12	0	1	4	6	12	16
12	365.1	913.7	0	1	0	2	10	6	0	1	0	5	6	10
15	741.3	914.0	0	0	1	5	6	14	0	0	3	8	4	3
18	539.0	911.7	0	0	2	0	4	5	0	1	1	8	6	6
21	829.7	914.7	0	0	0	2	0	2	0	0	2	6	3	10
24	460.5	911.8	0	0	0	1	3	2	0	2	1	1	1	2
27	847.3	915.8	0	0	0	1	6	4	1	0	2	8	1	2
30	975.7	911.7	0	0	0	0	5	8	2	1	3	4	8	9
33	312.4	912.7	0	0	0	0	0	1	1	1	1	3	5	2
36	661.5	918.2	0	0	0	0	3	1	1	1	1	4	4	0
39	804.2	912.8	0	0	0	1	2	3	0	0	2	3	2	1
42	487.8	912.2	0	0	0	2	3	0	0	0	1	3	3	1
45	668.0	913.1	0	0	0	3	4	2	0	0	1	6	2	0
48	1019.3	917.7	0	0	0	3	1	5	0	0	1	4	3	1
51	797.2	913.9	0	0	0	5	5	1	0	0	4	2	1	0
54	869.5	923.3	0	0	0	3	5	0	0	0	0	1	3	0
57	967.6	925.2	0	0	1	8	3	2	0	0	2	2	1	2
60	939.0	912.2	0	2	0	1	2	1	0	0	1	2	2	0
63	486.4	914.3	0	1	0	1	2	0	1	1	3	3	1	0
66	586.7	913.8	0	0	1	5	2	0	0	0	2	0	2	1
69	766.1	915.5	0	0	0	2	0	0	0	0	1	4	2	0
72	587.5	923.6	0	0	1	0	0	0	0	0	1	2	1	0
75	600.1	913.4	0	0	0	0	1	0	0	0	0	1	2	1
78	519.8	913.5	0	0	0	0	1	1	0	0	3	0	0	0
81	602.8	914.2	0	1	0	1	0	0	0	1	3	0	1	0
84	640.3	915.7	0	1	1	1	0	0	0	0	1	1	0	1
87	806.7	917.4	0	0	0	0	1	0	0	0	2	2	2	0
90	638.8	915.2	0	0	1	1	0	0	0	0	1	1	0	0
93	707.3	915.5	0	0	0	0	0	0	0	0	1	2	0	0
96	646.9	917.3	0	0	0	0	0	0	0	1	1	1	0	0
99	478.0	915.5	0	0	1	1	1	0	0	0	1	2	0	0
102	804.6	914.2	0	0	0	0	0	0	0	0	1	1	1	0
105	802.0	914.8	0	0	0	0	0	0	0	0	1	0	0	0
Total	692.0	915.1	0	8	16	68	102	92	7	12	57	112	101	97

	-6.35	-5.6 +4.0	-4.0 +2.8	-2.8 +2.0	-2.0 +1.4	-1.4 +1.0
	+5.6 mm	mm	mm	mm	mm	mm
Total Particles to Overflow	0	8	16	68	102	92
Total Particles to Underflow	7	12	57	112	101	97
Total Particles Remaining in Bed	48	73	54	36	3	0
Total Feed	55	93	127	216	206	189

Experiment Date	15/01/2010
Feed Rate (g/min sand)	536
Underflow rate (g/min sand)	305
Vibration Rate	595V
Gas rate (%)	25
Experiment run time (min)	105

		1600 kg/m ³ density particles											
Time (min)	Adjusted Time (min)	Number of particles to Overflow						Number of Particles to Underflow					
		-6.35 +5.6 mm	-5.6 +4.0 mm	-4.0 +2.8 mm	-2.8 +2.0 mm	-2.0 +1.4 mm	-1.4 +1.0 mm	-6.35 +5.6 mm	-5.6 +4.0 mm	-4.0 +2.8 mm	-2.8 +2.0 mm	-2.0 +1.4 mm	-1.4 +1.0 mm
3		-	-	-	-	-	-	-	-	-	-	-	-
6		-	-	-	-	-	-	-	-	-	-	-	-
9		-	-	-	-	-	-	-	-	-	-	-	-
12	2	0	0	0	0	0	0	0	0	0	0	0	0
15	5	0	0	2	7	10	13	0	0	4	4	9	10
18	8	0	1	2	3	15	26	0	0	2	4	5	8
21	11	0	0	4	8	24	26	0	1	0	1	5	10
24	14	0	1	4	5	10	8	0	0	2	2	6	14
27	17	0	1	0	8	6	14	0	0	2	4	5	3
30	20	0	0	0	8	12	10	0	0	2	2	4	4
33	23	0	0	1	3	7	2	0	0	1	2	4	4
36	26	0	0	1	6	4	3	1	0	3	3	2	0
39	29	0	0	4	9	7	7	0	0	3	3	1	0
42	32	0	0	1	6	4	1	0	0	2	3	1	0
45	35	0	1	4	6	3	1	0	0	3	1	0	1
48	38	0	1	6	9	6	12	0	0	0	5	0	0
51	41	0	0	6	6	1	5	0	0	1	1	0	0
54	44	0	0	3	8	2	1	0	0	1	0	2	0
57	47	0	2	4	5	3	2	0	0	0	0	0	0
60	50	0	3	5	4	2	1	0	0	1	0	0	0
63	53	0	1	1	2	2	0	0	0	0	0	1	0
66	56	1	2	2	3	1	0	0	1	0	1	1	0
69	59	0	0	1	2	1	0	0	0	0	1	0	0
72	62	0	0	0	1	0	0	0	0	0	0	1	0
75	65	0	1	2	0	2	0	0	0	0	0	0	0
78	68	0	1	0	0	0	0	0	0	0	0	0	0
81	71	0	2	3	3	1	0	0	0	0	0	0	0
84	74	0	1	0	0	1	0	0	0	0	0	0	0
87	77	0	0	0	0	0	0	0	0	1	0	0	0
90	80	0	1	3	1	0	0	0	0	1	0	0	0
93	83	0	0	2	1	0	0	0	0	1	2	0	0
96	86	0	0	1	0	0	0	0	0	0	1	0	0
99	89	0	0	1	1	0	0	0	0	1	0	0	0
102	92	0	0	0	1	0	0	0	0	0	0	0	0
105	95	0	0	0	0	0	0	0	0	0	0	0	0
Total		1	19	63	116	124	132	1	2	31	40	47	54

	-6.35 +5.6 mm	-5.6 +4.0 mm	-4.0 +2.8 mm	-2.8 +2.0 mm	-2.0 +1.4 mm	-1.4 +1.0 mm
Total Particles to Overflow	1	19	63	116	124	132
Total Particles to Underflow	1	2	31	40	47	54
Total Particles Remaining in Bed	50	76	46	15	1	0
Total Feed	52	97	140	171	172	186

Experiment Date	15/01/2010
Feed Rate (g/min sand)	536
Underflow rate (g/min sand)	305
Vibration Rate	595V
Gas rate (%)	25
Experiment run time (min)	105

		2100 kg/m ³ density particles													
Time (min)	Adjusted Time (min)	Number of particles to Overflow						Number of Particles to Underflow							
		-6.35 +5.6 mm	-5.6 +4.0 mm	-4.0 +2.8 mm	-2.8 +2.0 mm	-2.0 +1.4 mm	-1.4 +1.0 mm	-6.35 +5.6 mm	-5.6 +4.0 mm	-4.0 +2.8 mm	-2.8 +2.0 mm	-2.0 +1.4 mm	-1.4 +1.0 mm		
3		-	-	-	-	-	-	-	-	-	-	-	-	-	
6		-	-	-	-	-	-	-	-	-	-	-	-	-	
9		-	-	-	-	-	-	-	-	-	-	-	-	-	
12		-	-	-	-	-	-	-	-	-	-	-	-	-	
15		-	-	-	-	-	-	-	-	-	-	-	-	-	
18		-	-	-	-	-	-	-	-	-	-	-	-	-	
21	1	0	0	0	0	0	0	0	0	0	0	0	0	0	
24	4	0	0	0	0	0	0	0	7	6	5	2	9	7	
27	7	0	0	0	0	0	0	5	7	7	10	7	15	21	
30	10	0	0	0	0	0	0	0	0	0	0	0	0	0	
33	13	0	0	0	0	0	0	3	0	2	1	6	10	7	
36	16	0	0	0	0	0	0	3	0	1	3	5	1	12	
39	19	0	0	0	0	0	0	2	0	1	3	0	7	7	
42	22	0	0	0	0	1	4	0	0	0	2	4	6	6	
45	25	0	0	0	0	3	1	0	0	3	4	5	3	8	
48	28	0	0	0	1	4	7	0	0	2	4	7	4	5	
51	31	0	0	1	1	1	3	0	0	1	11	5	2	7	
54	34	0	0	0	1	1	4	0	0	1	1	5	4	2	
57	37	0	0	0	1	1	8	0	0	2	5	0	3	3	
60	40	0	0	1	0	2	3	0	0	0	1	2	2	0	
63	43	0	0	0	1	0	0	0	0	0	1	1	3	3	
66	46	0	0	0	2	2	3	0	0	0	1	5	1	2	
69	49	0	0	0	1	0	2	0	0	0	0	6	2	1	
72	52	0	0	0	0	0	1	0	0	0	1	3	2	1	
75	55	0	0	1	0	1	1	0	0	1	0	3	2	2	
78	58	0	0	0	0	0	1	0	0	0	5	1	0	1	
81	61	0	0	0	1	2	2	0	0	3	2	2	3	1	
84	64	0	0	1	1	1	1	0	0	0	0	0	1	1	
87	67	0	0	0	0	1	0	0	0	0	1	6	2	0	
90	70	0	0	0	0	1	0	0	0	1	1	1	2	0	
93	73	0	0	0	0	0	1	1	0	0	6	4	1	0	
96	76	0	0	0	0	0	0	0	0	1	3	2	2	0	
99	79	0	0	0	0	0	0	0	0	3	1	1	0	1	
102	82	0	0	0	0	0	0	0	0	2	1	5	3	0	
105	85	0	0	0	0	0	0	0	0	0	1	1	0	1	
Total		0	0	4	10	21	55	15	37	74	89	90	99		

	-6.35 +5.6 mm	-5.6 +4.0 mm	-4.0 +2.8 mm	-2.8 +2.0 mm	-2.0 +1.4 mm	-1.4 +1.0 mm
Total Particles to Overflow	0	0	4	10	21	55
Total Particles to Underflow	15	37	74	89	90	99
Total Particles Remaining in Bed	29	54	44	56	15	5
Total Feed	44	91	122	155	126	159

Experiment Date	15/01/2010
Feed Rate (g/min sand)	536
Underflow rate (g/min sand)	305
Vibration Rate	595V
Gas rate (%)	25
Experiment run time (min)	105

		1300 kg/m ³ density particles											
Time (min)	Adjusted Time (min)	Number of particles to Overflow						Number of Particles to Underflow					
		-6.35 +5.6 mm	-5.6 +4.0 mm	-4.0 +2.8 mm	-2.8 +2.0 mm	-2.0 +1.4 mm	-1.4 +1.0 mm	-6.35 +5.6 mm	-5.6 +4.0 mm	-4.0 +2.8 mm	-2.8 +2.0 mm	-2.0 +1.4 mm	-1.4 +1.0 mm
3		-	-	-	-	-	-	-	-	-	-	-	-
6		-	-	-	-	-	-	-	-	-	-	-	-
9		-	-	-	-	-	-	-	-	-	-	-	-
12		-	-	-	-	-	-	-	-	-	-	-	-
15		-	-	-	-	-	-	-	-	-	-	-	-
18		-	-	-	-	-	-	-	-	-	-	-	-
21		-	-	-	-	-	-	-	-	-	-	-	-
24		-	-	-	-	-	-	-	-	-	-	-	-
27		-	-	-	-	-	-	-	-	-	-	-	-
30		-	-	-	-	-	-	-	-	-	-	-	-
33	3	0	0	0	1	0	0	0	0	1	1	0	1
36	6	0	2	10	13	26	29	0	2	1	3	7	13
39	9	3	4	36	46	43	42	0	0	0	1	6	9
42	12	1	10	15	22	21	20	0	0	1	3	2	3
45	15	5	8	17	25	23	18	0	0	0	1	3	2
48	18	13	21	32	22	22	19	0	0	0	0	2	1
51	21	5	9	11	13	6	4	0	0	0	0	0	0
54	24	9	10	3	5	5	7	0	0	0	0	0	0
57	27	8	11	5	11	1	1	0	0	0	0	0	0
60	30	4	6	2	3	2	1	0	0	0	0	0	0
63	33	1	0	2	0	0	0	0	0	0	0	0	1
66	36	1	0	1	0	0	0	0	0	0	0	1	0
69	39	0	3	0	2	1	1	0	0	0	0	0	0
72	42	2	0	0	1	0	0	0	0	0	0	0	0
75	45	0	1	0	0	1	0	0	0	0	0	0	0
78	48	0	0	0	0	0	0	0	0	0	0	0	0
81	51	0	0	0	0	0	0	0	0	0	0	0	0
84	54	1	0	1	0	0	0	0	0	0	0	0	0
87	57	0	0	0	0	0	0	0	0	0	0	0	0
90	60	1	1	0	0	0	0	0	0	0	0	0	0
93	63	0	0	0	0	0	0	0	0	0	0	0	0
96	66	1	0	0	0	0	0	0	0	0	0	0	0
99	69	0	0	0	0	0	0	0	0	0	0	0	0
102	72	0	0	0	0	0	0	0	0	0	0	0	0
105	75	0	0	0	0	0	0	0	0	0	0	0	0
Total		55	86	135	164	151	142	0	2	3	9	21	30

	-6.35 +5.6 mm	-5.6 +4.0 mm	-4.0 +2.8 mm	-2.8 +2.0 mm	-2.0 +1.4 mm	-1.4 +1.0 mm
Total Particles to Overflow	55	86	135	164	151	142
Total Particles to Underflow	0	2	3	9	21	30
Total Particles Remaining in Bed	2	2	0	1	0	0
Total Feed	57	90	138	174	172	172

Experiment Date	15/01/2010
Feed Rate (g/min sand)	536
Underflow rate (g/min sand)	305
Vibration Rate	595V
Gas rate (%)	25
Experiment run time (min)	105

		2400 kg/m ³ density particles													
Time (min)	Adjusted Time (min)	Number of particles to Overflow						Number of Particles to Underflow							
		-6.35 +5.6 mm	-5.6 +4.0 mm	-4.0 +2.8 mm	-2.8 +2.0 mm	-2.0 +1.4 mm	-1.4 +1.0 mm	-6.35 +5.6 mm	-5.6 +4.0 mm	-4.0 +2.8 mm	-2.8 +2.0 mm	-2.0 +1.4 mm	-1.4 +1.0 mm		
3		-	-	-	-	-	-	-	-	-	-	-	-	-	
6		-	-	-	-	-	-	-	-	-	-	-	-	-	
9		-	-	-	-	-	-	-	-	-	-	-	-	-	
12		-	-	-	-	-	-	-	-	-	-	-	-	-	
15		-	-	-	-	-	-	-	-	-	-	-	-	-	
18		-	-	-	-	-	-	-	-	-	-	-	-	-	
21		-	-	-	-	-	-	-	-	-	-	-	-	-	
24		-	-	-	-	-	-	-	-	-	-	-	-	-	
27		-	-	-	-	-	-	-	-	-	-	-	-	-	
30		-	-	-	-	-	-	-	-	-	-	-	-	-	
33		-	-	-	-	-	-	-	-	-	-	-	-	-	
36		-	-	-	-	-	-	-	-	-	-	-	-	-	
39		-	-	-	-	-	-	-	-	-	-	-	-	-	
42	2	0	0	0	0	0	0	0	0	0	0	0	0	1	
45	5	0	0	0	0	0	0	1	40	38	25	38	25	24	
48	8	0	0	0	0	0	3	5	2	7	22	13	16	21	
51	11	0	0	0	1	1	1	5	1	1	4	10	6	11	
54	14	0	0	0	0	1	1	2	1	3	4	3	15	10	
57	17	0	0	0	0	0	0	3	0	2	6	5	7	11	
60	20	0	0	1	0	2	7		1	1	1	5	10	12	
63	23	0	0	0	0	2	1		0	1	3	2	5	4	
66	26	0	0	0	0	0	1		1	1	2	6	8	4	
69	29	0	0	0	0	0	1		1	0	1	4	2	8	
72	32	0	0	0	0	0	0		0	2	6	8	6	4	
75	35	0	0	0	0	2	1		0	4	4	3	3	6	
78	38	0	0	0	0	0	1		0	2	9	1	3	1	
81	41	0	0	0	1	3	0		0	0	2	2	2	4	
84	44	0	0	0	0	0	1		0	1	3	3	3	8	
87	47	0	0	0	0	0	0		0	2	2	2	4	3	
90	50	0	0	0	0	0	2		0	2	3	7	2	2	
93	53	0	0	0	0	0	1		0	1	1	2	5	1	
96	56	0	0	0	0	0	0		0	1	2	3	2	1	
99	59	0	0	0	0	0	0		1	1	1	2	3	0	
102	62	0	0	0	0	0	0		0	0	1	1	0	1	
105	65	0	0	0	0	0	0		0	0	3	3	2	0	
Total		0	0	1	2	14	32		48	70	105	123	129	137	

	-6.35 +5.6 mm	-5.6 +4.0 mm	-4.0 +2.8 mm	-2.8 +2.0 mm	-2.0 +1.4 mm	-1.4 +1.0 mm
Total Particles to Overflow	0	0	1	2	14	32
Total Particles to Underflow	48	70	105	123	129	137
Total Particles Remaining in Bed	5	21	36	35	23	12
Total Feed	53	91	142	160	166	181

Experiment Date	18/01/2010
Feed Rate (g/min sand)	563
Underflow rate (g/min sand)	264
Vibration Rate	595V
Gas rate (%)	25
Experiment run time (min)	114

1800 kg/m ³ density particles																					
Time (min)	Mass of Sand to Overflow (g)	Mass of Sand to Underflow (g)	Number of particles to Overflow						Number of Particles to Underflow												
			-6.35 +5.6 mm	-5.6 mm	+4.0 mm	-4.0 mm	+2.8 mm	-2.8 mm	+2.0 mm	-2.0 mm	+1.4 mm	-1.4 mm	+1.0 mm	-6.35 +5.6 mm	-5.6 mm	+4.0 mm	-4.0 mm	+2.8 mm	-2.8 mm	+2.0 mm	-2.0 mm
3	725.0	832.3	0	2	0	6	15	4	0	0	1	0	2	3							
6	806.2	739.7	7	11	10	25	37	24	0	0	3	6	12	8							
9	1153.1	829.1	12	12	20	32	45	27	1	0	0	4	5	10							
12	728.3	737.6	3	10	10	17	18	18	0	0	1	5	8	11							
15	861.2	831.1	1	2	4	12	7	11	0	0	1	1	2	2							
18	738.1	832.8	0	0	3	2	6	10	0	0	0	6	4	4							
21	999.5	740.2	0	0	1	6	3	4	0	1	0	2	2	4							
24	732.9	832.7	0	0	2	2	7	2	0	0	2	2	0	2							
27	1013.8	743.7	0	0	0	3	8	7	0	0	1	2	1	2							
30	653.3	834.2	0	0	0	0	2	1	0	1	6	10	3	7							
33	838.2	739.6	0	0	0	2	5	3	0	0	0	0	1	2							
36	983.5	836.5	0	0	0	3	2	5	0	0	2	5	2	0							
39	770.1	739.0	0	0	0	1	3	0	0	0	1	0	0	0							
42	902.4	831.2	0	0	0	6	3	5	0	0	1	2	1	1							
45	856.4	839.5	0	0	0	3	0	2	0	0	2	0	1	1							
48	916.5	740.9	0	0	0	2	1	1	0	0	1	2	0	0							
51	694.1	831.3	0	0	0	4	0	0	0	0	0	1	1	0							
54	1064.3	738.4	0	0	3	3	0	2	0	0	1	0	0	0							
57	908.0	833.2	0	0	2	5	0	1	0	0	0	1	0	0							
60	793.6	740.8	0	0	0	4	0	1	0	0	0	0	1	0							
63	1314.8	829.3	0	0	0	2	2	0	0	0	1	1	0	0							
66	926.0	829.6	0	0	1	7	1	0	0	0	0	0	0	0							
69	955.3	738.8	0	1	0	0	0	0	0	0	0	1	0	0							
72	1047.2	820.8	0	1	1	2	0	0	0	0	0	2	0	0							
75	1049.7	748.8	0	0	3	2	0	0	0	1	1	1	2	0							
78	787.7	839.5	0	1	1	1	0	0	0	0	0	0	0	0							
81	1006.0	743.3	0	1	0	4	0	0	0	0	1	1	0	0							
84	807.3	830.0	0	1	2	1	0	0	0	0	0	0	0	0							
87	796.9	831.0	0	0	0	1	0	0	0	0	0	2	0	0							
90	1079.3	744.9	0	2	0	0	0	0	0	0	0	0	0	0							
93	639.8	829.6	0	0	0	0	0	0	0	0	0	0	0	0							
96	872.1	738.3	0	0	0	1	0	0	0	0	1	1	1	0							
99	942.9	831.8	0	0	0	0	0	0	0	0	0	0	0	0							
102	736.3	738.4	0	0	0	1	0	0	0	0	1	1	0	0							
105	1138.7	832.1	0	0	0	2	0	0	0	0	0	0	0	0							
108	658.4	738.9	0	0	1	0	0	0	0	0	0	0	0	0							
111	1033.9	831.3	0	0	0	0	0	0	0	0	0	0	0	0							
114	950.4	739.6	0	0	0	0	0	0	0	0	0	0	0	0							
Total	891.6	791.0	23	44	64	162	165	128	1	3	28	59	49	57							

	-6.35 +5.6 mm	-5.6 mm	+4.0 mm	-4.0 mm	+2.8 mm	-2.8 mm	+2.0 mm	-2.0 mm	+1.4 mm	-1.4 mm	+1.0 mm
Total Particles to Overflow	23	44	64	162	165	128					
Total Particles to Underflow	1	3	28	59	49	57					
Total Particles Remaining in Bed	30	39	37	17	0	1					
Total Feed	54	86	129	238	214	186					

Experiment Date	18/01/2010
Feed Rate (g/min sand)	563
Underflow rate (g/min sand)	264
Vibration Rate	595V
Gas rate (%)	25
Experiment run time (min)	114

		1600 kg/m ³ density particles											
Time (min)	Adjusted Time (min)	Number of particles to Overflow						Number of Particles to Underflow					
		-6.35 +5.6 mm	-5.6 +4.0 mm	-4.0 +2.8 mm	-2.8 +2.0 mm	-2.0 +1.4 mm	-1.4 +1.0 mm	-6.35 +5.6 mm	-5.6 +4.0 mm	-4.0 +2.8 mm	-2.8 +2.0 mm	-2.0 +1.4 mm	-1.4 +1.0 mm
3		-	-	-	-	-	-	-	-	-	-	-	-
6		-	-	-	-	-	-	-	-	-	-	-	-
9		-	-	-	-	-	-	-	-	-	-	-	-
12	2	0	0	0	0	0	0	0	0	0	0	0	0
15	5	0	3	6	16	15	26	0	0	1	2	5	8
18	8	1	0	8	13	20	29	0	1	2	4	8	10
21	11	0	1	7	12	20	19	0	0	2	2	1	9
24	14	1	1	3	10	14	21	0	0	2	0	8	3
27	17	0	2	10	26	26	24	0	0	0	4	5	5
30	20	0	0	2	1	2	2	1	0	0	1	1	1
33	23	0	1	2	7	6	9	0	1	1	1	3	2
36	26	1	2	4	8	8	4	0	0	0	2	2	1
39	29	0	0	2	5	3	2	0	0	0	2	1	0
42	32	0	2	7	5	7	3	0	0	0	2	0	0
45	35	0	0	4	5	1	2	0	1	2	2	0	0
48	38	0	1	2	5	2	4	0	0	0	0	0	0
51	41	0	0	1	2	1	1	0	0	0	0	0	0
54	44	0	1	6	3	5	0	0	0	0	0	1	0
57	47	0	0	2	4	0	1	0	0	0	1	0	0
60	50	0	1	3	3	0	0	0	0	0	1	0	0
63	53	1	0	6	9	1	1	0	0	0	0	0	0
66	56	2	10	5	4	0	0	0	0	0	0	0	0
69	59	0	2	2	2	2	0	0	0	0	0	0	0
72	62	3	1	1	1	0	1	0	1	0	0	0	0
75	65	0	2	2	1	0	0	0	0	0	0	0	0
78	68	2	4	1	0	1	0	0	0	0	0	0	0
81	71	1	4	2	0	0	1	0	0	2	0	0	0
84	74	2	1	3	2	0	0	0	0	0	1	0	0
87	77	1	3	4	1	1	0	0	0	0	0	0	0
90	80	0	2	0	0	0	0	0	0	0	0	0	0
93	83	0	1	2	1	0	0	0	0	0	0	0	0
96	86	0	3	1	2	0	0	0	0	0	0	0	0
99	89	0	0	0	0	0	0	0	0	0	0	0	0
102	92	0	0	0	0	0	0	0	0	0	0	0	0
105	95	0	0	0	0	0	0	0	0	0	0	0	0
108	98	0	0	0	2	0	0	0	0	1	0	0	0
111	101	0	0	0	0	0	0	0	0	0	0	0	0
114	104	0	1	1	1	0	1	0	0	0	0	0	0
Total		15	49	99	151	135	151	1	4	13	25	35	39

	-6.35 +5.6 mm	-5.6 +4.0 mm	-4.0 +2.8 mm	-2.8 +2.0 mm	-2.0 +1.4 mm	-1.4 +1.0 mm
Total Particles to Overflow	15	49	99	151	135	151
Total Particles to Underflow	1	4	13	25	35	39
Total Particles Remaining in Bed	36	51	20	2	0	0
Total Feed	52	104	132	178	170	190

Experiment Date	18/01/2010
Feed Rate (g/min sand)	563
Underflow rate (g/min sand)	264
Vibration Rate	595V
Gas rate (%)	25
Experiment run time (min)	114

		2100 kg/m ³ density particles											
Time (min)	Adjusted Time (min)	Number of particles to Overflow						Number of Particles to Underflow					
		-6.35 +5.6 mm	-5.6 +4.0 mm	-4.0 +2.8 mm	-2.8 +2.0 mm	-2.0 +1.4 mm	-1.4 +1.0 mm	-6.35 +5.6 mm	-5.6 +4.0 mm	-4.0 +2.8 mm	-2.8 +2.0 mm	-2.0 +1.4 mm	-1.4 +1.0 mm
3		-	-	-	-	-	-	-	-	-	-	-	-
6		-	-	-	-	-	-	-	-	-	-	-	-
9		-	-	-	-	-	-	-	-	-	-	-	-
12		-	-	-	-	-	-	-	-	-	-	-	-
15		-	-	-	-	-	-	-	-	-	-	-	-
18		-	-	-	-	-	-	-	-	-	-	-	-
21	1	0	0	0	0	0	0	0	0	0	0	0	0
24	4	0	0	0	0	1	1	1	4	2	6	5	7
27	7	0	0	0	1	4	17	4	4	5	14	13	11
30	10	0	0	0	0	0	0	0	0	0	0	0	0
33	13	0	0	0	0	1	7	0	2	4	4	2	10
36	16	0	0	0	0	1	14	0	0	4	6	6	7
39	19	0	0	0	0	5	5	0	0	1	1	4	2
42	22	0	0	0	0	3	10	0	0	4	7	5	1
45	25	0	0	0	0	3	4	0	1	1	5	4	8
48	28	0	0	0	0	2	2	2	0	2	3	5	3
51	31	0	0	0	1	3	4	0	1	1	3	4	4
54	34	0	0	0	1	3	0	1	0	4	4	4	0
57	37	0	0	0	0	0	5	0	2	7	4	4	5
60	40	0	0	0	1	1	1	0	2	2	6	2	3
63	43	0	0	0	0	2	3	0	3	3	0	5	0
66	46	0	0	0	2	5	8	1	0	2	2	2	3
69	49	0	0	0	0	1	1	2	1	2	5	2	2
72	52	0	0	0	0	1	2	2	1	5	5	2	1
75	55	0	1	0	1	1	1	1	0	4	1	3	3
78	58	0	0	1	1	1	1	1	2	0	3	6	0
81	61	0	0	0	1	1	0	0	3	0	1	1	0
84	64	0	0	0	1	2	0	0	0	3	3	0	0
87	67	0	0	1	2	1	0	0	1	3	0	2	0
90	70	0	0	0	0	0	1	0	0	0	1	0	1
93	73	0	0	0	1	0	0	0	1	0	2	1	1
96	76	0	0	0	0	1	0	2	2	0	0	0	0
99	79	0	0	0	0	0	0	0	2	2	1	0	1
102	82	0	0	0	0	1	0	0	0	2	2	0	0
105	85	0	0	0	0	0	0	0	0	2	1	0	0
108	88	0	0	0	1	0	0	0	0	0	1	1	0
111	91	0	0	0	0	1	0	0	0	0	2	0	0
114	94	0	0	0	0	0	0	0	0	1	1	0	0
Total		0	1	2	14	45	87	17	32	66	94	83	73

	-6.35 +5.6 mm	-5.6 +4.0 mm	-4.0 +2.8 mm	-2.8 +2.0 mm	-2.0 +1.4 mm	-1.4 +1.0 mm
Total Particles to Overflow	0	1	2	14	45	87
Total Particles to Underflow	17	32	66	94	83	73
Total Particles Remaining in Bed	33	62	46	43	17	1
Total Feed	50	95	114	151	145	161

Experiment Date	18/01/2010
Feed Rate (g/min sand)	563
Underflow rate (g/min sand)	264
Vibration Rate	595V
Gas rate (%)	25
Experiment run time (min)	114

		1300 kg/m ³ density particles													
Time (min)	Adjusted Time (min)	Number of particles to Overflow						Number of Particles to Underflow							
		-6.35 +5.6 mm	-5.6 +4.0 mm	-4.0 +2.8 mm	-2.8 +2.0 mm	-2.0 +1.4 mm	-1.4 +1.0 mm	-6.35 +5.6 mm	-5.6 +4.0 mm	-4.0 +2.8 mm	-2.8 +2.0 mm	-2.0 +1.4 mm	-1.4 +1.0 mm		
3		-	-	-	-	-	-	-	-	-	-	-	-	-	
6		-	-	-	-	-	-	-	-	-	-	-	-	-	
9		-	-	-	-	-	-	-	-	-	-	-	-	-	
12		-	-	-	-	-	-	-	-	-	-	-	-	-	
15		-	-	-	-	-	-	-	-	-	-	-	-	-	
18		-	-	-	-	-	-	-	-	-	-	-	-	-	
21		-	-	-	-	-	-	-	-	-	-	-	-	-	
24		-	-	-	-	-	-	-	-	-	-	-	-	-	
27		-	-	-	-	-	-	-	-	-	-	-	-	-	
30		-	-	-	-	-	-	-	-	-	-	-	-	-	
33	3	0	1	2	2	3	2	0	0	0	1	0	3		
36	6	6	13	35	53	64	38	0	0	1	4	7	8		
39	9	6	11	24	33	35	31	0	0	0	2	2	9		
42	12	10	17	34	34	27	23	0	0	0	0	3	4		
45	15	3	12	11	13	15	17	0	0	0	0	1	0		
48	18	6	5	9	12	13	11	0	0	0	0	0	2		
51	21	5	7	3	8	2	3	0	0	0	0	0	0		
54	24	8	7	8	8	11	5	0	0	0	0	0	1		
57	27	4	4	4	0	1	3	0	0	0	0	0	0		
60	30	1	1	4	1	0	1	0	0	0	0	0	0		
63	33	3	3	3	2	0	0	0	0	0	0	0	0		
66	36	2	1	0	0	0	0	0	0	0	0	0	0		
69	39	1	0	1	0	0	0	0	0	0	0	0	0		
72	42	3	1	1	0	0	0	0	0	0	0	0	0		
75	45	0	3	0	0	0	0	0	0	0	0	0	0		
78	48	0	0	0	0	0	0	0	0	0	0	0	0		
81	51	0	0	0	0	0	0	0	0	0	0	0	0		
84	54	0	0	0	1	0	0	0	0	0	0	0	0		
87	57	0	0	0	0	0	0	0	0	0	0	0	0		
90	60	0	0	0	0	0	0	0	0	0	0	0	0		
93	63	0	0	0	0	0	0	0	0	0	0	0	0		
96	66	0	0	0	0	0	0	0	0	0	0	0	0		
99	69	0	0	0	0	0	0	0	0	0	0	0	0		
102	72	0	0	0	0	0	0	0	0	0	0	0	0		
105	75	0	0	0	0	0	0	0	0	0	0	0	0		
108	78	0	0	0	0	0	0	0	0	0	0	0	0		
111	81	0	0	0	0	0	0	0	0	0	0	0	0		
114	84	0	0	0	0	0	0	0	0	0	0	0	0		
Total		58	86	139	167	171	134	0	0	1	7	13	27		

	-6.35 +5.6 mm	-5.6 +4.0 mm	-4.0 +2.8 mm	-2.8 +2.0 mm	-2.0 +1.4 mm	-1.4 +1.0 mm
Total Particles to Overflow	58	86	139	167	171	134
Total Particles to Underflow	0	0	1	7	13	27
Total Particles Remaining in Bed	0	0	0	0	0	0
Total Feed	58	86	140	174	184	161

Experiment Date	18/01/2010
Feed Rate (g/min sand)	563
Underflow rate (g/min sand)	264
Vibration Rate	595V
Gas rate (%)	25
Experiment run time (min)	114

		2400 kg/m ³ density particles												
Time (min)	Adjusted Time (min)	Number of particles to Overflow						Number of Particles to Underflow						
		-6.35 +5.6 mm	-5.6 +4.0 mm	-4.0 +2.8 mm	-2.8 +2.0 mm	-2.0 +1.4 mm	-1.4 +1.0 mm	-6.35 +5.6 mm	-5.6 +4.0 mm	-4.0 +2.8 mm	-2.8 +2.0 mm	-2.0 +1.4 mm	-1.4 +1.0 mm	
3		-	-	-	-	-	-	-	-	-	-	-	-	
6		-	-	-	-	-	-	-	-	-	-	-	-	
9		-	-	-	-	-	-	-	-	-	-	-	-	
12		-	-	-	-	-	-	-	-	-	-	-	-	
15		-	-	-	-	-	-	-	-	-	-	-	-	
18		-	-	-	-	-	-	-	-	-	-	-	-	
21		-	-	-	-	-	-	-	-	-	-	-	-	
24		-	-	-	-	-	-	-	-	-	-	-	-	
27		-	-	-	-	-	-	-	-	-	-	-	-	
30		-	-	-	-	-	-	-	-	-	-	-	-	
33		-	-	-	-	-	-	-	-	-	-	-	-	
36		-	-	-	-	-	-	-	-	-	-	-	-	
39		-	-	-	-	-	-	-	-	-	-	-	-	
42	2	0	0	0	0	0	0	0	0	0	0	0	0	
45	5	0	0	0	0	0	0	1	39	52	38	23	18	13
48	8	0	0	0	0	1	3	4	7	19	23	22	23	
51	11	0	0	0	0	1	5	0	0	6	8	14	13	
54	14	0	0	0	1	2	8	1	2	2	5	8	4	
57	17	0	0	0	0	3	7	0	0	3	9	8	5	
60	20	0	0	0	0	2	6	1	1	3	3	12	6	
63	23	0	0	0	0	1	5	0	0	3	2	4	12	
66	26	0	0	0	0	0	3	0	0	2	4	6	9	
69	29	0	0	0	0	3	3	0	2	7	6	3	5	
72	32	0	0	0	0	0	1	1	1	4	4	2	4	
75	35	0	0	0	0	1	1	1	2	2	8	7	6	
78	38	0	0	0	1	1	4	0	0	2	1	2	5	
81	41	0	0	1	1	3	2	0	2	1	1	3	2	
84	44	0	0	1	2	1	1	2	2	1	2	4	3	
87	47	0	0	0	1	0	1	0	1	1	3	1	2	
90	50	0	0	0	0	0	0	1	0	0	4	1	2	
93	53	0	0	0	0	0	0	0	1	2	0	3	2	
96	56	0	0	0	0	0	1	2	0	1	1	4	1	
99	59	0	0	0	0	0	1	0	1	1	2	1	0	
102	62	0	0	0	0	0	0	0	0	0	0	0	0	
105	65	0	0	0	0	0	2	1	0	2	1	0	0	
108	68	0	0	0	0	1	0	0	0	2	0	0	1	
111	71	0	0	0	0	0	0	0	1	1	3	0	0	
114	74	0	0	0	0	0	0	0	0	4	3	1	0	
Total		0	0	2	6	20	55	53	75	107	116	124	118	

	-6.35 +5.6 mm	-5.6 +4.0 mm	-4.0 +2.8 mm	-2.8 +2.0 mm	-2.0 +1.4 mm	-1.4 +1.0 mm
Total Particles to Overflow	0	2	6	20	55	
Total Particles to Underflow	53	75	107	116	124	118
Total Particles Remaining in Bed	2	13	31	40	18	14
Total Feed	55	88	140	162	162	187

Experiment Date	20/01/2010
Feed Rate (g/min sand)	549
Underflow rate (g/min sand)	372
Vibration Rate	595V
Gas rate (%)	25
Experiment run time (min)	117

1800 kg/m ³ density particles														
Time (min)	Mass of Sand to Overflow (g)	Mass of Sand to Underflow (g)	Number of particles to Overflow						Number of Particles to Underflow					
			-6.35 +5.6 mm	-5.6 +4.0 mm	-4.0 +2.8 mm	-2.8 +2.0 mm	-2.0 +1.4 mm	-1.4 +1.0 mm	-6.35 +5.6 mm	-5.6 +4.0 mm	-4.0 +2.8 mm	-2.8 +2.0 mm	-2.0 +1.4 mm	-1.4 +1.0 mm
3	439.2	1116.7	0	0	0	0	0	0	0	2	0	3	3	2
6	484.9	1112.6	0	0	0	0	0	0	0	8	8	11	27	21
9	500.0	1113.3	0	0	0	0	3	2	1	4	4	8	19	9
12	622.6	1119.0	0	0	0	0	2	9	2	3	5	6	13	8
15	366.9	1115.1	0	0	0	0	1	4	1	0	6	7	7	10
18	230.0	1117.2	0	0	0	0	1	1	0	0	2	7	7	8
21	685.8	1116.5	0	0	0	0	3	2	0	0	2	7	5	4
24	675.1	1117.5	0	0	0	0	3	9	0	0	4	5	7	6
27	490.0	1113.0	0	0	0	0	5	8	0	0	2	10	7	3
30	767.4	1117.5	0	0	0	0	0	1	2	5	1	12	15	8
33	190.1	1123.3	0	0	0	0	0	2	0	1	3	6	4	6
36	457.1	1117.0	0	0	0	0	3	2	0	2	1	7	8	3
39	630.1	1115.8	0	0	0	0	1	3	0	0	3	8	2	8
42	566.3	1114.1	0	0	0	0	0	4	0	0	5	3	1	1
45	583.5	1156.7	0	0	0	1	5	4	0	3	5	2	3	0
48	641.3	1111.0	0	0	0	2	3	1	0	1	1	4	5	2
51	601.1	1113.0	0	0	0	0	2	4	0	0	2	6	4	1
54	528.4	1112.7	0	0	0	4	4	3	0	1	3	2	2	0
57	512.1	1114.4	0	0	0	2	0	2	0	1	4	2	4	2
60	624.7	1110.9	0	0	0	1	0	2	0	0	1	2	2	1
63	790.8	1110.1	0	0	0	0	3	1	0	2	2	4	0	0
66	560.1	1109.3	0	0	0	0	0	0	0	0	2	3	1	0
69	417.4	1109.6	0	0	1	1	2	1	0	0	0	5	2	0
72	756.5	1115.5	0	0	0	0	0	0	0	2	1	5	1	4
75	259.7	1108.8	0	0	0	0	0	0	0	0	0	2	3	1
78	583.2	1110.2	0	0	1	0	1	0	0	0	1	1	3	1
81	624.9	1109.8	0	0	0	0	2	1	0	1	1	2	1	0
84	283.2	1107.6	0	0	0	0	0	0	0	1	2	2	2	0
87	722.0	1110.7	0	0	0	2	1	0	0	0	0	5	1	1
90	369.9	1107.9	0	0	0	0	0	0	0	1	1	1	1	0
93	701.5	1107.5	0	0	0	0	1	0	0	1	1	1	0	0
96	633.8	1107.4	0	0	0	1	1	1	0	0	2	2	0	1
99	248.9	1107.6	0	0	0	0	1	0	0	0	2	3	1	1
102	865.1	1105.4	0	0	0	0	1	0	0	0	0	3	1	0
105	258.1	1109.4	0	0	0	0	0	0	0	0	1	1	0	0
108	547.2	1109.4	0	0	0	0	0	0	0	0	0	1	1	0
111	439.7	1108.7	0	0	0	1	0	0	0	0	1	2	1	0
114	302.2	1112.1	0	0	0	0	0	0	0	0	0	0	2	0
117	633.6	1110.3	0	0	0	0	0	0	0	0	0	1	0	0
Total	528.1	1113.5	0	0	2	15	49	67	14	39	82	178	159	112

	-6.35 +5.6 mm	-5.6 +4.0 mm	-4.0 +2.8 mm	-2.8 +2.0 mm	-2.0 +1.4 mm	-1.4 +1.0 mm
Total Particles to Overflow	0	0	2	15	49	67
Total Particles to Underflow	14	39	82	178	159	112
Total Particles Remaining in Bed	42	57	37	34	9	2
Total Feed	56	96	121	227	217	181

Experiment Date	20/01/2010
Feed Rate (g/min sand)	549
Underflow rate (g/min sand)	372
Vibration Rate	595V
Gas rate (%)	25
Experiment run time (min)	117

		1600 kg/m ³ density particles												
Time (min)	Adjusted Time (min)	Number of particles to Overflow						Number of Particles to Underflow						
		-6.35 +5.6 mm	-5.6 mm	+4.0 mm	-4.0 mm	+2.8 mm	-2.8 mm	+2.0 mm	-2.0 mm	+1.4 mm	-1.4 mm	+1.0 mm		
3		-	-	-	-	-	-	-	-	-	-	-	-	
6		-	-	-	-	-	-	-	-	-	-	-	-	
9		-	-	-	-	-	-	-	-	-	-	-	-	
12	2	0	0	0	0	0	0	0	0	0	0	0	0	
15	5	0	0	0	0	0	0	1	1	1	6	6	18	28
18	8	0	0	0	0	0	0	1	1	1	3	8	11	15
21	11	0	0	1	0	8	14	0	0	0	3	4	8	9
24	14	0	0	1	2	8	17	0	0	0	0	7	7	6
27	17	0	1	0	6	11	16	0	0	0	0	7	8	5
30	20	0	0	0	1	5	2	0	1	1	5	5	6	2
33	23	0	0	0	1	0	4	0	0	0	2	2	5	4
36	26	0	0	0	1	2	7	0	0	0	0	4	5	3
39	29	0	0	0	3	3	6	0	0	0	0	6	2	5
42	32	0	0	1	1	4	1	0	0	3	3	3	5	1
45	35	0	0	0	0	8	3	0	0	0	0	5	1	0
48	38	0	0	1	3	4	6	0	0	0	0	4	4	1
51	41	0	0	0	1	3	4	0	0	1	1	3	1	1
54	44	0	0	2	4	1	2	0	1	1	1	2	4	2
57	47	0	0	0	2	3	3	0	0	0	2	3	1	1
60	50	0	0	2	4	2	2	0	0	0	2	3	1	0
63	53	0	0	1	0	2	0	0	0	0	2	4	5	1
66	56	0	0	1	4	1	0	0	1	1	1	3	0	0
69	59	0	1	4	4	2	1	0	1	1	1	2	2	0
72	62	0	0	0	2	0	0	0	0	0	1	0	2	0
75	65	0	0	0	1	1	0	0	2	1	0	0	0	0
78	68	0	0	1	0	0	0	0	0	0	1	1	0	0
81	71	0	0	1	3	1	1	0	0	1	1	1	0	0
84	74	0	0	0	1	0	0	0	0	0	0	3	3	0
87	77	0	1	0	5	2	0	0	0	0	0	1	0	0
90	80	0	0	0	2	2	0	0	0	0	1	1	2	0
93	83	0	0	2	2	0	0	0	0	0	2	1	2	0
96	86	0	0	1	1	0	0	0	0	0	0	1	0	0
99	89	0	0	2	0	0	0	0	0	1	1	2	0	0
102	92	0	0	0	0	1	0	0	0	0	0	0	0	0
105	95	0	0	0	0	0	0	0	0	0	3	0	0	0
108	98	1	0	1	1	0	0	0	0	1	1	1	0	0
111	101	0	0	1	1	0	0	0	0	0	0	1	0	0
114	104	0	0	1	0	0	0	0	1	1	1	0	0	0
117	107	0	0	2	0	0	0	0	0	0	0	0	1	0
Total		1	3	26	56	74	91	2	9	45	94	104	84	

	-6.35 +5.6 mm	-5.6 mm	+4.0 mm	-4.0 mm	+2.8 mm	-2.8 mm	+2.0 mm	-2.0 mm	+1.4 mm	-1.4 mm	+1.0 mm
Total Particles to Overflow	1	3	26	56	74	91					
Total Particles to Underflow	2	9	45	94	104	84					
Total Particles Remaining in Bed	51	78	73	24	4	0					
Total Feed	54	90	144	174	182	175					

Experiment Date	20/01/2010
Feed Rate (g/min sand)	549
Underflow rate (g/min sand)	372
Vibration Rate	595V
Gas rate (%)	25
Experiment run time (min)	117

		2100 kg/m ³ density particles													
Time (min)	Adjusted Time (min)	Number of particles to Overflow						Number of Particles to Underflow							
		-6.35 +5.6 mm	-5.6 mm	+4.0 mm	-4.0+2.8 mm	-2.8+2.0 mm	-2.0+1.4 mm	-1.4+1.0 mm	-6.35 +5.6 mm	-5.6 mm	+4.0 mm	-4.0+2.8 mm	-2.8+2.0 mm	-2.0+1.4 mm	-1.4+1.0 mm
3		-	-	-	-	-	-	-	-	-	-	-	-	-	-
6		-	-	-	-	-	-	-	-	-	-	-	-	-	-
9		-	-	-	-	-	-	-	-	-	-	-	-	-	-
12		-	-	-	-	-	-	-	-	-	-	-	-	-	-
15		-	-	-	-	-	-	-	-	-	-	-	-	-	-
18		-	-	-	-	-	-	-	-	-	-	-	-	-	-
21	1	0	0	0	0	0	0	0	0	0	0	0	0	0	0
24	4	0	0	0	0	0	0	0	12	10	7	9	18	16	
27	7	0	0	0	0	0	0	0	9	12	19	24	28	30	
30	10	0	0	0	0	0	0	0	0	0	0	0	0	0	
33	13	0	0	0	0	0	0	0	0	3	9	7	7	8	
36	16	0	0	0	0	0	0	3	0	0	2	5	5	11	
39	19	0	0	0	0	0	1	1	0	1	3	8	10	12	
42	22	0	0	0	0	0	0	3	0	1	2	5	7	6	
45	25	0	0	0	0	0	0	2	1	3	3	3	3	6	
48	28	0	0	0	0	0	0	4	4	0	4	9	2	5	
51	31	0	0	0	0	0	0	1	0	3	2	4	3	6	
54	34	0	0	0	0	0	0	1	0	2	2	2	2	4	
57	37	0	0	0	0	0	0	1	0	0	1	2	3	3	
60	40	0	0	0	0	0	0	0	0	0	1	5	3	2	
63	43	0	0	0	0	0	0	1	0	0	3	6	1	1	
66	46	0	0	0	0	0	1	1	0	1	3	2	3	0	
69	49	0	0	0	0	0	0	1	0	0	1	1	4	2	
72	52	0	0	0	0	0	0	2	0	2	3	1	1	2	
75	55	0	0	0	0	0	0	1	0	1	3	2	1	1	
78	58	0	0	0	0	0	0	0	0	2	0	5	2	1	
81	61	0	0	0	0	0	0	0	0	0	0	3	1	1	
84	64	0	0	0	0	0	0	0	0	1	0	0	1	0	
87	67	0	0	0	0	0	1	2	0	0	3	0	2	1	
90	70	0	0	0	0	0	0	0	1	2	3	3	3	4	
93	73	0	0	0	0	0	0	1	0	0	1	3	0	2	
96	76	0	0	0	0	0	0	0	0	0	0	2	0	2	
99	79	0	0	0	0	0	0	0	0	0	1	0	0	2	
102	82	0	0	0	0	0	0	0	0	2	1	1	0	1	
105	85	0	0	0	0	0	0	0	1	2	1	1	1	0	
108	88	0	0	0	1	0	0	0	1	1	2	5	1	1	
111	91	0	0	0	1	0	0	0	0	0	0	0	1	0	
114	94	0	0	0	0	0	0	0	0	1	2	0	1	0	
117	97	0	0	0	0	0	0	0	0	0	1	1	1	0	
Total		0	0	0	2	3	25		29	50	83	119	115	130	

	-6.35 +5.6 mm	-5.6 mm	+4.0 mm	-4.0+2.8 mm	-2.8+2.0 mm	-2.0+1.4 mm	-1.4+1.0 mm
Total Particles to Overflow	0	0	0	2	3	25	
Total Particles to Underflow	29	50	83	119	115	130	
Total Particles Remaining in Bed	19	38	41	28	11	3	
Total Feed	48	88	124	149	129	158	

Experiment Date	20/01/2010
Feed Rate (g/min sand)	549
Underflow rate (g/min sand)	372
Vibration Rate	595V
Gas rate (%)	25
Experiment run time (min)	117

		1300 kg/m ³ density particles											
Time (min)	Adjusted Time (min)	Number of particles to Overflow						Number of Particles to Underflow					
		-6.35 +5.6 mm	-5.6+4.0 mm	-4.0+2.8 mm	-2.8+2.0 mm	-2.0+1.4 mm	-1.4+1.0 mm	-6.35 +5.6 mm	-5.6+4.0 mm	-4.0+2.8 mm	-2.8+2.0 mm	-2.0+1.4 mm	-1.4+1.0 mm
3		-	-	-	-	-	-	-	-	-	-	-	-
6		-	-	-	-	-	-	-	-	-	-	-	-
9		-	-	-	-	-	-	-	-	-	-	-	-
12		-	-	-	-	-	-	-	-	-	-	-	-
15		-	-	-	-	-	-	-	-	-	-	-	-
18		-	-	-	-	-	-	-	-	-	-	-	-
21		-	-	-	-	-	-	-	-	-	-	-	-
24		-	-	-	-	-	-	-	-	-	-	-	-
27		-	-	-	-	-	-	-	-	-	-	-	-
30		-	-	-	-	-	-	-	-	-	-	-	-
33	3	0	0	0	0	0	0	0	0	0	2	0	1
36	6	0	0	2	0	2	6	0	2	2	3	7	16
39	9	0	3	10	26	34	25	0	0	0	2	3	10
42	12	1	6	10	33	30	41	0	0	1	1	4	5
45	15	3	7	19	22	28	19	0	0	0	1	1	3
48	18	4	6	19	23	17	13	0	0	0	0	1	1
51	21	3	7	9	14	14	10	0	0	1	0	0	3
54	24	0	4	8	9	6	4	0	0	0	0	2	0
57	27	6	4	10	6	6	1	0	0	1	0	1	5
60	30	3	8	10	11	3	2	0	0	1	0	2	0
63	33	2	1	5	2	1	2	0	0	0	2	0	1
66	36	0	2	4	6	2	0	0	0	0	0	0	0
69	39	4	5	1	2	1	0	0	0	0	0	0	1
72	42	0	3	3	1	2	2	0	0	0	0	0	1
75	45	0	1	0	0	1	0	0	0	0	0	0	0
78	48	1	2	0	1	0	0	0	0	0	0	0	0
81	51	1	1	3	2	0	0	0	0	0	0	0	0
84	54	0	1	0	0	0	0	0	0	0	0	0	0
87	57	6	8	4	0	1	0	0	0	0	0	0	0
90	60	2	2	2	0	0	0	0	0	0	0	0	0
93	63	2	1	2	2	0	0	0	0	0	0	0	0
96	66	1	2	1	0	0	0	0	0	0	0	0	0
99	69	0	0	0	0	0	0	0	0	0	0	0	0
102	72	4	1	0	1	0	0	0	0	0	0	0	0
105	75	2	1	0	0	0	0	0	0	0	0	0	0
108	78	1	2	1	0	0	0	0	0	0	0	0	0
111	81	0	1	1	0	0	0	0	0	0	0	0	0
114	84	0	0	0	0	0	0	0	0	0	0	0	0
117	87	2	2	2	0	0	0	0	0	0	0	0	0
Total		48	81	126	161	148	125	0	2	6	11	21	47

	-6.35 +5.6 mm	-5.6+4.0 mm	-4.0+2.8 mm	-2.8+2.0 mm	-2.0+1.4 mm	-1.4+1.0 mm
Total Particles to Overflow	48	81	126	161	148	125
Total Particles to Underflow	0	2	6	11	21	47
Total Particles Remaining in Bed	7	9	4	0	0	0
Total Feed	55	92	136	172	169	172

Experiment Date	20/01/2010
Feed Rate (g/min sand)	549
Underflow rate (g/min sand)	372
Vibration Rate	595V
Gas rate (%)	25
Experiment run time (min)	117

		2400 kg/m ³ density particles													
Time (min)	Adjusted Time (min)	Number of particles to Overflow						Number of Particles to Underflow							
		-6.35 +5.6 mm	-5.6 mm	+4.0 mm	-4.0+2.8 mm	-2.8+2.0 mm	-2.0+1.4 mm	-1.4+1.0 mm	-6.35 +5.6 mm	-5.6 mm	+4.0 mm	-4.0+2.8 mm	-2.8+2.0 mm	-2.0+1.4 mm	-1.4+1.0 mm
3		-	-	-	-	-	-	-	-	-	-	-	-	-	-
6		-	-	-	-	-	-	-	-	-	-	-	-	-	-
9		-	-	-	-	-	-	-	-	-	-	-	-	-	-
12		-	-	-	-	-	-	-	-	-	-	-	-	-	-
15		-	-	-	-	-	-	-	-	-	-	-	-	-	-
18		-	-	-	-	-	-	-	-	-	-	-	-	-	-
21		-	-	-	-	-	-	-	-	-	-	-	-	-	-
24		-	-	-	-	-	-	-	-	-	-	-	-	-	-
27		-	-	-	-	-	-	-	-	-	-	-	-	-	-
30		-	-	-	-	-	-	-	-	-	-	-	-	-	-
33		-	-	-	-	-	-	-	-	-	-	-	-	-	-
36		-	-	-	-	-	-	-	-	-	-	-	-	-	-
39		-	-	-	-	-	-	-	-	-	-	-	-	-	-
42	2	0	0	0	0	0	0	0	0	0	0	0	0	0	0
45	5	0	0	0	0	0	0	0	50	53	55	52	31	36	
48	8	0	0	0	0	0	0	1	3	8	21	20	16	27	
51	11	0	0	0	0	0	0	2	0	1	6	8	9	16	
54	14	0	0	0	0	0	0	0	0	2	2	7	8	8	
57	17	0	0	0	0	0	1	0	0	2	4	7	7	12	
60	20	0	0	0	0	0	0	0	1	1	4	8	6	7	
63	23	0	0	0	0	0	0	1	0	1	4	6	12	9	
66	26	0	0	0	0	0	0	0	0	0	2	5	2	3	
69	29	0	0	0	0	0	0	0	0	1	2	3	5	4	
72	32	0	0	0	0	0	0	0	0	0	3	3	4	4	
75	35	0	0	0	0	0	0	0	0	0	1	3	6	9	
78	38	0	0	0	0	0	0	1	0	1	1	3	7	5	
81	41	0	0	0	0	0	1	0	0	2	4	1	3	9	
84	44	0	0	0	0	0	0	0	0	1	1	2	5	5	
87	47	0	0	0	0	0	0	0	0	1	1	3	2	2	
90	50	0	0	0	0	0	0	0	0	0	2	3	2	3	
93	53	0	0	0	0	0	0	0	0	1	2	3	6	0	
96	56	0	0	0	0	0	0	2	0	0	2	0	4	3	
99	59	0	0	0	0	0	0	0	0	0	3	3	5	2	
102	62	0	0	0	0	0	0	0	0	0	1	1	2	3	
105	65	0	0	0	0	0	0	0	0	1	0	1	2	1	
108	68	0	0	0	0	0	0	0	0	0	0	1	1	0	
111	71	0	0	0	0	0	0	0	0	0	2	2	1	1	
114	74	0	0	0	0	0	0	0	0	0	2	3	1	0	
117	77	0	0	0	0	0	0	0	1	1	0	2	0	1	
Total		0	0	0	0	2	7		55	77	125	150	147	170	

	-6.35 +5.6 mm	-5.6 mm	+4.0 mm	-4.0+2.8 mm	-2.8+2.0 mm	-2.0+1.4 mm	-1.4+1.0 mm
Total Particles to Overflow	0	0	0	0	2	7	
Total Particles to Underflow	55	77	125	150	147	170	
Total Particles Remaining in Bed	2	10	10	13	15	8	
Total Feed	57	87	135	163	164	185	

Experiment Date	22/01/2010
Feed Rate (g/min sand)	552
Underflow rate (g/min sand)	373
Vibration Rate	595V
Gas rate (%)	30
Experiment run time (min)	114

1800 kg/m ³ density particles																					
Time (min)	Mass of Sand to Overflow (g)	Mass of Sand to Underflow (g)	Number of particles to Overflow						Number of Particles to Underflow												
			-6.35 +5.6 mm	-5.6 mm	+4.0 mm	-4.0 mm	+2.8 mm	-2.8 mm	+2.0 mm	-2.0 mm	+1.4 mm	-1.4 mm	+1.0 mm	-6.35 +5.6 mm	-5.6 mm	+4.0 mm	-4.0 mm	+2.8 mm	-2.8 mm	+2.0 mm	-2.0 mm
3	468.0	1119.1	0	0	0	0	0	0	0	0	0	0	1	2	4	11	6				
6	510.8	1120.5	0	0	1	6	4	4	0	2	5	19	22	21							
9	408.1	1121.8	0	0	0	1	5	3	2	2	6	13	12	13							
12	442.2	1118.7	0	0	1	1	8	9	0	3	2	4	4	13							
15	659.5	1115.4	0	0	1	8	11	18	0	1	2	8	13	10							
18	437.6	1117.8	0	0	0	1	4	3	1	0	0	12	8	6							
21	495.1	1117.8	0	0	0	1	4	4	0	2	7	16	11	4							
24	636.4	1132.8	0	0	0	3	3	4	0	2	4	11	11	10							
27	790.3	1117.2	0	0	3	6	7	3	0	1	3	6	9	7							
30	285.0	1113.8	0	0	0	1	0	4	1	3	3	8	12	20							
33	673.3	1120.3	6	6	7	8	6	3	2	2	4	5	6	3							
36	382.8	1111.0	4	4	5	16	5	4	0	0	2	3	5	3							
39	665.6	1108.1	1	4	6	4	8	2	0	0	2	2	4	1							
42	389.6	1199.3	0	2	0	2	1	1	0	0	1	2	3	0							
45	570.5	1108.3	13	11	15	10	4	2	0	0	1	2	1	0							
48	684.0	1107.2	6	12	4	8	2	4	0	1	1	5	0	1							
51	349.8	1103.8	4	3	2	2	3	0	0	0	1	1	1	0							
54	397.3	1106.9	1	0	1	2	2	0	0	0	2	1	0	0							
57	804.7	1113.3	1	2	3	5	3	1	1	0	0	0	0	1							
60	572.1	1111.9	2	0	2	1	2	0	0	0	1	1	2	0							
63	388.1	1114.4	1	1	3	0	0	0	0	0	1	4	0	1							
66	586.6	1117.4	0	0	3	0	0	0	0	1	0	0	0	0							
69	452.7	1116.5	2	0	0	0	0	0	0	0	0	3	0	0							
72	506.5	1120.5	0	0	1	0	1	0	0	1	1	2	1	1							
75	890.7	1119.1	0	0	0	1	1	0	0	0	0	0	0	0							
78	260.1	1118.6	0	0	0	0	0	0	0	1	0	0	0	0							
81	770.4	1119.9	0	0	0	0	0	0	0	0	2	1	0	0							
84	609.4	1116.5	0	0	0	0	0	1	0	0	0	0	0	0							
87	746.7	1115.1	0	0	0	0	0	0	0	0	0	1	0	0							
90	303.6	1115.9	0	0	0	0	0	0	0	1	1	1	0	0							
93	964.3	1116.1	0	0	0	0	0	0	0	0	0	0	0	0							
96	602.3	1114.7	0	0	0	0	0	0	0	0	0	1	0	0							
99	694.6	1121.3	0	0	0	0	0	0	0	1	1	0	0	0							
102	593.0	1112.0	0	0	0	0	0	0	0	0	0	0	0	0							
105	540.5	1114.1	0	0	0	0	0	0	0	0	0	1	0	0							
108	471.4	1111.2	0	0	0	0	0	0	0	2	1	0	0	0							
111	411.3	1115.4	0	0	0	0	1	0	0	0	0	0	0	0							
114	692.0	1114.5	0	0	0	0	0	0	0	0	0	0	0	0							
Total	555.4	1117.8	41	45	58	87	85	70	7	27	56	137	136	121							

	-6.35 +5.6 mm	-5.6 mm	+4.0 mm	-4.0 mm	+2.8 mm	-2.8 mm	+2.0 mm	-2.0 mm	+1.4 mm	-1.4 mm	+1.0 mm
Total Particles to Overflow	41	45	58	87	85	70					
Total Particles to Underflow	7	27	56	137	136	121					
Total Particles Remaining in Bed	8	21	6	6	0	0					
Total Feed	56	93	120	230	221	191					

Experiment Date	22/01/2010
Feed Rate (g/min sand)	552
Underflow rate (g/min sand)	373
Vibration Rate	595V
Gas rate (%)	30
Experiment run time (min)	114

		1600 kg/m ³ density particles											
Time (min)	Adjusted Time (min)	Number of particles to Overflow						Number of Particles to Underflow					
		-6.35 +5.6 mm	-5.6 +4.0 mm	-4.0 +2.8 mm	-2.8 +2.0 mm	-2.0 +1.4 mm	-1.4 +1.0 mm	-6.35 +5.6 mm	-5.6 +4.0 mm	-4.0 +2.8 mm	-2.8 +2.0 mm	-2.0 +1.4 mm	-1.4 +1.0 mm
3		-	-	-	-	-	-	-	-	-	-	-	-
6		-	-	-	-	-	-	-	-	-	-	-	-
9		-	-	-	-	-	-	-	-	-	-	-	-
12	2	0	0	0	0	0	0	0	0	0	0	1	1
15	5	0	0	2	3	11	10	1	4	3	18	26	22
18	8	0	0	1	1	6	9	0	1	2	10	7	21
21	11	0	2	0	9	9	8	0	0	2	2	9	17
24	14	1	0	5	6	21	11	1	0	2	5	8	12
27	17	0	4	6	9	5	16	0	1	2	6	6	11
30	20	0	0	5	1	4	3	1	0	3	3	3	1
33	23	7	11	12	12	7	8	0	2	4	4	7	3
36	26	4	8	14	7	5	2	1	1	2	2	5	2
39	29	1	3	5	4	5	4	0	0	1	4	4	2
42	32	0	7	9	4	1	2	0	0	2	1	0	2
45	35	14	13	20	9	4	3	0	0	0	0	2	1
48	38	3	9	9	11	4	3	0	1	1	5	2	2
51	41	5	3	4	7	2	0	0	0	0	2	1	2
54	44	1	4	1	3	1	0	0	0	0	0	1	0
57	47	1	3	2	5	1	2	0	0	0	0	0	1
60	50	3	4	3	4	2	0	0	0	0	1	0	0
63	53	2	1	4	2	0	0	0	0	0	1	1	0
66	56	1	0	3	1	0	0	0	0	1	0	0	0
69	59	1	4	0	1	0	0	0	0	0	1	0	0
72	62	0	0	0	0	0	0	0	0	0	0	0	0
75	65	0	0	0	1	0	0	0	0	0	1	0	0
78	68	0	0	0	0	0	0	0	0	1	0	0	0
81	71	0	0	0	0	0	0	0	0	0	0	0	0
84	74	0	0	0	2	0	0	0	0	0	0	0	1
87	77	0	0	1	0	0	0	0	0	0	0	0	0
90	80	0	0	0	0	0	0	0	0	0	0	0	0
93	83	1	0	0	0	0	0	0	0	0	0	0	0
96	86	0	0	1	0	0	0	0	0	0	0	0	0
99	89	0	0	0	1	0	0	0	0	0	0	0	0
102	92	0	0	0	0	0	0	0	0	0	0	0	0
105	95	0	0	0	0	0	0	0	0	0	0	0	0
108	98	0	0	1	0	0	0	0	0	0	1	0	0
111	101	0	0	0	0	0	0	0	0	0	0	0	0
114	104	0	0	0	0	0	0	0	0	0	0	0	0
Total		45	76	108	103	88	81	4	10	26	67	83	101

	-6.35 +5.6 mm	-5.6 +4.0 mm	-4.0 +2.8 mm	-2.8 +2.0 mm	-2.0 +1.4 mm	-1.4 +1.0 mm
Total Particles to Overflow	45	76	108	103	88	81
Total Particles to Underflow	4	10	26	67	83	101
Total Particles Remaining in Bed	4	14	4	1	0	0
Total Feed	53	100	138	171	171	182

Experiment Date	22/01/2010
Feed Rate (g/min sand)	552
Underflow rate (g/min sand)	373
Vibration Rate	595V
Gas rate (%)	30
Experiment run time (min)	114

		2100 kg/m ³ density particles											
Time (min)	Adjusted Time (min)	Number of particles to Overflow						Number of Particles to Underflow					
		-6.35 +5.6 mm	-5.6 +4.0 mm	-4.0 +2.8 mm	-2.8 +2.0 mm	-2.0 +1.4 mm	-1.4 +1.0 mm	-6.35 +5.6 mm	-5.6 +4.0 mm	-4.0 +2.8 mm	-2.8 +2.0 mm	-2.0 +1.4 mm	-1.4 +1.0 mm
3		-	-	-	-	-	-	-	-	-	-	-	-
6		-	-	-	-	-	-	-	-	-	-	-	-
9		-	-	-	-	-	-	-	-	-	-	-	-
12		-	-	-	-	-	-	-	-	-	-	-	-
15		-	-	-	-	-	-	-	-	-	-	-	-
18		-	-	-	-	-	-	-	-	-	-	-	-
21	1	0	0	0	0	0	0	0	0	0	0	0	0
24	4	0	0	0	0	0	0	3	5	5	6	12	12
27	7	0	0	1	0	3	6	2	3	12	11	11	14
30	10	0	0	0	0	0	0	0	0	0	0	0	0
33	13	2	3	5	4	8	11	0	0	6	8	14	5
36	16	3	9	8	10	4	12	1	1	2	5	10	13
39	19	0	1	2	2	9	4	0	5	5	11	3	10
42	22	1	0	2	7	3	3	0	1	4	2	3	7
45	25	4	0	11	11	8	3	2	0	0	4	1	5
48	28	2	7	4	15	7	5	2	4	4	4	1	5
51	31	2	4	4	6	3	1	0	1	0	2	3	1
54	34	1	3	0	2	0	2	1	1	1	3	1	0
57	37	0	1	3	1	2	5	0	2	1	1	5	3
60	40	0	2	3	6	1	0	3	0	1	1	2	1
63	43	0	0	3	2	1	0	0	1	1	0	3	0
66	46	0	3	1	3	0	0	0	0	1	1	2	2
69	49	0	0	0	0	1	0	2	0	3	2	1	2
72	52	0	0	0	0	0	0	0	0	0	3	1	0
75	55	0	0	0	0	1	0	0	0	0	2	1	0
78	58	0	0	0	0	0	1	0	2	4	0	0	1
81	61	0	0	0	0	0	0	2	3	2	2	1	0
84	64	0	0	0	0	0	0	0	1	0	0	1	0
87	67	0	0	0	0	0	0	1	0	1	3	1	1
90	70	0	0	0	0	0	0	1	2	2	0	0	0
93	73	0	0	0	0	0	0	0	1	1	1	0	0
96	76	0	0	0	0	0	0	1	0	1	2	0	0
99	79	0	0	0	0	0	0	0	0	1	1	0	0
102	82	0	0	0	0	0	0	0	0	1	0	0	0
105	85	0	0	0	0	0	1	0	0	0	0	0	0
108	88	0	0	0	0	0	0	0	0	1	1	1	0
111	91	0	0	0	0	0	0	0	0	0	0	0	0
114	94	0	0	0	0	0	0	0	0	1	0	0	0
Total		15	33	47	69	51	54	21	33	61	76	78	82

	-6.35 +5.6 mm	-5.6 +4.0 mm	-4.0 +2.8 mm	-2.8 +2.0 mm	-2.0 +1.4 mm	-1.4 +1.0 mm
Total Particles to Overflow	15	33	47	69	51	54
Total Particles to Underflow	21	33	61	76	78	82
Total Particles Remaining in Bed	14	21	11	9	3	0
Total Feed	50	87	119	154	132	136

Experiment Date	22/01/2010
Feed Rate (g/min sand)	552
Underflow rate (g/min sand)	373
Vibration Rate	595V
Gas rate (%)	30
Experiment run time (min)	114

		1300 kg/m ³ density particles											
Time (min)	Adjusted Time (min)	Number of particles to Overflow						Number of Particles to Underflow					
		-6.35 +5.6 mm	-5.6 +4.0 mm	-4.0 +2.8 mm	-2.8 +2.0 mm	-2.0 +1.4 mm	-1.4 +1.0 mm	-6.35 +5.6 mm	-5.6 +4.0 mm	-4.0 +2.8 mm	-2.8 +2.0 mm	-2.0 +1.4 mm	-1.4 +1.0 mm
3		-	-	-	-	-	-	-	-	-	-	-	-
6		-	-	-	-	-	-	-	-	-	-	-	-
9		-	-	-	-	-	-	-	-	-	-	-	-
12		-	-	-	-	-	-	-	-	-	-	-	-
15		-	-	-	-	-	-	-	-	-	-	-	-
18		-	-	-	-	-	-	-	-	-	-	-	-
21		-	-	-	-	-	-	-	-	-	-	-	-
24		-	-	-	-	-	-	-	-	-	-	-	-
27		-	-	-	-	-	-	-	-	-	-	-	-
30		-	-	-	-	-	-	-	-	-	-	-	-
33	3	13	17	29	33	34	31	0	1	3	2	5	3
36	6	13	18	23	28	19	23	0	1	1	6	14	16
39	9	4	10	22	35	20	20	0	0	1	2	13	11
42	12	7	7	13	13	10	10	0	1	0	2	3	7
45	15	10	15	14	10	13	11	0	0	0	1	2	3
48	18	3	6	13	10	13	6	0	0	1	1	0	2
51	21	1	3	5	4	6	2	0	0	0	0	0	3
54	24	1	1	6	7	1	1	0	0	0	1	0	1
57	27	1	2	5	3	8	3	0	0	0	0	0	3
60	30	2	2	1	3	2	2	0	0	0	0	1	1
63	33	0	1	4	1	0	2	0	0	0	0	0	0
66	36	1	1	0	0	1	0	0	0	0	0	0	0
69	39	0	0	1	0	0	0	0	0	0	0	1	0
72	42	0	3	1	0	1	0	0	0	0	0	0	0
75	45	1	0	0	1	2	1	0	0	0	0	0	0
78	48	0	0	0	0	0	0	0	0	0	0	0	0
81	51	0	0	0	0	1	0	0	0	0	0	0	0
84	54	0	0	0	0	0	1	0	0	0	0	0	0
87	57	0	0	0	1	0	0	0	0	0	0	0	0
90	60	0	0	0	0	0	0	0	0	0	0	0	0
93	63	0	0	0	0	0	0	0	0	0	0	0	0
96	66	0	0	0	0	0	0	0	0	0	0	0	0
99	69	0	0	0	0	0	0	0	0	0	0	0	0
102	72	0	0	0	0	0	0	0	0	0	0	0	0
105	75	0	1	0	0	0	0	0	0	0	0	0	0
108	78	0	0	0	0	0	0	0	0	0	0	0	0
111	81	0	0	0	0	0	0	0	0	0	0	0	0
114	84	0	0	0	0	0	0	0	0	0	0	0	0
Total		57	87	137	149	131	113	0	3	6	15	39	50

	-6.35 +5.6 mm	-5.6 +4.0 mm	-4.0 +2.8 mm	-2.8 +2.0 mm	-2.0 +1.4 mm	-1.4 +1.0 mm
Total Particles to Overflow	57	87	137	149	131	113
Total Particles to Underflow	0	3	6	15	39	50
Total Particles Remaining in Bed	0	0	0	0	0	0
Total Feed	57	90	143	164	170	163

Experiment Date	22/01/2010
Feed Rate (g/min sand)	552
Underflow rate (g/min sand)	373
Vibration Rate	595V
Gas rate (%)	30
Experiment run time (min)	114

		2400 kg/m ³ density particles											
Time (min)	Adjusted Time (min)	Number of particles to Overflow						Number of Particles to Underflow					
		-6.35 +5.6 mm	-5.6 +4.0 mm	-4.0 +2.8 mm	-2.8 +2.0 mm	-2.0 +1.4 mm	-1.4 +1.0 mm	-6.35 +5.6 mm	-5.6 +4.0 mm	-4.0 +2.8 mm	-2.8 +2.0 mm	-2.0 +1.4 mm	-1.4 +1.0 mm
3		-	-	-	-	-	-	-	-	-	-	-	-
6		-	-	-	-	-	-	-	-	-	-	-	-
9		-	-	-	-	-	-	-	-	-	-	-	-
12		-	-	-	-	-	-	-	-	-	-	-	-
15		-	-	-	-	-	-	-	-	-	-	-	-
18		-	-	-	-	-	-	-	-	-	-	-	-
21		-	-	-	-	-	-	-	-	-	-	-	-
24		-	-	-	-	-	-	-	-	-	-	-	-
27		-	-	-	-	-	-	-	-	-	-	-	-
30		-	-	-	-	-	-	-	-	-	-	-	-
33		-	-	-	-	-	-	-	-	-	-	-	-
36		-	-	-	-	-	-	-	-	-	-	-	-
39		-	-	-	-	-	-	-	-	-	-	-	-
42	2	0	2	2	3	5	5	2	2	0	1	0	0
45	5	0	5	10	16	13	14	7	13	7	8	11	12
48	8	4	7	12	16	30	22	11	7	5	11	11	22
51	11	0	4	2	11	6	8	4	1	4	1	11	14
54	14	0	0	1	7	4	7	5	0	2	12	7	7
57	17	0	1	1	2	5	7	3	4	3	7	4	11
60	20	0	0	3	3	7	8	1	3	3	2	5	10
63	23	0	1	2	3	1	2	3	2	5	8	6	6
66	26	0	0	0	2	0	1	1	3	6	1	3	5
69	29	0	0	0	2	2	0	2	2	7	4	4	1
72	32	0	0	0	0	0	1	1	3	5	1	3	2
75	35	0	0	0	0	1	1	0	2	3	4	0	2
78	38	0	0	0	0	0	0	1	0	4	6	2	3
81	41	0	0	0	0	0	0	1	3	4	6	2	1
84	44	0	0	0	0	0	0	0	0	2	3	1	0
87	47	0	0	0	0	0	0	2	1	2	3	1	5
90	50	0	0	0	0	0	0	1	1	2	0	0	0
93	53	0	0	0	0	0	1	2	2	2	3	0	1
96	56	0	0	0	0	0	0	0	0	1	1	4	0
99	59	0	0	0	0	0	0	1	0	3	3	2	0
102	62	0	0	0	0	0	0	1	2	3	3	0	1
105	65	0	0	0	0	0	0	1	1	1	3	4	0
108	68	0	0	0	0	0	0	1	1	0	1	1	1
111	71	0	0	0	0	0	0	0	4	2	2	0	0
114	74	0	0	0	0	0	0	0	2	1	1	2	2
Total		4	20	33	65	74	77	51	59	77	95	84	106

	-6.35 +5.6 mm	-5.6 +4.0 mm	-4.0 +2.8 mm	-2.8 +2.0 mm	-2.0 +1.4 mm	-1.4 +1.0 mm
Total Particles to Overflow	4	20	33	65	74	77
Total Particles to Underflow	51	59	77	95	84	106
Total Particles Remaining in Bed	4	9	22	9	3	2
Total Feed	59	88	132	169	161	185

Experiment Date	25/01/2010
Feed Rate (g/min sand)	554
Underflow rate (g/min sand)	374
Vibration Rate	595V
Gas rate (%)	35
Experiment run time (min)	114

1800 kg/m ³ density particles														
Time (min)	Mass of Sand to Overflow (g)	Mass of Sand to Underflow (g)	Number of particles to Overflow						Number of Particles to Underflow					
			-6.35 +5.6 mm	-5.6 mm	+4.0 mm	-4.0+2.8 mm	-2.8+2.0 mm	-2.0+1.4 mm	-1.4+1.0 mm	-6.35 +5.6 mm	-5.6 mm	+4.0 mm	-4.0+2.8 mm	-2.8+2.0 mm
3	566.0	1123.4	4	4	5	21	23	17	1	2	8	4	11	4
6	281.5	1125.4	1	4	7	14	9	10	1	2	2	13	21	22
9	417.4	1124.1	2	4	11	15	12	16	0	1	1	11	20	12
12	361.9	1219.1	1	1	3	8	2	5	1	2	8	8	13	13
15	523.7	1031.5	3	1	2	6	16	9	0	0	4	6	7	11
18	436.1	1124.7	6	8	6	12	12	10	0	1	4	10	8	6
21	768.0	1123.2	3	1	7	11	10	10	0	1	2	6	8	6
24	300.5	1121.3	1	2	2	2	3	3	0	2	3	7	9	3
27	568.0	1121.7	0	0	1	1	3	4	1	0	2	4	1	0
30	812.5	1123.2	4	5	13	16	15	13	1	1	6	13	21	13
33	853.0	1118.2	6	14	0	8	3	3	0	0	1	5	4	3
36	138.9	1118.6	0	0	0	1	2	0	1	0	0	2	1	0
39	498.3	1117.8	0	0	2	2	0	0	0	0	0	2	2	0
42	439.1	1121.7	0	0	1	2	0	0	0	1	0	2	0	3
45	706.4	1114.8	1	4	2	3	1	0	0	0	0	1	1	0
48	650.6	1117.9	2	3	2	0	0	1	0	1	0	0	0	0
51	925.6	1130.7	6	6	7	3	1	0	0	2	2	1	0	0
54	303.9	1121.7	0	0	0	1	0	0	0	1	0	1	0	0
57	875.2	1117.6	1	3	5	2	0	0	0	0	1	0	0	0
60	140.3	1116.3	0	0	0	0	0	0	0	0	0	1	0	0
63	882.8	1119.6	4	1	3	0	0	1	0	0	0	0	0	0
66	399.1	1117.0	1	0	0	2	0	0	0	0	0	0	0	0
69	275.0	1118.0	0	0	1	1	0	0	0	1	0	2	0	0
72	635.5	1119.5	0	0	0	0	0	0	0	1	0	1	0	0
75	412.4	1124.0	0	0	0	0	0	0	0	0	0	0	0	0
78	371.9	1121.5	0	0	0	0	0	0	0	0	0	0	0	0
81	664.0	1121.1	1	1	0	0	0	0	0	0	0	0	0	0
84	922.6	1118.4	0	0	2	0	0	0	0	0	0	0	0	0
87	163.3	1118.2	0	0	0	0	0	0	0	0	0	0	0	0
90	969.8	1115.4	1	0	0	0	0	0	1	0	0	0	0	0
93	541.4	1120.5	0	0	0	0	0	0	0	1	1	0	0	0
96	570.0	1122.3	0	0	0	0	0	0	0	1	0	0	0	0
99	969.4	1115.7	1	1	2	1	0	0	0	0	0	0	0	0
102	408.4	1115.0	0	0	0	0	0	0	0	0	0	0	0	0
105	536.2	1112.9	3	0	0	0	0	0	0	0	0	0	0	0
108	713.9	1111.1	1	0	0	0	0	0	0	0	0	0	0	0
111	730.6	1110.8	0	1	0	0	0	0	0	0	0	0	0	0
114	450.3	1107.7	0	0	0	0	0	0	0	0	0	0	0	0
Total	557.5	1119.5	53	64	84	132	112	102	7	21	45	100	127	96

	-6.35 +5.6 mm	-5.6 mm	+4.0 mm	-4.0+2.8 mm	-2.8+2.0 mm	-2.0+1.4 mm	-1.4+1.0 mm
Total Particles to Overflow	53	64	84	132	112	102	
Total Particles to Underflow	7	21	45	100	127	96	
Total Particles Remaining in Bed	3	1	1	0	0	0	
Total Feed	63	86	130	232	239	198	

Experiment Date	25/01/2010
Feed Rate (g/min sand)	554
Underflow rate (g/min sand)	374
Vibration Rate	595V
Gas rate (%)	35
Experiment run time (min)	114

1600 kg/m ³ density particles													
Time (min)	Adjusted Time (min)	Number of particles to Overflow						Number of Particles to Underflow					
		-6.35 +5.6 mm	-5.6 +4.0 mm	-4.0 +2.8 mm	-2.8 +2.0 mm	-2.0 +1.4 mm	-1.4 +1.0 mm	-6.35 +5.6 mm	-5.6 +4.0 mm	-4.0 +2.8 mm	-2.8 +2.0 mm	-2.0 +1.4 mm	-1.4 +1.0 mm
3		-	-	-	-	-	-	-	-	-	-	-	-
6		-	-	-	-	-	-	-	-	-	-	-	-
9		-	-	-	-	-	-	-	-	-	-	-	-
12	2	0	1	0	0	2	0	0	0	0	3	2	1
15	5	6	7	24	27	21	17	1	1	11	7	24	27
18	8	8	18	20	19	21	20	0	2	2	5	6	14
21	11	6	10	14	27	10	25	0	0	4	9	8	18
24	14	2	2	3	8	7	6	0	0	2	5	7	5
27	17	1	5	2	2	8	9	0	1	1	2	6	4
30	20	2	3	7	10	8	3	0	1	4	4	4	3
33	23	8	11	9	11	9	7	0	0	2	2	0	2
36	26	0	0	1	0	0	0	0	1	0	2	3	4
39	29	0	1	4	4	0	2	1	0	1	1	2	0
42	32	0	1	0	1	1	4	0	1	0	4	1	1
45	35	4	1	6	3	2	2	0	0	0	0	2	0
48	38	2	3	1	5	2	0	0	0	0	0	1	1
51	41	1	1	7	4	2	1	0	0	1	0	0	1
54	44	1	0	0	0	1	0	0	0	0	2	1	0
57	47	1	5	3	1	3	0	0	1	1	1	0	1
60	50	0	0	0	0	0	0	0	0	0	0	0	1
63	53	0	2	5	0	0	0	0	0	1	0	0	0
66	56	0	1	0	1	0	0	0	0	1	0	0	0
69	59	1	0	0	0	0	0	0	0	0	0	0	0
72	62	0	0	0	0	0	0	0	0	0	0	0	0
75	65	0	0	0	0	1	0	0	0	0	0	1	0
78	68	0	0	0	1	0	0	0	0	0	0	0	0
81	71	0	0	0	0	0	0	0	0	0	1	0	0
84	74	0	0	0	0	0	0	0	0	0	0	0	0
87	77	0	1	0	0	0	0	0	0	0	0	0	0
90	80	0	1	0	0	0	0	0	0	0	0	0	0
93	83	0	0	0	0	0	0	0	0	0	0	0	0
96	86	0	0	0	0	0	0	0	1	0	0	0	0
99	89	0	0	0	0	0	0	0	0	0	0	0	0
102	92	0	0	0	0	0	0	0	0	0	0	0	0
105	95	0	0	0	0	0	0	0	0	0	0	0	0
108	98	0	0	0	1	0	0	0	0	0	0	0	0
111	101	0	0	0	0	0	0	0	0	0	0	0	0
114	104	0	0	0	0	0	0	0	0	0	0	0	0
Total		43	74	106	125	98	96	2	9	31	48	68	83

	-6.35 +5.6 mm	-5.6 +4.0 mm	-4.0 +2.8 mm	-2.8 +2.0 mm	-2.0 +1.4 mm	-1.4 +1.0 mm
Total Particles to Overflow	43	74	106	125	98	96
Total Particles to Underflow	2	9	31	48	68	83
Total Particles Remaining in Bed	0	0	0	0	0	0
Total Feed	45	83	137	173	166	179

Experiment Date	25/01/2010
Feed Rate (g/min sand)	554
Underflow rate (g/min sand)	374
Vibration Rate	595V
Gas rate (%)	35
Experiment run time (min)	114

		2100 kg/m ³ density particles													
Time (min)	Adjusted Time (min)	Number of particles to Overflow						Number of Particles to Underflow							
		-6.35 +5.6 mm	-5.6 mm	+4.0 -4.0+2.8 mm	-2.8 +2.0 mm	-2.0 +1.4 mm	-1.4 +1.0 mm	-6.35 +5.6 mm	-5.6 mm	+4.0 -4.0+2.8 mm	-2.8 +2.0 mm	-2.0 +1.4 mm	-1.4 +1.0 mm		
3		-	-	-	-	-	-	-	-	-	-	-	-	-	
6		-	-	-	-	-	-	-	-	-	-	-	-	-	
9		-	-	-	-	-	-	-	-	-	-	-	-	-	
12		-	-	-	-	-	-	-	-	-	-	-	-	-	
15		-	-	-	-	-	-	-	-	-	-	-	-	-	
18		-	-	-	-	-	-	-	-	-	-	-	-	-	
21	1	0	0	0	0	0	0	0	0	0	0	0	0	0	
24	4	0	0	0	1	0	1	3	6	12	11	15	20		
27	7	0	0	0	0	4	6	1	5	7	12	15	23		
30	10	0	0	0	0	0	0	0	0	0	0	0	0		
33	13	2	10	11	10	11	22	1	1	4	10	9	13		
36	16	0	0	0	2	1	0	0	2	5	7	6	9		
39	19	0	1	0	2	0	5	3	3	5	2	4	5		
42	22	0	0	0	1	0	0	2	3	4	5	5	3		
45	25	3	2	1	7	3	6	0	1	4	8	6	3		
48	28	1	1	1	4	2	3	4	2	2	9	6	4		
51	31	3	7	4	3	2	3	3	3	1	4	2	1		
54	34	0	1	0	1	0	2	2	1	4	3	0	0		
57	37	0	2	2	0	1	2	2	3	4	3	5	3		
60	40	0	0	1	0	1	0	3	1	3	5	1	1		
63	43	0	1	2	0	0	0	1	1	0	1	0	1		
66	46	0	0	1	0	0	0	0	1	2	1	0	2		
69	49	0	1	0	0	0	0	1	0	2	2	3	1		
72	52	0	0	0	0	0	0	1	3	1	3	0	0		
75	55	0	0	0	0	0	0	0	2	2	1	0	1		
78	58	0	0	0	0	0	0	1	2	1	0	0	1		
81	61	0	0	0	0	1	0	0	1	1	0	0	0		
84	64	0	0	0	1	1	0	1	1	2	2	0	2		
87	67	0	0	0	0	0	0	1	1	2	0	1	1		
90	70	0	1	0	1	0	0	0	2	1	0	0	0		
93	73	0	0	0	0	0	0	0	1	0	2	0	0		
96	76	0	0	0	0	0	0	2	0	2	0	0	0		
99	79	2	5	0	2	0	0	0	0	0	0	1	0		
102	82	0	0	0	0	0	0	0	0	2	0	0	0		
105	85	1	2	0	0	0	0	0	0	0	0	0	0		
108	88	0	2	0	0	0	0	0	1	1	0	0	0		
111	91	0	0	0	0	0	0	1	0	0	0	0	0		
114	94	0	0	0	0	0	0	0	0	0	0	0	0		
Total		12	36	23	35	27	50	33	47	74	91	79	94		

	-6.35 +5.6 mm	-5.6 mm	+4.0 -4.0+2.8 mm	-2.8 +2.0 mm	-2.0 +1.4 mm	-1.4 +1.0 mm
Total Particles to Overflow	12	36	23	35	27	50
Total Particles to Underflow	33	47	74	91	79	94
Total Particles Remaining in Bed	2	4	1	1	0	0
Total Feed	47	87	98	127	106	144

Experiment Date	25/01/2010
Feed Rate (g/min sand)	554
Underflow rate (g/min sand)	374
Vibration Rate	595V
Gas rate (%)	35
Experiment run time (min)	114

1300 kg/m ³ density particles													
Time (min)	Adjusted Time (min)	Number of particles to Overflow						Number of Particles to Underflow					
		-6.35 +5.6 mm	-5.6 +4.0 mm	-4.0 +2.8 mm	-2.8 +2.0 mm	-2.0 +1.4 mm	-1.4 +1.0 mm	-6.35 +5.6 mm	-5.6 +4.0 mm	-4.0 +2.8 mm	-2.8 +2.0 mm	-2.0 +1.4 mm	-1.4 +1.0 mm
3		-	-	-	-	-	-	-	-	-	-	-	-
6		-	-	-	-	-	-	-	-	-	-	-	-
9		-	-	-	-	-	-	-	-	-	-	-	-
12		-	-	-	-	-	-	-	-	-	-	-	-
15		-	-	-	-	-	-	-	-	-	-	-	-
18		-	-	-	-	-	-	-	-	-	-	-	-
21		-	-	-	-	-	-	-	-	-	-	-	-
24		-	-	-	-	-	-	-	-	-	-	-	-
27		-	-	-	-	-	-	-	-	-	-	-	-
30		-	-	-	-	-	-	-	-	-	-	-	-
33	3	21	31	54	43	44	20	0	2	1	4	6	3
36	6	6	5	8	10	8	13	1	0	2	6	8	21
39	9	8	16	16	19	25	26	0	0	3	3	5	8
42	12	3	6	7	22	15	8	0	0	1	1	5	4
45	15	7	11	18	18	12	17	0	0	0	5	4	5
48	18	5	5	14	6	11	9	0	0	1	3	1	3
51	21	2	3	11	11	4	7	0	0	0	1	2	4
54	24	2	0	0	1	3	2	0	0	0	0	1	2
57	27	2	3	3	4	5	4	0	0	0	0	0	0
60	30	0	1	0	1	0	0	0	0	0	0	0	1
63	33	0	1	3	2	0	3	0	0	0	0	0	1
66	36	0	1	0	1	0	0	0	0	0	0	0	0
69	39	0	0	0	0	1	0	0	0	0	0	1	0
72	42	0	0	0	1	1	0	0	0	0	0	0	0
75	45	0	0	0	0	0	0	0	0	0	0	1	0
78	48	0	0	0	0	1	0	0	0	0	0	0	0
81	51	0	0	0	1	0	0	0	0	0	0	0	0
84	54	1	2	0	0	0	0	0	0	0	0	0	0
87	57	0	0	0	0	0	0	0	0	0	0	0	0
90	60	0	1	0	0	0	0	0	0	0	0	0	0
93	63	0	0	0	0	0	0	0	0	0	0	0	0
96	66	0	0	0	0	0	0	0	0	0	0	0	0
99	69	0	0	0	0	0	0	0	0	0	0	0	0
102	72	0	0	0	0	0	0	0	0	0	0	0	0
105	75	0	0	0	0	0	0	0	0	0	0	0	0
108	78	0	0	0	0	0	0	0	0	0	0	0	0
111	81	0	0	0	0	0	0	0	0	0	0	0	0
114	84	0	0	0	0	0	0	0	0	0	0	0	0
Total		57	86	134	140	130	109	1	2	8	23	34	52

	-6.35 +5.6 mm	-5.6 +4.0 mm	-4.0 +2.8 mm	-2.8 +2.0 mm	-2.0 +1.4 mm	-1.4 +1.0 mm
Total Particles to Overflow	57	86	134	140	130	109
Total Particles to Underflow	1	2	8	23	34	52
Total Particles Remaining in Bed	0	0	0	0	0	0
Total Feed	58	88	142	163	164	161

Experiment Date	25/01/2010
Feed Rate (g/min sand)	554
Underflow rate (g/min sand)	374
Vibration Rate	595V
Gas rate (%)	35
Experiment run time (min)	114

2400 kg/m ³ density particles													
Time (min)	Adjusted Time (min)	Number of particles to Overflow						Number of Particles to Underflow					
		-6.35 +5.6 mm	-5.6+4.0 mm	-4.0+2.8 mm	-2.8+2.0 mm	-2.0+1.4 mm	-1.4+1.0 mm	-6.35 +5.6 mm	-5.6+4.0 mm	-4.0+2.8 mm	-2.8+2.0 mm	-2.0+1.4 mm	-1.4+1.0 mm
3		-	-	-	-	-	-	-	-	-	-	-	-
6		-	-	-	-	-	-	-	-	-	-	-	-
9		-	-	-	-	-	-	-	-	-	-	-	-
12		-	-	-	-	-	-	-	-	-	-	-	-
15		-	-	-	-	-	-	-	-	-	-	-	-
18		-	-	-	-	-	-	-	-	-	-	-	-
21		-	-	-	-	-	-	-	-	-	-	-	-
24		-	-	-	-	-	-	-	-	-	-	-	-
27		-	-	-	-	-	-	-	-	-	-	-	-
30		-	-	-	-	-	-	-	-	-	-	-	-
33		-	-	-	-	-	-	-	-	-	-	-	-
36		-	-	-	-	-	-	-	-	-	-	-	-
39		-	-	-	-	-	-	-	-	-	-	-	-
42	2	0	0	0	0	0	0	1	0	0	0	0	0
45	5	0	2	2	6	11	9	15	16	23	25	35	30
48	8	0	0	4	4	6	10	2	5	12	25	17	26
51	11	3	6	11	12	7	18	6	7	10	12	11	16
54	14	0	0	2	1	2	3	2	6	9	16	12	15
57	17	1	1	5	5	5	12	3	3	6	5	7	12
60	20	0	0	0	0	1	0	6	5	5	5	6	6
63	23	1	0	2	5	1	4	0	2	3	4	7	4
66	26	0	0	0	0	2	0	1	4	1	2	3	4
69	29	0	0	1	0	0	2	0	0	2	7	1	2
72	32	0	0	0	0	0	1	2	8	7	3	3	2
75	35	0	0	0	0	0	0	3	0	13	3	3	2
78	38	0	0	0	0	0	0	0	1	3	2	0	1
81	41	0	0	0	0	0	0	1	2	1	4	5	2
84	44	0	0	0	1	1	1	1	0	0	3	3	1
87	47	0	0	0	0	0	0	0	1	1	2	0	0
90	50	0	0	1	0	1	0	1	1	1	3	2	2
93	53	0	0	0	0	0	0	1	0	1	4	0	0
96	56	0	0	0	0	0	0	0	0	2	1	1	0
99	59	1	0	2	2	1	0	1	3	1	0	2	1
102	62	0	0	0	1	0	0	0	0	1	0	1	0
105	65	1	0	0	1	0	0	0	1	0	1	0	0
108	68	0	0	1	1	0	0	1	0	0	0	0	0
111	71	0	0	1	1	0	0	0	0	0	0	0	0
114	74	1	0	0	0	0	1	0	1	0	0	0	0
Total		8	9	32	40	38	61	47	66	102	127	119	126

	-6.35 +5.6 mm	-5.6+4.0 mm	-4.0+2.8 mm	-2.8+2.0 mm	-2.0+1.4 mm	-1.4+1.0 mm
Total Particles to Overflow	8	9	32	40	38	61
Total Particles to Underflow	47	66	102	127	119	126
Total Particles Remaining in Bed	0	8	3	2	1	0
Total Feed	55	83	137	169	158	187

Appendix F: Continuous tracer particle Raw Data – Vertical

Experiment Date	28/10/2009
Feed Rate (g/min sand)	569
Underflow rate (g/min sand)	307
Vibration Rate	595V
Gas rate (%)	25
Experiment run time (min)	99

		1800 kg/m ³ density particles													
Time (min)	Mass of Sand to Overflow (g)	Mass of Sand to Underflow (g)	Number of particles to Overflow						Number of Particles to Underflow						
			-6.35 +5.6 mm	-5.6 mm	+4.0 mm	-4.0 mm	+2.8 mm	-2.8 mm	+2.0 mm	-2.0 mm	+1.4 mm	-1.4 mm	+1.0 mm		
3	792.3	920.3	0	0	0	0	0	0	0	0	0	0	0	0	0
6	633.1	958.4	0	0	0	0	0	0	45	61	74	116	74	63	
9	956.2	918.8	0	0	0	0	0	0	0	6	14	32	50	51	
12	737.0	919.9	0	0	0	0	0	0	1	1	6	12	13	14	
15	876.0	924.4	0	0	0	0	0	0	0	0	1	3	5	4	
18	762.5	916.8	0	0	1	1	5	5	0	0	0	1	1	0	
21	909.7	913.7	0	0	0	5	16	15	0	0	0	0	0	1	
24	476.0	910.0	0	0	0	3	6	8	0	0	0	0	0	0	
27	787.6	912.5	0	0	0	5	7	9	0	0	0	0	0	0	
30	607.8	913.3	0	0	0	0	1	0	1	1	9	14	19	27	
33	890.5	927.1	0	1	3	10	9	9	0	0	0	0	0	0	
36	794.0	918.2	1	1	2	6	10	5	0	0	0	0	0	0	
39	932.0	916.3	0	1	5	9	9	4	0	0	0	0	0	0	
42	691.5	918.3	2	1	4	6	3	2	0	0	0	0	0	0	
45	567.3	1067.2	0	1	0	5	3	2	0	0	0	0	0	0	
48	725.4	921.6	0	0	0	3	4	7	0	0	0	0	0	0	
51	808.6	926.5	0	1	0	0	0	0	0	0	0	0	0	0	
54	695.3	925.9	0	2	1	2	0	0	0	0	0	0	0	0	
57	729.3	927.9	0	0	0	1	1	1	0	0	0	0	0	0	
60	791.0	928.4	0	0	0	0	0	0	0	0	0	0	0	0	
63	702.5	929.4	0	0	0	1	0	1	0	0	0	0	0	0	
66	890.6	927.1	0	0	1	1	0	0	0	0	0	0	0	0	
69	885.2	926.9	1	0	4	6	0	0	0	0	0	0	0	0	
72	872.7	922.4	0	1	0	1	0	0	0	0	0	0	0	0	
75	1052.8	917.8	1	2	3	1	0	0	0	0	0	0	0	0	
78	776.1	1096.6	1	0	0	0	0	0	0	0	0	0	0	0	
81	927.8	637.7	0	1	0	0	0	0	0	0	0	0	0	0	
84	608.2	907.9	0	0	0	0	0	0	0	0	0	0	0	0	
87	621.3	906.1	0	0	0	0	0	0	0	0	0	0	0	0	
90	1055.3	903.8	0	0	0	0	0	0	0	0	0	0	0	0	
93	623.0	904.2	0	0	0	0	0	0	0	0	0	0	0	0	
96	630.3	903.1	0	0	0	0	0	0	0	0	0	0	0	0	
99	766.6	902.3	0	0	0	0	0	0	0	0	0	0	0	0	
Total	775.0	920.3	6	12	24	66	74	68	47	69	104	178	162	160	

	-6.35 +5.6 mm	-5.6 mm	+4.0 mm	-4.0 mm	+2.8 mm	-2.8 mm	+2.0 mm	-2.0 mm	+1.4 mm	-1.4 mm	+1.0 mm
Total Particles to Overflow	6	12	24	66	74	68					
Total Particles to Underflow	47	69	104	178	162	160					
Total Particles Remaining in Bed	3	2	1	0	0	0					
Total Feed	56	83	129	244	236	228					

Experiment Date	28/10/2009
Feed Rate (g/min sand)	569
Underflow rate (g/min sand)	307
Vibration Rate	595V
Gas rate (%)	25
Experiment run time (min)	99

		1600 kg/m ³ density particles													
Time (min)	Adjusted Time (min)	Number of particles to Overflow						Number of Particles to Underflow							
		-6.35 +5.6 mm	-5.6 +4.0 mm	-4.0 +2.8 mm	-2.8 +2.0 mm	-2.0 +1.4 mm	-1.4 +1.0 mm	-6.35 +5.6 mm	-5.6 +4.0 mm	-4.0 +2.8 mm	-2.8 +2.0 mm	-2.0 +1.4 mm	-1.4 +1.0 mm		
3		-	-	-	-	-	-	-	-	-	-	-	-	-	
6		-	-	-	-	-	-	-	-	-	-	-	-	-	
9		-	-	-	-	-	-	-	-	-	-	-	-	-	
12	2	0	0	0	0	0	0	0	0	0	0	0	0	0	
15	5	0	0	0	0	0	0	0	17	19	22	18	16	16	
18	8	0	0	0	0	0	0	0	7	26	38	44	53	53	
21	11	0	0	0	0	0	1	0	2	3	9	12	28	30	
24	14	0	0	0	1	0	1		0	0	0	1	2	9	
27	17	1	1	0	5	4	11		0	0	0	0	2	1	
30	20	0	0	1	3	6	3		0	0	0	0	0	0	
33	23	3	12	9	20	17	19		0	0	0	0	0	0	
36	26	5	9	16	19	21	24		0	0	0	0	0	0	
39	29	12	7	17	17	13	18		0	0	0	0	0	0	
42	32	4	8	12	7	8	5		0	0	0	0	0	0	
45	35	0	5	0	6	3	6		0	0	0	0	0	0	
48	38	2	1	1	7	2	3		0	0	0	0	0	0	
51	41	1	3	4	2	1	5		0	0	0	0	0	0	
54	44	0	0	2	1	1	1		0	0	0	0	0	0	
57	47	2	2	0	1	0	1		0	0	0	0	0	0	
60	50	1	1	0	2	2	0		0	0	0	0	0	0	
63	53	0	1	0	2	0	0		0	0	0	0	0	0	
66	56	0	1	1	4	0	0		0	0	0	0	0	0	
69	59	1	0	1	0	1	0		0	0	0	0	0	0	
72	62	0	0	0	0	0	0		0	0	0	0	0	0	
75	65	0	0	0	1	1	0		0	0	0	0	0	0	
78	68	0	0	0	0	0	0		0	0	0	0	0	0	
81	71	0	0	0	0	0	0		0	0	0	0	0	0	
84	74	0	0	0	0	0	0		0	0	0	0	0	0	
87	77	0	0	0	0	0	0		0	0	0	0	0	0	
90	80	0	0	0	0	0	0		0	0	0	0	0	0	
93	83	0	0	0	0	0	0		0	0	0	0	0	0	
96	86	0	0	0	0	0	0		0	0	0	0	0	0	
99	89	0	0	0	0	0	0		0	0	0	0	0	0	
Total		32	51	64	98	81	97		26	48	69	75	101	109	

	-6.35 +5.6 mm	-5.6 +4.0 mm	-4.0 +2.8 mm	-2.8 +2.0 mm	-2.0 +1.4 mm	-1.4 +1.0 mm
Total Particles to Overflow	32	51	64	98	81	97
Total Particles to Underflow	26	48	69	75	101	109
Total Particles Remaining in Bed	0	0	1	0	0	0
Total Feed	58	99	134	173	182	206

Experiment Date	28/10/2009
Feed Rate (g/min sand)	569
Underflow rate (g/min sand)	307
Vibration Rate	595V
Gas rate (%)	25
Experiment run time (min)	99

		2100 kg/m ³ density particles											
Time (min)	Adjusted Time (min)	Number of particles to Overflow						Number of Particles to Underflow					
		-6.35 +5.6 mm	-5.6 +4.0 mm	-4.0 +2.8 mm	-2.8 +2.0 mm	-2.0 +1.4 mm	-1.4 +1.0 mm	-6.35 +5.6 mm	-5.6 +4.0 mm	-4.0 +2.8 mm	-2.8 +2.0 mm	-2.0 +1.4 mm	-1.4 +1.0 mm
3		-	-	-	-	-	-	-	-	-	-	-	-
6		-	-	-	-	-	-	-	-	-	-	-	-
9		-	-	-	-	-	-	-	-	-	-	-	-
12		-	-	-	-	-	-	-	-	-	-	-	-
15		-	-	-	-	-	-	-	-	-	-	-	-
18		-	-	-	-	-	-	-	-	-	-	-	-
21	1	0	0	0	0	0	0	0	0	0	0	0	0
24	4	0	0	0	0	0	0	33	31	25	16	11	9
27	7	0	0	0	0	0	0	10	30	30	56	43	53
30	10	0	0	0	0	0	0	0	0	0	0	0	0
33	13	0	0	0	0	2	2	0	2	0	5	4	11
36	16	0	0	0	0	5	1	1	1	0	1	0	1
39	19	0	0	0	5	3	15	1	0	0	0	0	0
42	22	0	1	3	8	7	13	0	0	0	0	0	0
45	25	0	0	0	1	4	9	0	0	0	0	1	0
48	28	0	0	3	3	3	8	0	0	0	0	0	0
51	31	0	0	0	4	3	7	0	0	0	0	0	0
54	34	0	0	1	2	1	5	0	0	0	0	0	0
57	37	0	0	2	1	4	8	0	0	0	0	0	0
60	40	0	0	2	2	2	3	0	0	0	0	1	0
63	43	0	0	0	1	5	3	0	0	0	0	0	0
66	46	0	0	0	4	3	6	0	0	0	0	0	0
69	49	0	0	2	5	6	6	0	0	0	0	0	0
72	52	0	0	6	9	7	4	0	0	0	0	0	0
75	55	0	0	8	7	5	2	0	0	0	0	0	0
78	58	0	1	3	0	3	1	0	0	0	0	0	0
81	61	0	0	4	6	3	1	0	0	0	0	0	0
84	64	0	1	1	1	1	3	0	0	0	0	0	0
87	67	0	0	0	0	0	0	0	0	0	0	0	0
90	70	0	0	1	1	1	0	0	0	0	0	0	0
93	73	0	0	0	0	2	0	0	0	0	0	0	0
96	76	0	0	0	0	0	0	0	0	0	0	0	0
99	79	0	0	0	0	0	0	0	0	0	0	0	0
Total		0	3	36	60	70	97	45	64	55	78	60	74

	-6.35 +5.6 mm	-5.6 +4.0 mm	-4.0 +2.8 mm	-2.8 +2.0 mm	-2.0 +1.4 mm	-1.4 +1.0 mm
Total Particles to Overflow	0	3	36	60	70	97
Total Particles to Underflow	45	64	55	78	60	74
Total Particles Remaining in Bed	4	22	26	16	6	2
Total Feed	49	89	117	154	136	173

Experiment Date	28/10/2009
Feed Rate (g/min sand)	569
Underflow rate (g/min sand)	307
Vibration Rate	595V
Gas rate (%)	25
Experiment run time (min)	99

		1300 kg/m ³ density particles													
Time (min)	Adjusted Time (min)	Number of particles to Overflow						Number of Particles to Underflow							
		-6.35 +5.6 mm	-5.6 +4.0 mm	-4.0 +2.8 mm	-2.8 +2.0 mm	-2.0 +1.4 mm	-1.4 +1.0 mm	-6.35 +5.6 mm	-5.6 +4.0 mm	-4.0 +2.8 mm	-2.8 +2.0 mm	-2.0 +1.4 mm	-1.4 +1.0 mm		
3		-	-	-	-	-	-	-	-	-	-	-	-	-	
6		-	-	-	-	-	-	-	-	-	-	-	-	-	
9		-	-	-	-	-	-	-	-	-	-	-	-	-	
12		-	-	-	-	-	-	-	-	-	-	-	-	-	
15		-	-	-	-	-	-	-	-	-	-	-	-	-	
18		-	-	-	-	-	-	-	-	-	-	-	-	-	
21		-	-	-	-	-	-	-	-	-	-	-	-	-	
24		-	-	-	-	-	-	-	-	-	-	-	-	-	
27		-	-	-	-	-	-	-	-	-	-	-	-	-	
30		-	-	-	-	-	-	-	-	-	-	-	-	-	
33	3	0	0	0	0	0	0	0	0	0	0	0	0	0	
36	6	0	0	0	0	0	0	0	0	1	6	5	15		
39	9	8	15	10	7	4	0	0	0	1	5	8	22		
42	12	28	30	32	32	21	17	0	0	2	2	9	7		
45	15	16	23	34	33	30	19	0	0	1	4	8	6		
48	18	3	16	20	30	32	35	0	0	1	6	0	3		
51	21	0	5	15	17	24	31	0	0	1	1	1	3		
54	24	1	2	5	19	16	11	0	0	0	2	0	1		
57	27	0	0	2	7	7	4	0	0	0	0	2	2		
60	30	0	0	3	3	0	4	0	0	0	1	1	0		
63	33	0	0	0	1	3	3	0	0	0	1	0	0		
66	36	0	0	0	3	2	2	0	0	0	0	0	0		
69	39	0	0	0	0	2	2	0	0	0	0	0	0		
72	42	0	0	0	0	1	0	0	0	0	0	0	0		
75	45	0	0	0	0	0	0	0	0	0	0	0	0		
78	48	0	0	0	2	0	0	0	0	0	0	0	0		
81	51	0	1	1	0	0	0	0	0	0	0	0	0		
84	54	0	0	0	0	0	0	0	0	0	0	0	0		
87	57	0	0	0	0	0	0	0	0	0	0	0	0		
90	60	0	0	0	0	0	0	0	0	0	0	0	0		
93	63	0	0	0	0	0	0	0	0	0	0	0	0		
96	66	0	0	0	0	0	0	0	0	0	0	0	0		
99	69	0	0	0	0	0	0	0	0	0	0	0	0		
Total		56	92	122	154	142	128	0	0	7	28	34	59		

	-6.35 +5.6 mm	-5.6 +4.0 mm	-4.0 +2.8 mm	-2.8 +2.0 mm	-2.0 +1.4 mm	-1.4 +1.0 mm
Total Particles to Overflow	56	92	122	154	142	128
Total Particles to Underflow	0	0	7	28	34	59
Total Particles Remaining in Bed	0	0	0	0	0	0
Total Feed	56	92	129	182	176	187

Experiment Date	28/10/2009
Feed Rate (g/min sand)	569
Underflow rate (g/min sand)	307
Vibration Rate	595V
Gas rate (%)	25
Experiment run time (min)	99

		2400 kg/m ³ density particles											
Time (min)	Adjusted Time (min)	Number of particles to Overflow						Number of Particles to Underflow					
		-6.35 +5.6 mm	-5.6 +4.0 mm	-4.0 +2.8 mm	-2.8 +2.0 mm	-2.0 +1.4 mm	-1.4 +1.0 mm	-6.35 +5.6 mm	-5.6 +4.0 mm	-4.0 +2.8 mm	-2.8 +2.0 mm	-2.0 +1.4 mm	-1.4 +1.0 mm
3		-	-	-	-	-	-	-	-	-	-	-	-
6		-	-	-	-	-	-	-	-	-	-	-	-
9		-	-	-	-	-	-	-	-	-	-	-	-
12		-	-	-	-	-	-	-	-	-	-	-	-
15		-	-	-	-	-	-	-	-	-	-	-	-
18		-	-	-	-	-	-	-	-	-	-	-	-
21		-	-	-	-	-	-	-	-	-	-	-	-
24		-	-	-	-	-	-	-	-	-	-	-	-
27		-	-	-	-	-	-	-	-	-	-	-	-
30		-	-	-	-	-	-	-	-	-	-	-	-
33		-	-	-	-	-	-	-	-	-	-	-	-
36		-	-	-	-	-	-	-	-	-	-	-	-
39		-	-	-	-	-	-	-	-	-	-	-	-
42	2	0	0	0	0	0	0	0	0	0	0	0	0
45	5	0	0	0	0	0	0	48	81	106	71	65	52
48	8	0	0	0	0	0	0	1	3	14	35	38	41
51	11	0	0	0	0	0	0	0	1	0	4	4	14
54	14	0	0	0	0	0	1	1	0	1	0	2	2
57	17	0	0	0	0	1	2	0	2	1	0	0	1
60	20	0	0	0	0	0	2	1	0	0	1	0	1
63	23	0	0	0	0	2	4	0	0	1	0	0	0
66	26	0	0	0	0	2	5	0	0	0	1	0	1
69	29	0	0	0	1	5	9	0	0	0	0	0	0
72	32	0	0	0	3	9	18	0	0	0	0	0	0
75	35	0	0	1	5	7	9	0	0	0	0	0	0
78	38	0	0	0	4	5	6	0	0	0	0	0	0
81	41	0	0	1	0	2	2	0	0	0	0	0	0
84	44	0	0	0	1	1	5	0	0	0	0	0	0
87	47	0	0	0	1	0	2	0	0	0	0	0	0
90	50	0	0	0	0	2	0	0	0	0	0	0	0
93	53	0	0	0	0	1	2	0	0	0	0	0	0
96	56	0	0	0	0	1	0	0	0	0	0	0	0
99	59	0	0	0	0	1	2	0	0	0	0	0	0
Total		0	0	2	15	39	69	51	87	123	112	109	112

	-6.35 +5.6 mm	-5.6 +4.0 mm	-4.0 +2.8 mm	-2.8 +2.0 mm	-2.0 +1.4 mm	-1.4 +1.0 mm
Total Particles to Overflow	0	0	2	15	39	69
Total Particles to Underflow	51	87	123	112	109	112
Total Particles Remaining in Bed	0	2	13	45	23	13
Total Feed	51	89	138	172	171	194

Experiment Date	4/11/2009
Feed Rate (g/min sand)	574
Underflow rate (g/min sand)	465
Vibration Rate	595V
Gas rate (%)	25
Experiment run time (min)	105

1800 kg/m ³ density particles														
Time (min)	Mass of Sand to Overflow (g)	Mass of Sand to Underflow (g)	Number of particles to Overflow						Number of Particles to Underflow					
			-6.35 +5.6 mm	-5.6 mm	+4.0 mm	-4.0+2.8 mm	-2.8+2.0 mm	-2.0+1.4 mm	-1.4+1.0 mm	-6.35 +5.6 mm	-5.6+4.0 mm	-4.0+2.8 mm	-2.8+2.0 mm	-2.0+1.4 mm
3	147.6	1384.8	0	0	0	0	0	0	12	7	7	5	6	4
6	277.5	1412.3	0	0	0	0	0	0	27	70	78	147	152	128
9	602.5	1390.2	0	0	0	0	0	0	1	2	7	19	29	38
12	118.9	1395.7	0	0	0	0	0	0	0	0	1	4	4	6
15	156.6	1396.3	0	0	0	0	0	0	1	0	21	0	2	2
18	276.1	1411.7	0	0	0	0	0	0	0	0	0	0	0	0
21	208.7	1391.2	0	0	0	0	0	0	0	0	0	0	0	1
24	25.9	1457.0	0	0	0	0	0	0	0	0	0	0	1	0
27	420.5	1396.1	0	0	0	0	0	1	0	0	0	0	0	0
30	296.5	1391.0	0	0	0	0	0	0	1	2	5	9	11	10
33	49.4	1390.0	0	0	0	0	0	0	1	0	0	0	0	0
36	358.9	1384.8	0	0	0	0	0	0	0	0	4	1	1	2
39	281.8	1385.1	0	0	0	0	0	1	0	0	1	1	2	0
42	310.4	1382.2	0	0	0	0	1	0	0	0	0	0	0	0
45	353.8	1457.9	0	0	0	0	0	0	0	0	0	0	0	0
48	334.7	1388.4	0	0	0	0	0	0	0	0	0	0	0	0
51	355.5	1389.1	0	0	0	0	0	0	0	0	0	0	0	0
54	550.3	1388.3	0	0	0	0	0	0	0	0	0	0	0	0
57	228.5	1388.8	0	0	0	0	3	1	0	0	0	0	0	0
60	502.3	1389.1	0	0	0	0	2	3	0	0	0	0	0	0
63	522.8	1392.2	0	0	0	1	0	0	0	0	0	0	0	0
66	372.3	1393.2	0	0	0	3	0	2	0	0	0	0	0	0
69	317.8	1397.0	0	0	0	1	1	1	0	0	0	0	0	0
72	575.4	1397.4	0	0	0	4	1	3	0	0	0	0	0	0
75	454.0	1397.0	0	0	0	1	3	0	0	0	0	0	0	0
78	382.2	1391.9	0	0	0	1	1	2	0	0	0	0	0	0
81	190.1	1393.4	0	0	0	0	0	0	0	0	0	0	0	0
84	445.1	1387.6	0	0	0	0	0	0	0	0	0	0	0	0
87	396.1	1386.4	0	0	1	4	0	0	0	0	0	0	0	0
90	303.3	1380.7	0	0	0	2	1	0	0	0	0	0	0	0
93	507.9	1378.0	0	0	0	1	4	0	0	0	0	0	0	0
96	386.9	1378.8	0	0	1	0	1	0	0	0	0	0	0	0
99	366.6	1380.1	0	0	0	2	0	1	0	0	0	0	0	0
102	476.5	1378.3	0	0	1	5	2	0	0	0	0	0	0	0
105	423.3	1295.7	0	0	0	1	0	1	0	0	0	0	0	0
Total	342.2	1391.4	0	0	3	26	20	16	43	81	124	186	208	191

	-6.35 +5.6 mm	-5.6+4.0 mm	-4.0+2.8 mm	-2.8+2.0 mm	-2.0+1.4 mm	-1.4+1.0 mm
Total Particles to Overflow	0	0	3	26	20	16
Total Particles to Underflow	43	81	124	186	208	191
Total Particles Remaining in Bed	11	9	21	27	12	3
Total Feed	54	90	148	239	240	210

Experiment Date	4/11/2009
Feed Rate (g/min sand)	574
Underflow rate (g/min sand)	465
Vibration Rate	595V
Gas rate (%)	25
Experiment run time (min)	105

		1600 kg/m ³ density particles											
Time (min)	Adjusted Time (min)	Number of particles to Overflow						Number of Particles to Underflow					
		-6.35 +5.6 mm	-5.6+4.0 mm	-4.0+2.8 mm	-2.8+2.0 mm	-2.0+1.4 mm	-1.4+1.0 mm	-6.35 +5.6 mm	-5.6+4.0 mm	-4.0+2.8 mm	-2.8+2.0 mm	-2.0+1.4 mm	-1.4+1.0 mm
3		-	-	-	-	-	-	-	-	-	-	-	-
6		-	-	-	-	-	-	-	-	-	-	-	-
9		-	-	-	-	-	-	-	-	-	-	-	-
12	2	0	0	0	0	0	0	0	0	0	0	0	1
15	5	0	0	0	0	0	0	19	34	43	65	53	65
18	8	0	0	0	0	0	0	9	16	34	42	54	63
21	11	0	0	0	0	0	0	0	0	3	6	16	20
24	14	0	0	0	0	0	0	0	0	1	1	5	4
27	17	0	0	0	0	0	0	0	0	0	1	0	1
30	20	0	0	0	0	0	1	1	0	0	0	0	0
33	23	0	0	0	0	0	0	0	0	0	0	1	1
36	26	0	0	1	1	0	1	0	0	0	0	1	0
39	29	0	0	0	1	1	0	0	0	0	0	0	0
42	32	0	0	0	3	1	3	0	0	0	0	0	0
45	35	0	0	0	2	1	6	0	0	0	0	0	0
48	38	0	0	0	3	2	3	0	0	0	0	0	0
51	41	1	0	2	4	3	4	0	0	0	0	0	0
54	44	0	2	2	3	2	4	0	0	0	0	0	0
57	47	0	0	3	3	3	2	0	0	0	0	0	0
60	50	0	2	3	4	8	2	0	0	0	0	0	0
63	53	1	2	6	2	4	4	0	0	0	1	0	0
66	56	1	3	3	3	4	4	0	0	0	0	0	0
69	59	1	1	0	1	1	2	0	0	0	0	0	0
72	62	2	3	5	6	5	4	0	0	0	0	0	0
75	65	2	3	4	3	3	0	0	0	0	0	0	0
78	68	2	2	2	1	1	2	0	0	0	0	0	0
81	71	1	3	0	0	0	0	0	0	0	0	0	0
84	74	0	1	2	2	1	2	0	0	0	0	0	0
87	77	1	1	1	4	3	0	0	0	0	0	0	0
90	80	0	0	1	2	2	1	0	0	0	0	0	0
93	83	2	0	0	1	1	2	0	0	0	0	0	0
96	86	1	1	2	1	2	0	0	0	0	0	0	0
99	89	3	0	2	1	1	0	0	0	0	0	0	0
102	92	1	0	0	2	0	1	0	0	0	0	0	0
105	95	0	1	0	1	1	0	0	0	0	0	0	0
Total		19	25	39	54	50	48	29	50	81	116	130	155

	-6.35 +5.6 mm	-5.6+4.0 mm	-4.0+2.8 mm	-2.8+2.0 mm	-2.0+1.4 mm	-1.4+1.0 mm
Total Particles to Overflow	19	25	39	54	50	48
Total Particles to Underflow	29	50	81	116	130	155
Total Particles Remaining in Bed	12	17	20	15	2	4
Total Feed	60	92	140	185	182	207

Experiment Date	4/11/2009
Feed Rate (g/min sand)	574
Underflow rate (g/min sand)	465
Vibration Rate	595V
Gas rate (%)	25
Experiment run time (min)	105

		2100 kg/m ³ density particles													
Time (min)	Adjusted Time (min)	Number of particles to Overflow						Number of Particles to Underflow							
		-6.35 +5.6 mm	-5.6 mm	+4.0 mm	-4.0 mm	+2.8 mm	-2.8 mm	+2.0 mm	-2.0 mm	+1.4 mm	-1.4 mm	+1.0 mm			
3		-	-	-	-	-	-	-	-	-	-	-	-	-	
6		-	-	-	-	-	-	-	-	-	-	-	-	-	
9		-	-	-	-	-	-	-	-	-	-	-	-	-	
12		-	-	-	-	-	-	-	-	-	-	-	-	-	
15		-	-	-	-	-	-	-	-	-	-	-	-	-	
18		-	-	-	-	-	-	-	-	-	-	-	-	-	
21	1	0	0	0	0	0	0	0	0	0	0	0	0	0	
24	4	0	0	0	0	0	0	0	41	69	83	99	60	58	
27	7	0	0	0	0	0	0	0	3	15	20	41	64	91	
30	10	0	0	0	0	0	0	0	0	0	0	0	0	0	
33	13	0	0	0	0	0	0	0	0	2	2	1	6	3	
36	16	0	0	0	0	0	0	0	1	0	0	0	1	0	
39	19	0	0	0	0	0	0	0	0	0	0	0	0	0	
42	22	0	0	0	0	0	0	1	0	0	0	0	0	0	
45	25	0	0	0	0	0	0	1	0	1	1	0	0	1	
48	28	0	0	0	0	0	0	0	0	0	0	0	0	1	
51	31	0	0	0	0	0	0	0	0	0	0	0	0	0	
54	34	0	0	0	0	0	0	0	0	0	0	1	0	0	
57	37	0	0	0	0	0	0	0	0	0	0	0	0	0	
60	40	0	0	0	0	0	0	0	0	0	0	0	0	0	
63	43	0	0	0	0	0	1	0	0	0	0	0	0	0	
66	46	0	0	0	0	0	0	1	0	0	0	0	0	0	
69	49	0	0	0	0	0	0	0	0	0	0	0	0	0	
72	52	0	0	0	0	0	0	1	0	0	0	0	0	0	
75	55	0	0	0	0	0	2	1	0	0	0	0	0	0	
78	58	0	0	0	0	0	0	1	0	0	0	0	1	0	
81	61	0	0	0	0	0	0	0	0	0	0	0	0	0	
84	64	0	0	0	0	0	0	0	0	0	0	0	0	0	
87	67	0	0	0	0	0	0	0	0	0	0	0	0	0	
90	70	0	0	0	0	0	0	1	0	0	0	0	0	0	
93	73	0	0	0	0	0	0	0	0	0	0	0	0	0	
96	76	0	0	0	0	0	0	0	0	0	0	0	0	0	
99	79	0	0	0	0	0	0	1	0	0	0	0	0	0	
102	82	0	0	1	0	0	0	1	0	0	0	0	0	0	
105	85	0	0	0	0	0	0	0	0	0	0	0	0	0	
Total		0	0	1	0	3	9		45	87	106	142	132	154	

	-6.35 +5.6 mm	-5.6 mm	+4.0 mm	-4.0 mm	+2.8 mm	-2.8 mm	+2.0 mm	-2.0 mm	+1.4 mm	-1.4 mm	+1.0 mm
Total Particles to Overflow	0	0	1	0	3	9					
Total Particles to Underflow	45	87	106	142	132	154					
Total Particles Remaining in Bed	0	3	5	17	10	9					
Total Feed	45	90	112	159	145	172					

Experiment Date	4/11/2009
Feed Rate (g/min sand)	574
Underflow rate (g/min sand)	465
Vibration Rate	595V
Gas rate (%)	25
Experiment run time (min)	105

		1300 kg/m ³ density particles											
Time (min)	Adjusted Time (min)	Number of particles to Overflow						Number of Particles to Underflow					
		-6.35 +5.6 mm	-5.6 +4.0 mm	-4.0 +2.8 mm	-2.8 +2.0 mm	-2.0 +1.4 mm	-1.4 +1.0 mm	-6.35 +5.6 mm	-5.6 +4.0 mm	-4.0 +2.8 mm	-2.8 +2.0 mm	-2.0 +1.4 mm	-1.4 +1.0 mm
3		-	-	-	-	-	-	-	-	-	-	-	-
6		-	-	-	-	-	-	-	-	-	-	-	-
9		-	-	-	-	-	-	-	-	-	-	-	-
12		-	-	-	-	-	-	-	-	-	-	-	-
15		-	-	-	-	-	-	-	-	-	-	-	-
18		-	-	-	-	-	-	-	-	-	-	-	-
21		-	-	-	-	-	-	-	-	-	-	-	-
24		-	-	-	-	-	-	-	-	-	-	-	-
27		-	-	-	-	-	-	-	-	-	-	-	-
30		-	-	-	-	-	-	-	-	-	-	-	-
33	3	0	0	0	0	0	0	0	0	0	0	0	0
36	6	0	0	0	0	0	0	1	1	13	44	61	55
39	9	0	0	0	0	0	0	4	7	22	27	25	40
42	12	1	0	0	1	0	0	1	6	15	23	20	14
45	15	11	3	1	0	2	1	5	6	10	8	8	3
48	18	12	11	9	2	1	1	0	3	3	1	1	1
51	21	10	9	10	7	5	4	0	1	0	0	0	1
54	24	9	17	21	3	9	6	0	0	0	0	1	0
57	27	0	6	2	9	8	10	0	2	0	0	0	0
60	30	1	6	10	11	12	7	0	0	0	0	0	0
63	33	1	5	7	15	7	8	0	0	0	0	0	0
66	36	1	1	5	9	9	5	0	0	0	0	0	0
69	39	0	2	3	1	3	3	0	0	0	0	0	0
72	42	1	1	3	5	7	2	0	0	0	0	0	0
75	45	2	0	2	2	3	6	0	0	0	0	0	0
78	48	0	0	1	0	2	1	0	0	0	0	0	0
81	51	0	1	0	0	0	2	0	0	0	0	0	0
84	54	0	1	0	3	0	0	0	0	0	0	0	0
87	57	0	0	1	1	2	2	0	0	0	0	0	0
90	60	0	0	0	1	1	0	0	0	0	0	0	0
93	63	0	0	0	0	2	0	0	0	0	0	0	0
96	66	0	0	0	0	0	0	0	0	0	0	0	0
99	69	0	0	0	0	1	0	0	0	0	0	0	0
102	72	0	0	1	0	1	1	0	0	0	0	0	0
105	75	0	1	0	0	0	0	0	0	0	0	0	0
Total		49	64	76	70	75	59	11	26	63	103	116	114

	-6.35 +5.6 mm	-5.6 +4.0 mm	-4.0 +2.8 mm	-2.8 +2.0 mm	-2.0 +1.4 mm	-1.4 +1.0 mm
Total Particles to Overflow	49	64	76	70	75	59
Total Particles to Underflow	11	26	63	103	116	114
Total Particles Remaining in Bed	0	0	0	0	0	2
Total Feed	60	90	139	173	191	175

Experiment Date	4/11/2009
Feed Rate (g/min sand)	574
Underflow rate (g/min sand)	465
Vibration Rate	595V
Gas rate (%)	25
Experiment run time (min)	105

		2400 kg/m ³ density particles													
Time (min)	Adjusted Time (min)	Number of particles to Overflow						Number of Particles to Underflow							
		-6.35 +5.6 mm	-5.6 mm	+4.0 mm	-4.0+2.8 mm	-2.8+2.0 mm	-2.0+1.4 mm	-1.4+1.0 mm	-6.35 +5.6 mm	-5.6 mm	+4.0 mm	-4.0+2.8 mm	-2.8+2.0 mm	-2.0+1.4 mm	-1.4+1.0 mm
3		-	-	-	-	-	-	-	-	-	-	-	-	-	-
6		-	-	-	-	-	-	-	-	-	-	-	-	-	-
9		-	-	-	-	-	-	-	-	-	-	-	-	-	-
12		-	-	-	-	-	-	-	-	-	-	-	-	-	-
15		-	-	-	-	-	-	-	-	-	-	-	-	-	-
18		-	-	-	-	-	-	-	-	-	-	-	-	-	-
21		-	-	-	-	-	-	-	-	-	-	-	-	-	-
24		-	-	-	-	-	-	-	-	-	-	-	-	-	-
27		-	-	-	-	-	-	-	-	-	-	-	-	-	-
30		-	-	-	-	-	-	-	-	-	-	-	-	-	-
33		-	-	-	-	-	-	-	-	-	-	-	-	-	-
36		-	-	-	-	-	-	-	-	-	-	-	-	-	-
39		-	-	-	-	-	-	-	-	-	-	-	-	-	-
42	2	0	0	0	0	0	0	2	0	1	0	0	0	0	0
45	5	0	0	0	0	0	0	52	83	115	125	93	97		
48	8	0	0	0	0	0	0	0	1	5	15	26	50		
51	11	0	0	0	0	0	0	0	0	3	5	9	8		
54	14	0	0	0	0	0	0	0	1	0	0	1	2		
57	17	0	0	0	0	0	0	0	1	3	1	0	1		
60	20	0	0	0	0	0	0	0	0	2	0	0	0		
63	23	0	0	0	0	0	0	0	1	1	0	0	0		
66	26	0	0	0	0	0	0	0	0	1	0	0	0		
69	29	0	0	0	0	0	0	0	0	0	0	1	1		
72	32	0	0	0	0	0	2	0	0	0	0	0	0		
75	35	0	0	0	0	0	0	0	0	0	0	0	0		
78	38	0	0	0	0	0	1	0	0	0	0	0	0		
81	41	0	0	0	0	0	0	0	0	0	0	0	0		
84	44	0	0	0	0	0	0	0	0	0	0	0	0		
87	47	0	0	0	0	0	0	0	0	0	0	0	0		
90	50	0	0	0	0	1	1	0	0	0	0	0	0		
93	53	0	0	0	0	0	2	0	0	0	0	0	0		
96	56	0	0	0	0	1	0	0	0	0	0	0	0		
99	59	0	0	0	0	0	1	0	0	0	0	0	0		
102	62	0	0	0	0	0	0	0	0	0	0	0	0		
105	65	0	0	0	0	0	0	0	0	0	0	0	0		
Total		0	0	0	0	2	7	54	87	131	146	130	159		

	-6.35 +5.6 mm	-5.6 mm	+4.0 mm	-4.0+2.8 mm	-2.8+2.0 mm	-2.0+1.4 mm	-1.4+1.0 mm
Total Particles to Overflow	0	0	0	0	2	7	
Total Particles to Underflow	54	87	131	146	130	159	
Total Particles Remaining in Bed	0	0	3	23	37	26	
Total Feed	54	87	134	169	169	192	

Experiment Date	6/11/2009
Feed Rate (g/min sand)	554
Underflow rate (g/min sand)	363
Vibration Rate	58
Gas rate (%)	595V
Experiment run time (min)	114

1800 kg/m ³ density particles															
Time (min)	Mass of Sand to Overflow (g)	Mass of Sand to Underflow (g)	Number of particles to Overflow						Number of Particles to Underflow						
			-6.35 +5.6 mm	-5.6 mm	+4.0 mm	-4.0 mm	+2.8 mm	-2.8 mm	+2.0 mm	-2.0 mm	+1.4 mm	-1.4 mm	+1.0 mm		
3	559.2	1084.2	0	0	0	0	0	0	2	2	0	1	0	0	
6	774.3	1085.5	0	0	0	0	0	0	26	50	56	84	79	76	
9	546.5	1078.1	0	0	0	0	0	0	2	9	22	43	49	35	
12	484.2	1079.7	0	0	0	0	0	0	0	0	3	6	12	13	
15	626.7	1086.2	0	0	0	0	2	1	0	0	0	3	8	8	
18	533.7	1085.4	0	0	0	0	2	2	0	0	0	2	5	0	
21	555.0	1084.5	0	0	1	3	3	4	0	0	0	0	0	1	
24	411.4	1147.5	0	0	0	3	1	0	0	0	0	0	1	0	
27	778.6	1079.5	0	1	0	5	7	4	0	0	0	0	0	0	
30	551.7	1079.5	0	0	0	0	0	0	0	3	7	17	22	32	
33	654.5	1081.3	0	0	1	6	4	7	0	0	0	0	0	0	
36	406.7	1080.8	0	1	0	3	3	4	0	0	0	0	0	0	
39	455.2	1085.2	0	0	0	3	2	7	0	0	0	0	0	0	
42	318.9	1085.0	0	0	2	5	3	1	0	0	0	0	0	0	
45	372.8	1169.7	0	0	0	0	3	2	0	0	0	0	0	0	
48	382.8	1087.6	0	0	0	1	2	2	0	0	0	0	0	0	
51	779.6	1085.1	0	0	0	3	1	6	0	0	0	0	0	0	
54	585.4	1088.8	0	0	1	4	5	2	0	0	0	0	0	0	
57	487.1	1090.5	0	2	0	3	3	3	0	0	0	0	0	0	
60	703.5	1095.5	0	0	1	7	5	10	0	0	0	0	0	0	
63	671.4	1096.7	2	2	6	8	3	2	0	0	0	0	0	0	
66	648.4	1096.1	1	3	5	4	2	3	0	0	0	0	0	0	
69	544.0	1087.5	0	1	2	4	1	1	0	0	0	0	0	0	
72	677.1	1082.6	0	1	0	4	2	0	0	0	0	0	0	0	
75	643.6	1082.1	0	0	1	2	2	0	0	0	0	0	0	0	
78	494.5	1080.5	0	0	1	1	5	0	0	0	0	0	0	0	
81	591.0	1078.9	0	0	1	0	0	0	0	0	0	0	0	0	
84	698.2	1081.8	0	0	1	1	0	0	0	0	0	0	0	0	
87	588.6	1078.1	0	0	0	2	1	0	0	0	0	0	0	0	
90	690.4	1082.5	0	0	1	0	0	0	0	0	0	0	0	0	
93	603.8	1083.1	0	1	1	0	1	0	0	0	0	0	0	0	
96	731.7	1085.9	0	0	2	0	1	1	0	0	0	0	0	0	
99	431.0	1085.2	0	0	0	1	0	0	0	0	0	0	0	0	
102	531.0	1086.0	0	0	0	0	2	0	0	0	0	0	0	0	
105	559.1	1085.6	0	0	0	0	1	0	0	0	0	0	0	0	
108	659.5	1087.8	0	1	0	2	2	0	0	0	0	0	0	0	
111	522.5	1086.7	0	0	0	0	0	0	0	0	0	0	0	0	
114	255.0	1089.6	0	0	0	0	0	0	0	0	0	0	0	0	
Total	566.0	1088.9	3	13	27	75	69	62	30	64	88	156	176	165	

	-6.35 +5.6 mm	-5.6 mm	+4.0 mm	-4.0 mm	+2.8 mm	-2.8 mm	+2.0 mm	-2.0 mm	+1.4 mm	-1.4 mm	+1.0 mm
Total Particles to Overflow	3	13	27	75	69	62					
Total Particles to Underflow	30	64	88	156	176	165					
Total Particles Remaining in Bed	18	15	11	10	0	0					
Total Feed	51	92	126	241	245	227					

Experiment Date	6/11/2009
Feed Rate (g/min sand)	554
Underflow rate (g/min sand)	363
Vibration Rate	58
Gas rate (%)	595V
Experiment run time (min)	114

		1600 kg/m ³ density particles													
Time (min)	Adjusted Time (min)	Number of particles to Overflow						Number of Particles to Underflow							
		-6.35 +5.6 mm	-5.6 mm	+4.0 mm	-4.0+2.8 mm	-2.8+2.0 mm	-2.0+1.4 mm	-1.4+1.0 mm	-6.35 +5.6 mm	-5.6 mm	+4.0 mm	-4.0+2.8 mm	-2.8+2.0 mm	-2.0+1.4 mm	-1.4+1.0 mm
3		-	-	-	-	-	-	-	-	-	-	-	-	-	-
6		-	-	-	-	-	-	-	-	-	-	-	-	-	-
9		-	-	-	-	-	-	-	-	-	-	-	-	-	-
12	2	0	0	0	0	0	0	0	0	0	0	0	0	0	0
15	5	0	0	0	0	0	0	0	11	10	17	27	37	32	32
18	8	0	0	0	0	0	0	0	24	44	47	59	53	72	72
21	11	0	0	0	0	0	0	0	1	6	11	24	29	31	31
24	14	0	0	0	0	1	1	0	0	5	9	16	17	9	9
27	17	0	0	1	2	2	4	0	0	0	1	2	0	3	3
30	20	0	1	1	7	7	7	0	0	0	0	0	0	0	0
33	23	4	2	5	7	5	9	0	0	0	0	0	0	0	0
36	26	1	2	3	2	0	3	0	0	0	0	0	0	0	0
39	29	1	2	3	8	4	6	0	0	0	0	0	0	0	0
42	32	1	2	1	4	3	3	0	0	0	0	0	0	0	0
45	35	0	0	0	2	4	3	0	0	0	0	0	0	0	0
48	38	0	0	0	1	5	4	0	0	0	0	0	0	0	0
51	41	1	2	5	5	8	5	0	0	0	0	1	0	0	0
54	44	2	2	5	5	1	3	0	0	0	0	0	0	0	0
57	47	0	3	4	5	4	4	0	0	0	0	0	0	0	0
60	50	1	5	4	3	4	4	0	0	0	0	0	0	0	0
63	53	1	3	2	1	4	1	0	0	0	0	0	0	0	0
66	56	1	2	2	2	3	1	0	0	0	0	0	0	0	0
69	59	4	1	2	3	0	0	0	0	0	0	0	0	0	0
72	62	0	2	1	1	1	1	0	0	0	0	0	0	0	0
75	65	0	1	2	1	1	1	0	0	0	0	0	0	0	0
78	68	0	0	0	0	1	0	0	0	0	0	0	0	0	0
81	71	0	0	1	2	0	0	0	0	0	0	0	0	0	0
84	74	3	0	0	0	0	0	0	0	0	0	0	0	0	0
87	77	1	0	1	0	0	0	0	0	0	0	0	0	0	0
90	80	0	0	0	0	0	0	0	0	0	0	0	0	0	0
93	83	1	0	0	0	0	0	0	0	0	0	0	0	0	0
96	86	1	0	0	1	0	0	0	0	0	0	0	0	0	0
99	89	0	0	1	0	0	0	0	0	0	0	0	0	0	0
102	92	0	0	1	0	0	0	0	0	0	0	0	0	0	0
105	95	0	0	0	0	0	0	0	0	0	0	0	0	0	0
108	98	0	0	0	0	0	0	0	0	0	0	0	0	0	0
111	101	0	0	0	0	0	0	0	0	0	0	0	0	0	0
114	104	0	0	0	0	0	0	0	0	0	0	0	0	0	0
Total		23	30	45	62	58	60	36	65	85	129	136	147		

	-6.35 +5.6 mm	-5.6 mm	+4.0 mm	-4.0+2.8 mm	-2.8+2.0 mm	-2.0+1.4 mm	-1.4+1.0 mm
Total Particles to Overflow	23	30	45	62	58	60	
Total Particles to Underflow	36	65	85	129	136	147	
Total Particles Remaining in Bed	0	0	1	1	0	0	
Total Feed	59	95	131	192	194	207	

Experiment Date	6/11/2009
Feed Rate (g/min sand)	554
Underflow rate (g/min sand)	363
Vibration Rate	58
Gas rate (%)	595V
Experiment run time (min)	114

2100 kg/m³ density particles

Time (min)	Adjusted Time (min)	Number of particles to Overflow						Number of Particles to Underflow					
		-6.35 +5.6 mm	-5.6 +4.0 mm	-4.0 +2.8 mm	-2.8 +2.0 mm	-2.0 +1.4 mm	-1.4 +1.0 mm	-6.35 +5.6 mm	-5.6 +4.0 mm	-4.0 +2.8 mm	-2.8 +2.0 mm	-2.0 +1.4 mm	-1.4 +1.0 mm
3		-	-	-	-	-	-	-	-	-	-	-	-
6		-	-	-	-	-	-	-	-	-	-	-	-
9		-	-	-	-	-	-	-	-	-	-	-	-
12		-	-	-	-	-	-	-	-	-	-	-	-
15		-	-	-	-	-	-	-	-	-	-	-	-
18		-	-	-	-	-	-	-	-	-	-	-	-
21	1	0	0	0	0	0	0	0	0	0	0	0	0
24	4	0	0	0	0	0	0	43	65	47	32	17	10
27	7	0	0	0	0	0	0	5	17	50	85	65	75
30	10	0	0	0	0	0	0	0	0	0	0	0	0
33	13	0	0	0	0	0	0	1	3	3	3	7	10
36	16	0	0	0	0	0	0	0	0	0	1	4	0
39	19	0	0	0	0	0	0	0	1	0	0	0	2
42	22	0	0	0	0	0	1	0	0	1	0	0	0
45	25	0	0	0	0	0	1	0	0	0	0	0	0
48	28	0	0	0	0	1	0	0	0	0	0	0	1
51	31	0	0	0	0	0	10	0	0	0	0	0	0
54	34	0	0	0	1	0	5	0	0	0	0	0	0
57	37	0	0	0	0	0	3	0	0	0	0	0	0
60	40	0	0	2	4	2	9	0	0	0	0	0	0
63	43	0	0	1	0	0	5	0	0	0	0	0	0
66	46	0	0	0	1	2	5	0	0	0	0	0	0
69	49	0	0	0	0	6	3	0	0	0	0	0	0
72	52	0	1	0	2	1	0	0	0	0	0	0	0
75	55	0	0	0	1	4	2	0	0	0	0	0	0
78	58	0	0	0	1	3	1	0	0	0	0	0	0
81	61	0	0	0	1	3	2	0	0	0	0	0	0
84	64	0	0	0	2	1	1	0	0	0	0	0	0
87	67	0	0	0	0	1	0	0	0	0	0	0	0
90	70	0	0	0	2	2	0	0	0	0	0	0	0
93	73	0	0	0	1	2	1	0	0	0	0	0	0
96	76	0	0	1	0	1	0	0	0	0	0	0	0
99	79	0	0	0	1	1	1	0	0	0	0	0	0
102	82	0	0	0	3	0	1	0	0	0	0	0	0
105	85	0	0	0	0	1	0	0	0	0	0	0	0
108	88	0	0	0	0	1	0	0	0	0	0	0	0
111	91	0	0	0	1	0	0	0	0	0	0	0	0
114	94	0	0	0	0	0	0	0	0	0	0	0	0
Total		0	1	4	21	32	51	49	86	101	121	93	98

	-6.35 +5.6 mm	-5.6 +4.0 mm	-4.0 +2.8 mm	-2.8 +2.0 mm	-2.0 +1.4 mm	-1.4 +1.0 mm
Total Particles to Overflow	0	1	4	21	32	51
Total Particles to Underflow	49	86	101	121	93	98
Total Particles Remaining in Bed	0	3	9	18	5	1
Total Feed	49	90	114	160	130	150

Experiment Date	6/11/2009
Feed Rate (g/min sand)	554
Underflow rate (g/min sand)	363
Vibration Rate	58
Gas rate (%)	595V
Experiment run time (min)	114

		1300 kg/m ³ density particles													
Time (min)	Adjusted Time (min)	Number of particles to Overflow						Number of Particles to Underflow							
		-6.35 +5.6 mm	-5.6 mm	+4.0 mm	-4.0+2.8 mm	-2.8+2.0 mm	-2.0+1.4 mm	-1.4+1.0 mm	-6.35 +5.6 mm	-5.6 mm	+4.0 mm	-4.0+2.8 mm	-2.8+2.0 mm	-2.0+1.4 mm	-1.4+1.0 mm
3		-	-	-	-	-	-	-	-	-	-	-	-	-	-
6		-	-	-	-	-	-	-	-	-	-	-	-	-	-
9		-	-	-	-	-	-	-	-	-	-	-	-	-	-
12		-	-	-	-	-	-	-	-	-	-	-	-	-	-
15		-	-	-	-	-	-	-	-	-	-	-	-	-	-
18		-	-	-	-	-	-	-	-	-	-	-	-	-	-
21		-	-	-	-	-	-	-	-	-	-	-	-	-	-
24		-	-	-	-	-	-	-	-	-	-	-	-	-	-
27		-	-	-	-	-	-	-	-	-	-	-	-	-	-
30		-	-	-	-	-	-	-	-	-	-	-	-	-	-
33	3	0	0	0	0	0	0	0	0	0	0	0	0	0	1
36	6	0	0	0	0	0	0	0	0	0	2	3	20	16	
39	9	0	0	0	0	0	0	0	0	0	3	18	19	37	
42	12	0	0	0	0	0	0	0	0	0	1	7	20	13	
45	15	9	7	3	6	1	1	0	3	7	13	24	16		
48	18	11	10	6	6	1	3	0	0	3	3	1	5		
51	21	23	27	34	22	10	12	0	0	1	3	0	2		
54	24	9	17	27	26	24	16	0	0	0	0	1	0		
57	27	5	17	16	18	20	12	0	0	0	1	0	1		
60	30	1	7	17	18	14	16	0	0	0	0	0	0		
63	33	0	1	6	15	11	8	0	0	0	0	0	1		
66	36	1	1	2	7	9	13	0	0	0	0	0	0		
69	39	0	0	4	3	3	1	0	0	0	0	2	0		
72	42	0	0	3	1	2	4	0	0	0	0	0	0		
75	45	0	0	1	2	1	2	0	0	0	0	0	0		
78	48	0	0	1	0	0	0	0	0	0	0	0	0		
81	51	0	0	0	2	0	0	0	0	0	0	0	0		
84	54	0	0	0	1	0	0	0	0	0	0	0	0		
87	57	0	0	0	0	1	0	0	0	0	0	0	0		
90	60	0	0	1	0	0	0	0	0	0	0	0	0		
93	63	0	0	0	0	0	0	0	0	0	0	0	0		
96	66	0	0	0	0	0	0	0	0	0	0	0	0		
99	69	0	0	0	0	0	0	0	0	0	0	0	0		
102	72	0	0	0	0	0	0	0	0	0	0	0	0		
105	75	0	0	0	0	0	0	0	0	0	0	0	0		
108	78	0	0	0	0	0	0	0	0	0	0	0	0		
111	81	0	0	0	0	0	0	0	0	0	0	0	0		
114	84	0	0	0	0	0	0	0	0	0	0	0	0		
Total		59	87	121	127	97	88	0	3	17	48	87	92		

	-6.35 +5.6 mm	-5.6 mm	+4.0 mm	-4.0+2.8 mm	-2.8+2.0 mm	-2.0+1.4 mm	-1.4+1.0 mm
Total Particles to Overflow	59	87	121	127	97	88	
Total Particles to Underflow	0	3	17	48	87	92	
Total Particles Remaining in Bed	0	0	0	0	1	0	
Total Feed	59	90	138	175	185	180	

Experiment Date	6/11/2009
Feed Rate (g/min sand)	554
Underflow rate (g/min sand)	363
Vibration Rate	58
Gas rate (%)	595V
Experiment run time (min)	114

		2400 kg/m ³ density particles												
Time (min)	Adjusted Time (min)	Number of particles to Overflow						Number of Particles to Underflow						
		-6.35 +5.6 mm	-5.6 mm	+4.0 mm	-4.0 mm	+2.8 mm	-2.8 mm	+2.0 mm	-2.0 mm	+1.4 mm	-1.4 mm	+1.0 mm		
3		-	-	-	-	-	-	-	-	-	-	-	-	
6		-	-	-	-	-	-	-	-	-	-	-	-	
9		-	-	-	-	-	-	-	-	-	-	-	-	
12		-	-	-	-	-	-	-	-	-	-	-	-	
15		-	-	-	-	-	-	-	-	-	-	-	-	
18		-	-	-	-	-	-	-	-	-	-	-	-	
21		-	-	-	-	-	-	-	-	-	-	-	-	
24		-	-	-	-	-	-	-	-	-	-	-	-	
27		-	-	-	-	-	-	-	-	-	-	-	-	
30		-	-	-	-	-	-	-	-	-	-	-	-	
33		-	-	-	-	-	-	-	-	-	-	-	-	
36		-	-	-	-	-	-	-	-	-	-	-	-	
39		-	-	-	-	-	-	-	-	-	-	-	-	
42	2	0	0	0	0	0	0	0	0	0	0	0	0	
45	5	0	0	0	0	0	0	0	55	82	110	94	74	
48	8	0	0	0	0	0	0	0	0	2	19	39	50	
51	11	0	0	0	0	0	0	0	0	1	3	8	13	
54	14	0	0	0	0	0	0	0	0	0	0	0	3	
57	17	0	0	0	0	0	0	0	0	0	1	0	0	
60	20	0	0	0	0	0	0	4	0	0	0	0	1	
63	23	0	0	0	0	0	1	1	0	0	0	0	0	
66	26	0	0	0	0	0	1	2	0	0	0	0	0	
69	29	0	0	0	0	0	1	3	0	0	0	0	0	
72	32	0	0	0	0	2	3	3	0	0	0	0	0	
75	35	0	0	0	0	0	1	4	0	0	0	0	0	
78	38	0	0	0	0	0	1	3	0	0	0	0	0	
81	41	0	0	0	0	0	1	2	0	0	0	0	0	
84	44	0	0	0	0	0	1	1	0	0	0	0	0	
87	47	0	0	0	0	0	0	5	0	0	0	0	0	
90	50	0	0	0	0	0	1	0	0	0	0	0	0	
93	53	0	0	0	0	0	0	1	0	0	0	0	0	
96	56	0	0	0	0	0	3	0	0	0	0	0	0	
99	59	0	0	0	0	0	1	0	0	0	0	0	0	
102	62	0	0	0	0	0	1	2	0	0	0	0	0	
105	65	0	0	0	0	0	0	0	0	0	0	0	0	
108	68	0	0	0	0	0	0	1	0	0	0	0	0	
111	71	0	0	0	0	0	1	0	0	0	0	0	0	
114	74	0	0	0	0	0	0	0	0	0	0	0	0	
Total		0	0	0	2	17	32		55	85	133	141	141	152

	-6.35 +5.6 mm	-5.6 mm	+4.0 mm	-4.0 mm	+2.8 mm	-2.8 mm	+2.0 mm	-2.0 mm	+1.4 mm	-1.4 mm	+1.0 mm
Total Particles to Overflow	0	0	0	2	17	32					
Total Particles to Underflow	55	85	133	141	141	152					
Total Particles Remaining in Bed	0	0	7	25	21	11					
Total Feed	55	85	140	168	179	195					

Experiment Date	11/11/2009
Feed Rate (g/min sand)	537
Underflow rate (g/min sand)	261
Vibration Rate	595V
Gas rate (%)	25
Experiment run time (min)	90

1800 kg/m ³ density particles														
Time (min)	Mass of Sand to Overflow (g)	Mass of Sand to Underflow (g)	Number of particles to Overflow						Number of Particles to Underflow					
			-6.35 +5.6 mm	-5.6 +4.0 mm	-4.0 +2.8 mm	-2.8 +2.0 mm	-2.0 +1.4 mm	-1.4 +1.0 mm	-6.35 +5.6 mm	-5.6 +4.0 mm	-4.0 +2.8 mm	-2.8 +2.0 mm	-2.0 +1.4 mm	-1.4 +1.0 mm
3	866.8	726.5	0	0	0	0	0	0	0	0	1	0	0	0
6	830.5	825.2	0	0	0	0	0	0	4	3	4	11	17	15
9	962.8	833.6	0	0	3	6	4	6	10	7	9	13	16	26
12	560.8	733.2	0	0	2	9	18	12	3	6	4	7	8	6
15	1014.7	825.6	0	6	9	34	46	34	0	3	0	1	1	2
18	1014.8	735.1	8	18	30	69	53	43	0	1	0	2	0	0
21	825.5	826.3	2	6	16	20	25	17	0	0	0	0	2	0
24	799.8	742.9	3	4	15	20	16	9	0	0	0	0	0	2
27	855.4	817.0	2	3	7	17	17	10	0	0	0	0	0	0
30	691.4	825.2	0	0	1	1	3	2	1	14	18	15	7	15
33	832.1	734.7	1	3	5	4	1	0	0	0	0	0	0	0
36	655.5	825.1	0	0	1	0	2	2	0	0	0	0	0	0
39	849.2	734.6	0	1	2	2	3	0	0	0	0	0	0	0
42	725.0	821.9	0	1	3	3	0	1	0	0	0	0	0	0
45	1097.4	727.2	2	1	2	1	1	0	0	0	0	0	0	0
48	494.9	820.0	1	1	0	0	0	0	0	0	0	0	0	0
51	870.8	819.4	1	1	2	1	1	0	0	0	0	0	0	0
54	711.5	734.1	0	1	1	1	0	0	0	0	0	0	0	0
57	737.7	821.2	1	3	0	0	0	0	0	0	0	0	0	0
60	1021.6	732.0	3	5	3	0	0	0	0	0	0	0	0	0
63	770.6	823.6	0	3	0	0	1	0	0	0	0	0	0	0
66	951.6	733.2	1	1	0	0	0	0	0	0	0	0	0	0
69	787.9	823.5	2	1	0	0	0	0	0	0	0	0	0	0
72	498.0	734.4	2	1	0	0	0	0	0	0	0	0	0	0
75	1093.2	821.6	1	2	0	0	0	0	0	0	0	0	0	0
78	882.6	819.9	0	0	0	0	0	0	0	0	0	0	0	0
81	849.4	730.6	0	0	0	0	0	0	0	0	0	0	0	0
84	818.2	823.8	1	0	0	0	0	0	0	0	0	0	0	0
87	896.3	729.3	4	0	0	0	0	0	0	0	0	0	0	0
90	877.0	819.9	1	0	0	0	0	0	0	0	0	0	0	0
Total	828.1	784.0	36	62	102	188	191	136	18	34	36	49	51	66

	-6.35 +5.6 mm	-5.6 +4.0 mm	-4.0 +2.8 mm	-2.8 +2.0 mm	-2.0 +1.4 mm	-1.4 +1.0 mm
Total Particles to Overflow	36	62	102	188	191	136
Total Particles to Underflow	18	34	36	49	51	66
Total Particles Remaining in Bed	5	2	0	0	0	0
Total Feed	59	98	138	237	242	202

Experiment Date	11/11/2009
Feed Rate (g/min sand)	537
Underflow rate (g/min sand)	261
Vibration Rate	595V
Gas rate (%)	25
Experiment run time (min)	90

		1600 kg/m ³ density particles											
Time (min)	Adjusted Time (min)	Number of particles to Overflow						Number of Particles to Underflow					
		-6.35 +5.6 mm	-5.6 +4.0 mm	-4.0 +2.8 mm	-2.8 +2.0 mm	-2.0 +1.4 mm	-1.4 +1.0 mm	-6.35 +5.6 mm	-5.6 +4.0 mm	-4.0 +2.8 mm	-2.8 +2.0 mm	-2.0 +1.4 mm	-1.4 +1.0 mm
3		-	-	-	-	-	-	-	-	-	-	-	-
6		-	-	-	-	-	-	-	-	-	-	-	-
9		-	-	-	-	-	-	-	-	-	-	-	-
12	2	0	0	0	0	0	0	0	0	0	0	0	0
15	5	0	0	0	0	0	0	0	0	1	2	6	
18	8	2	4	2	9	11	1	0	0	0	1	7	11
21	11	12	14	26	36	29	23	0	0	1	4	3	8
24	14	7	23	34	40	27	32	0	0	0	0	1	5
27	17	9	15	17	33	35	40	0	0	0	0	0	1
30	20	0	3	2	9	4	5	0	0	0	0	1	0
33	23	4	6	14	12	13	17	0	0	0	0	0	0
36	26	1	4	3	7	6	5	0	0	0	0	0	0
39	29	5	4	7	5	10	7	0	0	0	0	0	0
42	32	1	4	5	2	2	5	0	0	1	0	1	1
45	35	5	3	3	5	10	5	0	0	0	0	0	0
48	38	3	0	0	2	2	0	0	0	0	0	0	0
51	41	1	1	1	3	0	3	0	0	0	0	0	1
54	44	0	0	2	0	0	1	0	0	0	0	0	0
57	47	0	1	0	0	2	0	0	0	0	0	1	1
60	50	2	0	0	0	1	2	0	0	1	0	0	0
63	53	0	1	1	1	1	1	1	0	0	0	0	1
66	56	0	1	0	1	4	1	0	0	0	0	0	0
69	59	0	0	1	1	0	2	0	0	0	0	0	1
72	62	0	0	2	0	0	2	0	0	0	0	0	0
75	65	0	1	1	0	1	3	0	0	0	0	0	0
78	68	0	0	0	0	0	0	0	0	0	0	0	0
81	71	0	0	0	0	0	0	0	0	0	0	0	0
84	74	0	0	0	0	0	0	0	0	0	0	0	0
87	77	0	0	0	0	0	0	0	0	0	0	0	0
90	80	1	0	0	0	0	0	0	0	0	0	0	0
Total		53	85	121	166	158	155	1	0	3	6	16	36

	-6.35 +5.6 mm	-5.6 +4.0 mm	-4.0 +2.8 mm	-2.8 +2.0 mm	-2.0 +1.4 mm	-1.4 +1.0 mm
Total Particles to Overflow	53	85	121	166	158	155
Total Particles to Underflow	1	0	3	6	16	36
Total Particles Remaining in Bed	0	0	0	0	0	0
Total Feed	54	85	124	172	174	191

Experiment Date	11/11/2009
Feed Rate (g/min sand)	537
Underflow rate (g/min sand)	261
Vibration Rate	595V
Gas rate (%)	25
Experiment run time (min)	90

		2100 kg/m ³ density particles													
Time (min)	Adjusted Time (min)	Number of particles to Overflow						Number of Particles to Underflow							
		-6.35 +5.6 mm	-5.6 mm	+4.0 mm	-4.0+2.8 mm	-2.8+2.0 mm	-2.0+1.4 mm	-1.4+1.0 mm	-6.35 +5.6 mm	-5.6 mm	+4.0 mm	-4.0+2.8 mm	-2.8+2.0 mm	-2.0+1.4 mm	-1.4+1.0 mm
3		-	-	-	-	-	-	-	-	-	-	-	-	-	-
6		-	-	-	-	-	-	-	-	-	-	-	-	-	-
9		-	-	-	-	-	-	-	-	-	-	-	-	-	-
12		-	-	-	-	-	-	-	-	-	-	-	-	-	-
15		-	-	-	-	-	-	-	-	-	-	-	-	-	-
18		-	-	-	-	-	-	-	-	-	-	-	-	-	-
21	1	0	0	0	0	0	0	0	0	0	0	0	0	0	1
24	4	0	0	0	0	0	0	8	6	2	1	2	2	5	
27	7	0	0	0	0	1	2	27	23	23	16	16	22		
30	10	0	0	0	0	0	0	0	0	0	0	0	0	0	
33	13	0	0	4	9	9	11	0	1	4	5	4	4		
36	16	0	1	0	5	11	13	0	1	2	6	3	4		
39	19	0	0	0	14	14	21	0	0	3	3	3	2		
42	22	0	0	1	4	17	11	0	0	0	0	0	1		
45	25	0	1	1	13	21	28	0	0	0	0	0	0		
48	28	0	0	2	5	17	6	0	0	0	0	0	2		
51	31	0	0	3	7	6	8	0	0	0	0	0	0		
54	34	0	0	3	10	3	4	0	0	0	0	0	0		
57	37	0	0	5	3	4	4	0	0	0	0	0	0		
60	40	0	4	10	14	6	7	0	0	0	0	0	0		
63	43	0	0	10	8	6	5	0	0	0	0	0	0		
66	46	0	5	5	7	2	0	0	0	0	0	0	0		
69	49	0	0	4	4	0	2	0	0	0	0	0	0		
72	52	0	0	2	3	0	0	0	0	0	0	0	0		
75	55	1	1	3	4	0	2	0	0	0	0	0	0		
78	58	0	0	2	1	1	1	0	0	0	0	0	0		
81	61	0	1	3	2	0	0	0	0	0	0	0	0		
84	64	0	0	1	0	1	0	0	0	0	0	0	0		
87	67	0	2	1	2	0	0	0	0	0	0	0	0		
90	70	0	1	0	1	0	0	0	0	0	0	0	0		
Total		1	16	60	116	119	125	35	31	34	31	28	41		

	-6.35 +5.6 mm	-5.6 mm	+4.0 mm	-4.0+2.8 mm	-2.8+2.0 mm	-2.0+1.4 mm	-1.4+1.0 mm
Total Particles to Overflow	1	16	60	116	119	125	
Total Particles to Underflow	35	31	34	31	28	41	
Total Particles Remaining in Bed	12	29	13	6	1	1	
Total Feed	48	76	107	153	148	167	

Experiment Date	11/11/2009
Feed Rate (g/min sand)	537
Underflow rate (g/min sand)	261
Vibration Rate	595V
Gas rate (%)	25
Experiment run time (min)	90

		1300 kg/m ³ density particles											
Time (min)	Adjusted Time (min)	Number of particles to Overflow						Number of Particles to Underflow					
		-6.35 +5.6 mm	-5.6 +4.0 mm	-4.0 +2.8 mm	-2.8 +2.0 mm	-2.0 +1.4 mm	-1.4 +1.0 mm	-6.35 +5.6 mm	-5.6 +4.0 mm	-4.0 +2.8 mm	-2.8 +2.0 mm	-2.0 +1.4 mm	-1.4 +1.0 mm
3		-	-	-	-	-	-	-	-	-	-	-	-
6		-	-	-	-	-	-	-	-	-	-	-	-
9		-	-	-	-	-	-	-	-	-	-	-	-
12		-	-	-	-	-	-	-	-	-	-	-	-
15		-	-	-	-	-	-	-	-	-	-	-	-
18		-	-	-	-	-	-	-	-	-	-	-	-
21		-	-	-	-	-	-	-	-	-	-	-	-
24		-	-	-	-	-	-	-	-	-	-	-	-
27		-	-	-	-	-	-	-	-	-	-	-	-
30		-	-	-	-	-	-	-	-	-	-	-	-
33	3	0	0	0	0	0	0	0	0	0	0	0	0
36	6	1	1	0	0	0	0	0	0	0	1	5	4
39	9	23	22	20	21	9	5	0	0	1	0	6	10
42	12	23	35	50	45	31	21	0	0	0	7	9	6
45	15	9	28	47	70	55	50	0	0	0	1	3	10
48	18	0	1	6	14	20	14	0	0	0	0	1	4
51	21	0	0	7	16	16	31	0	0	0	0	3	1
54	24	0	0	3	3	7	10	0	0	0	1	1	0
57	27	0	0	1	3	6	6	0	0	0	1	0	0
60	30	0	1	1	1	2	4	0	0	0	0	0	2
63	33	0	0	0	0	3	0	0	0	0	0	0	0
66	36	0	0	1	0	1	2	0	0	0	1	0	0
69	39	0	0	0	0	1	1	0	0	0	0	1	0
72	42	0	0	0	0	0	0	0	0	0	0	0	0
75	45	0	0	0	0	0	1	0	0	0	0	0	0
78	48	0	0	0	0	0	0	0	0	0	0	0	0
81	51	0	0	0	0	0	0	0	0	0	0	0	0
84	54	0	0	0	0	0	0	0	0	0	0	0	0
87	57	0	0	0	0	1	0	0	0	0	0	0	0
90	60	0	0	0	0	0	0	0	0	0	0	0	0
Total		56	88	136	173	152	145	0	0	1	12	29	37

	-6.35 +5.6 mm	-5.6 +4.0 mm	-4.0 +2.8 mm	-2.8 +2.0 mm	-2.0 +1.4 mm	-1.4 +1.0 mm
Total Particles to Overflow	56	88	136	173	152	145
Total Particles to Underflow	0	0	1	12	29	37
Total Particles Remaining in Bed	0	0	0	0	0	0
Total Feed	56	88	137	185	181	182

Experiment Date	11/11/2009
Feed Rate (g/min sand)	537
Underflow rate (g/min sand)	261
Vibration Rate	595V
Gas rate (%)	25
Experiment run time (min)	90

		2400 kg/m ³ density particles																	
Time (min)	Adjusted Time (min)	Number of particles to Overflow						Number of Particles to Underflow											
		-6.35 +5.6 mm	-5.6 mm	+4.0 -4.0	+2.8 mm	-2.8 mm	+2.0 -2.0	+1.4 mm	-1.4 mm	+1.0 mm	-6.35 +5.6 mm	-5.6 mm	+4.0 -4.0	+2.8 mm	-2.8 mm	+2.0 -2.0	+1.4 mm	-1.4 mm	+1.0 mm
3		-	-	-	-	-	-	-	-	-	-	-	-	-	-	-	-	-	-
6		-	-	-	-	-	-	-	-	-	-	-	-	-	-	-	-	-	-
9		-	-	-	-	-	-	-	-	-	-	-	-	-	-	-	-	-	-
12		-	-	-	-	-	-	-	-	-	-	-	-	-	-	-	-	-	-
15		-	-	-	-	-	-	-	-	-	-	-	-	-	-	-	-	-	-
18		-	-	-	-	-	-	-	-	-	-	-	-	-	-	-	-	-	-
21		-	-	-	-	-	-	-	-	-	-	-	-	-	-	-	-	-	-
24		-	-	-	-	-	-	-	-	-	-	-	-	-	-	-	-	-	-
27		-	-	-	-	-	-	-	-	-	-	-	-	-	-	-	-	-	-
30		-	-	-	-	-	-	-	-	-	-	-	-	-	-	-	-	-	-
33		-	-	-	-	-	-	-	-	-	-	-	-	-	-	-	-	-	-
36		-	-	-	-	-	-	-	-	-	-	-	-	-	-	-	-	-	-
39		-	-	-	-	-	-	-	-	-	-	-	-	-	-	-	-	-	-
42	2	0	0	0	0	0	0	0	0	0	0	0	0	0	0	0	0	0	0
45	5	0	0	0	0	0	0	0	48	63	53	31	15	8					
48	8	0	0	0	0	0	0	0	3	8	49	68	64	56					
51	11	0	0	0	0	0	0	0	1	6	3	9	13	31					
54	14	0	0	0	0	4	4	4	0	2	0	1	3	8					
57	17	0	0	0	0	2	8	8	1	0	0	0	1	1					
60	20	0	0	1	3	14	16	16	0	2	0	0	0	0					
63	23	0	0	0	7	9	12	12	0	0	0	0	0	2					
66	26	0	0	1	4	13	15	15	0	0	0	0	0	0					
69	29	0	0	2	5	10	9	9	0	0	0	0	0	0					
72	32	0	0	0	6	5	7	7	0	0	0	0	0	0					
75	35	0	1	1	17	6	8	8	0	0	0	0	0	0					
78	38	0	0	2	1	5	6	6	0	0	0	0	0	0					
81	41	0	0	1	3	4	2	2	0	0	0	0	0	0					
84	44	0	0	1	1	0	0	0	0	0	0	0	0	0					
87	47	0	0	0	2	2	1	1	0	0	0	0	0	0					
90	50	0	0	1	2	0	0	0	0	0	0	0	0	0					
Total		0	1	10	51	74	88	88	53	81	105	109	96	106					

	-6.35 +5.6 mm	-5.6 mm	+4.0 -4.0	+2.8 mm	-2.8 mm	+2.0 -2.0	+1.4 mm	-1.4 mm	+1.0 mm
Total Particles to Overflow	0	1	10	51	74	88			
Total Particles to Underflow	53	81	105	109	96	106			
Total Particles Remaining in Bed	0	6	19	16	7	1			
Total Feed	53	88	134	176	177	195			

Experiment Date	13/11/2009
Feed Rate (g/min sand)	583
Underflow rate (g/min sand)	368
Vibration Rate	595V
Gas rate (%)	35
Experiment run time (min)	90

1800 kg/m ³ density particles															
Time (min)	Mass of Sand to Overflow (g)	Mass of Sand to Underflow (g)	Number of particles to Overflow						Number of Particles to Underflow						
			-6.35 +5.6 mm	-5.6 mm	+4.0 mm	-4.0 mm	+2.8 mm	-2.8 mm	+2.0 mm	-2.0 mm	+1.4 mm	-1.4 mm	+1.0 mm		
3	918.5	1105.6	2	9	13	13	14	9	0	1	3	6	21	7	
6	77.6	1109.2	1	1	2	4	2	4	0	1	3	8	22	21	
9	1028.8	1110.9	14	33	39	68	43	39	0	0	0	3	7	16	
12	651.6	1112.2	6	12	16	32	25	17	0	0	1	2	13	6	
15	350.0	1111.6	3	5	1	10	9	9	0	0	0	0	2	7	
18	595.9	1107.8	4	4	7	15	8	10	0	0	0	3	4	4	
21	535.1	1106.0	1	2	7	10	6	4	0	0	0	1	5	3	
24	527.3	1103.5	6	4	7	10	7	4	0	0	0	2	5	6	
27	652.6	1102.0	4	6	8	9	8	5	0	0	0	0	2	1	
30	760.7	1102.5	2	7	13	17	22	14	0	0	1	1	3	11	
33	614.8	1103.1	1	2	4	5	3	6	0	0	0	0	2	3	
36	675.3	1100.5	2	1	1	7	3	6	0	0	0	0	0	1	
39	851.6	1102.1	1	5	1	3	4	2	0	0	0	0	2	0	
42	666.8	1100.3	1	2	2	1	3	0	0	0	0	0	0	1	
45	541.5	1129.1	1	0	0	2	1	0	0	0	0	0	0	1	
48	888.1	1103.2	1	0	1	0	1	0	0	0	0	0	0	0	
51	354.1	1104.0	0	0	0	0	0	0	0	0	0	0	0	0	
54	570.7	1105.7	1	0	0	0	0	0	0	0	0	0	0	0	
57	544.6	1102.8	0	0	0	0	0	0	0	0	0	0	0	0	
60	986.5	1103.4	0	0	1	2	0	3	0	0	0	0	0	0	
63	528.3	1103.9	0	0	0	1	1	0	0	0	0	0	0	0	
66	465.9	1104.0	0	0	0	0	0	0	0	0	0	0	0	0	
69	771.8	1102.8	0	0	1	0	0	0	0	0	0	0	0	0	
72	580.7	1101.6	0	0	0	1	1	0	0	0	0	0	0	0	
75	916.6	1100.1	0	2	1	0	0	0	0	0	0	0	0	0	
78	515.1	1099.8	0	0	0	0	0	0	0	0	0	0	0	0	
81	500.5	1097.1	0	0	0	0	0	0	0	0	0	0	0	0	
84	868.6	1100.3	1	0	0	0	0	0	0	0	0	0	0	0	
87	630.8	1099.1	0	0	0	0	0	0	0	0	0	0	0	0	
90	790.7	1098.2	0	0	0	0	0	0	0	0	0	0	0	0	
Total	645.4	1104.4	52	95	125	210	161	132	0	2	8	26	88	88	

	-6.35 +5.6 mm	-5.6 mm	+4.0 mm	-4.0 mm	+2.8 mm	-2.8 mm	+2.0 mm	-2.0 mm	+1.4 mm	-1.4 mm	+1.0 mm
Total Particles to Overflow	52	95	125	210	161	132					
Total Particles to Underflow	0	2	8	26	88	88					
Total Particles Remaining in Bed	0	0	0	0	0	0					
Total Feed	52	97	133	236	249	220					

Experiment Date	13/11/2009
Feed Rate (g/min sand)	583
Underflow rate (g/min sand)	368
Vibration Rate	595V
Gas rate (%)	35
Experiment run time (min)	90

		1600 kg/m ³ density particles											
Time (min)	Adjusted Time (min)	Number of particles to Overflow						Number of Particles to Underflow					
		-6.35 +5.6 mm	-5.6 mm	+4.0 mm	-4.0 mm	+2.8 mm	-2.8 mm	+2.0 mm	-2.0 mm	+1.4 mm	-1.4 mm	+1.0 mm	
3		-	-	-	-	-	-	-	-	-	-	-	-
6		-	-	-	-	-	-	-	-	-	-	-	-
9		-	-	-	-	-	-	-	-	-	-	-	-
12	2	5	4	9	11	9	5	0	0	0	0	0	0
15	5	9	16	20	17	12	9	0	0	2	7	17	27
18	8	19	27	26	32	27	24	0	0	2	0	8	9
21	11	10	8	16	31	21	12	0	0	0	4	9	18
24	14	6	10	14	21	13	13	0	0	0	1	2	12
27	17	5	6	17	25	17	10	0	0	0	0	2	10
30	20	2	5	5	9	7	2	0	0	0	0	0	1
33	23	1	5	9	6	9	11	0	0	0	0	2	2
36	26	0	2	6	14	7	9	0	0	0	1	0	2
39	29	0	1	3	4	4	11	0	0	0	0	0	0
42	32	0	3	0	1	4	3	0	0	0	1	1	2
45	35	0	1	1	2	2	0	0	0	0	0	0	1
48	38	0	0	0	2	1	2	0	0	0	0	0	0
51	41	0	0	2	1	0	1	0	0	0	0	0	0
54	44	0	0	0	1	3	1	0	0	0	0	0	0
57	47	0	0	0	0	0	0	0	0	0	0	0	0
60	50	0	0	0	0	0	0	0	0	0	0	0	0
63	53	0	0	0	0	0	0	0	0	0	0	0	0
66	56	0	0	0	0	0	0	0	0	0	0	0	0
69	59	0	0	0	0	0	0	0	0	0	0	0	0
72	62	0	0	0	0	0	0	0	0	0	0	0	0
75	65	0	0	0	0	0	1	0	0	0	0	0	0
78	68	0	0	0	0	0	0	0	0	0	0	0	0
81	71	0	0	0	0	0	0	0	0	0	0	0	0
84	74	0	0	0	0	0	0	0	0	0	0	0	0
87	77	0	0	0	0	0	0	0	0	0	0	0	0
90	80	0	0	0	0	0	0	0	0	0	0	0	0
Total		57	88	128	177	136	114	0	0	4	14	41	84

	-6.35 +5.6 mm	-5.6 mm	+4.0 mm	-4.0 mm	+2.8 mm	-2.8 mm	+2.0 mm	-2.0 mm	+1.4 mm	-1.4 mm	+1.0 mm
Total Particles to Overflow	57	88	128	177	136	114					
Total Particles to Underflow	0	0	4	14	41	84					
Total Particles Remaining in Bed	0	0	0	0	0	0					
Total Feed	57	88	132	191	177	198					

Experiment Date	13/11/2009
Feed Rate (g/min sand)	583
Underflow rate (g/min sand)	368
Vibration Rate	595V
Gas rate (%)	35
Experiment run time (min)	90

		2100 kg/m ³ density particles											
Time (min)	Adjusted Time (min)	Number of particles to Overflow						Number of Particles to Underflow					
		-6.35 +5.6 mm	-5.6 +4.0 mm	-4.0 +2.8 mm	-2.8 +2.0 mm	-2.0 +1.4 mm	-1.4 +1.0 mm	-6.35 +5.6 mm	-5.6 +4.0 mm	-4.0 +2.8 mm	-2.8 +2.0 mm	-2.0 +1.4 mm	-1.4 +1.0 mm
3		-	-	-	-	-	-	-	-	-	-	-	-
6		-	-	-	-	-	-	-	-	-	-	-	-
9		-	-	-	-	-	-	-	-	-	-	-	-
12		-	-	-	-	-	-	-	-	-	-	-	-
15		-	-	-	-	-	-	-	-	-	-	-	-
18		-	-	-	-	-	-	-	-	-	-	-	-
21	1	0	0	0	0	0	0	0	0	0	0	0	0
24	4	1	0	7	13	9	12	0	6	6	23	14	31
27	7	9	16	18	26	24	18	0	0	3	7	12	17
30	10	0	0	0	0	0	0	0	0	0	0	0	0
33	13	3	7	14	11	10	11	0	1	0	1	5	5
36	16	5	7	10	14	14	5	0	0	0	0	0	6
39	19	9	16	15	14	9	14	0	0	0	0	0	4
42	22	4	3	11	10	10	4	0	0	0	1	1	1
45	25	1	3	2	4	0	6	0	0	0	1	3	3
48	28	2	5	8	4	4	6	0	1	0	0	0	2
51	31	0	2	2	1	0	1	0	0	0	0	1	1
54	34	1	4	2	5	0	2	0	0	0	0	0	2
57	37	0	2	2	4	2	2	0	0	0	0	0	2
60	40	2	4	2	1	3	3	0	0	0	0	0	1
63	43	0	4	0	4	0	2	0	0	0	1	0	0
66	46	0	0	0	0	1	0	0	0	0	0	0	0
69	49	0	2	2	0	0	0	0	0	0	0	0	0
72	52	1	0	1	0	1	0	0	0	0	1	0	0
75	55	1	1	0	1	0	0	0	0	0	0	0	0
78	58	1	2	0	2	1	0	0	0	0	0	0	0
81	61	0	0	0	0	1	1	0	0	0	0	0	0
84	64	1	0	1	0	0	0	0	0	0	0	0	0
87	67	0	0	0	0	0	0	0	0	0	0	0	0
90	70	0	0	0	0	0	0	0	0	0	0	0	0
Total		41	78	97	114	89	87	0	8	9	35	36	75

	-6.35 +5.6 mm	-5.6 +4.0 mm	-4.0 +2.8 mm	-2.8 +2.0 mm	-2.0 +1.4 mm	-1.4 +1.0 mm
Total Particles to Overflow	41	78	97	114	89	87
Total Particles to Underflow	0	8	9	35	36	75
Total Particles Remaining in Bed	4	2	3	0	1	0
Total Feed	45	88	109	149	126	162

Experiment Date	13/11/2009
Feed Rate (g/min sand)	583
Underflow rate (g/min sand)	368
Vibration Rate	595V
Gas rate (%)	35
Experiment run time (min)	90

		1300 kg/m ³ density particles											
Time (min)	Adjusted Time (min)	Number of particles to Overflow						Number of Particles to Underflow					
		-6.35 +5.6 mm	-5.6 +4.0 mm	-4.0 +2.8 mm	-2.8 +2.0 mm	-2.0 +1.4 mm	-1.4 +1.0 mm	-6.35 +5.6 mm	-5.6 +4.0 mm	-4.0 +2.8 mm	-2.8 +2.0 mm	-2.0 +1.4 mm	-1.4 +1.0 mm
3		-	-	-	-	-	-	-	-	-	-	-	-
6		-	-	-	-	-	-	-	-	-	-	-	-
9		-	-	-	-	-	-	-	-	-	-	-	-
12		-	-	-	-	-	-	-	-	-	-	-	-
15		-	-	-	-	-	-	-	-	-	-	-	-
18		-	-	-	-	-	-	-	-	-	-	-	-
21		-	-	-	-	-	-	-	-	-	-	-	-
24		-	-	-	-	-	-	-	-	-	-	-	-
27		-	-	-	-	-	-	-	-	-	-	-	-
30		-	-	-	-	-	-	-	-	-	-	-	-
33	3	15	23	21	11	10	12	0	0	1	2	4	4
36	6	24	32	48	49	39	19	0	0	0	7	17	21
39	9	14	22	31	51	25	36	0	0	0	2	8	6
42	12	3	10	21	20	19	22	0	0	0	0	3	5
45	15	0	1	5	13	12	16	0	0	0	0	2	5
48	18	0	1	5	12	17	17	0	0	0	0	1	0
51	21	0	0	0	0	3	3	0	0	0	0	4	0
54	24	0	0	1	4	1	2	0	0	0	0	1	2
57	27	0	0	0	0	1	3	0	0	0	0	1	3
60	30	0	1	1	2	4	2	0	0	0	0	0	0
63	33	0	0	0	1	2	0	0	0	0	0	0	0
66	36	0	0	0	2	0	0	0	0	0	0	1	0
69	39	0	0	0	0	0	0	0	0	0	0	0	1
72	42	0	0	0	0	2	0	0	0	0	0	0	0
75	45	0	0	0	0	2	1	0	0	0	0	0	0
78	48	0	0	0	0	0	0	0	0	0	0	0	0
81	51	0	0	1	0	0	0	0	0	0	0	0	0
84	54	0	0	0	0	0	0	0	0	0	0	0	0
87	57	0	0	0	0	2	0	0	0	0	0	0	0
90	60	0	0	0	0	0	0	0	0	0	0	0	0
Total		56	90	134	165	139	133	0	0	1	11	42	47

	-6.35 +5.6 mm	-5.6 +4.0 mm	-4.0 +2.8 mm	-2.8 +2.0 mm	-2.0 +1.4 mm	-1.4 +1.0 mm
Total Particles to Overflow	56	90	134	165	139	133
Total Particles to Underflow	0	0	1	11	42	47
Total Particles Remaining in Bed	0	0	0	0	1	2
Total Feed	56	90	135	176	182	182

Experiment Date	13/11/2009
Feed Rate (g/min sand)	583
Underflow rate (g/min sand)	368
Vibration Rate	595V
Gas rate (%)	35
Experiment run time (min)	90

		2400 kg/m ³ density particles											
Time (min)	Adjusted Time (min)	Number of particles to Overflow						Number of Particles to Underflow					
		-6.35 +5.6 mm	-5.6 +4.0 mm	-4.0 +2.8 mm	-2.8 +2.0 mm	-2.0 +1.4 mm	-1.4 +1.0 mm	-6.35 +5.6 mm	-5.6 +4.0 mm	-4.0 +2.8 mm	-2.8 +2.0 mm	-2.0 +1.4 mm	-1.4 +1.0 mm
3		-	-	-	-	-	-	-	-	-	-	-	-
6		-	-	-	-	-	-	-	-	-	-	-	-
9		-	-	-	-	-	-	-	-	-	-	-	-
12		-	-	-	-	-	-	-	-	-	-	-	-
15		-	-	-	-	-	-	-	-	-	-	-	-
18		-	-	-	-	-	-	-	-	-	-	-	-
21		-	-	-	-	-	-	-	-	-	-	-	-
24		-	-	-	-	-	-	-	-	-	-	-	-
27		-	-	-	-	-	-	-	-	-	-	-	-
30		-	-	-	-	-	-	-	-	-	-	-	-
33		-	-	-	-	-	-	-	-	-	-	-	-
36		-	-	-	-	-	-	-	-	-	-	-	-
39		-	-	-	-	-	-	-	-	-	-	-	-
42	2	0	1	1	0	1	0	1	0	0	0	1	0
45	5	1	2	6	18	16	9	15	14	13	20	20	30
48	8	1	6	16	27	27	26	5	2	5	8	11	15
51	11	1	2	5	7	9	4	0	1	3	3	7	12
54	14	0	4	7	13	12	14	1	0	0	2	2	4
57	17	0	5	6	8	15	10	1	1	2	2	5	5
60	20	3	4	16	14	9	14	1	0	1	0	4	0
63	23	1	3	3	7	2	7	0	0	2	0	0	5
66	26	0	2	3	3	2	3	0	0	0	3	1	2
69	29	1	3	5	6	5	4	0	0	2	2	1	1
72	32	0	1	4	1	4	5	0	0	1	0	2	3
75	35	1	3	3	4	4	5	0	0	0	2	1	0
78	38	0	2	4	3	2	1	0	0	0	0	0	0
81	41	0	2	1	1	1	1	1	0	0	1	0	1
84	44	0	3	1	1	0	1	0	0	0	0	0	1
87	47	0	0	2	2	3	1	0	0	1	0	1	1
90	50	1	2	3	2	2	1	0	0	1	0	1	1
Total		10	45	86	117	114	106	25	18	31	43	57	81

	-6.35 +5.6 mm	-5.6 +4.0 mm	-4.0 +2.8 mm	-2.8 +2.0 mm	-2.0 +1.4 mm	-1.4 +1.0 mm
Total Particles to Overflow	10	45	86	117	114	106
Total Particles to Underflow	25	18	31	43	57	81
Total Particles Remaining in Bed	26	18	24	5	3	4
Total Feed	61	81	141	165	174	191

Experiment Date	18/11/2009
Feed Rate (g/min sand)	542
Underflow rate (g/min sand)	368
Vibration Rate	595V
Gas rate (%)	30
Experiment run time (min)	117

1800 kg/m ³ density particles																					
Time (min)	Mass of Sand to Overflow (g)	Mass of Sand to Underflow (g)	Number of particles to Overflow						Number of Particles to Underflow												
			-6.35 +5.6 mm	-5.6 mm	+4.0 mm	-4.0 mm	+2.8 mm	-2.8 mm	+2.0 mm	-2.0 mm	+1.4 mm	-1.4 mm	+1.0 mm	-6.35 +5.6 mm	-5.6 mm	+4.0 mm	-4.0 mm	+2.8 mm	-2.8 mm	+2.0 mm	-2.0 mm
3	638.0	1108.6	3	2	8	17	13	7	0	0	2	4	11	9							
6	372.6	1106.4	4	6	7	13	18	13	0	0	8	13	23	17							
9	435.7	1110.0	5	14	18	19	16	15	0	0	2	2	7	9							
12	568.2	1107.5	8	8	15	28	26	21	0	0	0	3	3	11							
15	533.6	1109.1	4	4	6	24	21	13	0	0	0	1	3	5							
18	616.4	1107.0	3	5	13	23	19	5	0	0	0	1	0	2							
21	711.5	1106.0	5	12	14	22	14	10	0	0	0	0	3	2							
24	514.8	1104.0	1	7	5	6	5	3	0	0	0	0	1	3							
27	331.1	1112.0	4	4	5	6	6	2	0	0	0	1	1	1							
30	607.4	1110.0	2	9	18	15	17	17	2	1	0	4	1	14							
33	768.8	1113.3	4	6	6	5	4	8	0	0	0	0	2	0							
36	624.8	1108.7	4	5	2	9	9	6	0	0	0	0	0	1							
39	371.1	1106.0	1	3	0	5	0	2	0	0	0	0	0	0							
42	347.7	1104.0	1	1	2	2	4	0	0	0	0	0	0	0							
45	490.6	1103.0	0	1	0	3	2	0	0	0	0	0	0	2							
48	749.0	1098.3	0	2	1	7	7	0	0	0	0	0	0	1							
51	493.9	1100.5	0	0	1	0	3	2	0	0	0	0	0	0							
54	356.1	1100.6	0	2	1	4	1	4	0	0	0	0	0	0							
57	853.3	1101.6	0	0	0	1	2	0	0	0	0	0	0	0							
60	83.5	1098.6	0	0	0	0	0	0	0	0	0	0	0	0							
63	379.5	1101.4	1	0	2	0	0	1	0	0	0	0	0	0							
66	707.3	1103.2	0	1	1	0	1	1	0	0	0	0	0	0							
69	409.3	1195.9	1	3	0	0	0	0	0	0	0	0	0	0							
72	321.6	1101.0	0	0	0	0	0	0	0	0	0	0	0	0							
75	415.7	1102.5	0	0	1	0	0	0	0	0	0	0	0	0							
78	564.6	1104.0	0	1	0	0	0	0	0	0	0	0	0	0							
81	638.3	1102.9	1	0	0	1	0	0	0	0	0	0	0	0							
84	600.2	1104.7	1	0	0	0	0	1	0	0	0	0	0	0							
87	444.0	1103.5	0	0	0	0	0	0	0	0	0	0	0	0							
90	641.6	1107.1	0	0	0	0	0	0	0	0	0	0	0	0							
93	269.9	1104.8	0	0	0	0	0	1	0	0	0	0	0	0							
96	747.7	1103.7	1	0	0	0	0	0	0	0	0	0	0	0							
99	363.0	1103.5	0	0	0	0	0	0	0	0	0	0	0	0							
102	450.2	1105.5	0	0	0	0	0	0	0	0	0	0	0	0							
105	659.1	1101.9	0	0	0	0	0	0	0	0	0	0	0	0							
108	602.3	1100.9	0	1	0	0	0	0	0	0	0	0	0	0							
111	597.4	1100.4	0	0	0	0	0	0	0	0	0	0	0	0							
114	370.3	1097.2	0	0	0	0	0	0	0	0	0	0	0	0							
117	581.4	1097.1	0	1	0	0	0	0	0	0	0	0	0	0							
Total	518.8	1104.3	54	98	126	210	188	132	2	1	12	29	55	77							

	-6.35 +5.6 mm	-5.6 mm	+4.0 mm	-4.0 mm	+2.8 mm	-2.8 mm	+2.0 mm	-2.0 mm	+1.4 mm	-1.4 mm	+1.0 mm
Total Particles to Overflow	54	98	126	210	188	132					
Total Particles to Underflow	2	1	12	29	55	77					
Total Particles Remaining in Bed	2	1	0	0	0	0					
Total Feed	58	100	138	239	243	209					

Experiment Date	18/11/2009
Feed Rate (g/min sand)	542
Underflow rate (g/min sand)	368
Vibration Rate	595V
Gas rate (%)	30
Experiment run time (min)	117

		1600 kg/m ³ density particles											
Time (min)	Adjusted Time (min)	Number of particles to Overflow						Number of Particles to Underflow					
		-6.35 +5.6 mm	-5.6 +4.0 mm	-4.0 +2.8 mm	-2.8 +2.0 mm	-2.0 +1.4 mm	-1.4 +1.0 mm	-6.35 +5.6 mm	-5.6 +4.0 mm	-4.0 +2.8 mm	-2.8 +2.0 mm	-2.0 +1.4 mm	-1.4 +1.0 mm
3		-	-	-	-	-	-	-	-	-	-	-	-
6		-	-	-	-	-	-	-	-	-	-	-	-
9		-	-	-	-	-	-	-	-	-	-	-	-
12	2	1	0	1	3	0	1	0	0	0	0	0	0
15	5	5	5	10	19	14	9	0	0	2	7	17	22
18	8	5	13	30	25	35	26	0	0	0	1	7	17
21	11	14	25	36	38	26	25	0	0	0	3	6	5
24	14	8	12	17	14	16	16	0	0	0	0	1	3
27	17	6	5	7	6	5	12	0	0	0	0	2	5
30	20	4	5	6	7	6	2	0	0	0	0	0	0
33	23	0	8	7	14	10	0	0	0	0	1	0	1
36	26	5	7	2	9	9	7	0	0	0	0	0	1
39	29	2	2	2	1	2	5	0	0	0	0	0	2
42	32	2	2	2	3	2	3	0	0	0	1	1	0
45	35	0	2	4	1	4	6	0	0	0	0	0	1
48	38	0	1	1	5	7	4	0	0	0	0	0	0
51	41	3	0	3	3	1	3	0	0	0	0	0	0
54	44	0	0	0	2	1	2	0	0	0	0	0	0
57	47	0	1	1	2	2	2	0	0	0	0	0	0
60	50	0	0	0	0	0	1	0	0	0	0	0	0
63	53	1	1	0	2	0	1	0	0	0	0	0	0
66	56	0	0	1	0	0	1	0	0	0	0	0	0
69	59	0	0	0	0	0	1	0	0	0	0	0	0
72	62	0	0	0	0	0	0	0	0	0	0	0	0
75	65	0	0	0	1	0	0	0	0	0	0	0	0
78	68	0	0	0	0	1	0	0	0	0	0	0	0
81	71	0	0	0	0	0	0	0	0	0	0	0	0
84	74	0	0	0	1	0	1	0	0	0	0	0	0
87	77	0	0	0	0	1	0	0	0	0	0	0	0
90	80	0	0	0	0	0	0	0	0	0	0	0	0
93	83	0	0	0	0	0	0	0	0	0	0	0	0
96	86	0	0	1	0	0	0	0	0	0	0	0	0
99	89	0	0	0	0	0	0	0	0	0	0	0	0
102	92	0	0	0	0	0	0	0	0	0	0	0	0
105	95	0	0	0	0	0	0	0	0	0	0	0	0
108	98	0	0	0	0	0	0	0	0	0	0	0	0
111	101	0	0	0	0	0	0	0	0	0	0	0	0
114	104	0	0	1	0	0	0	0	0	0	0	0	0
117	107	0	0	0	0	0	0	0	0	0	0	0	0
Total		56	89	132	156	142	128	0	0	2	13	34	57

	-6.35 +5.6 mm	-5.6 +4.0 mm	-4.0 +2.8 mm	-2.8 +2.0 mm	-2.0 +1.4 mm	-1.4 +1.0 mm
Total Particles to Overflow	56	89	132	156	142	128
Total Particles to Underflow	0	0	2	13	34	57
Total Particles Remaining in Bed	0	0	0	0	0	0
Total Feed	56	89	134	169	176	185

Experiment Date	18/11/2009
Feed Rate (g/min sand)	542
Underflow rate (g/min sand)	368
Vibration Rate	595V
Gas rate (%)	30
Experiment run time (min)	117

		2100 kg/m ³ density particles													
Time (min)	Adjusted Time (min)	Number of particles to Overflow						Number of Particles to Underflow							
		-6.35 +5.6 mm	-5.6 mm	+4.0 mm	-4.0+2.8 mm	-2.8+2.0 mm	-2.0+1.4 mm	-1.4+1.0 mm	-6.35 +5.6 mm	-5.6 mm	+4.0 mm	-4.0+2.8 mm	-2.8+2.0 mm	-2.0+1.4 mm	-1.4+1.0 mm
3		-	-	-	-	-	-	-	-	-	-	-	-	-	-
6		-	-	-	-	-	-	-	-	-	-	-	-	-	-
9		-	-	-	-	-	-	-	-	-	-	-	-	-	-
12		-	-	-	-	-	-	-	-	-	-	-	-	-	-
15		-	-	-	-	-	-	-	-	-	-	-	-	-	-
18		-	-	-	-	-	-	-	-	-	-	-	-	-	-
21	1	0	0	0	0	1	0	0	0	0	0	0	0	0	0
24	4	0	1	6	8	6	10	7	1	4	10	18	16		
27	7	0	3	0	14	13	6	1	3	5	3	10	15		
30	10	0	0	0	0	0	0	0	0	0	0	0	0		
33	13	3	4	14	24	17	17	0	1	0	1	2	4		
36	16	4	8	5	19	11	14	1	0	0	1	4	4		
39	19	1	6	1	9	8	5	1	0	0	1	3	3		
42	22	1	3	5	4	8	1	0	0	0	0	0	3		
45	25	1	1	3	5	4	4	0	0	0	0	2	0		
48	28	0	1	3	5	9	7	0	0	0	0	1	0		
51	31	3	8	5	6	4	4	0	0	0	0	0	0		
54	34	1	3	3	2	3	0	1	0	0	0	0	0		
57	37	0	2	3	6	1	8	0	0	0	0	0	0		
60	40	0	0	0	0	0	0	0	0	0	0	0	1		
63	43	1	1	4	3	2	2	0	0	0	0	0	1		
66	46	0	3	3	3	5	2	0	0	0	0	0	0		
69	49	0	4	5	7	1	0	0	0	0	0	0	0		
72	52	0	3	1	3	0	1	0	0	0	0	0	0		
75	55	0	0	1	1	0	0	0	0	0	0	0	0		
78	58	0	0	0	2	1	3	0	0	0	0	0	0		
81	61	0	0	0	0	0	0	0	0	0	0	0	0		
84	64	0	0	0	1	2	1	0	0	0	0	0	0		
87	67	0	0	0	0	0	1	0	0	0	0	0	0		
90	70	0	0	1	0	0	1	0	0	0	0	0	0		
93	73	0	0	1	1	0	0	0	0	0	0	0	0		
96	76	0	0	2	2	1	0	0	0	0	0	0	0		
99	79	0	1	0	0	1	1	1	0	0	0	0	0		
102	82	0	0	1	1	0	0	0	0	0	0	0	0		
105	85	1	4	0	1	0	1	0	0	0	0	0	0		
108	88	1	1	3	1	0	0	0	0	0	0	0	0		
111	91	0	1	2	1	0	0	0	0	0	0	0	0		
114	94	0	0	0	0	0	0	0	0	0	0	0	0		
117	97	1	1	0	1	0	0	0	0	0	0	0	0		
Total		18	59	72	130	98	89	12	5	9	16	40	47		

	-6.35 +5.6 mm	-5.6 mm	+4.0 mm	-4.0+2.8 mm	-2.8+2.0 mm	-2.0+1.4 mm	-1.4+1.0 mm
Total Particles to Overflow	18	59	72	130	98	89	
Total Particles to Underflow	12	5	9	16	40	47	
Total Particles Remaining in Bed	16	19	10	1	0	2	
Total Feed	46	83	91	147	138	138	

Experiment Date	18/11/2009
Feed Rate (g/min sand)	542
Underflow rate (g/min sand)	368
Vibration Rate	595V
Gas rate (%)	30
Experiment run time (min)	117

		1300 kg/m ³ density particles											
Time (min)	Adjusted Time (min)	Number of particles to Overflow						Number of Particles to Underflow					
		-6.35 +5.6 mm	-5.6+4.0 mm	-4.0+2.8 mm	-2.8+2.0 mm	-2.0+1.4 mm	-1.4+1.0 mm	-6.35 +5.6 mm	-5.6+4.0 mm	-4.0+2.8 mm	-2.8+2.0 mm	-2.0+1.4 mm	-1.4+1.0 mm
3		-	-	-	-	-	-	-	-	-	-	-	-
6		-	-	-	-	-	-	-	-	-	-	-	-
9		-	-	-	-	-	-	-	-	-	-	-	-
12		-	-	-	-	-	-	-	-	-	-	-	-
15		-	-	-	-	-	-	-	-	-	-	-	-
18		-	-	-	-	-	-	-	-	-	-	-	-
21		-	-	-	-	-	-	-	-	-	-	-	-
24		-	-	-	-	-	-	-	-	-	-	-	-
27		-	-	-	-	-	-	-	-	-	-	-	-
30		-	-	-	-	-	-	-	-	-	-	-	-
33	3	14	14	9	9	10	9	0	0	1	0	4	4
36	6	22	50	47	40	32	20	0	0	2	5	6	11
39	9	5	13	27	30	27	12	0	0	0	1	4	9
42	12	7	5	14	21	15	14	0	0	0	0	1	3
45	15	4	8	14	22	20	14	0	0	0	0	0	3
48	18	1	4	9	21	25	14	0	0	0	0	1	0
51	21	2	1	6	12	14	14	0	0	0	0	0	0
54	24	0	0	3	5	7	9	0	0	0	0	0	0
57	27	0	0	3	6	8	15	0	0	0	0	0	1
60	30	0	0	0	0	1	0	0	0	0	0	0	0
63	33	0	0	2	1	2	5	0	0	0	0	0	0
66	36	0	1	1	3	3	6	0	0	0	0	0	0
69	39	0	0	0	0	1	3	0	0	0	0	0	0
72	42	0	0	0	1	0	1	0	0	0	0	0	0
75	45	0	0	0	0	0	0	0	0	0	0	0	0
78	48	0	0	0	0	0	0	0	0	0	0	0	0
81	51	0	0	0	0	1	0	0	0	0	0	0	0
84	54	0	0	0	0	0	2	0	0	0	0	0	0
87	57	0	0	0	0	0	1	0	0	0	0	0	0
90	60	0	0	0	0	0	0	0	0	0	0	0	0
93	63	0	0	0	0	0	0	0	0	0	0	0	0
96	66	0	0	0	0	0	0	0	0	0	0	0	0
99	69	0	0	0	0	0	0	0	0	0	0	0	0
102	72	0	0	0	0	0	0	0	0	0	0	0	0
105	75	0	0	0	0	0	0	0	0	0	0	0	0
108	78	0	0	0	0	0	0	0	0	0	0	0	0
111	81	0	0	0	0	0	0	0	0	0	0	0	0
114	84	0	0	0	0	0	0	0	0	0	0	0	0
117	87	0	0	0	0	0	0	0	0	0	0	0	0
Total		55	96	135	171	166	139	0	0	3	6	16	31

	-6.35 +5.6 mm	-5.6+4.0 mm	-4.0+2.8 mm	-2.8+2.0 mm	-2.0+1.4 mm	-1.4+1.0 mm
Total Particles to Overflow	55	96	135	171	166	139
Total Particles to Underflow	0	0	3	6	16	31
Total Particles Remaining in Bed	0	0	0	0	0	0
Total Feed	55	96	138	177	182	170

Experiment Date	18/11/2009
Feed Rate (g/min sand)	542
Underflow rate (g/min sand)	368
Vibration Rate	595V
Gas rate (%)	30
Experiment run time (min)	117

		2400 kg/m ³ density particles													
Time (min)	Adjusted Time (min)	Number of particles to Overflow						Number of Particles to Underflow							
		-6.35 +5.6 mm	-5.6 mm	+4.0 mm	-4.0+2.8 mm	-2.8+2.0 mm	-2.0+1.4 mm	-1.4+1.0 mm	-6.35 +5.6 mm	-5.6 mm	+4.0 mm	-4.0+2.8 mm	-2.8+2.0 mm	-2.0+1.4 mm	-1.4+1.0 mm
3		-	-	-	-	-	-	-	-	-	-	-	-	-	-
6		-	-	-	-	-	-	-	-	-	-	-	-	-	-
9		-	-	-	-	-	-	-	-	-	-	-	-	-	-
12		-	-	-	-	-	-	-	-	-	-	-	-	-	-
15		-	-	-	-	-	-	-	-	-	-	-	-	-	-
18		-	-	-	-	-	-	-	-	-	-	-	-	-	-
21		-	-	-	-	-	-	-	-	-	-	-	-	-	-
24		-	-	-	-	-	-	-	-	-	-	-	-	-	-
27		-	-	-	-	-	-	-	-	-	-	-	-	-	-
30		-	-	-	-	-	-	-	-	-	-	-	-	-	-
33		-	-	-	-	-	-	-	-	-	-	-	-	-	-
36		-	-	-	-	-	-	-	-	-	-	-	-	-	-
39		-	-	-	-	-	-	-	-	-	-	-	-	-	-
42	2	0	0	0	0	0	0	0	0	0	0	0	0	0	0
45	5	0	0	3	3	2	5	42	39	36	26	36	34		
48	8	0	0	2	6	6	9	10	15	14	22	13	26		
51	11	0	1	4	8	6	12	1	7	6	8	7	11		
54	14	0	0	0	4	5	10	1	2	2	2	7	7		
57	17	0	0	2	7	13	13	0	1	2	0	1	4		
60	20	0	0	1	0	0	2	0	0	1	2	0	0		
63	23	0	0	0	6	4	7	0	1	1	1	0	1		
66	26	0	0	4	10	9	8	0	1	1	1	0	0		
69	29	0	1	4	6	9	5	0	0	0	0	1	0		
72	32	0	0	2	2	4	1	0	0	0	0	0	0		
75	35	0	1	1	2	7	4	0	0	0	0	1	2		
78	38	0	0	2	0	5	5	0	0	0	0	0	0		
81	41	0	0	0	2	4	5	0	0	1	0	0	0		
84	44	0	1	1	2	7	2	0	0	0	1	0	0		
87	47	0	0	0	3	0	1	1	1	0	0	0	0		
90	50	0	0	1	2	0	1	0	2	1	0	0	0		
93	53	0	0	1	1	0	4	0	0	0	0	0	0		
96	56	0	1	1	3	4	0	0	0	0	0	0	0		
99	59	0	0	1	0	1	2	0	0	1	0	0	0		
102	62	0	0	1	1	2	0	0	1	0	0	0	0		
105	65	0	0	0	2	5	1	0	0	0	0	0	0		
108	68	0	3	3	3	2	0	0	0	0	0	0	0		
111	71	0	0	3	0	0	1	0	0	0	0	0	0		
114	74	0	1	1	2	0	0	0	0	0	0	0	0		
117	77	0	0	2	3	0	2	0	0	0	0	0	0		
Total		0	9	40	78	95	100	55	70	66	63	66	85		

	-6.35 +5.6 mm	-5.6 mm	+4.0 mm	-4.0+2.8 mm	-2.8+2.0 mm	-2.0+1.4 mm	-1.4+1.0 mm
Total Particles to Overflow	0	9	40	78	95	100	
Total Particles to Underflow	55	70	66	63	66	85	
Total Particles Remaining in Bed	0	10	35	26	4	0	
Total Feed	55	89	141	167	165	185	

Appendix G: Coal Separation Data

Coal Washability Data

-8.00 + 4.00mm				ROM Mass %			
				11.7			
Sink	Float	Mass %	Ash %	Sink	Float	Mass %	Ash %
	1.30	0.8	1.9		1.30	4.5	1.0
1.30	1.35	8.2	5.6	1.30	1.35	16.3	4.8
1.35	1.40	26.2	9.6	1.35	1.40	24.8	9.3
1.40	1.45	16.4	14.1	1.40	1.45	13.9	14.1
1.45	1.50	6.0	18.0	1.45	1.50	6.2	18.3
1.50	1.55	2.8	21.9	1.50	1.55	3.0	22.0
1.55	1.60	1.7	24.7	1.55	1.60	2.0	25.9
1.60	1.70	1.9	30.3	1.60	1.70	2.1	30.5
1.70	1.80	1.1	38.1	1.70	1.80	1.2	38.8
1.80	1.90	1.1	45.6	1.80	1.90	1.0	46.0
1.90	2.00	0.9	52.6	1.90	2.00	0.8	52.5
2.00	2.10	0.8	59.3	2.00	2.10	0.8	58.9
2.10	2.20	0.6	65.2	2.10	2.20	0.6	64.3
2.20		31.5	82.9	2.20		22.8	82.7

-2.00 + 1.00mm				ROM Mass %			
				7.7			
Sink	Float	Mass %	Ash %	Sink	Float	Mass %	Ash %
	1.30	9.4	1.0		1.30	9.4	1.0
1.30	1.35	23.2	4.2		1.35	23.2	4.2
1.35	1.40	21.7	8.8		1.40	21.7	8.8
1.40	1.45	12.7	13.7		1.45	12.7	13.7
1.45	1.50	5.5	18.5		1.50	5.5	18.5
1.50	1.55	3.0	22.0		1.55	3.0	22.0
1.55	1.60	2.0	25.8		1.60	2.0	25.8
1.60	1.70	1.1	31.1		1.70	1.1	31.1
1.70	1.80	2.1	38.3		1.80	2.1	38.3
1.80	1.90	0.9	45.4		1.90	0.9	45.4
1.90	2.00	0.7	52.5		2.00	0.7	52.5
2.00	2.10	0.7	58.6		2.10	0.7	58.6
2.10	2.20	0.6	63.6		2.20	0.6	63.6
2.20		16.4	82.0			16.4	82.0

Batch Coal Separations Data

595V (Figure 8-1, 8-3)

Size fraction (mm)	Flow	Mass (g)	Ash%
-8.0 +4.0	1	6.8	10.1
-4.0 +2.0	1	4.5	10.3
-2.0 +1.0	1	2.1	12.2
-8.0 +4.0	2	27.7	10.8
-4.0 +2.0	2	25.0	11.0
-2.0 +1.0	2	22.7	12.5
-8.0 +4.0	3	22.6	11.1
-4.0 +2.0	3	22.4	12.7
-2.0 +1.0	3	21.7	16.5
-8.0 +4.0	4	19.3	15.5
-4.0 +2.0	4	8.7	20.1
-2.0 +1.0	4	9.8	26.2
-8.0 +4.0	5	5.1	26.1
-4.0 +2.0	5	5.0	33.4
-2.0 +1.0	5	6.3	35.1
-8.0 +4.0	Underflow	34.9	76.5
-4.0 +2.0	Underflow	19.8	80.0
-2.0 +1.0	Underflow	6.3	78.6

595V (Figure 8-2)

Size fraction (mm)	Flow	Mass (g)	Ash%
-4.0 +2.0	1	47.6	11.3
-2.0 +1.0	1	27.3	12.8
-4.0 +2.0	2	107.1	14.2
-2.0 +1.0	2	95.4	15.7
-4.0 +2.0	3	81.6	18.0
-2.0 +1.0	3	99.0	20.1
-4.0 +2.0	4	25.1	34.0
-2.0 +1.0	4	19.2	40.9
-4.0 +2.0	5	10.9	49.2
-2.0 +1.0	5	8.3	58.6
-4.0 +2.0	Underflow	13.5	79.6
-2.0 +1.0	Underflow	50.3	81.4

750M (Figure 8-2)

Size fraction (mm)	Flow	Mass (g)	Ash%
-4.0 +2.0	1	36.7	11.0
-2.0 +1.0	1	21.4	12.4
-4.0 +2.0	2	144.3	14.1
-2.0 +1.0	2	143.7	15.9
-4.0 +2.0	3	10.6	33.1
-2.0 +1.0	3	31.5	33.8
-4.0 +2.0	4	4.6	52.5
-2.0 +1.0	4	8.3	64.7
-4.0 +2.0	Underflow	53.4	80.6
-2.0 +1.0	Underflow	9.0	81.0

No Vibration (Figure 8-2)

Size fraction (mm)	Flow	Mass (g)	Ash%
-4.0 +1.0	1	101.5	17.0
-4.0 +1.0	2	171.7	24
-4.0 +1.0	3	163.3	27.9
-4.0 +1.0	4	13.6	63.5
-4.0 +1.0	Underflow	6.8	71.9

Continuous Coal Separation Data

Time (min)	Overflow		Underflow		Feed	
	Sand (g)	Coal (g)	Sand (g)	Coal (g)	Sand (g)	Coal (g)
10	1976.3	123.4	4484.8	30.7	5794.3	620.7
20	1305.5	177.9	4454.8	70.7	5794.3	620.7
30	1184.2	147.9	4551.0	95.3	5794.3	620.7
40	1245.0	179.4	4374.6	108.8	5794.3	620.7
50	1526.0	179.9	4286.2	138.1	5794.3	620.7
60	1701.3	259.4	4421.5	142.6	5794.3	620.7
70	1054.2	179.3	4250.6	109.2	5794.3	620.7
80	1466.1	244.7	4361.9	117.9	5794.3	620.7
90	2773.1	399.1	3581.4	106.3	5794.3	620.7
100	1349.6	195.0	3499.9	92.7	5794.3	620.7
110	2802.4	281.6	3432.9	88.6	5794.3	620.7
120	2108.6	239.0	3521.9	89.7	5794.3	620.7
130	3166.8	341.8	3503.5	88.8	5794.3	620.7
140	1702.1	226.2	3578.7	101.8	5794.3	620.7
150	2065.9	272.7	3395.0	95.1	5794.3	620.7
160	2127.7	273.3	3474.8	100.5	5794.3	620.7
170	2628.3	298.6	3452.6	87.7	5794.3	620.7
180	2621.8	349.0	2939.0	72.0	5794.3	620.7
190	2760.7	266.7	2959.2	68.6	5794.3	620.7
200	3448.1	312.9	2867.9	76.5	5794.3	620.7
210	2311.6	239.3	2962.1	75.2	5794.3	620.7

<i>70 minutes</i>	Size (mm)	Overflow			Underflow			Feed		
		Mass (g)	Mass %	Ash (%)	Mass (g)	Mass %	Ash (%)	Mass (g)	Mass %	Ash (%)
	-5.6+4.0	49.5	28.0	24.1	16.4	15.3	75.2	84.8	23.6	36.4
	-4.0+2.8	40.2	22.7	23	16.4	15.3	59.7	62.3	17.3	29.1
	-2.8+2.0	34.2	19.3	20.4	20.2	18.8	45.1	70.0	19.5	29.1
	-2.0+1.4	30.9	17.5	19.1	27.2	25.3	34.5	76.3	21.2	23.1
	-1.4+1.0	22.2	12.5	17.6	27.2	25.3	26.2	66.5	18.5	23.1

<i>80 minutes</i>	Size (mm)	Overflow			Underflow			Feed		
		Mass (g)	Mass %	Ash (%)	Mass (g)	Mass %	Ash (%)	Mass (g)	Mass %	Ash (%)
	-5.6+4.0	54.5	22.5	18	20.7	17.8	75.8	84.8	23.6	36.4
	-4.0+2.8	51.6	21.3	16.5	15.9	13.7	60.5	62.3	17.3	29.1
	-2.8+2.0	52.4	21.7	16.8	21.4	18.4	47.7	70.0	19.5	29.1
	-2.0+1.4	49	20.2	15.7	29.2	25.2	33.5	76.3	21.2	23.1
	-1.4+1.0	34.5	14.3	15.5	28.8	24.8	27.2	66.5	18.5	23.1

<i>160 minutes</i>	Size (mm)	Overflow			Underflow			Feed		
		Mass (g)	Mass %	Ash (%)	Mass (g)	Mass %	Ash (%)	Mass (g)	Mass %	Ash (%)
	-5.6+4.0	52.3	19.3	15.7	21.5	22.4	78.8	84.8	23.6	36.4
	-4.0+2.8	55.5	20.5	16.6	17.9	18.6	69.9	62.3	17.3	29.1
	-2.8+2.0	58	21.4	17.2	16.4	17.1	55	70.0	19.5	29.1
	-2.0+1.4	59.1	21.9	17.3	20.2	21.0	39.7	76.3	21.2	23.1
	-1.4+1.0	45.5	16.8	17.5	20	20.8	29.5	66.5	18.5	23.1

<i>170 minutes</i>	Size (mm)	Overflow			Underflow			Feed		
		Mass (g)	Mass %	Ash (%)	Mass (g)	Mass %	Ash (%)	Mass (g)	Mass %	Ash (%)
	-5.6+4.0	84.1	28.4	32	21	24.2	77.8	84.8	23.6	36.4
	-4.0+2.8	60.6	20.4	28.5	14.8	17.1	71.2	62.3	17.3	29.1
	-2.8+2.0	58.5	19.7	27.3	14.7	17.0	54.4	70.0	19.5	29.1
	-2.0+1.4	53.6	18.1	24.7	17.8	20.5	38	76.3	21.2	23.1
	-1.4+1.0	39.6	13.4	21.8	18.4	21.2	29.6	66.5	18.5	23.1

<i>210 minutes</i>	Size (mm)	Overflow			Underflow			Feed		
		Mass (g)	Mass %	Ash (%)	Mass (g)	Mass %	Ash (%)	Mass (g)	Mass %	Ash (%)
	-5.6+4.0	41	17.3	12.6	18.8	25.3	77.9	84.8	23.6	36.4
	-4.0+2.8	46.7	19.7	14.2	12.4	16.7	71.5	62.3	17.3	29.1
	-2.8+2.0	51.5	21.7	16	12.5	16.8	57	70.0	19.5	29.1
	-2.0+1.4	55.1	23.2	17	15.4	20.7	41.5	76.3	21.2	23.1
	-1.4+1.0	42.9	18.1	17.8	15.2	20.5	31.2	66.5	18.5	23.1

Appendix H: Continuous Tracer Particle Partition Curve Data

The following tables contain the details of the best fits to the partition curves for both the Reflux Classifier and the vertical fluidised bed as discussed in Chapter 7. The Σe^2 term in the partition curve data is the sum of the square difference between the partition curve value and the experimental data point that was minimised to produce the partition curve.

After the partition curve data, the fitted values of Equation (7-1) are given.

Table H-1: The partition curve constants for the Reflux Classifier with changing overflow rate.

Tracer Particle Size (mm)	Overflow Feed	τ_{50}	E_p	Σe^2
-6.35 +5.6	0.160	1.800	0.060	0.0006
	0.322	1.562	0.060	0.0002
	0.431	1.600	0.060	0.0006
	0.530	1.939	0.070	0.0124
-5.6 +4.0	0.160	1.779	0.090	0.0001
	0.322	1.534	0.066	0.0002
	0.431	1.769	0.082	0.0006
	0.530	1.941	0.090	0.0204
-4.0 +2.8	0.160	1.678	0.166	0.0049
	0.322	1.557	0.084	0.0004
	0.431	1.672	0.114	0.0014
	0.530	1.864	0.097	0.0067
-2.8 +2.0	0.160	1.587	0.183	0.0045
	0.322	1.551	0.106	0.0003
	0.431	1.741	0.159	0.0014
	0.530	1.899	0.135	0.0088
-2.0 +1.4	0.160	1.560	0.273	0.0008
	0.322	1.572	0.176	0.0045
	0.431	1.801	0.252	0.0023
	0.530	1.990	0.247	0.0097
-1.4 +1.0	0.160	1.418	0.444	0.0024
	0.322	1.619	0.329	0.0016
	0.431	1.859	0.397	0.0047
	0.530	2.130	0.465	0.0037

Table H-2: The partition curve constants for the Reflux Classifier with changing gas rate.

Tracer Particle Size (mm)	Gas Rate (%)	τ_{50}	Ep	$-e^2$
-6.35 +5.6	25	1.562	0.060	0.006
	30	2.048	0.163	0.003
	35	2.002	0.128	0.014
-5.6 +4.0	25	1.534	0.066	0.017
	30	2.069	0.326	0.008
	35	2.033	0.220	0.000
-4.0 +2.8	25	1.557	0.084	0.017
	30	2.000	0.392	0.008
	35	1.922	0.283	0.000
-2.8 +2.0	25	1.551	0.106	0.036
	30	1.968	0.661	0.067
	35	1.886	0.364	0.009
-2.0 +1.4	25	1.572	0.176	0.017
	30	1.852	1.037	0.051
	35	1.766	0.447	0.009
-1.4 +1.0	25	1.619	0.329	0.000
	30	1.667	1.229	0.035
	35	1.776	0.791	0.004

Table H-3: The partition curve constants for the vertical fluidised bed with changing overflow rate.

Tracer Particle Size (mm)	Overflow Feed	τ_{50}	Ep	$-e^2$
-6.35 +5.6	0.197	1.519	0.134	0.0131
	0.342	1.568	0.089	0.0028
	0.457	1.619	0.093	0.0006
	0.514	1.847	0.074	0.0001
-5.6 +4.0	0.197	1.453	0.163	0.0125
	0.342	1.542	0.114	0.0139
	0.457	1.612	0.110	0.0036
	0.514	1.957	0.174	0.0210
-4.0 +2.8	0.197	1.362	0.229	0.0153
	0.342	1.546	0.172	0.0121
	0.457	1.645	0.273	0.1185
	0.514	2.124	0.195	0.0341
-2.8 +2.0	0.197	1.223	0.351	0.0127
	0.342	1.512	0.313	0.0174
	0.457	1.721	0.415	0.0686
	0.514	2.278	0.241	0.0254
-2.0 +1.4	0.197	1.193	0.342	0.0069
	0.342	1.277	0.639	0.0098
	0.457	1.750	0.730	0.0891
	0.514	2.405	0.423	0.0325
-1.4 +1.0	0.197	1.075	0.403	0.0042
	0.342	1.062	1.046	0.0184
	0.457	1.726	1.491	0.0679
	0.514	2.468	0.757	0.0261

Table H-4: The partition curve constants for the vertical fluidised bed with changing gas rate.

Tracer Particle Size (mm)	Gas Rate (%)	τ_{50}	Ep	$-e^2$
-6.35 +5.6	25	1.568	0.089	0.0028
	30	2.126	0.070	0.0011
	35	2.412	0.037	0.0000
-5.6 +4.0	25	1.542	0.114	0.0139
	30	2.264	0.073	0.0001
	35	2.713	0.278	0.0003
-4.0 +2.8	25	1.546	0.172	0.0121
	30	2.339	0.138	0.0064
	35	2.835	0.368	0.0007
-2.8 +2.0	25	1.512	0.313	0.0174
	30	2.483	0.284	0.0120
	35	2.969	0.660	0.0029
-2.0 +1.4	25	1.277	0.639	0.0098
	30	2.643	0.719	0.0016
	35	4.061	2.650	0.0069
-1.4 +1.0	25	1.062	1.046	0.0184
	30	2.578	1.133	0.0066
	35	2.616	1.964	0.0117

Table H-5: The fitted constants of Equation (7-1) for the Reflux Classifier with changing overflow rate.

Tracer Particle Size (mm)	A	n	C
-6.35 +5.6	24.33	7.31	1.64
-5.6 +4.0	27.59	7.31	1.67
-4.0 +2.8	67.08	8.85	1.62
-2.8 +2.0	4.88	4.16	1.56
-2.0 +1.4	4.04	3.39	1.53
-1.4 +1.0	3.00	2.13	1.36

Table H-6: The fitted constants of Equation (7-1) for the Reflux Classifier with changing gas rate.

Tracer Particle Size (mm)	A	n	C
-6.35 +5.6	17.78	0.06	-20.03
-5.6 +4.0	20.17	0.06	-22.95
-4.0 +2.8	16.51	0.06	-18.15
-2.8 +2.0	14.93	0.06	-16.30
-2.0 +1.4	8.68	0.06	-8.81
-1.4 +1.0	0.00	2.19	1.46

Table H-7: The fitted constants of Equation (7-1) for the vertical fluidised bed with changing overflow rate.

Tracer Particle Size (mm)	A	n	C
-6.35 +5.6	27.15	6.80	1.53
-5.6 +4.0	41.26	6.80	1.47
-4.0 +2.8	61.41	6.80	1.42
-2.8 +2.0	87.62	6.80	1.32
-2.0 +1.4	113.25	6.80	1.19
-1.4 +1.0	136.57	6.80	1.02

Table H-8: The fitted constants of Equation (7-1) for the vertical fluidised bed with changing gas rate.

Tracer Particle Size (mm)	A	n	C
-6.35 +5.6	12.10	0.13	-16.96
-5.6 +4.0	16.77	0.13	-24.15
-4.0 +2.8	18.41	0.13	-26.66
-2.8 +2.0	20.89	0.13	-30.48
-2.0 +1.4	39.54	0.13	-59.42
-1.4 +1.0	22.60	0.13	-33.40

Appendix I: Continuous Tracer Particle Error Bars

Table I-1: Error bar data for the Reflux Classifier

Particle Size (mm)	Gas rate (%)	Overflow Feed	π_{50}	$\pi_{50 \text{ max}}$	$\pi_{50 \text{ min}}$
-6.35 +5.6	25	0.160	1.800	1.885	1.582
	25	0.322	1.562	1.828	1.534
	25	0.431	1.600	1.946	1.560
	25	0.530	1.900	2.032	1.768
	30	0.332	2.048	2.084	2.009
	35	0.332	2.002	2.008	1.997
-5.6 +4.0	25	0.160	1.779	1.916	1.610
	25	0.322	1.534	1.786	1.523
	25	0.431	1.769	1.973	1.631
	25	0.530	1.931	2.059	1.836
	30	0.332	2.069	2.120	2.003
	35	0.332	2.033	2.053	2.032
-4.0 +2.8	25	0.160	1.678	1.813	1.605
	25	0.322	1.557	1.647	1.537
	25	0.431	1.672	1.819	1.647
	25	0.530	1.864	1.966	1.839
	30	0.332	2.000	2.058	1.985
	35	0.332	1.922	1.928	1.922
-2.8 +2.0	25	0.160	1.587	1.654	1.575
	25	0.322	1.551	1.576	1.548
	25	0.431	1.741	1.844	1.740
	25	0.530	1.899	1.982	1.906
	30	0.332	1.968	1.996	1.953
	35	0.332	1.886	1.889	1.886
-2.0 +1.4	25	0.160	1.560	1.582	1.545
	25	0.322	1.572	1.583	1.573
	25	0.431	1.801	1.837	1.796
	25	0.530	1.990	2.026	1.991
	30	0.332	1.852	1.863	1.847
	35	0.332	1.766	1.767	1.766
-1.4 +1.0	25	0.160	1.418	1.419	1.401
	25	0.322	1.619	1.623	1.619
	25	0.431	1.859	1.875	1.858
	25	0.530	2.130	2.153	2.127
	30	0.332	1.667	1.668	1.666
	35	0.332	1.776	1.776	1.776

Table I-2: Error bar data for the Vertical Fluidised Bed

Particle Size (mm)	Gas rate (%)	Overflow Feed	π_{50}	$\pi_{50 \text{ max}}$	$\pi_{50 \text{ min}}$
-6.35 +5.6	25	0.197	1.519	1.556	1.516
	25	0.342	1.568	1.599	1.565
	25	0.457	1.619	1.624	1.618
	25	0.514	1.847	1.907	1.836
	30	0.320	2.126	2.134	2.095
	35	0.369	2.370	2.389	2.325
-5.6 +4.0	25	0.197	1.453	1.483	1.453
	25	0.342	1.542	1.556	1.540
	25	0.457	1.612	1.617	1.611
	25	0.514	1.957	2.024	1.950
	30	0.320	2.264	2.268	2.221
	35	0.369	2.593	2.595	2.489
-4.0 +2.8	25	0.197	1.362	1.382	1.361
	25	0.342	1.546	1.560	1.545
	25	0.457	1.645	1.683	1.641
	25	0.514	2.124	2.151	2.112
	30	0.320	2.339	2.378	2.314
	35	0.369	2.695	2.699	2.562
-2.8 +2.0	25	0.197	1.223	1.281	1.201
	25	0.342	1.512	1.523	1.511
	25	0.457	1.721	1.779	1.716
	25	0.514	2.278	2.298	2.270
	30	0.320	2.483	2.519	2.433
	35	0.369	2.933	2.936	2.879
-2.0 +1.4	25	0.197	1.193	1.329	1.162
	25	0.342	1.277	1.332	1.261
	25	0.457	1.750	1.783	1.746
	25	0.514	2.405	2.419	2.396
	30	0.320	2.643	2.651	2.624
	35	0.369	3.939	3.957	3.824
-1.4 +1.0	25	0.197	1.075	1.213	1.034
	25	0.342	1.062	1.123	1.051
	25	0.457	1.726	1.743	1.719
	25	0.514	2.468	2.470	2.463
	30	0.320	2.578	2.579	2.568
	35	0.369	2.572	2.589	2.552

Appendix J: Sample Calculations

First Order Elutriation constant

In Chapter 6, the batch elutriation data was fitted to a first order elutriation model of the form:

$$M_{bed,t+1} = M_{bed,t}(1 - k)$$

where $M_{bed,t}$ is the mass of particles in the bed at time t and k the first order elutriation constant.

The raw experimental data from the batch experiments gave the values of $M_{bed,t}$ and the value of k for each set of data was calculated using a SOLVER routine in excel by minimising the square difference between the theoretical and experimental values.

Partition Curve

In Chapter 6 and Chapter 7, partition curves were used to analyse the tracer particle data. The partition curves took the form of:

$$P = \frac{1}{1 + \exp\left(\frac{\ln 3(\rho_p - \rho_{50})}{Ep}\right)}. \quad (4-1)$$

The experimental values of the partition numbers P , were fitted to Equation (4-1) using a Solver routine in EXCEL to minimise the sum of the square difference between the experimental and fitted values.

Levenspiel Equation

The particle elutriation data were fitted to a two-parameter model for dispersed plug flow with open boundary conditions at each end (Levenspiel, 1972):

$$\dot{m} = \frac{U}{\sqrt{4\pi Dt}} \exp\left[\frac{-(L - Ut)^2}{4Dt}\right], \quad (0-1)$$

where \dot{m} is the mass fraction rate (1/s), U the species velocity (m/s), D the dispersion coefficient (m^2/s), t the time (s) and L the length (m) of the Reflux Classifier. The mass fraction rate is determined by dividing the mass of particles elutriated in a time interval by the width of the time interval and the total mass of particles of that size fraction in the initial tracer charge.

Equation (6-4) was fitted to the experimental data by calculating the experimental mass fraction rate as:

$$\dot{m} = \frac{m_t}{m_T t}$$

where m_t is the mass of particles exiting in time interval t (length in seconds) and m_T is the total number of particles in the feed in that size fraction. So for example, if 1 g of particles exited the bed in a 2 minute time interval, from a total feed of 50 g, the mass fraction rate is:

$$\dot{m} = \frac{m_t}{m_T t} = \frac{1}{50 \times 120} = \frac{1}{6000} = 0.000167s^{-1}$$

The best fit values of U and D were then calculated by minimising the sum of the square difference of the experimental and calculated values of the mass fraction rate using a solver routine in Excel.

Theoretical U_{conv}

The theoretical sand convective velocity $U_{conv,t}$, is given by,

$$U_{conv,t} = \frac{\dot{M}_{feed} L}{M_{bed}} \quad (0-2)$$

where \dot{M}_{feed} is the rate of sand addition (kg/s), M_{bed} is the steady state hold-up (kg) of sand as given in Figure 6-3 and L is the length of the column (m). So for example, if a feed of 300 g/min of sand is fed into a bed of length L with a total mass of sand in the bed of 7000 g, then:

$$U_{conv,t} = \frac{\dot{M}_{feed} L}{M_{bed}} = \frac{0.005 \times 3}{7000} = 0.00214m/s.$$

Bed Voidage

The void fraction, ε , is calculated using the following equation:

$$\varepsilon = \frac{V_{Total} - V_{particles}}{V_{Total}}$$

And so in a 0.006 m^3 bed with a total mass of sand of 7000 g, at a density of 2600 kg/m^3 , corresponding to a volume of 0.00269 m^3 , the voidage of the bed is:

$$\varepsilon = \frac{V_{Total} - V_{particles}}{V_{Total}} = \frac{0.006 - 0.00269}{0.006} = \frac{0.00331}{0.006} = 0.55.$$

U_{slip} in the Intermediate Regime

The terminal free settling velocity of a particle in the Intermediate regime with diameter d_p and density ρ_p in a fluid of density ρ_f and viscosity μ_f was given in Chapter 3 as (Vance & Moulton, 1965):

$$U_{TFS} = 0.153 \frac{d_p^{8/7} (\rho_p - \rho_f)^{5/7} g^{5/7}}{\mu_f^{3/7} \rho_f^{2/7}} . \quad (3-7)$$

And so, for a particle of density 1300 kg/m^3 and diameter 3 mm in a fluid of density 1500 kg/m^3 and viscosity 22 Pa s , the UTFS is calculated as:

$$\begin{aligned} U_{TFS} &= 0.153 \frac{d_p^{8/7} (\rho_p - \rho_f)^{5/7} g^{5/7}}{\mu_f^{3/7} \rho_f^{2/7}} \\ &= 0.153 \frac{0.003^{8/7} (1300 - 1500)^{5/7} 9.81^{5/7}}{22^{3/7} 1500^{2/7}} \\ &= \frac{-0.045}{30.393} \\ &= 0.0015 \text{ m/s} \end{aligned}$$

Tracer Particle Concentration

The Concentration of tracer particles in the bed layer, as reported in Figure 7-3, was calculated as follows. If the layer contained 495 g of sand, and 5 g of tracer particles, the concentration was calculated to be:

$$\text{Concentration} = 5/500 = 0.01 \text{ g/g.}$$

Appendix K: Photos of Reflux Classifier

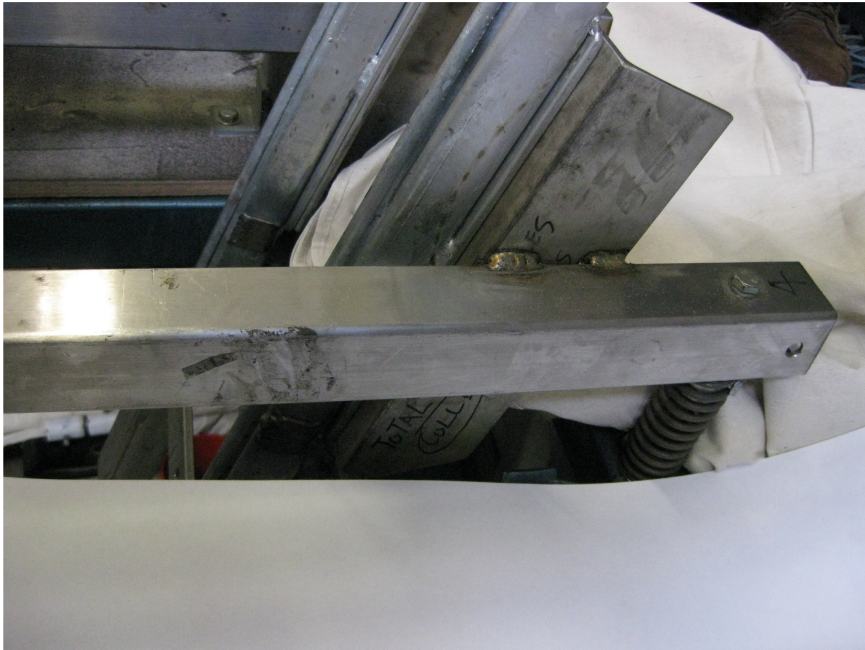


Figure 1: Photograph showing how the supporting frames were attached to the horizontal bar via angled struts. Can also see one of the four springs in the bottom right hand corner.

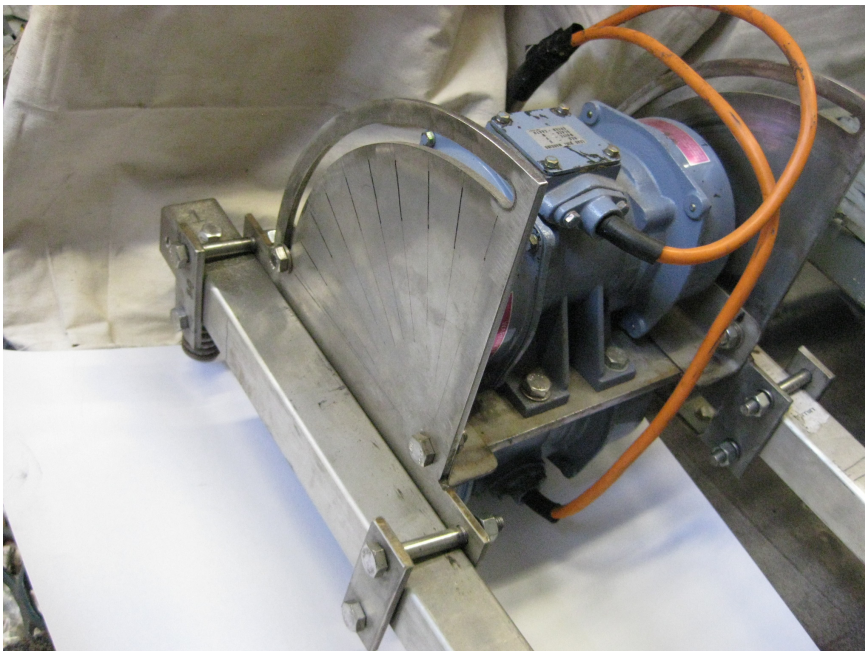


Figure 2: Photograph showing how the motors were mounted one above the other. Also showing how the angle of the motors could be changed by rotating the frame and how the motors frame was attached to the horizontal bars. One of the four springs can be seen at the left.



Figure 3: Photograph showing the N1000 frame and the struts used to mount the Reflux Classifier apparatus onto the frame.



Figure 4: Photographs of the overflow arrangement showing the stainless steel that was used for the majority of experiments as well as the polycarbonate arrangement to give insight into the internals of the stainless steel.

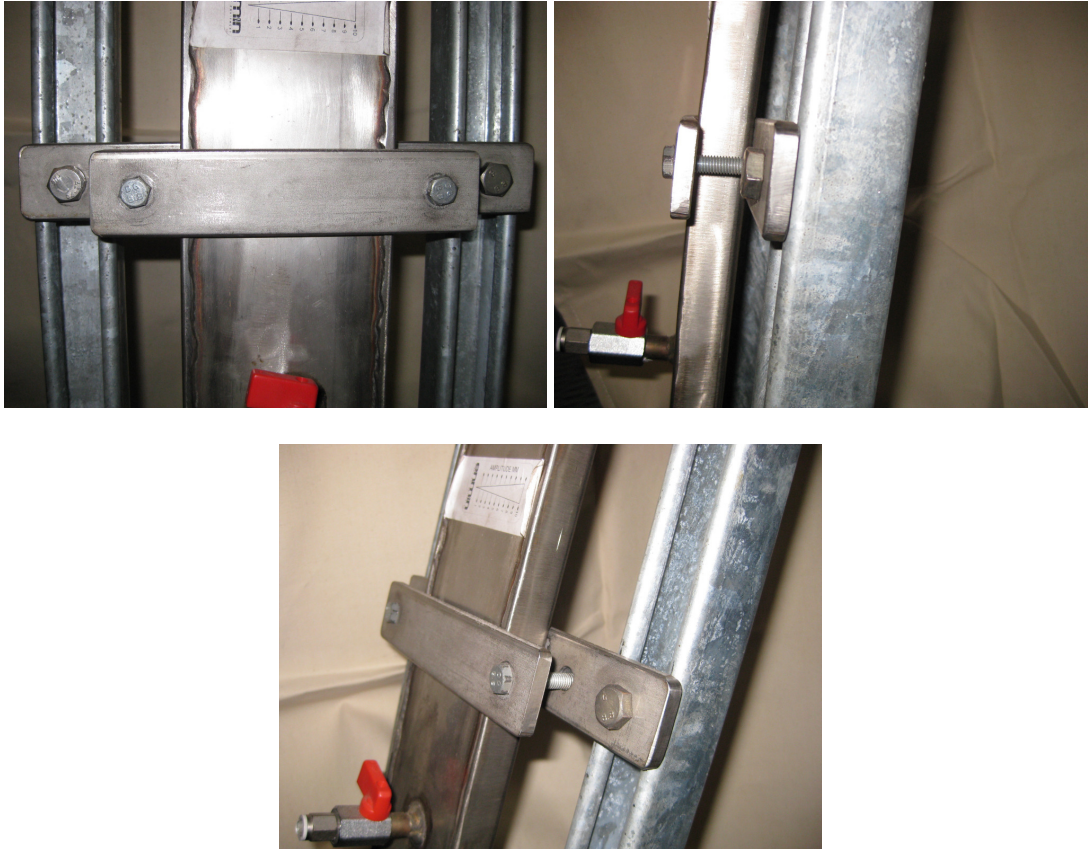


Figure 5: Photographs showing the way that the channel of the bed was attached to the frame.



Figure 6: Showing the pinch valves below the pyramid section.

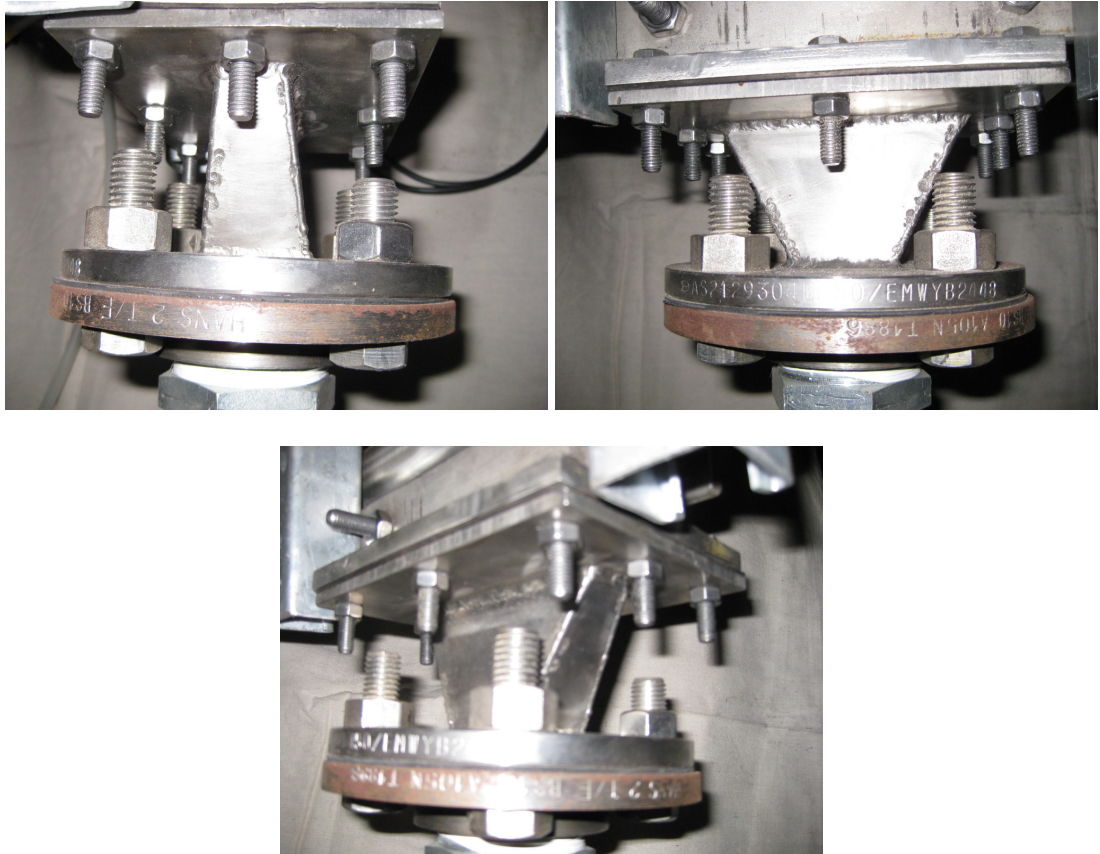


Figure 7: Illustrating the pyramid section that moved the particles from the continuous gas distributor to the pinch valves.



Figure 8: Photograph illustrating the feed inlet on the vertical section.

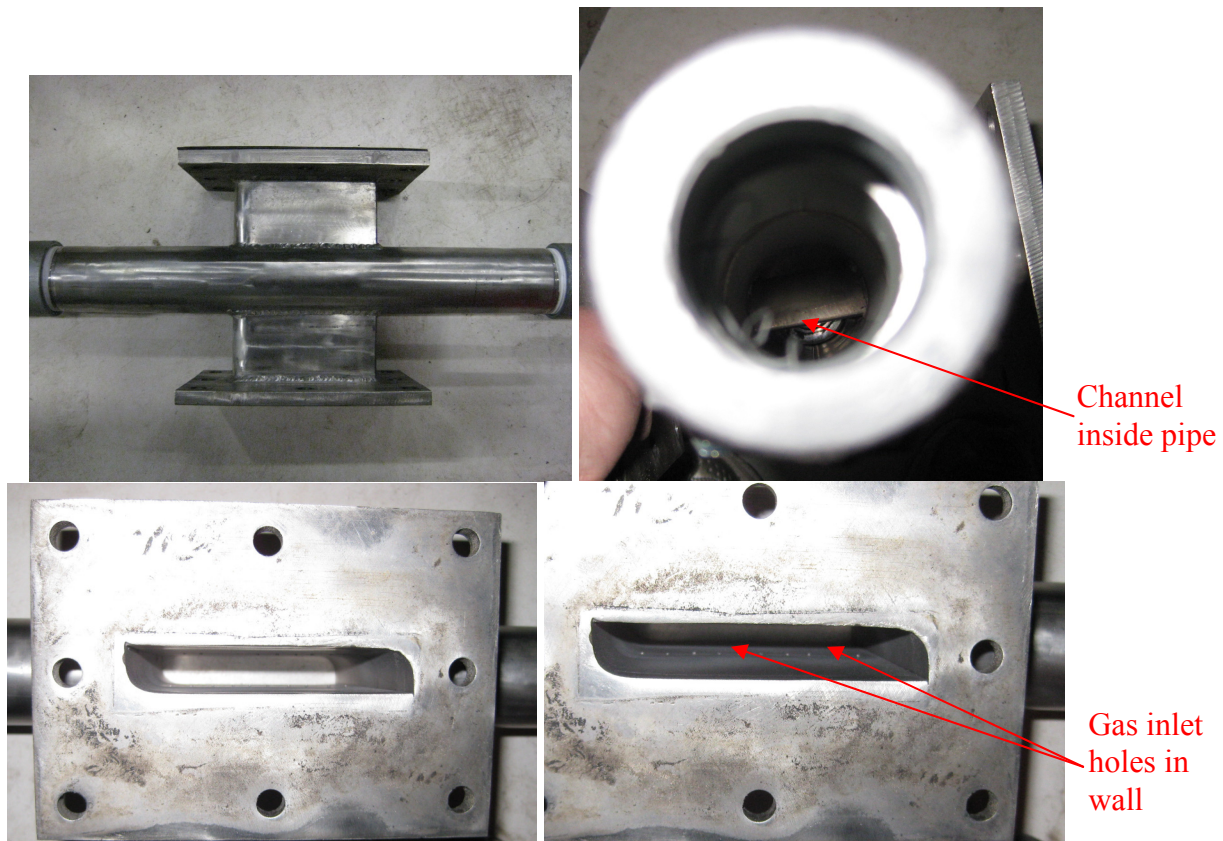


Figure 9: Photographs illustrating the gas distributor for the continuous system showing the pipe plenum chamber, the channel walls inside the pipe and the holes in the channel walls that acted as the distributor plate.

Appendix L: Spring Design

Part No. : 4.5x29x127x12.3

Details :

Spring Type: ROUND WIRE COMPRESSION

Material: BS 5216 Patented Carbon

Youngs Mod (E) = 206800 N/mm²

End Type: Closed & Ground

Dead Coils = 1.50

Tip Thick = 25.00%

Rigidity Mod (G) = 79300 N/mm²

Density = 0.00000783 Kg/mm³

0-49% Unprestress 49-70% Prestress

End Fix : Both Ends Fixed & Guided

Wire Dia. = 4.50 mm

Outside Dia. = 38.00 mm

Total Coils = 12.30

Stress Data LOWER

% TENSILE

Tensile Solid Working

Spring Rate = 10.01 *C N/mm

Free Length = 127.00 mm

Grade 1 1130 72 O 24 U

Grade 2 1330 61 P 20 U

Calculated Data

Solid Length = 53.10 mm

Solid Load = 739.81 N

Solid Stress = 821.54 N/mm²

Active Coils = 10.80

Stress Factor = 1.19

Spring Index = 7.44 SPECIFIED

NO DATA

Grade 3 1530 53 P 18 U

Grade 4 NO DATA

Grade 5 NO DATA

Working Positions 1

Length (mm) 102.00

Load (N) 250.27

Deflec. (mm) 25.00

Stress (N/mm²) 277

% Solid 33

Inside Dia. = 29.00 mm

Helix Angle = 6.15 Deg

Wire Length = 1301.22 mm

Weight per 100 = 16.20 Kg

Nat.Frequency = 7978.30 RPM

Buckling (Pos)= STABLE

Buckling (Def)=

PRINTOUT OF LOAD AT LENGTH CHARACTERISTICS

% % TENSILE (LOWER) LOAD TOL OD

LENGTH	LOAD	DEFL	STRESS	DFL	1	2	3	4	5	G1	G2	EXP
102.00	250.27	25.00	277 33	24	20	18	27.25	40.88	.0846			